Exosomal Protein Deficiencies: How Abnormal RNA Metabolism Results in Childhood-Onset Neurological Diseases

A thesis submitted for the degree of Doctor of Philosophy at Newcastle University

October 2016

Michele Giunta

Institute of Genetic Medicine

Newcastle University

Institute of Genetic Medicine

Author’s declaration

This thesis is submitted for the degree of Doctor of Philosophy at Newcastle University. I, Michele Giunta, declare that the work described here is my own, unless where clearly acknowledged and stated otherwise. I certify that I have not submitted any of the material in this thesis for a degree qualification at this or any other university.

Abstract

RNA metabolism is of critical importance for normal cellular functions and needs to be finely tuned in order to maintain stable conditions within the cell. The exosome complex is the most important RNA processing machinery, responsible for the correct processing of many different types of RNAs and interacting with different co-factors which bind and carry specific subtypes of RNA for degradation to the complex. Mutations in exosome complex subunits (*EXOSC3, EXOSC8*) were reported to cause severe childhood onset complex neurological disorders presenting with pontocerebellar hypoplasia type 1 (PCH1), spinal muscular atrophy (SMA) and central nervous system hypomyelination. We have recently identified a homozygous pathogenic mutation in RNA Binding Motif Protein 7 *RBM7*, a subunit of the nuclear exosome targeting (NEXT) complex in a single patient with SMA-like phenotype and proved that *RBM7* is a novel human disease gene related to the exosome complex.

In order to understand the disease mechanism in *RBM7* deficiency and to explore the role of exosome complex in neurodevelopment, we performed gene expression studies (RT-PCR, RNA sequencing) in human cells of patients carrying mutations in *EXOSC8* and *RBM7*. Furthermore we performed functional studies in zebrafish (*D. rerio*) by morpholino oligonucleotide mediated knock-down of *rbm7*, *exosc8* and *exosc3* and also by introducing pathogenic mutations in exosomal protein genes in zebrafish embryos by the CRISPR/Cas9 system.

We showed that mutations in *RBM7* and *EXOSC8* mutant fibroblasts cause differential expression of several different transcripts, 62 of them being shared between the two cell lines. Altered gene expression of some AU-rich element containing genes may potentially contribute to the clinical presentation.

Knock-down of *rbm7*, *exosc8* and *exosc3* caused impaired neurodevelopment in zebrafish, illustrated by abnormal growth of motor neuron axons and failure to differentiate cerebellar Purkinje cells. RT-PCR analysis in zebrafish showed a dramatic increase in expression of *atxn1b* (an AU-rich element containing homolog of the human *ATXN1* gene) in *rbm7*, *exosc8* and *exosc3* downregulated fish, which may be responsible for the cerebellar defects. We have successfully introduced several germline mutations with CRISPR/Cas9 technology in *rbm7*. Phenotype of the F1 mutants is milder than what observed with the morpholino oligonucleotide injected fish. Mutants at a closer look do not show any morphological defect but further experiment may indicate similar characteristics to the morphants, although more

subtle. Further studies on the CRISPR/Cas9 generated zebrafish models will extend our knowledge on the disease mechanisms caused by defective RNA metabolism.

Acknowledgements

The last three years have been a great experience for me, I am grateful to the following people:

firstly I would like to thank my supervisor Professor Rita Horvath, she has been always supportive and available for fruitful discussions throughout all my PhD.

Dr. Juliane Mueller and Dr. Veronika Boczonadi for helping me with day to day life in the lab and in the pub.

Dr. Aurora Gomez-Duran for helping with all the transcriptome-related-issues.

Dr Angela Pyle and Dr. Jennifer Duff for being the cornerstones of the lab, I don't know how I would have done without you.

Rafiqul Hussain has always been on my (right-hand) side, no matter what. He has taught me every secret of the Agilent Bioanalyzer.

I have been lucky to share these three years of work and fun with people from the mitochondrial group and stem cell group: Gavin Hudson, Jonathan Coxhead, Beccie Brennan, Padraig Flannery, Emily McIlwayne, David Moore, Marina Bartsakoulia, Florence Burte, George Cairns, Marzena Kurzawa-Akanbi, George Anyfantis, Valeria Chichagova, Katja Gassner, Ellie Meader, Joseph Collin, Carla Mellough, Boglarka Bansagi, Mikael Pezet.

Thank you mum, dad, Elisa and all the people who have supported me until here through all my life.

Thanks to the electron microscopy and zebrafish facilities staff: Kathryn White, Tracey Davey, Michael Robson, Paul Cairns.

Finally, thanks to the Marie-Curie 'MEET' project co-ordination team: Prof. Giuseppe Gasparre and Serena Paterlini, University of Bologna, Italy.

Table of contents

List of figures

List of tables

List of abbreviations

αBGTX	Alpha bungarotoxin
β-act	beta actin
AA	amino acid
AChRs	Acetylcholine receptors
Air2/ ZCCHC7	Zinc Finger CCHC-Type Containing 7
AMPD2	Adenosine Monophosphate Deaminase 2
AP	Antero-posterior
ARE	AU-rich element
ARS2	Arsenite-Resistance Protein 2
ATOH1	Atonal BHLH Transcription Factor 1
ATP	adenosine 5'-triphosphate
atxn1	ataxin 1
AUG	start codon
BLAST	Basic Local Alignment Search Tool
BMI1	BMI1 Polycomb Ring Finger Oncogene
BMP2B	Bone Morphogenetic Protein 2B
BS	Bayes Factor
BSA	Bovine Serum Albumine
$Ca2^{+}$	Calcium Ion
CaCl	Calcium Chloride
CACNA1G	Calcium Voltage-Gated Channel Subunit Alpha1 G
Ca(NO3)2	Calcium Nitrate
CaP	Caudal Primary Motor Neuron
Cas9	CRISPR associated protein 9
CBC	Cap Binding Complex
Cce	corpus cerebelli
cDNA	complementary DNA
CHD	Chordin
CHMP1A	Charged Multivesicular Body Protein 1A
CLP1	Cleavage And Polyadenylation Factor I Subunit 1
CNS	Central Nervous System
COL6A3	Collagen Type VI Alpha 3
CRISPR	Clustered Regularly Interspaced Short Palindromic Repeats
Csl4/EXOSC1	Exosome Component 1
CTP	cytidine 5'-triphosphate
CTRL	control
DARS	Aspartyl-TRNA Synthetase
DCN	Deep Cerebellar Nuclei
dH_2O	distilled water
DIS3L	DIS3 Like Exosome 3'-5' Exoribonuclease
DMEM	Dulbecco's modified eagle medium
DNA	Deoxyribonucleic acid
Dpf	days post fecundation
D.r.	Danio rerio
EARS2	Glutamyl-TRNA Synthetase 2, Mitochondrial
EDTA	Ethylenediaminetetraacetic acid
ef1α	Elongation factor 1-alpha
EG	eminentia granularis

ENU (mutagenesis)	N-ethyl-N-nitrosourea
ESF	Exosome Specific Factor
Ex	exon
FGF8	Fibroblasts Growth factor 8
GABA	gamma-Aminobutyric acid
GARS	Glycyl-TRNA Synthetase
GCL	Granule Cell Layer
gDNA	genomic DNA
gRNA	guide RNA
GTP	guanosine 5'-triphosphate
HARS	Histidyl-TRNA Synthetase
Hpf	Hours post fecundation
HRP	Horseradish Peroxidase
H.s.	Homo sapiens
IARS	Isoleucyl-TRNA Synthetase
In	intron
INK4A/cdkn2a	Cyclin-Dependent Kinase Inhibitor 2A
KARS	Lysyl-TRNA Synthetase
KCl	Potassium Chloride
LCa	lobus caudalis cerebelli
lncRNA	long-non-coding RNA
LAMP2	Lysosomal Associated Membrane Protein 2
M	Molar
MBP	Myelin Basic Protein
MiP	Middle Primary Motor Neuron
miRNA	microRNA
MgSO4	Magnesium sulphate
Mhb	midbrain-hindbrain boundary
MISO	mixture of isoforms
ML	Molecular Layer
MO	morpholino
mM	Millimolar
MN	Motor Neuron
MOBP	Myelin-Associated Oligodendrocyte Basic Protein
MRI	Magnetic Resonance Imaging
mRNA	messenger RNA
MTR4/DOB1/SKIV2L2	Ski2 Like RNA Helicase 2
Mtr3/EXOSC6	Exosome Component 6
NaCl	Sodium chloride
NaOH	Sodium hydroxide
NCAM	Neural Cell Adhesion Molecule 1
ncRNA	non-coding RNA
NEXT	Nuclear Exosome Targeting complex
NGD	no-go decay
Nkx6	NK6 homeobox
NMD	non-sense mediated decay
NSD	non-stop decay
Olig2	Oligodendrocyte Lineage Transcription Factor 2
OMIM	Online Mendelian Inheritance in Man
Otx2	Orthodenticle Homeobox 2
P0	Myelin Protein Zero

P53	Tumor Protein P53
PAM	Proto-spacer adjacent motif
Pax6	Paired Box 6
PBS	Phosphate-buffered saline
PBST	PBS + Tween20
PCs	Purkinje cells
PCH	pontocerebellar hypoplasia
PCLO	Piccolo Presynaptic Cytomatrix Protein
PCR	Polymerase Chain reaction
PFA	Paraformaldehyde
Plc	Polycomb protein
PLP	proteolipid protein
PNS	Peripheral Nervous System
Ppm	parts per million
PROMPT	PROMoter uPstream Transcript
PSI	Percentage Spliced In
Ptf1a	Pancreas Specific Transcription Factor, 1a
PVALB7	Parvalbumin 7
PVDF	polyvinylidene difluoride
QARS	Glutaminyl-TRNA Synthetase
qRT-PCR	quantitative Reverse Transcriptase PCR
R	Arginine
RA	Retinoic Acid
RARS	Arginyl-TRNA Synthetase
RARS2	mitochondrial argynil-tRNA synthetase 2
RBM7	RNA Binding Motif Protein 7
RIN	RNA integrity number
RNA	Ribonucleic acid
RNA-seq	RNA sequencing
RoP	Rostral Primary Motor Neuron
RPL17	Ribosomal Protein L17
RRM	RNA Recognition Motif
Rrp4/EXOSC2	Exosome Component 2
Rrp6/EXOSC10	Exosome Component 10
Rrp40/EXOSC3	Exosome Component 3
Rrp41/EXOSC4	Exosome Component 4
Rrp42/EXOSC7	Exosome Component 7
Rrp43/EXOSC8	Exosome Component 8
Rrp44/DIS3/EXOSC11	Exosome Component 11
Rrp45/EXOSC9	Exosome Component 9
Rrp46/EXOSC5	Exosome Component 5
rRNA	ribosomal RNA
RT	Room Temperature
RT-PCR	Reverse Transcriptase PCR
SD	syndromic diarrhea
sema3a1	sempahorin 3a1
sgRNA	single guide RNA
SHH	Sonic Hedgehog
siRNA	small interference RNA
SKI	SuperKiller complex
Ski2/SKI2W/SKIV2L	Ski2 Like RNA Helicase
Ski3/TTC37	Tetratricopeptide Repeat Domain 37

SMA	Spinal Muscular Atrophy
SMN1	Survival Of Motor Neuron 1
SNX15	Sorting Nexin 15
SNV	single nucleotide variant
SPL	splicing
SV2	Synaptic Vesicle Protein 2
TBST	Tris-Buffered Saline Tween20
Tg(Isl1:GFP)	Transgenic(islet1:Green Fluorescent Protein)
THES	thrico-hepato-enteric syndrome
TMEM116	Transmembrane Protein 116
TOE1	Target Of EGR1, Member 1
TRAMP	Trf4/5-Air1/2-Mtr4 polyadenylation complex
Trf4/5/PAPD5	PAP Associated Domain Containing 5
Tris-HCl	Tris Hydrochloride
tRNA	transfer RNA
TSNE54	TRNA Splicing Endonuclease Subunit 54
TUNEL	Terminal deoxynucleotidyl transferase dUTP nick end labelling
TUBB	Tubulin beta
UTP	uridine 5'-triphosphate
UTR	Untranslated Region
Va	valvula cerebelli
VaP	Variable Primary Motor Neuron
VDCC	Voltage-dependent calcium channels
Vglut1	Vesicular glutamate transporter 1
VRK1	Vaccinia Related Kinase 1
WDR74	WD Repeat Domain 74
WES	Whole Exome Sequencing
WNT	Wingless-Type
WT	Wild Type
YARS	Tyrosyl-TRNA Synthetase
ZCCHC8	Zinc Finger CCHC-Type Containing 8
ZC3H18/ NHN1	Zinc Finger CCCH-Type Containing 18
ZFNS	Zinc Finger Nucleases

Chapter 1: Introduction

1.1 RNA processing and disease

Transcriptional and post-transcriptional regulation is of fundamental importance for correct cellular functions (Lee and Young, 2013) (Kiebler et al., 2013).

Fine tuning of coding and non-coding RNA (ncRNA) levels is very important: either too much or too little transcript within the cell can give rise to an unbalance of protein synthesis and then defects of cellular processes (Moraes, 2010). Such a complex task is performed through precise integration of transcription and degradation steps of cellular RNAs, in order to achieve correct protein expression levels (Rogowska, 2005) (Dori-Bachash et al., 2011).

RNA processing including splicing (Seng et al., 2015), capping and poly-adenylation is also very important for correct cellular functions (Poulos et al., 2011). Furthermore, regulatory elements such as ncRNAs also need to be correctly transcribed, processed and degraded. Although they do not get translated into proteins, they are known to play key roles in epigenetic, transcriptional and post-transcriptional regulation (Schmitz et al., 2016). Said that, our knowledge about ncRNAs is still very limited (Chi, 2016).

All this complexity comes at a price: it is not surprising that a faulty machinery within the system can give rise to disease. A number of conditions have been linked to impaired RNA processing: cancer, neuromuscular diseases, neurological disorders (Cooper et al., 2009).

Among the large number of defects due to impaired RNA metabolism, a novel group of neurological disorders caused by defective functionality of the exosome complex has begun to be increasingly important in the field.

Our lab started investigating this subset of neurological disorders soon after the first mutation on an exosome complex sub-unit (*EXOSC3*) was discovered in 2012 by Wan and colleagues (Wan et al., 2012).

We initially focused on some patients of Roma ethnic background with complex overlapping symptoms of pontocerebellar hypoplasia type 1 (PCH1), spinal muscular atrophy (SMA), central nervous system demyelination and mitochondrial disease (Boczonadi et al., 2014) (Pyle et al., 2015) and identified a novel disease gene:

EXOSC8. Subsequently, we identified and investigated the role of a new mutation in a sub-unit of a co-factor of the exosome complex (RBM7; Giunta et al., 2016) in a Palestinian patient with motor neuron disease. Results of some of the experiments I performed for the investigation of functions of *EXOSC8* and *RBM7* are explained in this thesis.

Furthermore, here I show some data (not yet published) about the CRISPR/Cas9 driven gene inactivation of *RBM7* homolog in zebrafish (*D. rerio*) and identification of new patients with mutation on *EXOSC3* and *TSEN54*, which also causes PCH. It is worth to say that, as a complementary model, Dr. Juliane Mueller (Newcastle University) has created in parallel a mutant line of *EXOSC8* in the same organism, however, these data are not shown here.

1.2 The exosome complex

The exosome complex is the main RNA metabolism machinery within the cell, responsible for many functions regarding RNA degradation and quality control (Houseley et al., 2006). The structure and functions of the exosome complex are highly conserved through all forms of life.

The exosome is a large multi-subunit complex formed, in all eukaryotic and archaea cells, by 9 proteins (called Exo-9). Six of them (Rrp41/EXOSC4, Rrp42/EXOSC7, Rrp43/EXOSC8, Rrp45/EXOSC9, Rrp46/EXOSC5 and Mtr3/EXOSC6) form the barrel-like structure, where the RNA filament passes through (in a 3'-5' direction) in order to be degraded. Three proteins (Rrp40/EXOSC3, Csl4/EXOSC1 and Rrp4/EXOSC2) form the "cap" of the complex, with RNA binding properties (Oddone et al., 2007) (Januszyk and Lima, 2010).

This barrel-like structure seems to be catalytically active in prokaryotes through three active sites situated in the internal side of the channel (Makino et al., 2013). However, in eukaryotes the Exo-9 structure seems to be enzymatically inactive due to some amino acid changes. The functionality of Exo-9 in the cytoplasm in eukaryotes resides in an additional subunit, Rrp44/DIS3/EXOSC11, a hydrolytic exonuclease belonging to the RNase R family that, when bound to Exo-9, forms the functional structure Exo-10 (Januszyk and Lima, 2010) (Oddone et al., 2007).

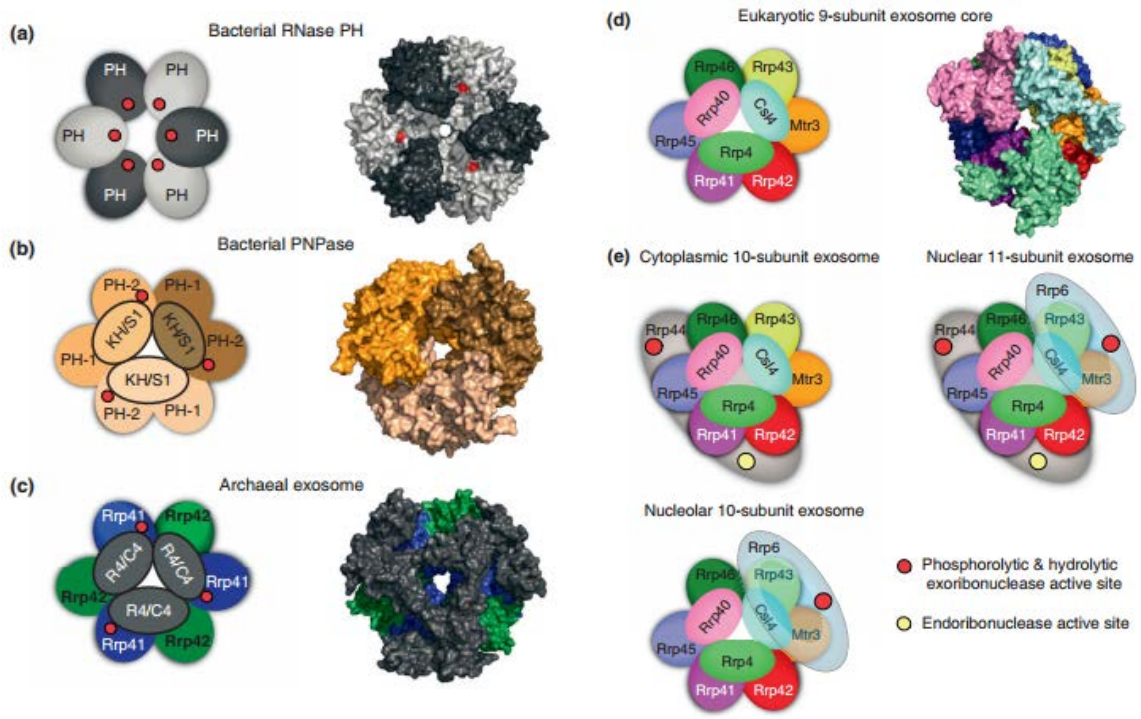

Figure 1.1 **Structures of Prokaryotic and Eukaryotic exosome complex.** The Eukaryotic exosome complex has different cytoplasmic, nuclear and nucleolar forms. Modified from Januszyk and Lima, 2014.

The cytosol active Exo-10 requires an additional sub-unit to become catalytically active in the nucleus: Rrp6/EXOSC10, forming an 11 subunit nuclear exosome called Exo-11 (Januszyk and Lima, 2014). A paralog of DIS3 is indispensable for exonuclease activity (DIS3L1) and is only present in the cytoplasmic form (Sudo et al., 2016). The exosome complex also has endonucleolytic activities (Januszyk and Lima, 2014).

The exosome complex is directly involved in metabolism of almost all types of RNA within the cell.

As mentioned earlier, the exosome carries out a variety of functions related to gene expression regulation through mRNA decay (Houseley et al., 2006): other than performing 3'-5' turnover of normal mRNAs (Kilchert et al., 2016), the exosome complex in human cells is also responsible for degradation of AU-rich sequence elements (AREs). AREs can be found in 3' UTR of mRNAs that encode for proteins for which only a transient expression is required (Chen et al., 2001). AREs can be loosely categorized as sequences with the presence of various copies of an AUUUA pentanucleotide and a high content of uridylate and sometimes also adenylate residues (Chen and Shyu, 1994). Also called AU instability elements, AREs have been found to interact directly with the exosome complex (Mukherjee et al., 2002) suggesting this complex has a direct involvement in ARE-containing mRNA turnover.

The exosome complex is also responsible for processing non-functional RNAs; accumulation of faulty RNAs can be harmful to the cell as they can compete for the good ones for cofactors (Kilchert et al., 2016). The exosome degrades RNAs with a premature stop codon through the *non-sense mediated decay* pathway (NMD; Lejeune et al., 2003); the *non-stop decay* (NSD) pathway degrades mRNAs that lack a termination codon (Frischmeyer et al., 2002) and the *no-go decay* (NGD) pathway targets mRNAs on which translation has stopped (Doma and Parker, 2006).

Although rare, failure in performing those decay pathways can give rise to disease in humans such as PEHO (Nahorski et al., 2016), MNGIE with neuropathy (Torres-Torronteras et al., 2011).

Furthermore, the exosome complex is involved in degradation of non-coding RNAs such as tRNAs (Lubas et al., 2015), long-non coding RNAs (lncRNAs; Chlebowski et al., 2013), PROMoter uPstream Transcripts (PROMPTs; Norbury, 2011), which are transcribed antisense of most protein coding genes and which functions are not completely understood, but thought to act as transcriptional regulators (Preker et al., 2008) (Lloret-Llinares et al., 2016). Finally, the exosome complex is secondarily involved in splicing regulation, being primarily responsible of metabolism of splicing factors (Zhang et al., 2015).

The exosome complex itself is highly unspecific (Kilchert et al., 2016). One open question is how the exosome can be loaded on so many different substrates, performing these tasks so efficiently and specifically (Kilchert et al., 2016).

High substrate specificity of the exosome complex is guaranteed by the interaction with exosome-specificity factors (ESFs) which lead to specific processing or degradation pathways. Indeed, experimental evidence shows that different classes of RNAs are recognized by different co-factors which subsequently determines its fate (Schmidt and Butler, 2013) (Kilchert et al., 2016).

1.2.1 Exosome-Specificity Factors

To date, four complexes have been identified as cofactors of the exosome complex, responsible for binding and helping with the degradation/processing of specific subtypes of RNAs.

1.2.2 The TRAMP complex

The Trf4/5-Air1/2-Mtr4 polyadenylation (TRAMP) complex is involved in two catalytic activities: the TRf4-Air2 is a poly(A)polymerase sub-complex, Mtr4 carries out

helicase activities (Falk et al., 2014) in yeast. The TRAMP complex predominantly acts promoting exosomal decay by the oligoadenylation and unwinding of RNA targets (Lubas et al., 2015). A part from Mtr4, the other proteins have little sequence similarity in human. In mammalian cells, a homolog of the TRAMP complex has been proposed, formed by PAPD5 (Trf4/5 homolog), ZCCHC7 (Air1/2 homolog) and MTR4/DOB1/SKIV2L2. EXOSC10/Rrp6 seems to play an important role in TRAMP stable assembly (Sudo et al., 2016). In yeast, the TRAMP complex targets aberrant coding and non-coding RNAs. Another MTR4 related protein is WDR74 (Hiraishi et al., 2015). MTR4 sub-unit participates in another stable co-factor of the exosome complex, the nuclear exosome-targeting (NEXT) complex (Norbury, 2011) (Lubas et al., 2011).

1.2.3 The NEXT complex

The NEXT complex - which is not found in yeast - consists of a putative RNA binding protein (RBM7) and other two proteins: ZCCHC8 and MTR4. Opposite to ZCCHC7 which is only localized in the nucleolus, ZCCHC8 and RBM7 are localized in the nucleus. Therefore it seems that different RNA substrates in different nuclear localizations are targeted by the NEXT complex or the TRAMP complex (Sudo et al., 2016). The NEXT complex facilitates the exosome-driven degradation of RNA polymerase II transcripts including non-coding RNAs such as the PROMPTs (Lubas et al., 2011) and other ncRNAs (Hrossova et al., 2015) (Sofos et al., 2016). RBM7 sub-unit binds with high affinity to U-rich stretches in RNA (Hrossova et al., 2015) suggesting it may also be involved in ARE genes degradation. RBM7 was also previously reported to be involved in splicing (Guo et al., 2003).

1.2.4 The SKI complex

The SKI complex as it is found in yeast is a heterotetramer that channels RNAs toward the exosome complex, activating the NMD, NGD and NSD (Synowsky and Heck, 2007) (Halbach et al., 2013) (Chlebowski et al., 2013).

It consists of a Ski2 sub-unit, a Ski3 sub-unit and 2 Ski8 sub-units. The human homolog of the SKI complex, hSKI, has a hSKI8 sub-unit (Zhu et al., 2005), a SKI2W/SKIV2L (Ski2 homolog) sub-unit (Dangel et al., 1995) and a TTC37 (Ski3 homolog) sub-unit.

1.2.5 The CBC complex

A fourth complex, the human cap-binding complex (CBC) is also functionally connected to the exosome (Andersen et al., 2013). It associates with arsenic resistance protein 2 (ARS2) forming the CBC-ARS2 complex and then connects (together with ZC3H18/ NHN1 protein) to the NEXT complex, therefore forming the CBC-NEXT complex.

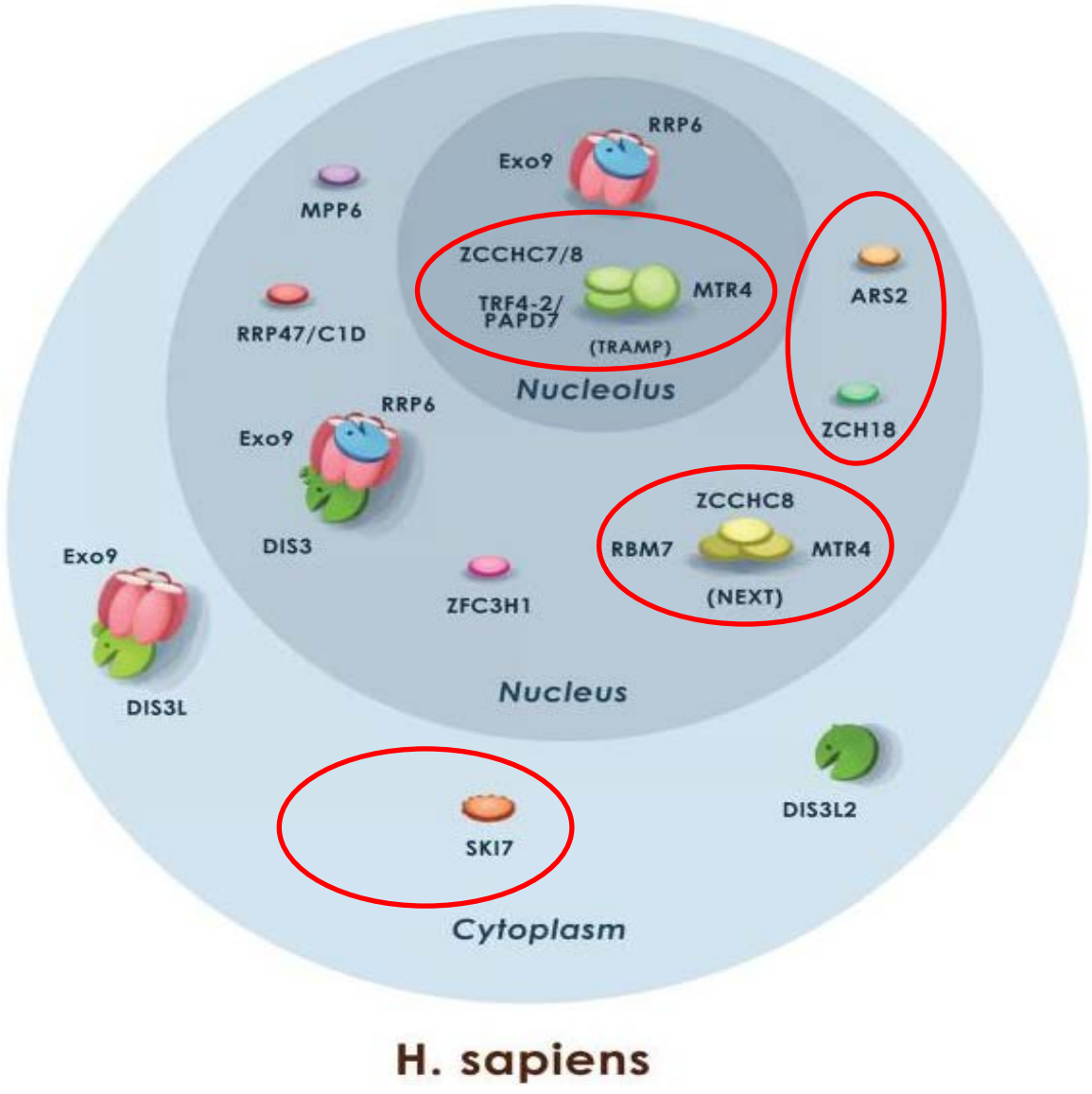

Figure 1.2 **Cellular localization of the Exosome Specific Factors.** Each factor seems to target specific subtypes of RNA in different cellular compartments. Modified from Januszyk and Lima, 2014. TRAMP complex's functions are mainly oligoadenylation and unwinding of RNAs; NEXT binds and facilitates exosome degradation of non-coding RNAs and SKI complex is involved in NGD, NSD and NMD pathways.

1.3 The exosome complex in health and disease

Impaired functionality of any of the exosome complex sub-units or Exosome-Specificity Factors can give rise to a wide variety of diseases. Mutations on *EXOSC3*, *EXOSC8*, *EXOSC2* cause a predominant neurological phenotype with PCH (Wan et al., 2012) (Boczonadi et al., 2014) (Di Donato et al., 2016).

1.3.1 Symptoms caused by EXOSC3 mutations

The first pathogenic mutations on an exosome complex sub-unit (*EXOSC3*) were identified by Wan and colleagues in 2012. Patients presented with severe pontocerebellar hypoplasia and spinal motor neuron degeneration. Six different pathogenic mutations (one of them intronic) were described in this study (Fig. 1.3): missense, deletions and splice mutations.

EXOSC3/Rrp40 is part of the exosome “cap”, and is an RNA binding subunit of the exosome complex (Luz et al., 2007). Probably the binding activity is performed through interaction with other sub-units (Oddone et al., 2007). It has been hypothesized that EXOSC3/Rrp40 might also have a hydrolytic activity (Luz et al., 2007).

In order to understand functions of EXOSC3 in neurodevelopment, Wan and colleagues performed functional studies in zebrafish knocking down functions of *exosc3*, the zebrafish homolog of the human gene.

Downregulation of *exosc3* in zebrafish with morpholino (MO) showed reduction of levels of *pvalb7 and atoh1a* (respectively a Purkinje cells (PCs) marker and a dorsal hindbrain progenitor-specific marker) transcripts tested by *in situ* hybridization.

Morpholinos act reducing gene expression binding to the mRNA and resulting in a non-functional protein, therefore co-injection of a functional mRNA should ideally rescue the phenotype caused by the impaired endogenous mRNA.

Co-injection of human and zebrafish WT mRNA and *exosc3*-MO in zebrafish largely rescued the phenotype, which was not rescued by co-injection of either human or zebrafish mutant mRNA and morpholino.

Subsequently other studies identified more mutations in *EXOSC3*, which can cause a broad spectrum of PCH1 symptoms (Tab. 1), and showed that *EXOSC3* mutations may account for about half of the total cases of PCH1 worldwide (Eggens et al., 2014) (Eggens, 2016).

	1	2	3	4	5-I	5-II	6	7-I
Nucleotide change	c.92G > C	c.92G > C	c.92G > C	c.92G > C	c.92G > C	c.92G > C	c.395A > C	c.395A > C
Amino acid change	p.G31A	p.G31A	p.G31A	p.G31A	p.G31A	p.G31A	p.D132A	p.D132A
Ethnic background	Roma	Roma	Roma	Roma	Roma	Roma	Caucasian	Caucasian
Pregnancy duration	39w, CS	at term	38w	37w	37w	40w	39w	u
Hypotonia at birth	+	+	+	+	+	+	+	+
OFC (SD)[a] (age)	−4 (1.5 m)	−2.5 (birth)	0 (birth)	+3 (4.5mo)	0 (4mo)	+2.5 (4mo)	+3 (4.5mo)	−0.5 (11y)
Nystagmus	-	-	u	+	-	-	+	+
Optic atrophy	Pale optic disc	-	u	-	-	-	-	u
Seizures	-	-	-	-	-	-	-	+
Dyskinesia/dystonia	-	-	-	-	-	-	+ 1 episode, admitted with high temp and pneunomia	+
Tendon reflexes	absent	absent	absent	absent	absent	absent	brisk	brisk
Response on visual/ auditory stimuli	-	-	u	-	-	-	++	+
Age at death (cause)	4.5mo (cardiac arrest)	7mo (pneumonia, sepsis)	5d (respiratory failure)	5mo (u)	6mo (viral infection)	4mo (u)	7y (respiratory failure)	12y (GI failure)
Lower motor neuron signs	Neurogenic muscle atrophy	Neurogenic muscle atrophy	u, diagnosed following patient 5-II (cousin)	Tongue fasciculations, denervation (EMG), neurogenic muscle atrophy	u, diagnosed following patient 5-II (sister)	Muscle denervation (EMG)	u	u, diagnosed following patient 7-II (brother)

	7-II	8	9	10	11	12
Nucleotide change	c.395A > C	c.395A > C (he) g.del37781240-37787410 (he)	c.395A > C (he) c.743_749delinsA (he)	c.325-4_329dupGTAGTATGT (he) c.334G > A (he) c.395A > C (he)	c.325 T > A (he) c.395A > C (he)	c.404G > A
Amino acid change	p.D132A	p.D132A; deletion exon 1-3	p.D132A; p.L248*	p.P111*; p.V112I; p.D132A	p.Y109N; p.D132A	p.G135E
Ethnic background	Caucasian	Caucasian	Caucasian	Caucasian	Caucasian	Pakistan
Pregnancy duration	35w	39w	38w	42w	41w	40w
Hypotonia at birth	+	+	+	±	+	+
OFC (SD)[a] (age)	−2 (6.5y)	−1 (birth)	u	−0.5 (10w)	−1.5 (6.5mo)	−1 (8w)
Nystagmus	+	-	u	-	-	+
Optic atrophy	u	+	u	-	Small optic discs	Pale optic disc
Seizures	-	+ West syndrome at 5 mo	-	-	-	-
Dyskinesia/dystonia	+	-	-	-	-	-
Tendon reflexes	reduced	reduced	absent	reduced	absent	absent
Response on visual/ auditory stimuli	+	±	-	±	-	-
Age at death (cause)	10y (pseudomonas infection)	6mo (respiratory infection)	14w (respiratory failure)	6mo (respiratory infection)	8.5mo (respiratory failure)	8w (respiratory failure)
Lower motor neuron signs	Denervation (EMG)	Neurogenic muscle atrophy	Denervation (EMG)	Denervation (EMG), reduced motor nerve conduction velocity	Tongue fasciculations, neurogenic muscle atrophy	Denervation, neurogenic muscle atrophy

he = heterozygous; d = days; w = weeks; mo = months; y = years; u = unknown; ++ = markedly present; + = present; ± = mildly present; - = not present.
[a]SD for head circumference according to WHO standards (http://www.who.int/childgrowth/standards/hc_for_age/en/index.html).

Table 1. **Clinical data of 14 patients with EXOSC3 mutation (From Eggens et al., 2014).**

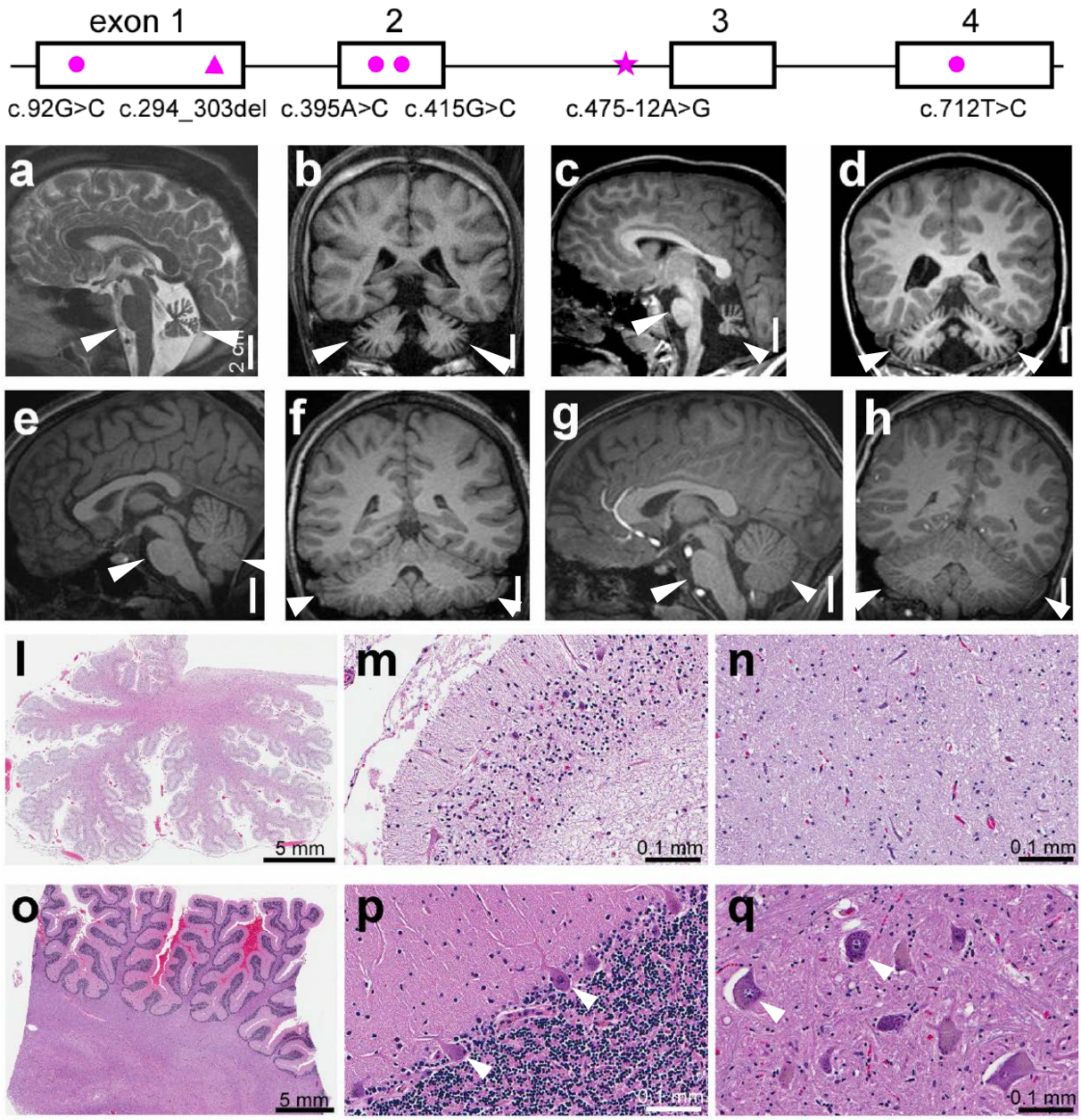

Figure 1.3. **Schematic representation of the *EXOSC3* pathogenic mutations and anatomical features of the patients.** Mutations identified in *EXOSC3* are missense (circle), deletions (triangle) or splice site mutations (star). Brain MRI of the patient (a, b) show a clear reduction in cerebellum size compared to an age matched control (e, f). For a second patient also reduction of cerebellum (c, d) is clear compared to an age matching control (g, h). Brain autopsy of the patient who died at age 18 shows cerebellar atrophy (l) compared to control (o). At higher magnification patient's brain show dysmorphic Purkinje cells and loss of granule cells (m) compared to control (p). Loss of motor neuorns in the anterior horn of the spinal cord is also present in the patient (n) compared to control (q). Images modified from Wan et al., 2012.

1.3.2 Symptoms caused by EXOSC8 mutations

Our group subsequently identified 2 pathogenic missense mutations (Fig. 1.4) on *EXOSC8* – which is one of the six subunits forming the barrel-like structure of the exosome complex - in 22 patients from three different families of Roma and Palestinian ethnic origin with cerebellar and corpus callosum hypoplasia (Fig. 1.4), abnormal myelination of the central nervous system (Fig. 1.4), spinal motor neuron disease and mitochondrial disease (Table 2; Boczonadi et al., 2014). Mutations were c.5C>T, p.Ala2Val in exon 1 and c.815G>C, p.Ser272Thr in exon 11. Extended functional studies in human fibroblasts, myoblasts and oligodendroglia cells as well as in zebrafish confirmed the pathogenicity of the mutations.

Patients fibroblasts and myoblasts were used to test gene expression of ARE genes such as *MBP, MOBP, SMN1* which levels resulted to be higher than in controls cells. Non ARE genes levels were not affected. In human oligodendroglia cells *EXOSC8* was downregulated by siRNA, resulting in a similar pattern of gene expression. Downregulation of *exosc8* in zebrafish also resulted in upregulation of some ARE genes. Particularly interesting is the overexpression of MBP, given its known key role in the myelination process and correspondent myelination issues in the patients. Myelination is a complex process that needs to be tightly regulated, overexpression of a fundamental protein such as MBP may indeed have toxic effects.

Further zebrafish experiments which will be better explained in results chapter 2 seem to indicate a direct involvement of *mbp* overexpression in myelination issues.

Patient	Onset/ Death	Clinical presentation							
		Neurological signs	Psychomo-tor ret.	Visual loss	Hearing loss	Respiratory problems	Other	Brain MRI	Other tests
P1 - V:20	2m/11m†	Severe muscle weakness and wasting, spastic tetraparesis	+	+	+	+	Facial dysmorphy, scoliosis, ing. hernia	No data	
P1 - V:10	2m/9m†	Severe muscle weakness and wasting, spastic tetraparesis	+	+	+	+	Tremor, irritability	Cortical atrophy, vermis hypoplasia, thin corpus callosum (2.5m)	Muscle biopsy: RC complex I+IV↓
P1 - V:9	4m/13m†	Muscle weakness, wasting, spasticity, facial dysmorphy	+	+	+	+	Inguinal hernia, axial hypotonia, no voice	Vermis hypoplasia (5m)	lactate↑
P1 - V:29	1m/14m†	Severe muscle weakness and wasting, spastic tetraparesis, contractures,	+	+	+	+	Tremor, axial hypotonia, brachy-cephalia, facial dysmorphy	Diffuse cortical and cerebellar atrophy (L>R), thin corpus callosum (11m)	Pathological BAEP
P1 - V:4	1.5m/18 m†	Severe tetraspasticity, muscle wasting, contractures, no spontaneous movements	+	+	+	+	Polyhydramnion dystrophy, tremor axial hypotonia	Thin corpus callosum, immature myelination (2m)	Metabolic acidosis, pathological BAEP, VEP
P1 - VI:3	12d/8m†	Severe spastic tetraparesis, reflexes↑	+	+	+	+	Tremor, feeding difficulties	No data	
P1 - V:2	2m/19m†	Severe spastic tetraparesis	+	+	+	+	Feeding difficulties, tremor, irritability	Some cortical atrophy (6m)	
P2 - II:7	1.5m/13 m†	Severe spastic tetraparesis, muscle wasting	+	+	+	+	Inguinal hernia, feeding difficulties, irritability, apnoe	No data	Transient ALT↑, GGT↑
P2 - II:10	2m/alive 9m	Severe spastic tetraparesis, muscle wasting	+	+	+	+	Feeding difficulties, irritability, apnoe	Thin corpus callosum, immature myelination (5m)	
P3 – II:1	6m/28m†	Severe muscle weakness and wasting, ankle contractures	+	-	-	+	Feeding difficulties	Vermis hypoplasia, mega cisterna magna	EMG: motor neuron lesion
P3 – II:3	4m/alive 5y	Severe muscle weakness, tongue fasciculations	+	-	-	+	Feeding difficulties	Vermis hypoplasia, mega cisterna magna	EMG: motor neuron lesion

Table 2. Clinical presentation of 9 patients from 2 pedigrees. Abbreviations: P: pedigree; m: month; ret.: retardation; BAEP: brainstem auditory evoked potentials, VEP: visual evoked potentials, ALT: alanine transaminase, GGT: gamma-glutamyl transferase. Table from Boczonadi et al. 2014.

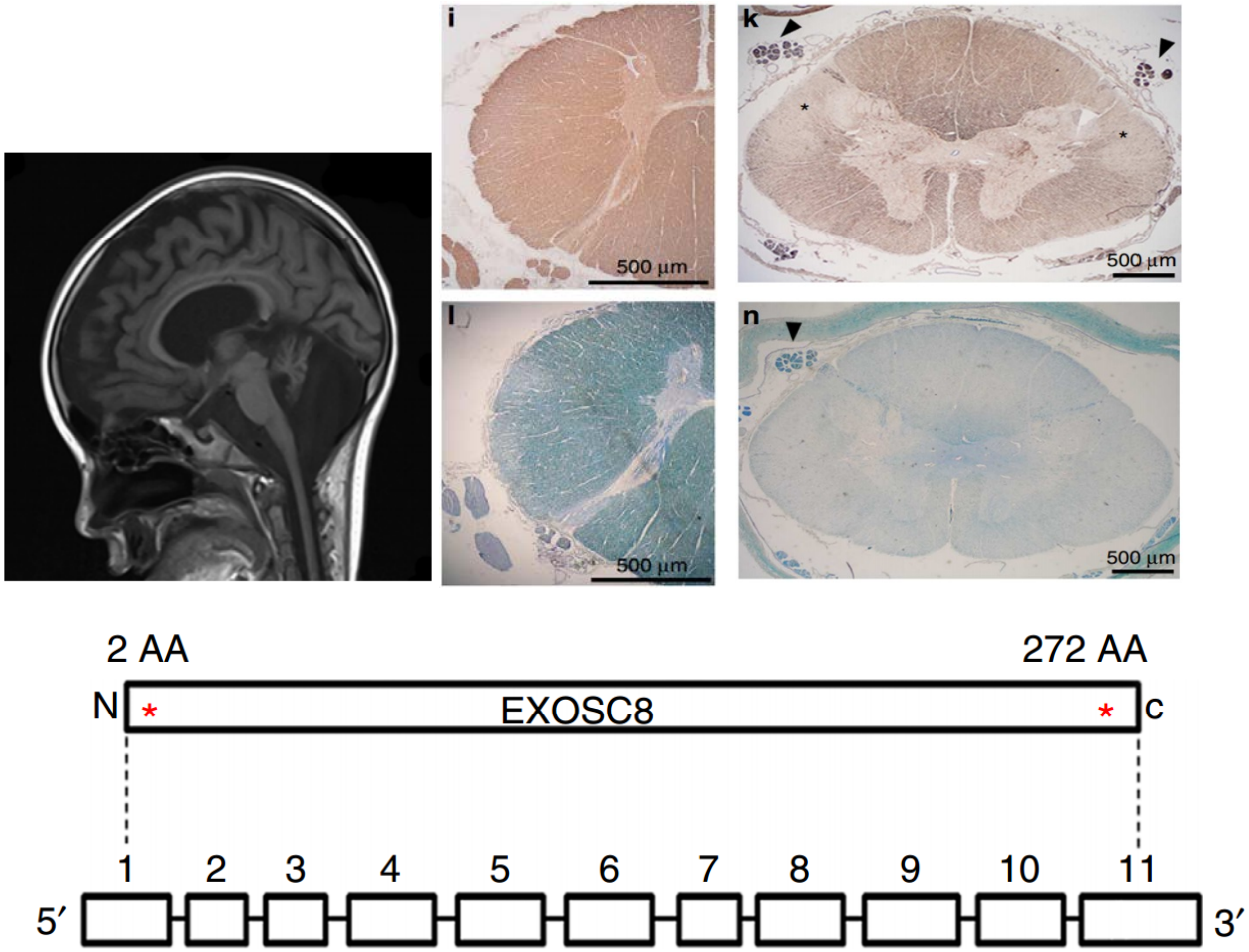

Figure 1.4. **MRI scan, autopsy staining of patients with EXOSC8 mutation and position of the mutations within the gene.** The MRI scan highlights reduced cerebellar volume and thin corpus callosum in the Palestinian patient (top). Spinal cord normal control (i, l) and patient V:20 of the Roma family. In EXOSC8 deficiency, myelin basic protein is present–apart from the longitudinal descending fibre tracts **(k, *).** Myelin is well preserved within the peripheral nerve roots (n, arrowhead) while indicates severe loss of myelin within the spinal cord (n). Images modified from Boczonadi et al., 2014.

1.3.3 Symptoms caused by EXOSC2 mutations

Di Donato and colleagues (Di Donato et al., 2016) published a study where they reported three patients from two unrelated, non-consanguineous German families with a novel syndrome with retinitis pigmentosa, progressive hearing loss, premature ageing, intellectual disability and facial dysmorphism caused by mutations in *EXOSC2*. *EXOSC2* is located in the 'cap' of the exosome complex, similarly to *EXOSC3*. They identified a homozygous missense mutation and a compound heterozygous mutation Brain MRI showed also hypomyelination and mild cerebellar hypoplasia. Unfortunately, no functional studies on cells or animal models were performed. Nevertheless, this study extends the knowledge of clinical symptoms caused by impaired RNA metabolism due to exosome complex deficiencies.

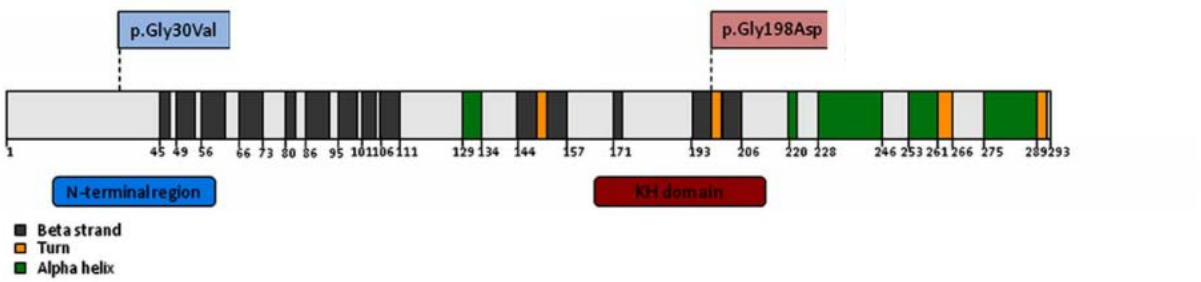

Figure1.5**. Domain organisation of the EXOSC2 protein (RRP4) with the localisation of the discovered mutations is shown (from Di Donato et al., 2016).**

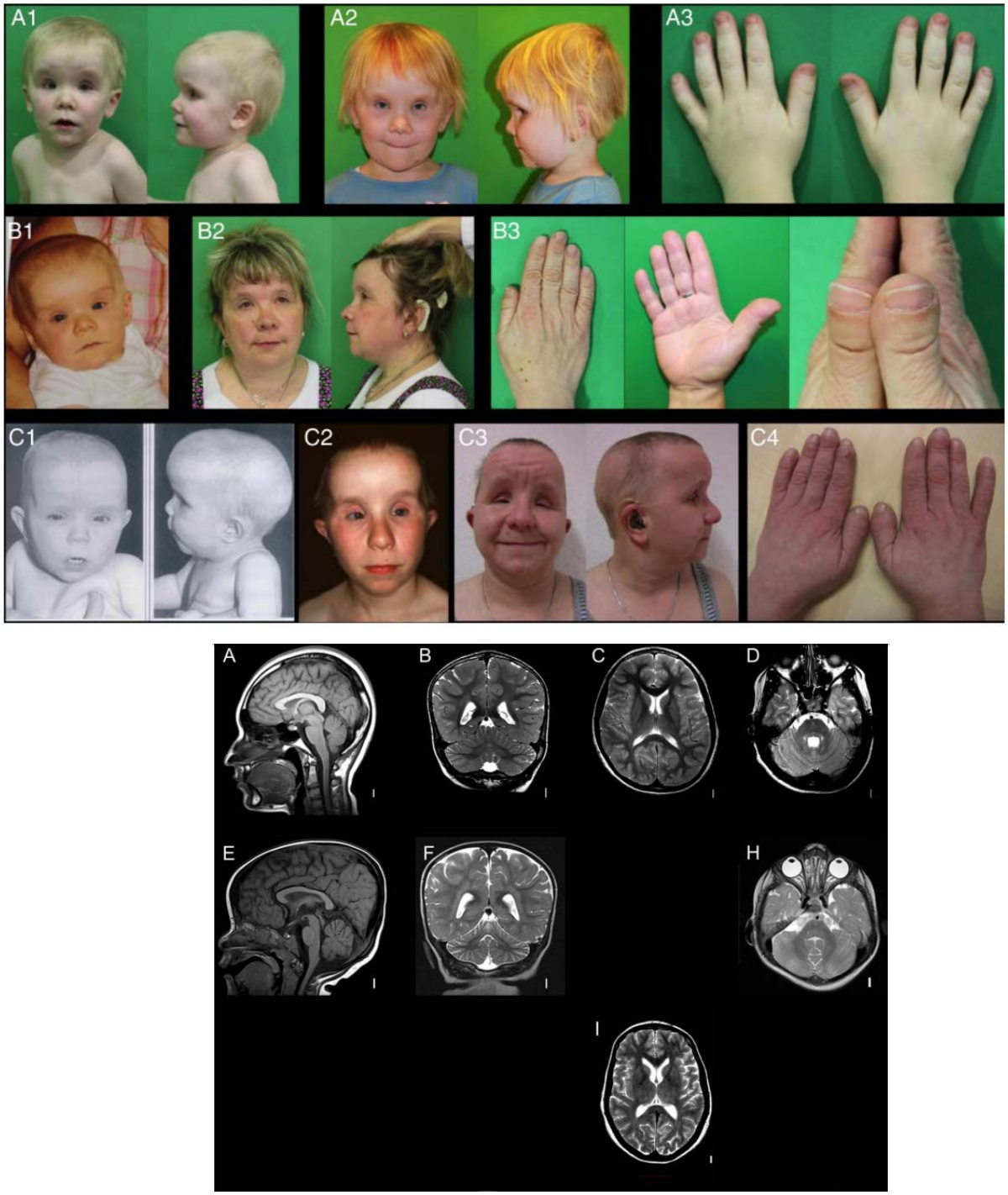

Figure1.6**. Morphological features of patients with mutations on EXOSC2 (top) and brain MRIs (bottom; from Di Donato et al., 2016).** Patient 1 Top figure A1, A3 (3 y/o) and A2 (6y/o). Brain MRI (A-C) shows mildly enlarged extra-axial spaces and borderline cerebellar hypoplasia. Patient 2, who is patient's 1 paternal aunt, is in top figure B1 (1 y/o) and B2,B3 (41 y/o). Her brain MRI at age 39 shows mild cortical and cerebellar atrophy with unremarkable white matter (H,I). Patient 3 at age of 1 year (top figure C1), 13 years (C2) and 28 years (C3, C4). His brain MRI was abnormal with diffuse dysmyelination, bilateral calcifications in the basal ganglia and thalamus and mild cortical and cerebellar atrophy (D-F).

	Patient 1	Patient 2	Patient 3
EXOSC2 mutation	NM_014285.5:c.89G>T (p.[Gly30Val]) homozygous	NM_014285.5:c.89G>T (p.[Gly30Val]) homozygous	NM_014285.5:c.[89G>T];[593G>A] (p.[Gly30Val];[Gly198Asp])
Sex	female	female	male
Age at the last follow-up	6 years 4 months	44 years	28 years
Mother's age at conception	26 years	19 years	25 years
Father's age at conception	28 years	24 years	30 years
Pregnancy complications	none	none	none
Neonatal History			
Gestational age at birth	38 GW	36 GW	37 GW
Birth length	46 cm (- 1.9 SD)	45 cm (- 1.3 SD)	48 cm (- 0.9 SD)
Birth weight	2510 g (-1.6 SD)	2400 g (- 0.8 SD)	2120 g (- 2.2 SD)
OFC at birth	35 cm (0.5 SD)	not documented	not documented [37 cm at the age of 2 months (- 1.7 SD)]
Complications at birth	no	no	no
Feeding difficulties	no	no	no
Respiratory failure	no	no	no
Growth measurements			
Age of the examination	2 years 11 months / 6 years 4 months	41 years	28 years
Height	88 cm (-2.4 SD) / 108 cm (- 2.4 SD)	145 cm (-3.3 SD)	139 cm (-4.8 SD)
Weight	13 kg (BMI 16.8) / 17.3 kg (BMI 14.8)	62 kg (BMI 29.49)	not documented
OFC	51.5 (1.7 SD) / not documented	56.5 cm (1.1 SD)	54 cm (-1.8 SD)
Short stature, age of onset	first year	first year	first year
Developmental milestones			
Sit	8 months	not documented	8 months
Walk	24 months	18 months	18 months
First words	18 months	18 months	very delayed (> 24 months)
3-word sentences	24 months	not documented	very delayed (> 24 months)
School education	Enrolled into the developmental program	Developmental school	Developmental school
Formal IQ testing	IQ 98 (HAWIVA test) at 6 years	not documented	IQ 82 at the age of 11 years, no recent testing documented
Occupation	not applicable	permanetly unable to work due to severe vision loss	Sheltered workshop
Hearing			
Hearing loss, age of onset	at birth	5-7 years	5-7 years
type	sensorineural bilateral	sensorineural bilateral	mixed sensorineural and conductive bilateral
severity (last follow up)	mild-moderate (right 50dB, left 60 dB)	severe, progressive from the 2nd decade (deafness)	severe, progressive from the 2nd decade (80-90 dB bilateral)
hearing aid, age of application	not necessary	17 years	7 years
cochlea implants, age	not necessary	35 years	none
Vision			
myopia	yes	yes	yes
age of diagnosis	first year of life	7-9 years	first year of life
severity in the childhood (dpt)	not applicable	severe	- 3.5 Dpt (1 year); - 10 Dpt (12 years)
Recent dpt	right - 5.5 Dpt; left -5.0 Dpt	not documented	not documented
Corneal dystrophy	no	yes (onset 25-27 years)	yes (onset 20-25 years)
Retinitis pigmentosa (RP)	no (no ERG done yet)	yes	yes
Nyctalopia, age of onset	no	10 years	10 years
RP age of diagnosis	not applicable	19 years	17 years
Glaucoma	no	yes	no
Age of onset	-	30 years	-
Strabismus	no	no	yes, operated
Nystagmus	no	no	yes
Hypothyroidism	no	yes	yes
Age of onset	not applicable	20 years	congenital
Skeletal features			
Brachydactyly	yes	yes	yes
Hand X-ray	short distal phalanges, middle phalanges, 4th metacarpals (right >left), bilateral mild ulnar negative variance	short distal phalanges most pronounced in thumb, 4th metacarpals, diffuse mild joint space narrowing in the carpal bones and of the radial carpal joint space	short distal phalanges and 4th metacarpals, angled distal articular surface of the radius, bilateral ulnar negative variance, narrowing of the radial carpal joints
Other skeletal features	none	none	scoliosis, bilateral shortening of the 4th metatarsals, splayfeet
Premature ageing	none	yes	yes
Hair loss	sparce hair	normal hair	very sparce hair, occipital alopecia from the age of 10 years
Arterial hypertension	none	yes, early third decade	yes, onset at the age of 10 years
Coronary disease	none	none	none
Diabetes mellitus	none	none	yes, onset at the age of 12 years
Arthritis	none	none	none
Neurological features			
Seizures, incl. fever seizures	no	no	no
Muscular hyoptonia	mild, transient during 1st year of life	no	no
Neuropathy	no	no	no
Spasticity	no	no	no
Brain MRI	borderline cerebellar atrophy, delayed myelination vs periventricular dysmyelination	mild cerebral and cerebellar atrophy	diffuse dysmyelination, bilateral calcifications in the basal ganglia and thalamus (first seen on CT at the age of 10 years), mild cortical and cerebellar atrophy
Other features	delayed closure of the anterior fontanell	none	none

Table 3. **Clinical data of EXOSC2 patients (from DiDonato et al., 2016)**

To complete the overview of diseases caused by dysfunction of the exosome complex, it's worth to mention that not only neurological syndromes are caused by reduced functionality of the exosome complex, other types of diseases have been linked to exosome complex defective functions:

Polymyositis/Scleroderma overlapping syndrome (PM/Scl) is an autoimmune disease which affects antigens PM/Scl75 and PM/Scl100 which are actually part of the human exosome complex (the antibodies target mainly hRrp4, hRrp40, hRrp41, hRrp42, hRrp46p, hCsl4) (Rick Brouwer et al., 2002).

Autoimmune diseases targeting aminoacyl-tRNA synthetases show a remarkable similarity to PM/Scl syndrome, representing again a similarity between exosome-driven pathologies and tRNAs driven pathologies (as explained better in the next paragraph) causing dermatomyositis, polymyositis, skin hyperkeratosis and other symptoms (Hamaguchi et al., 2013) (Mirrakhimov, 2015) having such a narrow spectrum of symptoms and such a specific etiology it is in fact referred to as "anti-synthetase syndrome".

Another disease caused by defective exosome complex functions is the thrico-hepato-enteric syndrome (THES), also called syndromic diarrhea (SD) which is caused by mutations on Ski2/SKIV2L/SKI2W and Ski3/TTC37, sub-units of the SKI complex (Monies et al., 2015).

1.4 RNA processing and pontocerebellar hypoplasias

Given the typical PCH features of the *EXOSC3*, *EXOSC8* and *EXOSC2* patients, Fabre and Badens hypothesized that the main RNA class which may be affected by mutations in these 3 sub-units may be tRNAs (Fabre and Badens, 2014).

A striking number of mutations on tRNA splicing endonuclease (TSEN) complex are often responsible for development of PCH. Mutations on TSEN54, TSEN2, TSEN15, TSEN34 (Simonati et al., 2011) (Bierhals et al., 2013) (Breuss et al., 2016) (Cassandrini et al., 2010) are responsible for this condition.

Other genes involved in tRNAs processing and which mutations are causative of PCH are CLP1 (Weitzer et al., 2015), RARS2 (mitochondrial argynil-tRNA synthetase 2; Edvardson et al., 2007).

This hypothesis of a defective tRNA-driven neural degeneration was subsequently backed by Weitzer and colleagues (Weitzer et al., 2015); it is worth mentioning that a direct interaction between tRNAs and EXOSC2 has been demonstrated in mammalian cells (Goodarzi et al., 2016), although in this study it is thought to be linked to cancer progression.

Many other aminoacyl-RNA synthetase mutations are known to cause neurological disorders and cerebellar degeneration: DARS (Taft et al., 2013); QARS (Zhang et al., 2014); EARS2 (Güngör et al., 2016); VARS2 (Baertling et al., 2016); GARS (Del Bo et al., 2006); HARS (Safka Brozkova et al., 2015); IARS (Kopajtich et al., 2016); KARS (McLaughlin et al., 2010); RARS (Wolf et al., 2014); YARS (Thomas et al., 2016).

In my thesis I describe the identification of a new mutation on *RBM7* in a single patient with motor neuron disease and functional experiments we performed in zebrafish (Giunta et al., 2016). Notably, RBM7 is likely to be involved in tRNAs processing and degradation of surplus of tRNAs (as well as other ncRNAs), as a high level of cross-linking between RBM7 protein and these RNA species has been observed (Lubas et al., 2015).

1.4.1 Subtypes of pontocerebellar hypoplasias

Pontocerebellar hypoplasia is a heterogeneous group of very rare developmental disorders with prenatal onset, characterized by abnormally small cerebellum and ventral pons. Most affected areas are cerebellar cortex, dentate nuclei, inferior olivary and ventral pontine nuclei (D'Arrigo et al., 2014). Estimated incidence is lower than 1:200,000 (Namavar et al., 2011a). Main symptom is severe psychomotor retardation. PCH often results in early death of the patient (Ekert et al., 2016).

Initially PCHs were classified in only 2 subtypes: with spinal motor neuron involvement (type 1) or without spinal motor neuron involvement (type 2). To date, 10 different subtypes of PCH have been clinically and genetically described (Eggens, 2016).

As mentioned before, **PCH1** (OMIM 607596) includes symptoms of pontocerebellar degeneration plus degeneration of anterior spinal horn, morphologically similar to spinal muscular atrophy (Eggens et al., 2014). Phenotype is actually very broad, cerebellar involvement can be very severe or milder and patient's survival can also be very different (from few days up to 18 years). PCH1 can be caused by mutations

in *EXOSC3* (estimated 50% of the cases), , *TSEN54*, *EXOSC8* (Eggens, 2016) and Vaccinia-related kinase 1 (*VRK1*), a nuclear serine/threonine protein kinase known to play multiple roles in cellular proliferation, cell cycle regulation, carcinogenesis, neuronal migration and neural stem cell differentiation (Vinograd-Byk et al., 2015).

PCH2 (OMIM 277470; 612389; 612390) is the most common subtype of pontocerebellar hypoplasia, mostly caused by mutations in tRNA splicing endonuclease subunit 54 (TSEN54). Other mutations in *TSEN2* and *TSEN34* have been identified. Clinically patients have a dragonfly-like pattern of the cerebellar hemispheres on coronal brain MRI, where the vermis is relatively intact, delayed myelination can occur as well as cortical atrophy (in 40% of the cases). Life expectancy can range from infancy to early puberty. (Namavar et al., 2011a) (Eggens, 2016)

PCH3 (OMIM 608027) is an extremely rare subtype of PCH. Patients suffer of hypotonia, microcephaly, optic atrophy and short stature (Namavar et al., 2011b). A pathogenic mutation was identified in *PCLO*, a gene only present in vertebrates which product is a large protein component of the presynaptic active zone, a specialized area mediating neurotransmitter release (Ahmed et al., 2015). It interacts with and controls the assembly of presynaptic F-actin. All the other cases of PCH3 remain unresolved.

Patients with **PCH4** (OMIM 225753) and **PCH5** (OMIM 610204) have the same characteristics of PCH2 but with an earlier and more severe onset (Eggens, 2016)

PCH6 (OMIM 611523) is a rare form and combines features of PCH with mitochondrial disease shown as elevated lactate levels. Mutations of mitochondrial Arginyl tRNA synthetase (RARS2) have been reported to cause this subtype (Eggens, 2016).

PCH7 (OMIM 614969) patients have brain and gonadal abnormalities, developmental delay. XY patients have impalpable testicles and micropenis; XX patients have atrophic ovaries. Brain MRI showed a hypoplastic pons and cerebellum, large ventricles and thin white matter. Mutations in *TOE1*, a putative splicing factor, have been associated with this subtype (Eggens, 2016).

PCH8 (OMIM 614961) was reported in six patients from 3 families. Patients showed severe psychomotor retardation, abnormal movements, hypotonia, spasticity, and variable visual defects. Brain MRI shows pontocerebellar hypoplasia, decreased cerebral white matter, and a thin corpus callosum (Mochida et al., 2012). It is caused by recessive mutation in Charged Multivesicular Body Protein 1A (CHMP1A) a member of the endosomal-sorting-complex-required-for-transport-III (ESCRT-III). CHMP1A also localizes in the nuclear matrix and is thought to regulate chromatin structure.

PCH9 (OMIM 615809) is characterized by severely delayed psychomotor development, progressive microcephaly, spasticity, seizures, and brain abnormalities, including brain atrophy, thin corpus callosum, and delayed myelination. PCH9 has been described in five families and linked to mutations in adenosine monophosphate deaminase 2 (AMPD2). AMPD2 encodes one of three known AMP deaminase homologues, which converts AMP to IMP (Akizu et al., 2013).

PCH10 (OMIM 615803) Patients suffer from both central and peripheral nervous system abnormalities. Brain MRI shows small pons, cerebellum and brainstem, as well as cortical involvement. Mutations in Cleavage And Polyadenylation Factor I Subunit 1(*CLP1*) has been associated with this subtype (Eggens, 2016). CLP1 is also a component of the tRNA splicing endonuclease and involved in tRNA metabolism (Weitzer et al., 2015).

1.5 Zebrafish as a model system

Zebrafish has become a widely used model for studying neurodevelopment and neurodegeneration. Most anatomical structures, developmental processes and protein structures are largely conserved between zebrafish and other vertebrates (Scalise et al., 2016) (Lyons and Talbot, 2015) (Babin et al., 2014).

Zebrafish has been largely used as a model to study developmental biology (Weis, 1968) and soon it gained its role as a new powerful tool to study human disease (Zon, 1999). Nowadays high quality zebrafish genome assembly have been generated (Howe et al., 2013) showing that 71.4% of human genes have at least one zebrafish orthologue with an average of 2.28 zebrafish genes for each human gene. This is due to a whole-genome duplication called the teleost-specific genome duplication (Meyer and Schartl, 1999). Zebrafish possess 26,206 protein-coding

genes (Howe et al., 2013). Continue genetic screening and phenotyping through mutagenesis, gene knock-down or gene overexpression has led to a great understand of molecular mechanisms which can be translated to human biology. Zebrafish have been used for modelling human muscle disease (Guyon et al., 2007) (Sztal et al., 2015) and neurological diseases (Stewart et al., 2014)

1.6 Zebrafish development

Zebrafish (*Danio rerio*) is a freshwater teleost which is found in nature in the Himalayan region. It has firstly become an important model to study developmental biology thanks to some of its features such as external fecundation and development, transparency of the body during the early stages of development (pigmentation starts developing at ~48 hpf) which allows direct observation, high number of eggs per lay (in the range of hundreds), short embryo development time (within 5 days all organs are completely developed), and of course developmental, anatomical, genetic similarity to human (Detrich et al., 1999), bridging the gap between *D. melanogaster* and *C. elegans* and mouse.

Zebrafish development cycle has been finely staged (Kimmel et al., 1995): since the 16 cells stage the fate of each cell has been established and it is now known which cells will form each of the three germ layers (ectoderm, mesoderm and endoderm) and therefore the tissues and organs which will develop from the respective layer (Fig. 1.1) (Strehlow et al., 1994) (Kimmel et al., 1990) (Gilbert and Raunio 1997).

Spatial gene expression analysis through *in situ* hybridization have shown that embryonic territories are very early defined through secretion of factors (such as BMP2B and CHD) with opposite roles from different cell populations (Schier and Talbot, 1998), therefore defining the polarization of the gastrula (Fig. 1.1). Therefore a left-right and a dorsal-ventral axis are established (Gilbert, 2000).

The neural tube formation is then induced by specific factors secreted by the underlying mesoderm, which turns part of the ectoderm into neuro ectoderm, neural

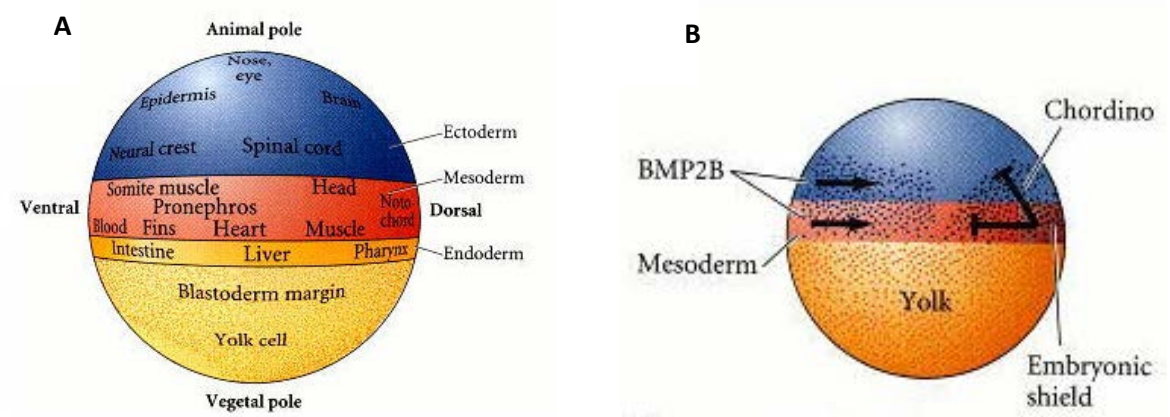

Figure 1.6. **Axis definition and fate map in zebrafish.** Experimental evidence (Kimmel et al;., 1990) has allowed to draw a fate map of the zebrafish blastula (A). Secreted factors (like CHD) from the embryonic shield in the dorsal side of the gastrula will inhibit the ventralizing factors such as BMP2B, defining the dorso-ventral axis (B). Images modified from Schier and Talbot, 1998 (B) and Gilbert and Raunio, 1997 (A).

plate and then neural tube (Schmidt et al., 2013). Neural tube formation starts after somitogenesis. Antero-posterior patterning of the neural tube is once again induced by secreted signals which establish a gradient of expression throughout the neural tube, polarizing it. Different anatomical areas act as organizers for the antero-posterior patterning. The anterior neural boundary organizes the definition of the anterior neural plate, secreting some antagonists of Wnt factors (Schmidt et al., 2013). Subsequently, other organizers that pattern the AP development of the neural system are intra-brain boundaries such as, for example, the intrathalamic boundary, characterised by *shh* expression which orchestrates the development of the thalamic complex in the diencephalon in zebrafish. The midbrain-hindbrain boundary is also a well established organizer, characterised by the secretion of *FGF8* (Schmidt et al., 2013).

The somites start developing at about 10.5 hpf at the sides of the notochord. The notochord itself exerts an important role in inducing the specification of surrounding tissues. Secreting factors such as *shh* toward the adjacent paraxial mesoderm, the first somite forms from the most rostral area of the presomitic mesoderm and somitogenesis continues caudally with the formation of a new pair of somites every ~30 minutes (Stickney et al., 2000). The somites then give rise to the development of the axial skeleton and skeletal muscle of the trunk.

1.6.1 Spinal cord and Spinal Motor Neuron development in zebrafish

The antero-posterior patterning of the spinal cord is defined by gradient of expression of genes such as FGF, Wnt, Retinoic Acid (RA). The polarization of the spinal cord seems to occur via a caudalization of an otherwise (by default) all-rostral structure. FGF and Wnt proteins initially suppress anterior gene expression in the posterior neural plate in an RA-independent manner. Then the same signals activate posterior genes, in an RA-dependant manner (Lewis and Eisen, 2003).

The neural tube has obviously a dorso-ventral patterning as well (Fig. 1.2). Dorsal sensory neurons and ventral motor neuron (MNs) are connected by a number of inter neurons. Identification of molecular markers in the last years has allowed to further categorize more neuronal sub groups within the neural tube. Dorsal neurons are divided into 6 subgroups in mouse; ventral neurons are divided into 5 groups (Lai et al., 2016). Each domain is characterized by the expression of specific markers (Wilson and Maden, 2005) (Lai et al., 2016). In addition to these there are 2 additional late-onset dorsal domains, which can be further divided into subgroups depending on axonal projections or neuropeptide secretion (Lai et al., 2016).

Motor neurons (and other neuronal types) in the ventral region are specified by repression of alternative cell fates through expression of transcriptional repressor factors (Davis-Dusenbery et al., 2014) such as *olig2* (Lee, 2005), *nkx6* (Hutchinson et al., 2007) (Sander, 2000) and *pax6* (Wilson and Maden, 2005). RA is important for activating expression of *olig2* and *pax6* (Paschaki et al., 2012).

MNs have distinct identities throughout the length of the spinal cord. Major differences in the antero-posterior identities of spinal motor neurons have been linked to actions of some members of the *Hox* gene family (Fig. 1.2) as their expression and functional profiles correlate with the AP positional identity of MNs (Wilson and Maden, 2005) (Bonanomi and Pfaff, 2010) (Lai et al., 2016). RA is a known regulator of *hox* genes expression in vertebrates (Cunningham and Duester, 2015).

The spinal cord in zebrafish (as for other anamniotes vertebrates) has both primary neurons and secondary neurons. These two neuronal cell types have anatomical and functional distinctions: primary neurons are larger in size, develop earlier and have sensory , motor and inter-neuronal functions (Higashijima, 2004)while secondary neurons have smaller size, develop later during embryo development and consist of only interneurons and motor neurons (Lewis and Eisen, 2003).

When positional identity of motor neurons is defined, they start extending processes: either axons or dendrites to connect each other with upstream and downstream neurons or tissues. MNs pathfinding seems to be driven by (but not only) semaphorins, a large class of secreted or transmembrane proteins, in vertebrates (Svensson et al., 2008). It may be that muscle-secreted semaphorins inhibit growth of axons, preventing them from reaching the wrong target (Lewis and Eisen, 2003). Mutant fish for *plexin A3*, a semaphorin receptor, show defects in exit position from the spinal cord (Palaisa and Granato, 2007), *sema3a1* is also important for MNs growth (Sato-Maeda, 2006).

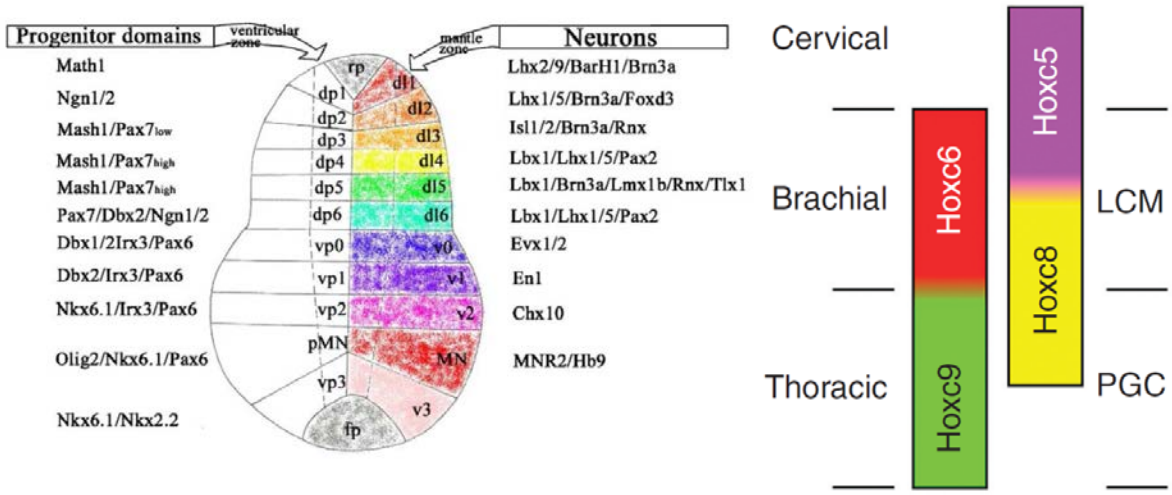

Figure 1.7 **Definition of dorso-ventral and antero-posterior neuronal identities in the vertebrates' spinal cord.** Many different subtypes of sensory, motor and interneuron are present in the vertebrate spinal cord, each of them characterised by the expression of specific markers (left). *Hox* genes play a key role in antero-posterior patterning of the spinal cord through gradients of expression, defining different subset of neurons which will innervate the limbs or the internal walls (right). Images modified from Wilson and Maden, 2005 (left) and Bonanomi and Pfaff, 2010 (right).

1.6.2 Myelination process in zebrafish

Zebrafish is considered a good model for studies of the myelination process and related human diseases (Buckley et al., 2010) (Sager et al., 2010) (Raphael and Talbot, 2011).

Myelin is an insulating membrane that surrounds nerves permitting a better signal transduction along the nerve fibres. In humans, the importance of myelin for correct neuronal functions is highlighted by the severity of diseases with an impairment of myelin. Such disorders are characterized by abortive impulse conduction and the

resulting loss of sensory, motor, and cognitive functions. Myelinating cells and the myelination process have been intensely studied and we now have knowledge of its structure, its formation and factors that might affect its functions.

Composed of about 70% lipid and 30% proteins (Buckley et al., 2008), myelin takes the form of overlapping sheaths around axons and is produced by oligodendrocytes in the central nervous system (CNS) and by Schwann cells in the peripheral nervous system (PNS). Myelination process in zebrafish starts at about 3 dpf, beginning from lateral line neurons and ventral motor neurons in the neural tube (Buckley et al., 2010). In all vertebrates Schwann cells originates from neural crest-derived precursors which associate with and proliferate along axonal tracts that grow out from the neural tube and peripheral ganglia (Jessen and Mirsky, 2005). Schwann cell precursors extend processes that envelop axon bundles and progressively segregate and subdivide them. Ultimately, each myelinating Schwann cell ensheaths a single axonal segment, then elaborates a multi-layered myelin sheath that gradually becomes compacted (Kazakova et al., 2006). Oligodendrocyte progenitors are generated by neuroepithelial precursors. They proliferate and migrate from their sites of origin before associating with axons and differentiating into oligodendrocytes, which elaborate myelin sheaths round single or multiple axons (Richardson et al., 2006). Myelination process requires the highly co-ordinated expression of specific structural and regulatory proteins (Brösamle and Halpern, 2002). Myelin basic protein (MBP), referred as the “executive molecule of myelin” is of fundamental importance for this process (Boggs, 2006). In mammals MBP accounts for about 8% of the total myelin proteins in CNS and PNS being the second most abundant after proteolipid protein (PLP) (Müller et al., 2013). MBP is a fundamental protein for the myelination process in the CNS, as highlighted by severe hypomyelination observed in different mutant mice, while almost a normal myelination is possible in mice lacking PLP. MBP is essential to provide adhesion of the myelin sheaths at the cytoplasmic interface, interacting electrostatically with the lipid layer (Min et al., 2009). Apparently in mice it is not indispensable for myelination of the PNS which can be explained by compensatory roles of P0 (Müller et al., 2013). Notably P0 in zebrafish PNS is less expressed than in mammals and does not work as a myelin adhesion protein (Buckley et al., 2008) therefore *mbp* in zebrafish is essential also for myelination of the PNS (Pogoda et al., 2006). Two *mbp* paralogs are present in zebrafish: *mbpa* (on chromosome 19) and *mbpb* (on chr 16), which have very similar but not identical

expression pattern (Nawaz et al., 2013) the second one being more closely related to the MBP present in tetrapods, both are abundant in zebrafish myelin. *mbpb* but not *mbpa* is expressed as early as 11 hpf in the polster, the hatching gland precursor underlying the developing forebrain (Nawaz et al., 2013). Both paralogs were found in association with the plasma membrane suggesting a structural function like MBP in mouse. Both paralogs have a complex splice structure and mbpb exists in a transcription unit from which two protein products emerge: MBPb and the unrelated GOLLI. The function of the second one is not completely understood, although mice lacking for the golli product of the mbp gene have a phenotype suggesting an involvement in the myelination process (Nawaz et al., 2013). Although MBP is mainly known to have structural function in myelin, it seems also to have other roles. There is evidence that one classic MBP isoform alone is capable of fulfilling this function in the absence of the other isoforms, making the roles of the other isoforms unclear (Campagnoni and Skoff, 2001). The complex splicing variants of MBP, its post-translational modifications and its tertiary structure that might be compatible with multiple protein associations, seem to indicate it has different functions within the cell (Müller et al., 2013).

Some studies in mouse showed different MBP isoforms play different roles at different developmental stages in different cell compartments. These non-myelin-related functions are various: some isoforms appear to be in the cytoplasm and nucleus but not in the plasma membrane (Smith et al., 2013), it interacts with cytoskeletal proteins influencing their polymerization (Hill et al., 2005), it has been connected to signalling pathways which are important for differentiation and myelination (Smith et al., 2012) (Kräm er-Albers and White, 2011), modulates voltage-operated Ca^{2+} channels (Smith et al., 2011) and also, a role of MBP as a transcription factor has been speculated (Staugaitis et al., 1996).

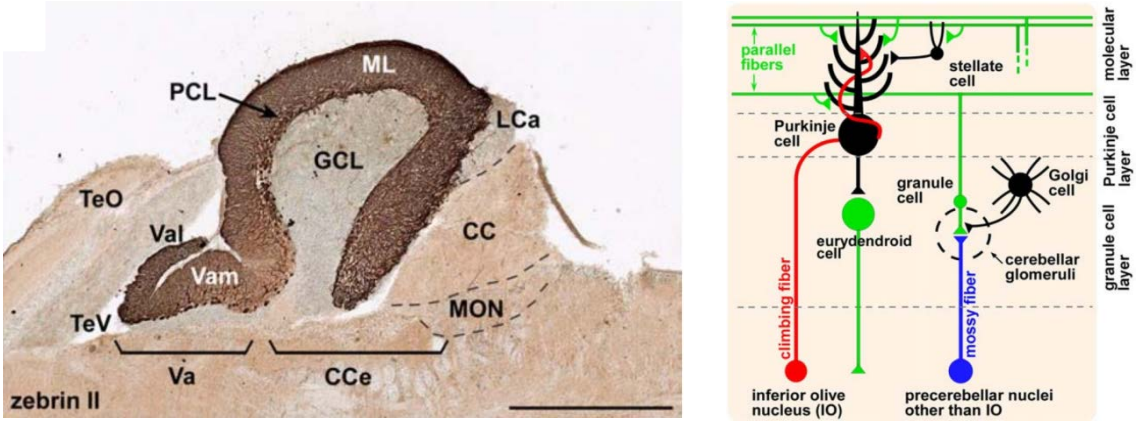

Figure 1.8 **All three cerebellar layers are easily recognizable upon immunostaining.** From external to internal: Molecular Layer (ML); Purkinje Cell Layer (PCL), Granule Cell Layer (GCL; left). Schematic representation of different cell types and their connections within zebrafish cerebellum (right). Images from Bae et al., 2009.

The presence of the GOLLI product within the same transcription unit makes the situation even more complicated as the golli-mbp gene seems to have other different neural and non-neural roles in mouse (Müller et al., 2013) (Fulton et al., 2010). GOLLI-MBP isoforms are expressed throughout the immune system in thymocytes and T-cells and also in the entire haemopoietic system (Feng, 2007) (Marty et al., 2002). Overall, it seems classic forms of mbp have many other roles with functions beyond that of serving as myelin structural proteins, playing a role also in oligodendrocyte and Schwann cells differentiation as well as regulating the myelination program.

1.6.3 Cerebellar development in zebrafish

Cerebellar functions are also highly conserved in vertebrates, integrating sensory and motor information. In mammals cerebellum is thought to perform also some higher cognitive and emotional tasks (Buckner, 2013).

Zebrafish cerebellum is formed by three layers of cells just like in mammals, from external to internal: a molecular layer, a PCs layer and a granule layer (Kani et al., 2010). The three layers are first detectable at 5 dpf (Bae et al., 2009). Zebrafish cerebellum can be divided in lobular structures from rostral to caudal, each of them containing all three cell layers: valvula cerebelli (Va), the corpus cerebelli (CCe), and the vestibulolateral lobe, which consists of the eminentia granularis (EG) and the

lobus caudalis cerebelli (LCa). The eminentia granularis contains only the granule cell layer (Bae et al., 2009; Fig. 1.3).

The different types of neurons in the zebrafish cerebellum, like in mammals, can be divided in GABAergic/glycinergic neurons (inhibitory) and glutamatergic neurons (excitatory), according to the main neurotransmitter they secrete. This differentiation begins 3 days post fecundation (Bae et al., 2009). Granule cells, eurydendroid cells (which are absent in mammals, substituted by the deep cerebellar nuclei) are glutamatergic; Purkinje cells and interneuron such as Golgi cells and stellate cells are inhibitory. PCs layer in all vertebrates receives information from the climbing fibres from the inferior olives, and the mossy fibres principally from the pontine nuclei (via granule cell parallel fibres). The pons (and pontine nuclei) are highly affected in PCH (D'Arrigo et al., 2014). The PCs in mammals send their inhibitory signals outside the cerebellar cortex thorugh the Deep Cerebellar Nuclei (DCN). The DCN in teleosts is substituted by the eurydendroid cells (Bae et al., 2009) (Heap et al., 2013).

Purkinje cells can be stained with *pvalb7* antibody, granule cells express instead *vglut1*. Either *vglut1* and *pvalb7* are initially expressed at 3 dpf (Bae et al., 2009). *pvalb7* may be expressed even earlier in PCs (2.8 dpf; Hamling et al., 2015). The signal of the 2 antibodies merges in the more external layer at 5 dpf, indicating that the molecular layer is completely formed by 5 dpf (Bae et al., 2009; Fig. 1.6).

Purkinje cells start differentiating at 2.8 dpf in dorsomedial clusters and ventrolateral clusters, symmetrically (Fig. 1.4; Hamling et al., 2015) from progenitor cells expressing *ptf1a* (Kani et al., 2010). By 4 dpf the PCs layer have acquired the distinctive "wing-shaped" pattern.

Mutations affecting cerebellar development compromise the formation of the PCs layer which can result scattered or with an inverted wing-shape (Fig. 1.5; Bae et al., 2009).

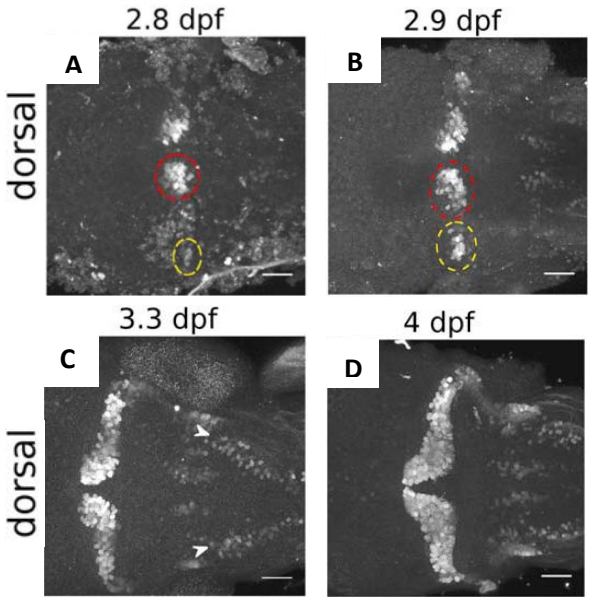

Figure 1.9 **Dorsal view of Purkinje cell layer development in zebrafish.** Clusters of PCs can be seen as early as 2.8 dpf in the dorsomedial region (red) and ventrolateral region (yellow). They progressively expand until they reach confluence (3.3 dpf) and form the classical wing-shaped structure. Images from Hamling et al., 2015.

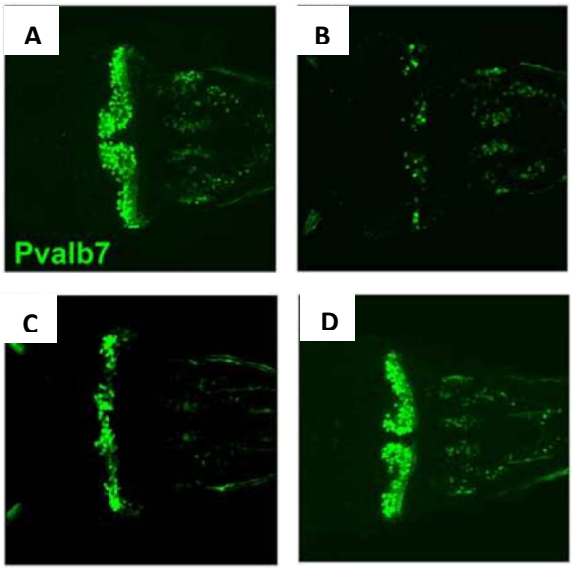

Figure 1.10 **Dorsal view of Purkinje cell layer in WT and mutant zebrafish.** Wild type (A); Mutations in genes affecting cerebellar development can cause the formation of scattered structures (B, C) or inverted structure (D), although the fish may not show any clear morphological phenotype. Images modified from Bae et al., 2009.

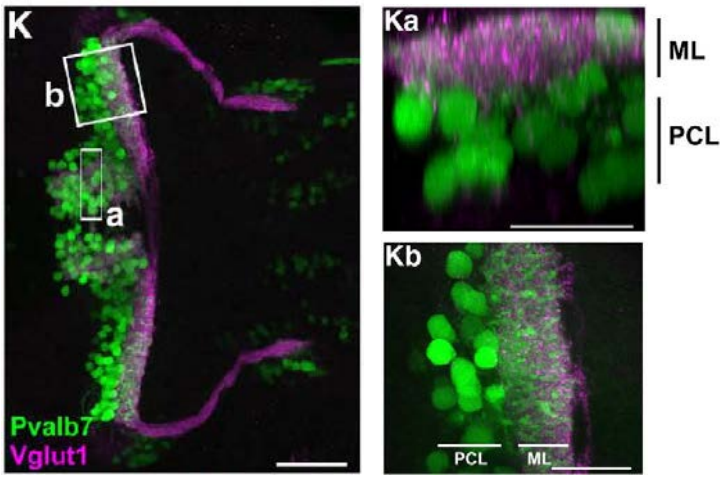

Figure1.11 **Purkinje cells and Granule cells in zebrafish.** Co-immunostaining of *pvalb7* and vglut1 show merged signal in the most dorsal part (Ka, top; Kb, right) at 5 dpf indicating that the ML is formed. K dorsal view; Ka and Kb show transverse sections obtained by manipulation of Z-stack from image K Image from Bae et al., 2009.

1.7 Zebrafish models of PCH

Zebrafish have been used as a model for a countless number of studies about neurodevelopment and neurodegeneration. It is a versatile and cost efficient model thanks to external fecundation and body transparency, which allows direct observation of anatomical defects caused either by gene knock down or mutagenesis (Schmidt et al., 2013) (Babin et al., 2014) (Martín-Jiménez et al., 2015). Here I will analyze the state of the art for the use of zebrafish as a model to specifically study pontocerebellar hypoplasias and motor neuron diseases.

Other than the previously mentioned studies about the investigation of functions of *EXOSC3* and *EXOSC8*, several other publications took advantage of this model system to study cerebellar development. Zebrafish cerebellum development has been well staged and studied (Hamling et al., 2015) (Kani et al., 2010).

1.7.1 TSEN54

Kasher and colleagues created knock-down and mutant zebrafish models of PCH targeting tRNA-splicing endonuclease subunit 54 (*tsen54*) and mitochondrial arginyl-tRNA synthetase (*rars2*; Kasher et al., 2011).

In the article, they show expression of *tsen54* in 24 hpf zebrafish through *in situ* hybridization. *tsen54* is expressed systemically, but a stronger signal is present within the midbrain-hindbrain boundary (mhb), in the telencephalon and hindbrain (Fig. 1.7).

Gene knock down with an antisense morpholino shows a defective development of the head region, which they state, it is not reflected in the general body morphology.

To study if there could be any analogy between the roles of *tsen54* and *rars2* in neurodevelopment, the authors performed gene knock-down of *rars2* as well, showing similar morphological defects in the brain. Specifically, the mhb is missing in both morphant fish. Defects were partially rescued through co-injection of WT (human or zebrafish) mRNA in both models. Notably, the mhb seems to partially develop in the rescued fish.

In situ hybridization was performed in both models to study brain development using *fgf8* and *otx2* as markers of brain development. Again similar defective expression patterns of the markers could be shown in both models, which was partially rescued by WT mRNA injection.

Acridine orange staining highlighted a higher cell death rate in the brain of both *tsen54* and *rars2* morphant models, resembling the patient phenotype that also show cell death in the pons.

Although the phenotypes were rescued through co-injection of mRNA (Fig. 1.7), therefore demonstrating the specificity of the phenotype, to avoid any doubt about the causes of brain cell death, a *p53*-MO co-injection could have been performed.

Finally, in the paper Kasher and colleagues report the creation of a *tsen54* mutant line but they only say the homozygous mutant fish die within 9 dpf. No phenotype could be seen and the causes of the sudden death are unknown. Hopefully this mutant line will be investigated further with a modern, comprehensive technique (e.g. RNA-seq) to study what patho-mechanisms lead to death of the mutant fish.

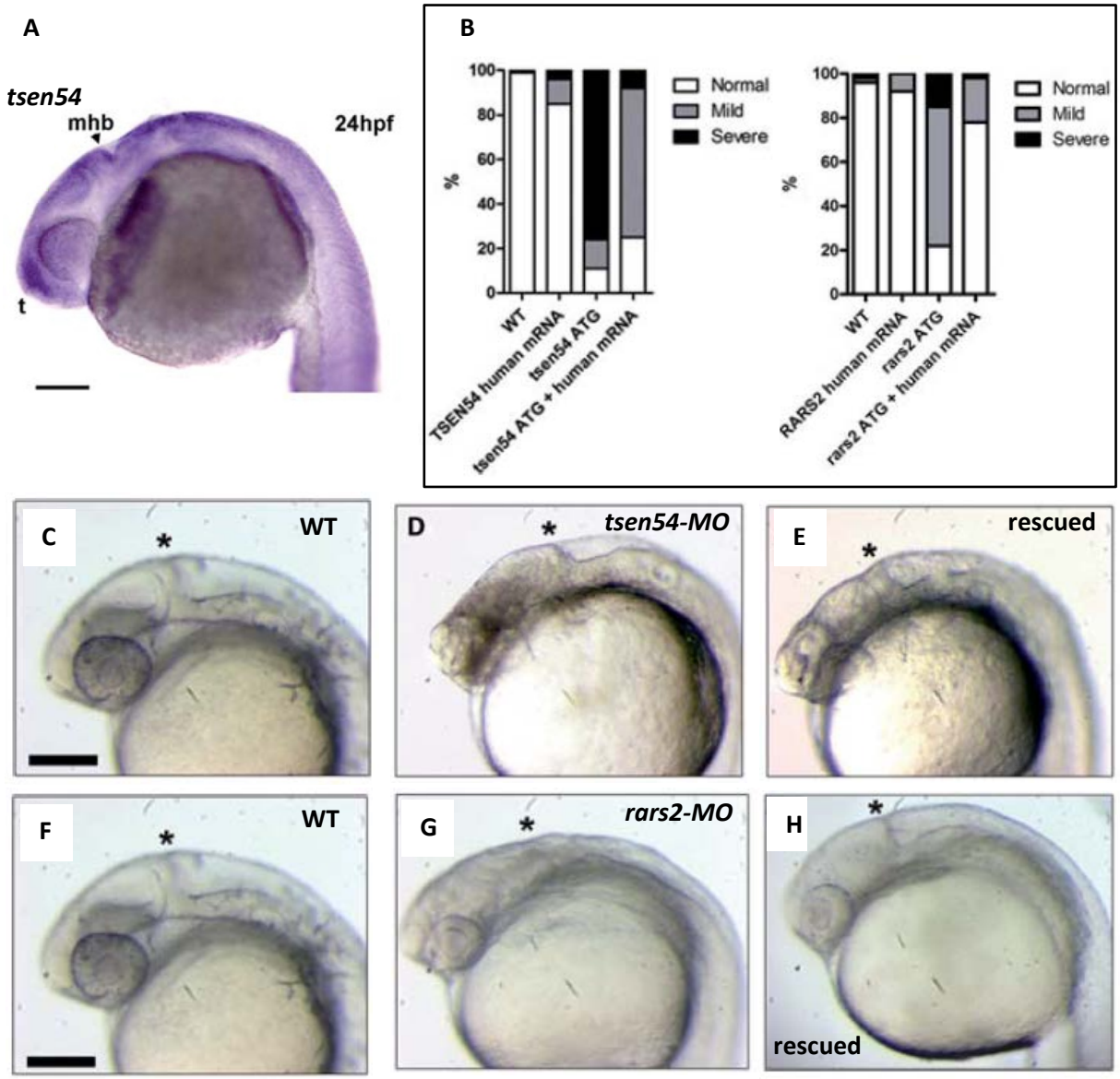

Figure 1.12 ***tsen54* expression and *tsen54* and *rars2* knock down.** *tsen54* is ubiquitously expressed but signal is stronger in mhb and telencephalon (A). Knock-down of *tsen54* (D) and *rars2* (G) cause defective development of brain and mhb compared to control (C, F). Co-injection of respective mRNAs and morpholinos rescued the brain phenotype, mhb is partially formed in both models (E, H). Graphs representing the percentage of defects in knock-down fish and rescued fish for *tsen54* experiments (B, left) and *rars2* experiments (B, right). Scale bar = 200 μm. Figures modified from Kasher et al., 2011

1.7.2 CLP1

Schaffer and colleagues show in their paper functional analysis of *clp1* in a zebrafish mutant strain (Schaffer et al., 2014).

They generated a *clp1* R44X mutant line by ENU mutagenesis which showed defective body morphology and *clp1* expression - tested by *in situ* hybridization. Mutant fish did not survive after 5 dpf, demonstrating an essential role of *clp1* during embryo development.

Expression of *otx2* as a marker of midbrain development was normal up to 24 hpf even in mutant fish. At 48 hpf mutants started displaying lower *otx2* expression (Fig. 1.8). Because of the sudden decrease in expression suggest neurodegeneration instead of defective differentiation, they tested for cell death with TUNEL, showing indeed an increased cell death rate in the brain of mutant fish. Injection of *p53*-MO partially rescued *otx2* expression in mutants suggesting that the neural apoptosis is *p53* dependent. Immunostaining of motor neuron with SV2 showed defects of these structures too (Fig. 1.8).

Injection of human WT *CLP1* mRNA showed body morphology phenotype as well as *otx2* expression rescue while injection of mutant *CLP1* mRNA did not, therefore suggesting that the human mutation lacks activity *in vivo* (Fig. 1.8).

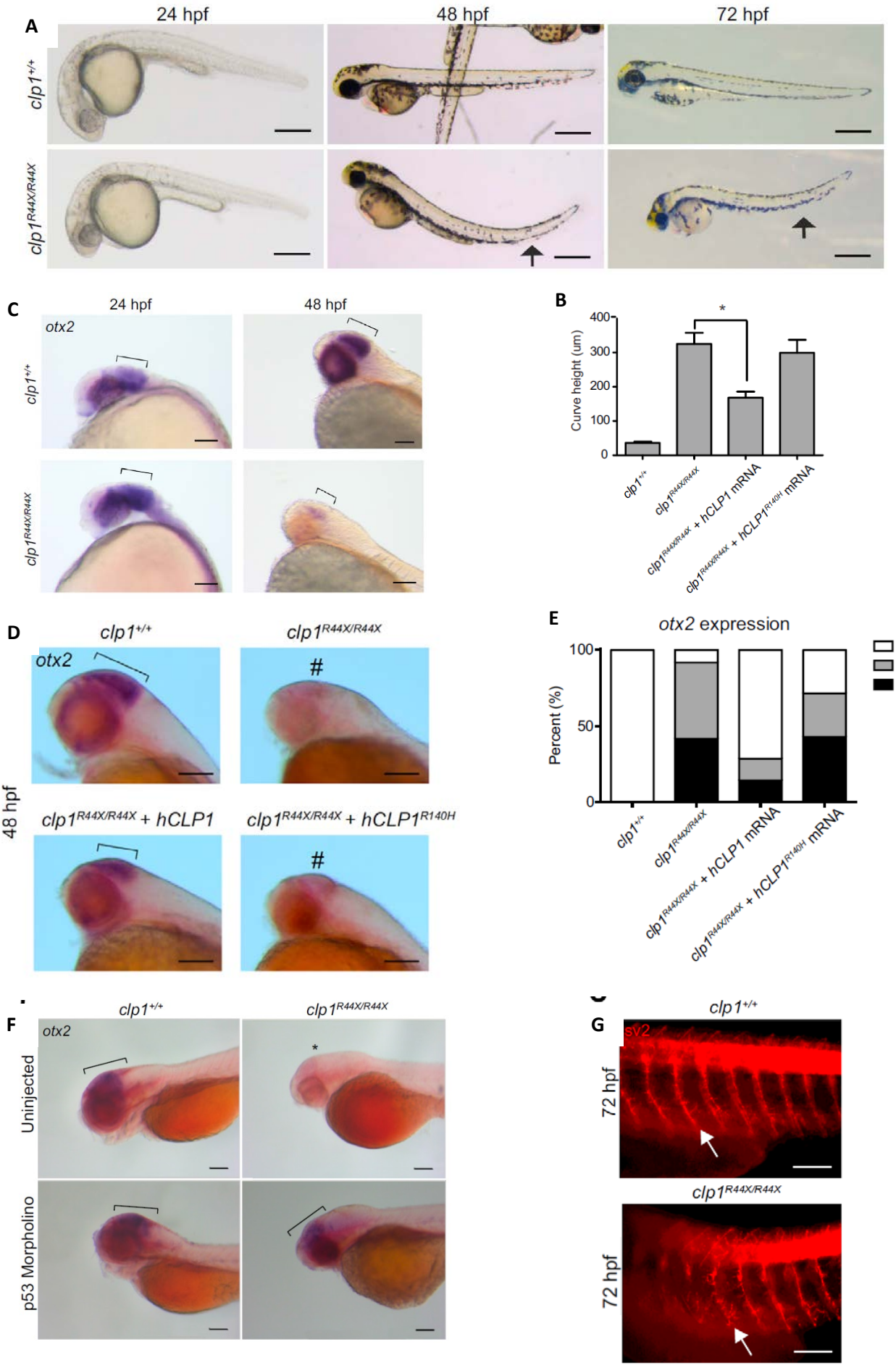
A
24 hpf
48 hpf
72 hpf
clp1+/+
clp1R44X/R44X
B
Curve height (um)
400
300
200
100
0
*
clp1+/+
clp1R44X/R44X
clp1R44X/R44X + hCLP1 mRNA
clp1R44X/R44X + hCLP1R140H mRNA
C
24 hpf
48 hpf
otx2
clp1+/+
clp1R44X/R44X
D
clp1+/+
clp1R44X/R44X
otx2
#
48 hpf
clp1R44X/R44X + hCLP1
clp1R44X/R44X + hCLP1R140H
#
E
otx2 expression
Normal
Reduced
Absent
Percent (%)
100
50
0
clp1+/+
clp1R44X/R44X
clp1R44X/R44X + hCLP1 mRNA
clp1R44X/R44X + hCLP1R140H mRNA
F
clp1+/+
clp1R44X/R44X
otx2
*
Uninjected
p53 Morpholino
G
clp1+/+
SV2
72 hpf
clp1R44X/R44X
72 hpf

Figure 1.13 ***clp1* is important for CNS and PNS development.** Mutant *clp1*$^{-/-}$ fish develop normally up to 48 hpf when they start showing a curved tail (A). They curvature of the tail was used to calculate the severity of the phenotype and to quantify the rescue by WT mRNA and mutant mRNA, demonstrating a lack of activity of the human mutant gene (B). Analysis of *otx2* expression as a marker of brain development show normal signal even in mutants at 24 hpf. Signal decreases at 48 hpf in mutants compared to controls (C). Injection of the WT mRNA rescues expression of *otx2* in brain of mutant fish. Injection of mutant mRNA does not rescue the expression (D). The graph shows the percentage of different phenotypes in mutant and rescued fish (E). Injection of *p53* morpholino rescues expression of *otx2* in the brain, indicating that brain degeneration is *p53* dependent (F). *clp1* inactivation affects also primary motor neurons (G). Images modified from Schaffer et al., 2014.

1.7.3 CHMP1A

CHMP1A was originally identified as binding to polycomb proteins (Plc) and to recruit in the cytoplasm the transcriptional repressor BMI1 which in turn inhibits expression of *INK4A*, a repressor of stem cell proliferation. Mochida and colleagues show that morpholino based gene knock-down of *chmp1a* causes reduced cerebellum size compared to control fish (Mochida et al., 2012; Fig. 1.9), similar to what caused by knock-down of zebrafish orthologs of BMI1: *bmi1a* and *bmi1b*. Cerebellar phenotype was partially rescued by injection of human WT mRNA (Fig. 1.9).

The authors then tested for interactions between *chmp1a* and the zebrafish ortholog of *INK4A*: *cdkn2a*. Double knock-down of *chmp1a* and *cdkn2a* resulted in partial rescue of the phenotype, accordingly to the molecular function of these 2 proteins.

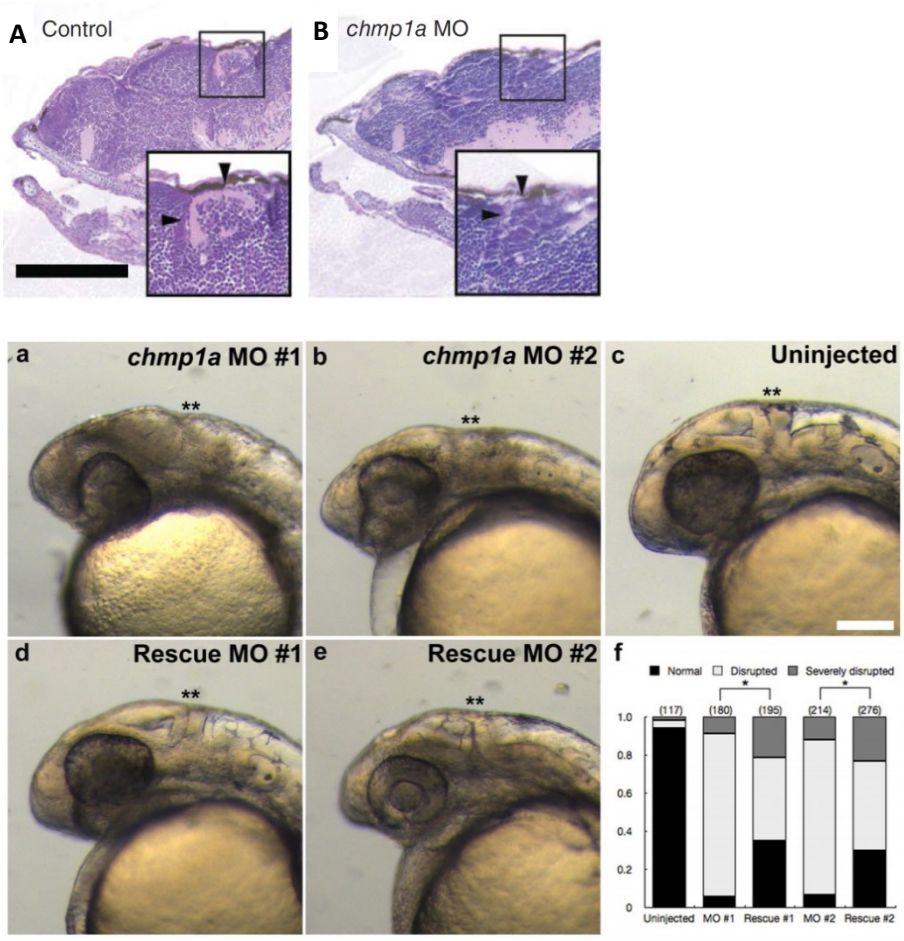

Figure 1.14 ***chmp1a* morpholino affects brain development.** Cerebellar morphology of 5 dpf morphnat fish is defective (B) compared to controls (A). Midbrain-hindbrain boundary is disrupted in morphant fish(a, b) compared to controls (c). Hindbrain structures are rescue through injection of WT mRNA (d, e). The graph shows percentage of phenotypes in moprhant and rescued fish (f). Image modified from Mochida et al., 2012.

1.7.4 QARS

QARS encodes for glutaminyl-tRNA synthetase, variants in this gene cause neurological symptoms and pontocerebellar hypoplasia. Zhang and colleagues took advantage of a previously published mutant *qars* zebrafish line and phenotyped it (Zhang et al., 2014). In their study they demonstrate that the onset of neurodegeneration starts at 3 dpf, presumably for compensation through maternal effect. Mutant *qars*$^{-/-}$ fish do not show any defect until that age, subsequently they develop smaller eyes and head. Eyes and head size is significantly smaller (Fig. 1.10). To test if neurogenesis was normal up to 2 dpf in mutant fish the authors performed immunostaining of fish head sections with anti-Pax6 (a marker of neural progenitors), anti-PH3 (a marker for mitotic cells) and anti-HuC/D (a marker for post-mitotic neurons), showing that mitosis was normal both in the eyes and brain in mutant fish compared to controls (Fig. 1.11).

Cell death tested by TUNEL staining was instead much higher in 6 dpf mutant fish compared to controls and comparable to WT in 2 dpf mutants indicating that the brain phenotype was indeed caused by neurodegeneration rather than defective neurodevelopment (Fig. 1.11).

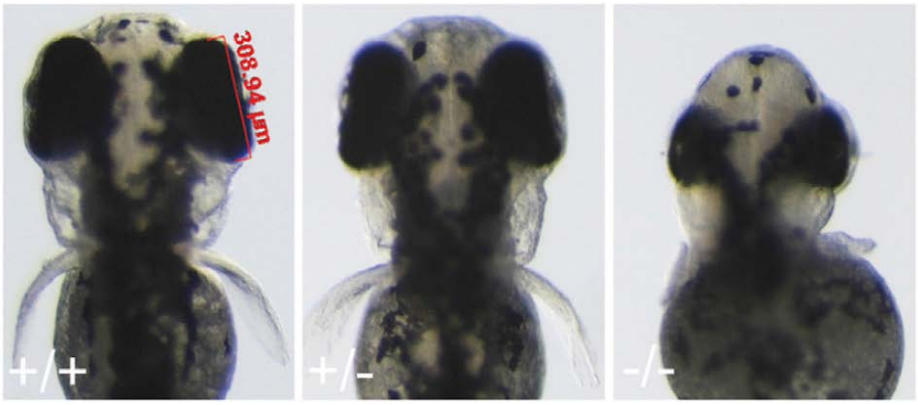

Figure 1.15 **Head and eyes have smaller size in *qars* mutant zebrafish.** Image from Zhang et al., 2014.

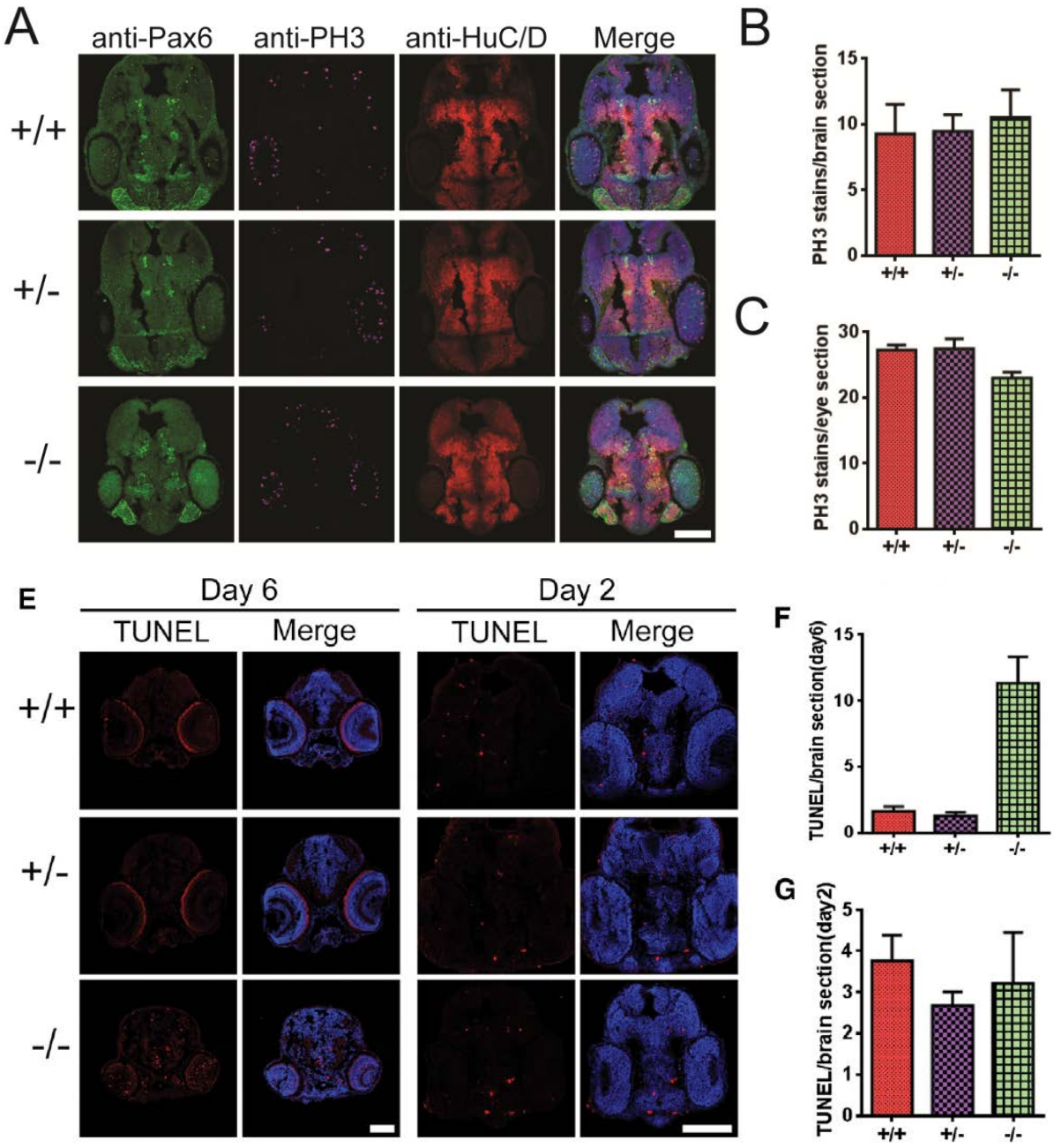

Figure 1.16 **Neurogenesis and cell death in control and *qars* mutant fish.** Neurogenesis is normal in mutant fish compared to control at 2 dpf (A-C). Neural progenitors stained with anti-Pax6, mitotic cells (anti-PH3) and postmitotic cells (anti-HuC/D) show a similar pattern (A). TUNEL staining shows a much stronger signal in mutants brain's section at 6 dpf compared to control. At 2 dpf TUNEL staining is comparable in mutants and controls (E-F). Image modified from Zhang et al., 2014.

2 Chapter 2: Materials & Methods

2.1 Next Generation sequencing (NGS)

2.1.1 Whole exome sequencing

Whole-exome sequencing was performed on one or several individuals from each pedigree depending on the mode of inheritance of the disease. Whole-exome sequencing was outsourced to AROS (AROS Applied Biotechnology A/S, Aarhus, Denmark). Genomic DNA was subjected to a library preparation using TruSeqTM DNA Sample Preparation Kit (Illumina Inc., San Diego, USA) and the targeted regions were captured using the Illumina Nextera Rapid Capture Exome Kit (37Mb) (Illumina Inc., San Diego, USA). The captured fragments were sequenced on an Illumina HiSeq 2500 platform (Illumina Inc., San Diego, USA) producing 100 bp paired-end reads.

2.1.2 Bioinformatic analysis

Bioinformatic analysis was performed using an in-house algorithm incorporating the published tools. The following was performed by Dr. Helen Griffin (Newcastle University): the reads were aligned to the human reference genome (UCSChg19) using Burrows-Wheeler Aligner (Li and Durbin, 2010), PCR duplicates were removed with Picard v1.85 (available at http://broadinstitute.github.io/picard/), single base variants (SBV) and insertions/deletions (indels) were identified with Varscan v2.2 (Koboldt et al., 2009) and Dindel v1.01 (Albers et al., 2011) respectively.

2.1.3 RNA-seq

For RNA sequencing experiments, total RNA was extracted from fibroblasts or muscle tissue using the mirVana™ miRNA Isolation Kit (Ambion) and DNAse treated with the DNA-free™ DNA Removal Kit (Ambion). RNA quality was tested with an Agilent 2100 Bioanalyzer and only samples with an RNA Integrity Number (RIN) >7 were sent for sequencing. RNAseq libraries were prepared using Illumina (Illumina, Inc. California, U.S.) TruSeq Stranded Total RNA with Ribo-Zero Human kit and were sequenced on an Illumina HiSeq 2500 platform using paired-end protocol.

2.1.4 Bioinformatic analysis

Bioinformatic analysis of *EXOSC8* and *RBM7* mutant fibroblasts was performed by Dr. Yaobo Xu (Newcastle University). The quality of sequencing reads was firstly checked with FastQC (http://www.bioinformatics.babraham.ac.uk/projects/fastqc/).

The 12 bp on the left ends and 4 bp of the right ends of all reads were clipped off with Seqtk (https://github.com/lh3/seqtk) to remove GC-content biased bases. The programme (https://github.com/optimuscoprime/autoadapt) was then used to remove low quality bases (Q < 20) and contaminations from standard Illumina paired-end sequencing adaptors on 3' ends of reads. Autoadapt uses FastQC to identify the exact sources of contaminations and uses cutadapt (Martin, 2011) to remove them automatically. Poly-N tails were trimmed off from reads with an in house Perl script. Only reads that were at least 20bp in length after trimming were kept. These high quality reads were then mapped to the human reference genome hg38 with Tophat2 (Kim et al., 2013). Number of reads mapped to genes were counted using HTSeq-count (Anders et al., 2014). Differentially expressed genes were then identified with Bionconductor (Gentleman et al., 2004) package DESeq2 (Love, et al., 2014). P-values of detected expression changes were corrected with Benjamini & Hochberg algorithm. Genes differentially expressed with P-values ≤ 0.05 and fold change ≥ 2 were considered as differentially expressed genes.

2.2 Sanger sequencing

2.2.1 Polymerase Chain Reaction

Primer oligonucleotide sequences specific for the genes of interest were designed using Primer 3 (v.0.4.0) software. Primer 3 specifies product size as well as melting temperature of the designed primers and their GC content (%). Target DNA sequences were uploaded into the online software and primer sequences selected to span the region of interest. The generated primer sequences were checked for specificity using the online program Basic Local Alignment Search Tool (BLAST) (http://blast.ncbi.nlm.nih.gov/Blast.cgi). A list of the primers used is provided below.

Gene	Exon	Fw primer	Rv primer	Ta (°C)	Size (bp)
EXOSC3	1	acggccatcaagcttcataaac	ctcttcttttgggaggtcttct	myTaq 63	539
EXOSC3	2	ggggtgcctaagagataatggag	gatagccttctggatatgtgagtgttc	myTaq 63	441
EXOSC3	3	tccccaagactcaactccaaag	atcagcccaccagaaactacacag	myTaq 63	539

EXOSC3	4	tggaagaaaggaggcagcaaatg	cacaaaagcgtgggtgaaaac	myTaq 63	515
EXOSC8	1	gtctgggcaggggaaagt	aggaaatggcaccccaac	myTaq 55	300
EXOSC8	11	tcacttggaggtcttgtgaa	ttggtttgcctaagtcattgc	myTaq 59	460
RBM7	1	gtttgtgacgccagggag	cgtcactttcggcctaaacg	myTaq 61	400
RBM7	2	ggaaatccgtgcatcattttca	ccatgtgtcaatgttacccgt	myTaq 61	475
RBM7	3	cccggccagtagtttgagat	acaacaaccccaaaaggcaa	myTaq 55 + Betaine	360
RBM7	4	tattctggctgcatgagagc	cagcccagtgaaaactaaaatga	myTaq 57	451
RBM7	5	tgctttagttgtggatccatct	tgtgacaacttgtaaagctgct	myTaq 59	600

Table 4. List of primers used for PCR reactions

PCR reaction was prepared using the following mix:

MyTaq™ DNA Polymerase (Bioline) …….. 0.2 μl
MyTaq™ reaction buffer (Bioline) …….. 5 μl
Fw primer (10 μM) …… 1 μl
Rv primer (10 μM) …… 1 μl
H_2O ……16.8 μl
DNA……...1 μl

Reaction times and T° were as following:
Step 1 – denaturation at 95 °C for 1 minute **}** 1 cycle

Step 2 – denaturation at 95 °C for 15 seconds
annealing T° user determined (see above), 10 secs per Kb
extension 72 ° for 10 seconds
} 25-35 cycles

2.2.2 Electrophoresis on agarose gel

40 μl/100ml of ethidium bromide was mixed into the molten 1-2 % agarose gel in 1xTAE buffer pH8.0 (Tris base, acetic acid and Ethylenediaminetetraacetic acid – EDTA). 5μl of PCR product was mixed with 1μl of loading dye (dH2O, 15% glycerol, 1% orange dye) and subjected to electrophoresis for a minimum of 30minutes at 75V

before being visualised under UV light. Gel images were captured on a GelDoc-It 310 Imaging system (UVP).

2.2.3 ExoFAP PCR clean up

Purification of PCR products was performed using 2 hydrolytic enzymes added to 3 or 5 μl of PCR product as following:

Exonuclease I (20 U/μL, Thermo Fisher)…….. 0.5 μl
FastAP Thermosensitive Alkaline Phosphatase (1 U/μL, Thermo Fisher)……..…. 1 μl

Reaction times and T° were as following:

1. Enzyme incubation 37 °C for 15 minutes
2. Enzyme inactivation 80 °C for 15 minutes
3. Hold at 4 °C indefinitely

2.2.4 BigDye Terminator cycle

BigDye® Terminator v3.1 (Applied Biosystems)…….. 1 μl

BigDye® Terminator v1.1 & v3.1 5X Sequencing Buffer…….. 2 μl

Fw or Rv primer (10 μM)……..……1 μl

H_2O……..……11 μl

Reaction times and T° were as following:

96 °C 1 min

96 °C 10 secs
50 °C 5 secs
60 °C 4 mins
} 25 cycles

4 °C ∞

2.2.5 Ethanol precipitation

20 μl of sequencing reaction were precipitated according to the following protocol:

1. Briefly spin the 96 well plate;
2. Add 2 μl of 125 mM EDTA to each well;
3. Add 2 μl of Sodium acetate solution (3M) to each well;
4. Add 70 μl of 100 ethanol to each well;
5. Seal the plate with a plate sealer and mix inverting several times;
6. Incubate at RT for 15 minutes;
7. Spin plate at 2,000 g for 30 mins;
8. Invert the plate on tissue paper and spin briefly at 100 g;

9. Add 70 μl of 70% ethanol to each well;
10. Spin the plate at 1,650 g for 15 minutes;
11. Invert the plate on tissue paper and spin briefly at 100 g;
12. Allow the plate to air dry in the dark (without lid) for 10 minutes;
13. Resuspend in 10 μl Hi-Di™ Formamide (Applied Biosystems)

2.2.6 Sanger Sequencing

DNA resuspended in Hi-Di™ was heated for 2 mins at 95 °C and then sequenced with a 3130xl Genetic Analyzer. Raw data were suddenly analysed with Seqscape® v2.6 (ThermoFisher) or Mutation Surveyor® v4.0.5 (Softgenetics).

2.3 RNA isolation

RNA was isolated using different methods depending on the downstream applications.

2.3.1 RNA isolation for miRNA qRT-PCR analysis and RNAseq from cells and tissues

Total RNA was isolated from cells or muscle tissue using the mirVana™ miRNA Isolation Kit (Ambion) following manufacturer instructions.

2.3.2 RNA isolation for qRT-PCR

Total RNA isolation for qRT-PCR application was performed through a customized protocol with the RNAeasy mini kit (Qiagen).

A first step to prevent RNA degradation due to RNAse action was done with β–mercaptoethanol in RLT Buffer (1:100, Qiagen). Lysate was then passed through QIAshredder columns to increase RNA yield. Subsequent steps were performed as indicated on RNAeasy mini kit protocol and RNA eluted in 30-50 μl of nuclease free water in order to have a minimum concentration of 200 ng/μl.

2.3.3 RNA isolation for RT-PCR

Samples were homogenized using 1 ml Trizol® (Ambion) and incubated 5 mins at RT. Following incubation, 200 μl of chloroform were added for each ml of Trizol®. Tubes were then shaken vigorously for 15 secs, incubated for 2-3 mins at RT and centrifuged at 12,000 g for 15 mins at 4°C. Once the top aqueous phase is removed and placed in a new tube, 500 μl of 100% isopropanol per ml of Trizol® were added,

incubated at RT for 10 minutes and then span at 12,000 g for 20 mins at 4°C. Optionally, 1 μl of linear polyacrylamide can be added to increase RNA precipitation during this step.

After centrifugation supernatant is removed and the RNA pellet washed with 1 ml of 75% of ethanol per ml of Trizol used. Sample is vortexed, span at 7,500 g for 5 mins, ethanol is removed and the pellet is left to air dry for 5-10 mins. The pellet is resuspended in 30 μl of water incubating for 10-15 minutes at 55-60 °C.

Human *WARS* primers:

Primers pair	Temp.
1F3R	61
8F11R	59
11F13R	61

2.4 cDNA reverse transcription

Total RNA extracted from cells or zebrafish was reverse transcribed with High-Capacity cDNA Reverse Transcription Kit (Applied Biosystems). A minimum of 2 μg of RNA were used for a single reverse transcription reaction.

2.5 qRT-PCR

qRT-PCR reaction was prepared using the following mix:

iTaq™ Universal SYBR® Green Supermix (BioRad)…….…… 12.5 μl
Fw primer (10 mM)…….…….. 1.25 μl
Rv primer (10 mM)…….…….. 1.25 μl
H_2O……9μl
cDNA…… 1 μl

Reactions were performed in a 96-well plate using a Bio-Rad iCycler Thermal Cycler equipped with a MyiQ™ Single-Color Real-Time PCR Detection System.

The following primers were used:

Gene	Species	Fw primer	Rv primer

atxn1a	*D.r.*	GGGTGGAAGACCTGAAAACA	GCCGAACACAAAGAAAGGAT
atxn1b	*D.r.*	TACAGACATCGCCCACAGAG	CAGCGGCACTCCTAATGCT
hoxc6b	*D.r.*	CTGCGTCTTGTCAAATAGCGA	GCTTCAGACCAAGGCAAGAC
hoxc8	*D.r.*	CTCTCCGAGCCTCATGTTCC	ACCAGATCTTCACCTGTCGT
hoxc9	*D.r.*	GGGAAGCACAAAGACGACAA	CCTTGCTACCTCATATCGCC
hoxc10	*D.r.*	GGAGGGAATACGCAGGAAGA	ACGGACACCTCTTCTTTCGA
hoxc11a	*D.r.*	CCAGAGGATGAGGAGGAACA	CGCTCCAGTTCACGAATCTG
hoxc11b	*D.r.*	TGGACATCGCTTCTTCCTCA	TGTCTTCAGTTCTCCGCAGT
hoxd10	*D.r.*	GTTAACCAGTTGCTCGTCGG	CGCTGGAGGAGAAGAATTGC
hoxd11	*D.r.*	ACCAAATCTTCACTTGTCGGTC	CCGTTTCAACCTGCGATGAA
hoxd13	*D.r.*	CTGACAGAATGAAGCCGCTG	GGTTCAGAGAGCAATGATGGG
hoxa13a	*D.r.*	ACTGCCGATGGAGAGTTACC	AACACGTTTCTTCCTTCCGC
hoxa13b	*D.r.*	ACTAACGGGTGGAGCAGTC	TTGTGGCATATTCTCGTTCTAGT
β-act	*D.r.*	CGAGCTGTCTTCCCATCCA	TCACCAACGTAGCTGTCTTTCTG
ef1α	*D.r.*	CTGGAGGCCAGCTCAAACAT	ATCAAGAAGAGTAGTAGTACCG CTAGCATTAC
HOXC6	*H.s.*	AAAAGAGGAAAAGCGGGAAG	CGAGGGAGAAAGGGAGAGAG
HOXC8	*H.s.*	GGGAGACGGAGAAACAGTGA	AGGTGGGAGTGTGGTGAGAG
HOXC9	*H.s.*	AGACGCTGGAACTGGAGAAG	AGGCTGGGTAGGGTTTAGGA

HOXC11	*H.s.*	TGACTCTCGCTGTGGGACA	GAGGATTGTTCGGCTCAGG
HOTAIR	*H.s.*	GGAGTGGGGAGTGGAGAGA	CGTGGCATTTCTGGTCTTGT
TUBB	*H.s.*	GCTGGTGGAAAACACAGATG	GTTGAGGTCCCCGTAGGTG

Table 5. List of primers used for qRT-PCR reactions.

2.6 Animal Models

2.6.1 Fish strains and maintenance

Zebrafish (*Danio rerio*) of the wild type *golden* strain and Tg*(Isl1:GFP)* strain expressing GFP in the cranial motor neurons under control of the *islet1* promoter were used for experiments.

Adult fish were kept in fresh water at 28.5 °C. Males and females were paired and kept separated by a net the night before the embryos were required. The following day the net was removed. Embryos were collected and raised in E3 medium ((5mM NaCl,0.17mM KCl, 0.33mM CaCl2, 0.33mM MgS04, 0.1PPM methylene blue) and staged in hours or days post fertilization according to Kimmel's criteria (Kimmel *et al*.).

After 24 hours embryos were dechorionated manually or using pronase (0.5-2 mg/ml, Roche). Embryos and larvae were then euthanized in 4mg/ml tricaine methanesulfonate E3 medium mix (1:2; Westerfield, 2000) and fixed in 4% Paraformaldehyde (PFA) or frozen in dry ice depending on the needs.

2.6.2 Antisense oligonucleotide morpholino preparation

Antisense morpholino oligonucleotide (MO, Gene Tools LLC) against *rbm7* were designed to target an intron-exon or an exon-intron boundary in order to cause defective splicing. The following morpholinos against *rbm7* were used:

SPL *rbm7_In1-Ex2* MO*:* 5'-ATGGCCCAGCCTAGTGGAAAAAGAA-3';
SPL *rbm7_Ex2-In2* MO: 5'-ACGCAATAAGGAAAGTCCTACCGGT-3'
Two previously published morpholino against *exosc3* (Wan et al., 2012) and *exosc8* (Boczonadi *et al*., 2014) both these morpholinos target the translation start site (AUG)
AUG *exosc3* MO: 5'- TCCATGATGGAGGAGCGGAAAACAC-3';
AUG *exosc8* MO: 5′-TTTAAAACCAGCCGCCATGATGTTT-3′;
AUG *mbpa* MO: 5'-GGCCATTCTAGGTGTTGATCTGTTC-3'

Gene tools' standard control morpholino which does not have a target in zebrafish was used as negative control oligo:

CTRL MO: 5′-CCTCTTACCTCAGTTACAATTTATA-3'.

The MOs were re-suspended in 1x Danieau solution (0.4mM MgSO4, 58 mM NaCl,0.7mM KCl, 5mM HEPES, 0.6 mM Ca(NO3)2; pH 7.6; Westerfield, 2000).

2.6.3 Micro-needle preparation and microinjection

Borosilicate glass capillaries (Article # 1403550, Hilgenberg GmbH, Malsfeld, Germany) were pulled with a P97 Flaming Brown Micropipette Puller with a heat of 695, a pull of 70 and velocity of 60. Needles were filled using Microloader Tips (Eppendorf) with a mix of Danieau Buffer, Morpholino and Phenol red. Embryos were injected up to 2 cells stage with an Eppendorf Femtojet microinjector. The following quantities were injected for each morpholino:

SPL *rbm7_In1-Ex2* MO: 2.2 ng

SPL *rbm7_Ex2-In2* MO: 1.1 ng

AUG *exosc3* MO: 1.5 ng

AUG *exosc8* MO: 10 ng

AUG *mbpa* MO: 1 ng

CTRL MO: 5 ng

Morphant embryos were then visualized with an epifluorescence stereomicroscope (Leica MZ16F).

2.6.4 RT-PCR

RNA was extracted from ~20-40 fish at different developmental stages using the RNAeasy kit (Qiagen) as described above and reverse transcribed using the High Capacity Reverse Transcription kit (ThermoFisher).

rbm7 primers and conditions were used as published before in Giunta et al., 2016

exosc8 primers and conditions were used as published in Boczonadi et al., 2014

mbpb primers and conditions were used as published in (Nawaz et al., 2013)

β-actin primers and conditions were used as published in (Argenton et al., 2004)

2.7 CRISPR/Cas9 mutagenesis

2.7.1 Design of gRNAs

Guide RNAs were designed using CRISPRscan (http://www.crisprscan.org/).

2 gRNAs (Oligo1) were chosen

*rbm7*_Exon2_gRNA: taatacgactcactataGGGATTTTAACCTTGATCAAgttttagagctagaa

*rbm7*_Exon4_gRNA:

taatacgactcactataGGCCTCTGCATGTGCTGTGGgttttagagctagaa

the BLUE part being the actual guide RNA, the RED part the T7 promoter, the GREEN the overlapping crRNA-TracrRNA sequence (Oligo2) which will anneal to the generic oligo2: 5'-AAA AGC ACC GAC TCG GTG CCA CTT TTT CAA GTT GAT AAC GGA CTA GCC TTA TTT TAA CTT GCT ATT TCT AGC TCT AAA AC-3'

2.7.2 Annealing:

Annealing mix of oligo 1 to oligo 2 was as following:

MyTaq™ DNA Polymerase (Bioline) ……..…….. 0.2 µl

MyTaq™ reaction buffer (Bioline) ……..…….. 5 µl

Oligo1 (100 µM) …… 2 µl

Oligo2 (100 µM) ……..…… 2 µl

H_2O ……..……16 µl

Annealing conditions were as following:

Denaturation 95 °C……..…….5 mins

89°C……15 secs

83°C……15 secs

77°C……15 secs

71°C……15 secs

65°C……15 secs

59°C……..…….15 secs

53°C……15 secs

Annealing 50°C……..…….10 mins

Extension 72°C……10 mins

4°C…… ∞

The size of product was verified on an agarose gel and the annealed product was purified with the QIAquick PCR Purification Kit (Qiagen).

2.7.3 In vitro transcription

Guide RNAs were transcribed in vitro using 8 μl of annealed DNA product (60-120 ng/μl) using the MEGAshortscript Kit (ThermoFisher) as follows:

T7 10x reaction buffer…… 2 μl

T7 ATP solution (75 μM)…… 2 μl

T7 CTP solution (75 μM)…… 2 μl

T7 GTP solution (75 μM)…… 2 μl

T7 UTP solution (75 μM)…… 2 μl

DNA template…… 8 μl

T7 enzyme mix…… 2 μl

The mix was incubated at 37 °C overnight then DNAse treated with TURBO DNAse (Thermo Fisher).

The RNA was then eluted to 300 μl and purified with the miRvana kit (Ambion) adding 1.25 volumes of ethanol, spin through the column, add 700 μl of solution 1, spin, add 500 μl of solution 2/3, spin, add 500 μl, spin, elute in nuclease free water.

Cas9 RNA was transcribed from pCS2-nCas9n plasmid (Plasmid #47929, Addgene).

Size and quality of RNA was then checked on a 2.5% agarose gel.

2.7.4 Microinjection

Fish at 1 cell stage were injected into the cell or just below it using the following mix:

1 μl gRNA

1 μl Cas9 RNA

2.5 μl Danieau buffer

0.5 μl Phenol Red

2.7.5 Screening for mutations

Fish of min 10-15 fish were collected, genomic DNA was extracted with DNeasy Blood & Tissue Kit (Qiagen) following manufacturer instructions.

PCR was performed with zebrafish genomic DNA using the following intronic primers (Ta 59 °C):

Exon2: Fw 5'-TTGCAGGCAATTTATAGTTCACAGAAA-3'

Rv 5'-GGCATGAGGGTATGCTGAAA-3'

Exon4: Fw 5'-TGAGAGTGATCACATTTACACCTG-3'

Rv 5'- AAATCGTGACAGGCCTATGTTT-3'

PCR product was run on a 2% gel and purified with QIAquick PCR Purification Kit (Qiagen).

The PCR product was suddenly ligated into pGEM-T Easy Vector (Promega) using the following mix.

Rapid Ligation Buffer (2X)…… 5 µl

pGEM-T Easy Vector……1 µl

PCR product……3 µl

T4 DNA Ligase……1 µl

Ligation conditions:

16°C……..……...10 hours

65°C……..……...20 minutes

4°C…….. ∞

Ligation was performed using JM109 High Efficiency Competent Cells (Promega) adding 2 µl of ligation product to 10 µl of competent cells and following the protocol provided with the kit (Heat-shocking for 45-50 seconds).

150 µl of transformed cells were plated on LB/ampicillin plates.

Each colony was then amplified by PCR. PCR product was then run on 2% agarose gel to check the presence of the fragment.

If positive, 3 µl of PCR were transferred to a new 96 well plate and an ExoFAP reaction was performed on this product to remove unwanted deoxynucleotides and primers. The subsequent sequencing steps were performed as previously described.

2.7.6 High throughput gDNA extraction

For gDNA isolation from F1 single embryos (at least 48 hpf; with or without chorion) we used a lysis buffer containing 500 µl of NaOH (2.5 M) 20 µl of EDTA (0.5 M) in 50 ml of deionized H_2O. Each embryo was placed in a well in a 96 well plate and 15 µl of the mix were added. The plate was placed at 95°C for 30 mins and rapidly cooled down on ice. The alkaline solution was neutralized adding 1 volume of neutralizing buffer (40 mM of Tris-HCl; 325 mg in 50 ml of deionized H_2O).

Samples were let on ice for 10 minutes and then 5 µl of supernatant were used as template for PCR (Wilkinson et al., 2013).

2.8 Immunostaining and confocal imaging

Embryos at 48 hpf or 4.5 dpf were collected and fixed in 4% PFA in PBS at 4°C overnight. The following day the PFA was removed and fish were washed three times in PBS and once in dH_2O and partially permeabilised in cold acetone (-20°C). Acetone was removed after 7 minutes at -20°C and fish washed in dH_2O.

Water is removed and fish are washed three times with PBS-Tween20 (0.1%) (PBST). Samples older than 48 hpf are treated with Collagenase A in PBST (1mg/ml) to further permeabilize the tissues. Depending on the age of the embryos, samples were incubated at RT in Collagenase A for:

- 30 minutes if 3 days old
- 1 hour if 4 days old
- 1.5 hours if 5 days old

Collagenase A was removed and samples washed three times with PBST.

Samples were suddenly blocked with 5% horse serum for at least 1 hour.

Primary antibody was added at the correct concentration in 5% horse serum and samples incubated overnight at 4°C. Purkinje cells were stained with Parvalbumin7 antibody (a kind gift of Prof. Masahiko Hibi, Nagoya University, Japan; 1:1000, mouse ascites); Synaptic vesicles were stained with SV2 antibody (1:200, Developmental Studies Hybridoma Bank, Iowa).

The following day samples were washed thoroughly with PBST and the secondary antibody was added at the correct dilution in 5% horse serum (Alexa Fluor 488, Invitrogen, 1:500). Acetylcholine receptors were visualized by using Alexa Fluor 594 conjugated α-bungarotoxin (1 μg/ml, Invitrogen).

Samples were incubated at RT for at least 2 hours and eventually imaged in methylcellulose 3% using a Nikon A1R confocal. Z-stack images were generated by scanning through the whole body with a 10x objective and then images manipulated to have the best resolution with NIS-element AR 3.2 64 bit software.

2.9 Western blot

2.9.1 Bradford assay

Serial dilutions of bovine serum albumin (BSA) were previously prepared at concentrations of 0 mg/ml; 0.05 mg/ml; 0.1 mg/ml; 0.2 mg/ml; 0.3 mg/ml; 0.4 mg/ml; 0.5 mg/ml.

Protein assay dye reagent concentrate (Bio-Rad) was diluted 1:5 in H_2O.

Cells were lysed with 50 μl of PathScan® Sandwich ELISA Lysis Buffer (1X; Cell Signaling technology) or RIPA buffer.

10 μl of cell lysate/standard (cell lysate eventually diluted 1:10) were added to 190 μl of diluted Protein assay dye reagent concentrate and the concentration was measured with an Infinite® F50 (Tecan) plate reader.
Absorbance readings and concentrations of the standards were plotted in a graph and then concentration of the samples was calculated.

2.9.2 Gel electrophoresis

A maximum volume of 20 μl of cell lysate was mixed with 7.5 μl NuPAGE® LDS Sample Buffer (4X; Life technologies) and 3 μl of reducing agent. Samples were then boiled at 70°C for 10 mins and then a maximum volume of 30 μl of cell lysate was loaded into a 4-12% SDS–polyacrylamide gel. Molecular weight of the bands was compared to SeeBlue® Plus2 Pre-stained Protein Standard (ThermoFisher).

500 μl of NuPAGE® Antioxidant (ThermoFisher) was added to the internal chamber of the tank using NuPAGE® MES SDS Running Buffer (20X) (ThermoFisher) previously diluted 20 times as running buffer.

2.9.3 Protein transfer

Proteins were transferred to a PVDF membrane with an iBlot®2 PVDF Mini transfer stack (ThermoFisher). Efficiency of protein transfer was checked by red Ponceau staining. Membrane was washed thoroughly with TTBS (20 ml Tris-HCl pH 7.5, 29.2 g NaCl, 1 ml Tween20, Top up to 1 litre with dH_2O) and then blocked with 5% milk powder in TTBS for at least 30 minutes at RT. Primary antibodies were added at the correct concentration (RBM7, Abcam ab84116, 1:600; SNX15, Abcam ab172534, 1:500; β-actin, Sigma A1978, 1:2000;) in 5% milk in TTBS and incubated overnight at 4°C.
The following day the antibody was removed and the membrane was washed 3 X 10/15 mins in TTBS and then the secondary antibody was added in 5% milk in TTBS and incubate at RT for at least 1 hour (polyclonal swine anti-rabbit immunoglobulins/HRP or Polyclonal Rabbit Anti-mouse immunoglobulins/HRP; Dako, Denmark) and washed 3 X 10/15 mins.

2.9.4 Blot development

The membrane was incubated for 5 min in a dark place with Clarity™ Western ECL Blotting Substrate peroxide solution:luminol/enhancer solution 1:1 (Bio-rad) and then imaged with an Amersham Imager 600 (GE Healthcare Life Science).

2.10 Tissue culture

Human primary fibroblasts and immortalized myoblasts were grown in plastic flasks (CELLSTAR®, Greiner Bio-One International, Item No: 690175 - 25 cm^2 and 658175 – 75 cm^2). Fibroblasts were grown in 1X Dulbecco Modified Eagle Medium (*Gibco*®), 10% FBS (F7524, Sigma), 1% Pen/Strep (10,000 U/mL, *Gibco®)* unless otherwise specified.

2.11 Electron microscopy

Zebrafish at 4 dpf were fixed in 2% glutaraldehyde in sodium cacodylate buffer at 4 °C overnight and suddenly washed three times (15 min each) in cacodylate buffer, and then stained with 1% osmium tetroxide (Agar Scientific) in dH2O for 1 h. Fish were dehydrated using graded acetone (25, 50 and 75% and twice in 100%). Fish were impregnated through increasing concentration of resin in acetone (25, 50, 75 and 100%) and then embedded in 100% resin at 60 °C for 24 h (TAAB Lab. Equip). Ultra-thin transverse sections of ~70 nm were cut using a diamond knife on a Reichert Ultracut E ultramicrotome. The sections were stretched with chloroform to eliminate compression and mounted on pioloform-filmed copper grids. The grids were then stained with 2% aqueous uranyl acetate lead citrate and subsequently examined using a Philips CM 100 Compustage (FEI) Transmission Electron Microscope and digital images were collected using an AMT CCD camera (Deben) at the Electron Microscopy Research Services, Newcastle University.

3 Chapter 3: Results – Exome Sequencing and RNA sequencing

3.1 Diseases caused by impaired functionality of the exosome complex

The first identified condition caused by defects in the exosome complex's functions was the polymyositis/scleroderma syndrome (Wolfe et al., 1977), an autoimmune syndrome caused by the presence of auto-antibodies against antigen PM1/Scl in these patients (which was subsequently recognized to be the human exosome complex). Symptoms caused by PM/Scl syndrome are not neurological like most of the other exosome complex related diseases known so far. Symptoms can include chronic muscle inflammation, weakening/loss of muscle mass, hardening of the skin and disposition of calcium under the skin (scleroderma) (Staals and Pruijn, 2011).

More recently, Wan and colleagues (Wan et al., 2012) identified the first mutations on an exosome complex sub-unit (*EXOSC3*) which causes a dysfunction of the exosome causing pontocerebellar hypoplasia type 1 (PCH1).

Subsequently, our group identified mutations on subunit *EXOSC8* with overlapping symptoms of PCH1 and hypomyelination of the central nervous system in 22 children from three independent pedigrees (Boczonadi et al., 2014).

Mutations on *EXOSC2* sub-unit were identified as cause of neurological disorders in two unrelated German families in 2016 (Di Donato et al., 2016) with symptoms of hypomyelination, retinitis pigmentosa, hearing loss, premature ageing and others.

Soon after, our group published a new study were we describe a patient with a mutation on *RBM7* (a component of an exosome complex co-factor) with an SMA-like phenotype (Giunta et al., 2016).

In an attempt to discover new exosome complex related pathologies, we searched for mutations on exosome complex subunits and/or co-factors in an unresolved cohort of neurological patients and in databases, based on the symptoms of the subjects. Transcriptome analysis of primary fibroblasts from 2 subjects was also performed, in order to understand which genes were differentially expressed or differentially spliced due to impaired exosome complex functions.

3.2 Overview of the techniques

3.2.1 Next Generation Sequencing for identifying new mutations involved in pontocerebellar hypoplasia.

In the last few years, the development of new technologies for genome and transcriptome sequencing known as “Next Generation Sequencing platforms” have reduced the cost of DNA and RNA sequencing by many orders of magnitude compared to Sanger sequencing or standard gene expression analysis techniques (Reon and Dutta, 2016). These technologies allow to have a high throughput screening potentially for all mutations in the coding sequences of a given genome as well as transcript levels by Whole Exome Sequencing (WES; Bamshad et al., 2011) and RNA-sequencing (RNA-seq; Reon and Dutta, 2016). The use of these technologies releases a huge amount of data (Hrdlickova et al., 2016). On average, exome sequencing identifies ~20,000 single nucleotide variants (SNV) in a European American genome (Bamshad et al., 2011). If we need to analyse or compare several different samples, there is a need to reduce the number of potentially interesting variants to an acceptable number through filtering of potentially interesting genes/transcripts.

3.2.2 Variants filtering of exome sequencing data

Out of all the SNV identified by exome sequencing, on average 95% are already known as polymorphisms and non-pathogenic (Bamshad et al., 2011). Techniques to screen this massive amount of data from the background of common non-pathogenic variants vary. One of the most used approaches is the comparison of exome sequencing of closely or not related individuals, sharing a common phenotype, with control subjects DNAs, available in public databases such as dbSNP93, 1000 Genomes Project (1000 Genomes Project Consortium et al., 2010) and Exome Variant Server (Johnston and Biesecker, 2013), screening for rare or novel alleles. The disease-causing variant might be present in the database as well, although with a very low frequency (usually less than 2%). Then a variant filtering methodology has to be designed, in order to further reduce the number of variants that will be analysed for segregation analysis in the families.

There is no optimal statistical test or filtering strategy, given the variability of the gene functions and functional mutations, it depends on the type of analysis that needs to be performed (Do et al., 2012).

3.2.3 Select variants based on gene functions

Some studies have shown data filtering is very useful when applied to searching for specific gene functions, noticeably increasing power. Most of the annotation tools commonly used such as ANNOVAR (Wang et al., 2010), PolyPhen2 (Adzhubei et al., 2013), SIFT (Kumar et al., 2009) also provide annotation on putative gene functions. Other databases such as KEGG (Kanehisa and Goto, 2000) and WikiPathways (Kutmon et al., 2016) provide functional annotations about metabolic pathways and enzymes. Including functional filtering in the exome sequencing analysis can greatly reduce the number of candidate variants (Friedrichs et al., 2016).

3.2.4 Select variants based on mode of inheritance

Mode of inheritance can be thought as filtering strategy for some diseases. For recessive models only homozygous (for consanguineous families) or compound heterozygous (for non-consanguineous families) variants should be considered (Fig. 3.1; Ku et al., 2011). The combination of more of the filtering strategies is usually applied and improves the detection rate.

3.2.5 Segregation analysis within families

In order to confirm the pathogenicity of a mutation identified by exome sequencing, it is important to analyse ancestors and/or progeny - preferably with a similar disease phenotype - to confirm the segregation within the family and to investigate the inheritance pattern of the disease. Study of the family tree can give much information about the pathology and the type of inheritance (Fig. 3.1; Becker et al., 2011). If no family member with the same symptoms is present, analysis of the parents (so called *trio* analysis) can be helpful to highlight genes which are heterozygous in non-affected subjects (if it is an autosomal recessive disease model) and therefore narrow down the number of total candidate genes (Zhu et al., 2015).

3.2.6 Ethnic and population differences

Special attention needs to be paid when analysing exome sequencing from small ethnic groups which are not frequently studied, even more if it is about consanguineous families (Foo et al., 2012) as some variants may be more frequent in some populations but absent in others. Alternatively, if a control database from an ethnically matched group is not available, it would be good to sequence at least a sufficient number of non-affected individuals from the same population.

3.2.7 RNA-sequencing

RNA-seq technology aims to provide a complete profile of the whole transcript of a cell or tissue. Transcriptomic analysis is very important in some cases, in order to understand what pathogenic or compensatory mechanisms have been triggered within the cell at a specific developmental stage. The trigger may be a mutation (Bova et al., 2016) or an exogenous factor such as a drug or an infection (Benson et al., 2016) (Rolfe et al., 2016). RNA-seq allows to identify differences in expression of mRNA as well as non-coding RNAs. Differences in RNA splicing can also be recognised (Griffith et al., 2015).

Something which is very important to consider when doing RNA-seq analysis is tissue specificity of gene expression, which becomes particularly relevant when it comes to tissue specific diseases, especially because obtaining biopsies from specifically affected tissues may be impossible. Brain and nerves can only be collected post-mortem and, unlike animal tissues which can be collected and conserved in a controlled environment, post-mortem tissues can only be collected naturally, which often causes degradation of RNA (Sidova et al., 2015). High RNA

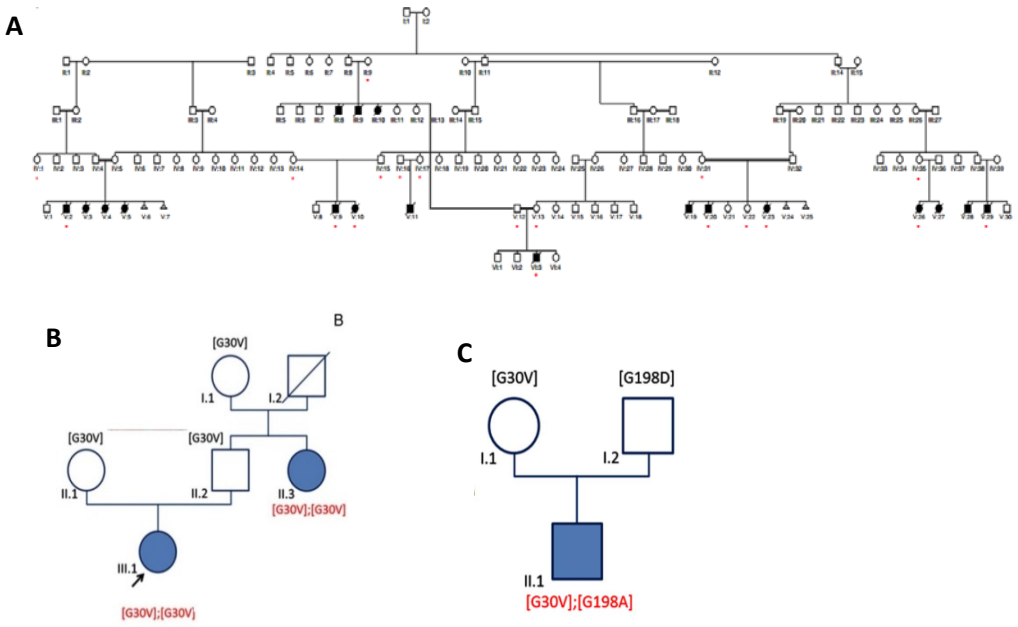

Figure 3.1 **Studying large consanguineous families genotype/phenotype correlation it is possible to easily identify recessive inheritance of a given mutation.** Here the example of *EXOSC8* mutation (A). For non-consanguineous families, *trio* analysis can help to identify either homozygous (B) or compound heterozygous mutations as for *EXOSC2* mutation (C). Images modified from Boczonadi et al., 2014 and Di Donato et al., 2016.

quality is fundamental for RNA-seq analysis.

Therefore in some cases transcriptomic analysis has to rely on primary fibroblasts, which are easily accessible, although gene expression may be undoubtedly different than in neurons. Gene expression analysis in fibroblast can be still useful to give indications of a potential molecular pathomechanism.

3.3 Results

3.3.1 PCH patients cohort – Identification of known mutations

In an attempt to discover new patients with exosomal deficiencies, Sanger sequencing was performed on 17 patients of Roma ethnic origin with pontocerebellar hypoplasia type 1, looking for two founder mutations on *EXOSC8* and *EXOSC3* which were previously reported to be disease causing (Wan et al., 2012) (Boczonadi et al., 2014).

A known homozygous c.92G>C; p.31G>A mutation on *EXOSC3* was identified in three patients (308/3, 792/3 and T.M.) with a predominant PCH1 phenotype.

All the other subjects were negative for mutations in *EXOSC8* and *EXOSC3*.

Whole Exome Sequencing (WES) was then performed on some of the remaining samples in order to identify the causes of the pathology.

Bioinformatic analysis and filtering was performed by Dr. Helen Griffin and Dr. Angela Pyle (Newcastle University), respectively. Another known c.919G>T; p.307A>S mutation in TSEN54 was identified in another patient (K.E.), which is a common cause for pontocerebellar hypoplasia type 1, 2, 4 and 5 (Simonati et al., 2011) (Namavar et al., 2011c). The variant was found to be heterozygous in both parents.

In other 2 patients, non-reported mutations on another gene (LAMP2) have been identified (c.1114_1116del and 1171G>A; p.391V>I).

LAMP2 (Lysosomal Associated Membrane Protein 2) is situated on Chr:X, the mutation is X-linked recessive in both male patients. The mother of one of the patients is a heterozygous healthy carrier. Reported mutations on LAMP2 so far have been linked to Danon disease (Di Mauro et al., 2007) with symptoms of cardiomyopathy, myopathy, mental retardation and cardiac failure.

Very recently our collaborators contacted our group upon identification of a patient who presented with cerebellar hypoplasia and spinal motor neuropathywith a homozygous mutation in another gene related to exosome complex functions. The mutation is heterozygous in both consanguineous parents of Hispanic origin and never been reported in human. We will perform further analysis of this mutation upon receipt of primary fibroblasts.

Patient code	Mutation	Clinical presentation	WES
308/3	*EXOSC3* c.92G>C; p.31G>A	PCH1	NO
792/3	*EXOSC3* c.92G>C; p.31G>A	PCH1	NO
T.M.	*EXOSC3* c.92G>C; p.31G>A	PCH1	YES
K.E.	TSEN54 c.919G>T; p.307A>S	PCH1	YES
K.R.	LAMP2 c.1114_1116del	PCH1	YES
EB/806	LAMP2 1171G>A; p.391V>I	PCH1	YES
P.1	*RBM7* c.236C > G; p.P79R	SMA-like	YES
P.2	New Gene	PCH1	YES

Table 6. Patients cohort with PCH symptoms and mutations identified.

3.3.2 Identification of a novel pathogenic mutation in RBM7

In an attempt to identify new mutations related to exosomal proteins deficiencies, a patient with a SMA-like phenotype was brought to our attention by Prof. O. Elpeleg and Dr. S. Edvardson (Hebrew University Medical Center, Jerusalem, Israel).

The patient was the youngest child of seven siblings of consanguineous parents of Palestinian background. Family history was negative for similar symptoms. Muscle weakness, both proximal and distal was apparent and required mechanical ventilation. During the last episode of respiratory decompensation the patient died at age 28 months (Giunta et al., 2016). Pregnancy, delivery and perinatal course were uneventfulexcept for breech presentation which necessitated caesarean section. Initial concerns were raised around one month of age as hypotonia with poor sucking and failure to thrive were observed. No developmental regression or cognitive difficulties were noted but gross motor abilities plateaued around 1 year of age when unsupported brief sitting was achieved (Giunta et al., 2016). At this time, muscle biopsy showed fibre type grouping of small and hypertrophic fibres, compatible with SMA (Fig. X). Paraffin embedded sections displayed sheets of foamy macrophages (CD68-immunopositive), and only few myofibers, consistent with macrophagic myofasciitis. Electromyography/nerve conduction velocity (NCV) was also compatible with SMA. SMN1 analysis showed two normal copies. No other significant alterations were evident on H&E, GTC, ATPase9.4, ATPase4.3, NADH, SDH/COX, PAS, PAS+ D and ORO stains (Giunta et al., 2016).

Exome sequencing analysis identified homozygous variants that segregate in the family in 2 different genes: *SNX15* and *RBM7*. Mutation in *SNX15* was discarded based on published gene functions. SNX15 published data show its involvement in protein trafficking and amyloid beta generation (Feng et al., 2015) (Phillips et al., 2001). Furthermore, western blot analysis showed a 63% reduction in RBM7 protein levels but no reduction of SNX15 (Fig. 3.2).

RBM7 is a sub-unit of NEXT, a co-factor of the exosome complex (Norbury, 2011) which is known to be responsible for binding and carry toward the exosome complex non-coding RNAs such as the PROMoter uPstream Transcripts (PROMPTs; Preker et al., 2011) and in splicing regulation (Guo et al., 2003).

The c.236C > G; p.Pro79Arg (Fig. 3.2) mutation is located within the highly conserved RNA Recognition Motif (RRM) Domain (Hrossova et al., 2015) and is

predicted to be pathogenic, affecting the structure of the binding domain as well as the splice site (according to MutationTaster), decreasing the stability of the protein structure (MuPro -http://www.ics.uci.edu/~baldig/mutation.html; Confidence Score: -0.068480655 and Confidence Score: -0.644794635393117). In silico analysis with PROVEAN (http://provean.jcvi.org/index.php) also predicted the mutation to be deleterious with a score of -4.49. Align-GVGD (http://agvgd.iarc.fr/agvgd_input.php) scored it Class C65 (most likely to interfere with protein functions). All these *in silico* prediction are overall in accord with the western blot analysis (Fig. 3.2) which show reduced protein levels in RBM7 mutant cells Given the predominantly neuromuscular phenotype and (partially) overlapping symptoms caused by mutations in different sub-units or co-factors of the exosome complex, an investigation was carried out in order to understand if any common molecular feature that links the pathologies may occur. RNA sequencing analysis on *EXOSC8* and *RBM7* mutant primary fibroblasts was then performed and compared to control primary fibroblasts data.

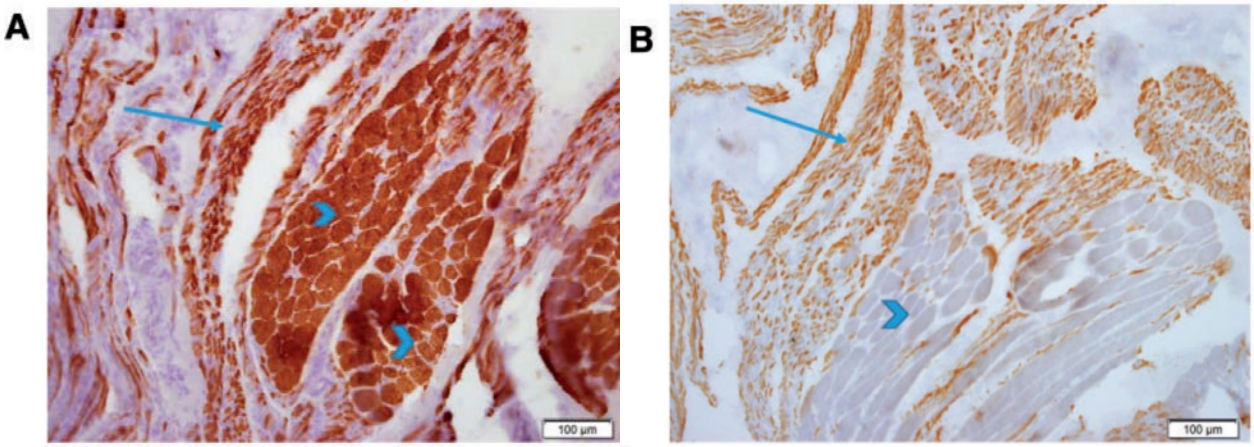

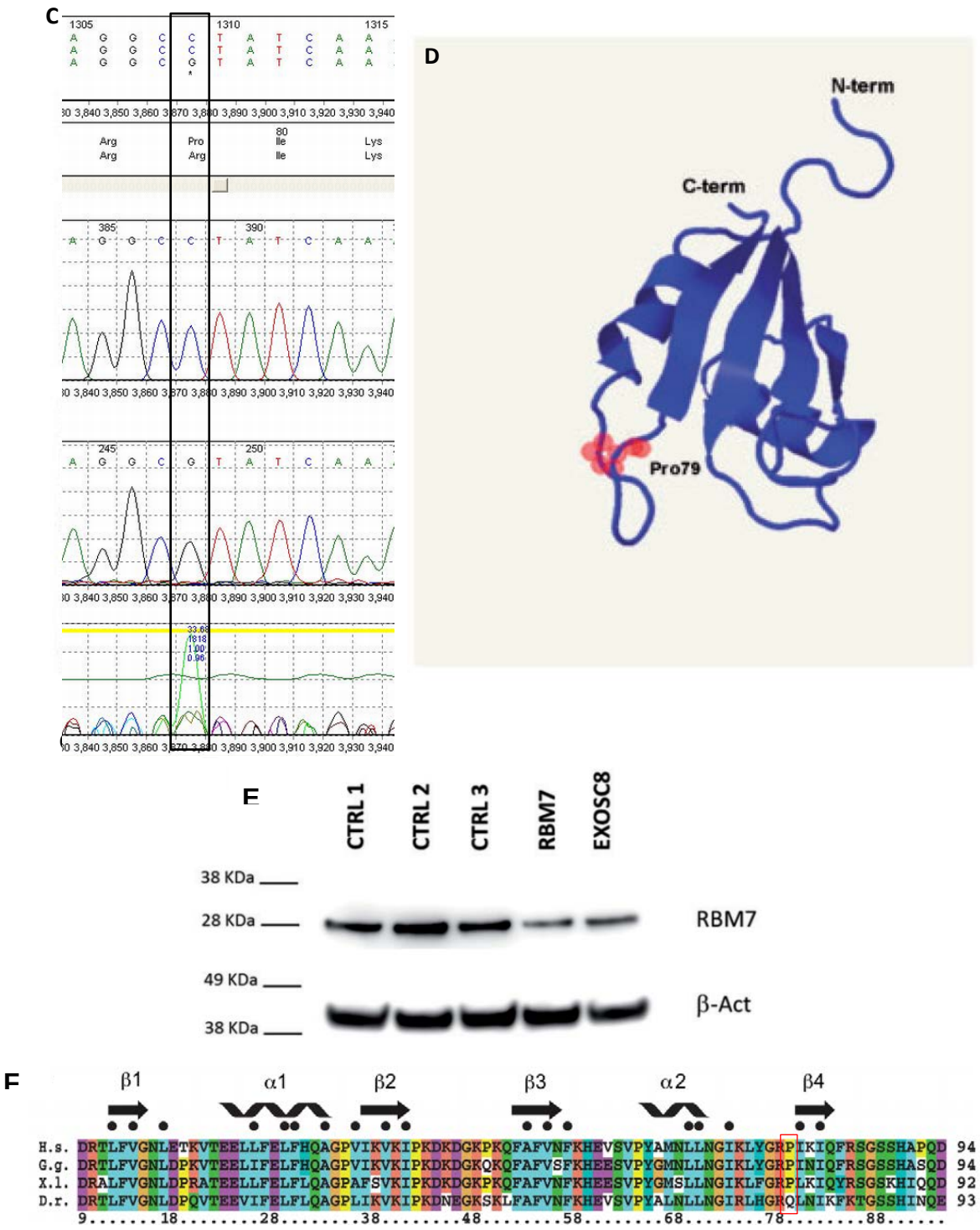

Figure 3.2 **Muscle biopsies**, e**lectropherogram showing the mutation P79G, protein structure and WB analysis. Below comparison of the highly conserved RBM7 RNA recognition motif.** Frozen sections stained with immunohistochemical stains for slow- (A) and fast-myosin (B) display striated muscle tissue with large group atrophy, includingatrophic myofibers of both types, alongside groups of hypertrophic myofibers, most of them type 1.Images showing position of the mutation in the highly conserved RNA recognition motif in RBM7 (C, D). 3D image was created using Phyre2 (Kelley et al., 2015) according to the structure presented by Hrossova et al., 2015; Western blot analysis shows reduced protein levels of RBM7 as well as EXOSC8 in *RBM7* mutant fibroblasts, compared to controls (E). In yeast, EXOSC3 mutations cause the impossibility of the protein to assemble to the exosome complex and the mutated EXOSC3 is eventually degraded by the proteasome (Fasken et al., 2017). It may be a similar degradation mechanism happens for RBM7; Comparison of the RRM in different species. The mutated P79 is highlighted in red (from Hrossova et al., 2015; F).

3.3.3 Agilent analysis of RNA sample quality

In order to proceed with RNA-seq analysis it is essential to have high quality RNA. RNA is easily degraded either before extraction from cells or tissues by endogenous RNAse or after, by chemical and physical reactions such as ion interaction with the single strand (Forconi and Herschlag, 2009). Tissues and cells need to be stored properly (ideally snap-frozen in liquid nitrogen and conserved at -80 °C). RNA can also be conserved for long times at -80 °C. Numerous freeze-thawing cycles are known to have a negative effect on RNA quality and integrity.
RNA quality can be assessed with an Agilent Bioanalyzer 2100 which is able to provide an RNA Integrity Number (RIN; Schroeder et al., 2006). RIN goes from 1 to 10 and is inversely related to degradation of the sample (higher the number, lower the degradation of the sample).
The machine is based on a microcapillary electrophoretic principle and is able to provide an electropherogram which shows the abundance and size of RNA based on peaks area and retention time (Fig. 3.3). A good quality RNA should show clearly two peaks which correspond to 18S and 28S rRNA, which in normal conditions are largely the most abundant. Noise or background in the electropherogram indicates degraded RNA. A reduction in the intensity of the 18S and 28S signal and increase in the signal toward the left indicates presence of short-fragmented RNA (Fig. 3.3). The electropherogram can be recapitulated by the representation of an agarose gel analysis on the right hand side of the screen.

3.3.4 Results of RNA quality control

Primary fibroblasts from patients and controls were cultured as described in Materials & Methods. The cell pellet was collected and frozen in dry ice straight away. Samples were then kept at -80 °*C.*

A big RIN variation could be noticed when re-analysing the same samples. This was probably due to genomic DNA contamination. We were able to obtain a repeatable high RIN treating the RNA sample with DNAse before the analysis (as described in materials & methods), therefore reducing gDNA contamination.

Only samples with a RIN >8 were sent for RNA-seq analysis. Three biological replicates for each cell line were analysed.

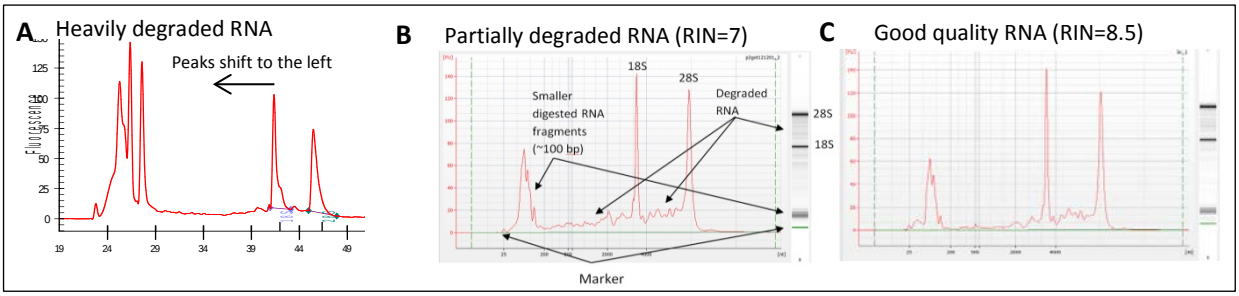

Figure 3.3 **Representative Agilent Bioanalyzer 2100 electropherograms.** Good quality RNA shows a graph with 2 higher peaks which represent 18S and 28S rRNA (C). The X-axis show the retention time and it is directly proportional to the size of the fragments. The lower peak at the left of the graph should be as little as possible, as it represents shorter, digested RNA fragments. The small noisy or background peaks in between are also an indication of degraded RNA. On the right hand side of each graph there is a representation of an agarose gel with the same RNA. Representation of an electropherogram of partially degraded RNA (B). The noisy peaks are slightly bigger than in (C). When RNA is heavily degraded, the peaks are shifted to the left (A).

3.3.5 RNA-seq analysis results

Total RNA-seq analysis was performed by AROS Applied Biotechnology A/S (Denmark) using the Illumina HiSeq 2500 platform. RNA-seq analysis of *RBM7* and *EXOSC8* cells versus control primary fibroblasts showed several transcripts differentially expressed including coding and non-coding RNAs (Table 4). Bioinformatic analysis was performed by Dr. Yaobo Xu, Newcastle University. Considering an adjusted p-value ≤ 0.05 and Log2-fold change of ±1, *RBM7* mutant cells showed 312 differentially expressed transcripts compared to controls and *EXOSC8* mutants showed 193 differentially expressed transcripts, 62 of them being shared between the 2 primary fibroblast lines compared to controls (Fig. 3.4). Three biological replicates were analysed for each cell line.

Notably, the two sets of transcripts show a high correlation following the same pattern of differential expression (as shown in Fig. 3.4) indicating a shared molecular mechanism that drives up or down regulation of a given gene. 13 of the common differentially expressed transcripts are involved in neurological functions: CACNA1G, HOXC8, PITX1, HOXC11, GNAZ, PCDH10, NTNG1, SOX11, HOXC9, HOXC10, HOXC6, HOTAIR, OMD (Fig. 3.5).

Only 8 of the 62 common differentially expressed genes are AU-rich. Notably, 50% of them belong to the group above - involved in neurological functions: OMD, HOXC6, NTNG1, SOX11, PDE4B, WNK3, TBX5, KLHL3 (Table 5).

18 of the 62 common differentially expressed transcripts are non-coding RNAs (Table 4).

RNA-seq data were confirmed through qRT-PCR (Fig 3.6). Expression levels of the 4 genes analysed show a high level of correlation either for *RBM7* mutant cells or for *EXOSC8* mutant cells (respectively $R^2 = 0.98$ and $R^2 = 0.99$).

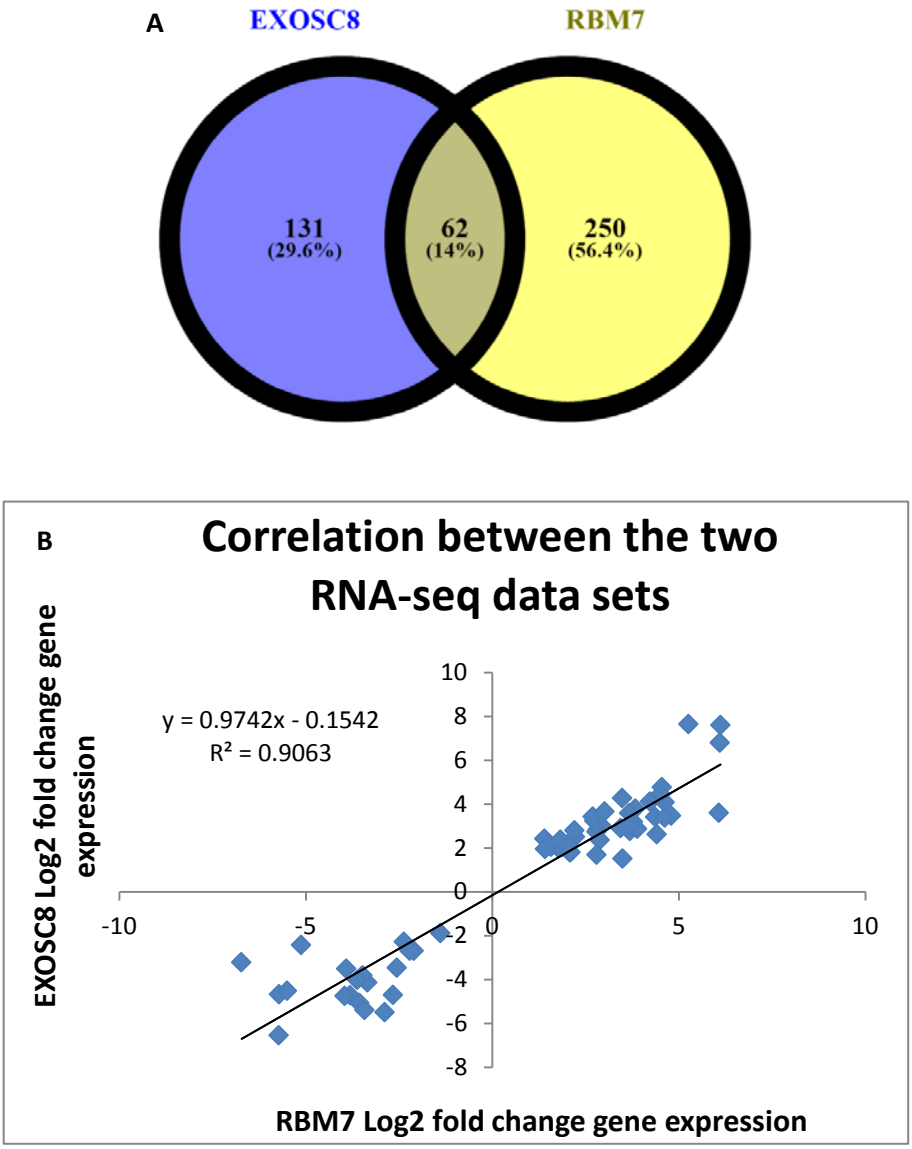

Figure 3.4 **Summary of RNA-seq data.** (A) Venn diagram showing number of differentially expressed transcripts for each mutant line. 14% of the total number is shared between the two. (B) The 62 shared transcripts follow same pattern of up or downregulation.

Gene	Gene name	RBM7 Log2 fold change	EXOSC8 Log2 fold change	Gene type
CACNA1G	calcium channel, voltage-dependent, T type, alpha 1G subunit	3.691032007	2.767291607	Protein coding
HOXC8	homeobox c8, transcription factor	1.396425863	2.419657474	Protein coding
DGAT2	Diacylglycerol O-Acyltransferase Homolog 2	4.410700623	2.622619732	Protein coding
PEG10	paternally expressed 10, imprinted gene	2.07534546	1.798544111	Protein coding
PITX1	paired-like homeodomain 1, transcription regulation	4.551147928	4.762613373	Protein coding
ZNF334	zinc finger protein	2.054463408	2.096171883	Protein coding
SFRP1	secreted frizzled-related protein 1, Wnt pathway	4.79885953	3.466095963	Protein coding
TCF21	transcription factor 21	4.364849155	3.415167911	Protein coding
HOXC6	homeobox c6, transcription factor	1.827229548	2.372816325	Protein coding
WNK3	lysine deficient protein kinase 3	2.694941819	3.429503882	Protein coding
HOXC11	homeobox c11, transcription factor	6.116841804	7.594757502	Protein coding
PTGER2	prostaglandin E receptor	2.795316287	1.692521515	Protein coding
PDE4B	phosphodiesterase 4B, cAMP-specific	1.417020499	1.944871591	Protein coding
GNAZ	guanine nucleotide binding protein	1.58414185	2.050887623	Protein coding
TCEAL7	transcription elongation factor A (SII)-like 7	1.865112273	2.035861836	Protein coding
HOXC10	homeobox c10, transcription factor	6.105422717	6.79186005	Protein coding
KCNMB4	potassium channel	3.774588508	3.18771346	Protein coding
IGF2BP3	(insulin-like growth factor 2 mRNA binding protein 3	3.445626323	2.902385839	Protein coding
PCDH10	protocadherin 10	3.888768259	2.866653042	Protein coding
MCTP2	(multiple C2 domains, transmembrane 2)	3.685804339	3.01777966	Protein coding
SLC14A1	solute carrier	3.835288902	3.786043531	Protein coding
KLHL3	kelch like family member 3	2.106158547	1.809268059	Protein coding
UCHL1	ubiquitin carboxyl-terminal esterase L1 (ubiquitin thiolesterase)	1.762819833	2.022851498	Protein coding

HOXC9	homeobox c9, transcription factor	2.207722452	2.803054114	Protein coding
NTNG1	netrin G1, axon guidance	2.735818992	3.235429173	Protein coding
TMEM155	transmembrane protein 155	2.225865777	2.509314216	Protein coding
RNF180	ring finger protein 180, ubiquitin protein ligase	2.844350479	2.852119379	Protein coding
ZMAT4	zinc finger matrin type 4	6.074879489	3.591657612	Protein coding
ZNF804A	zinc finger protein	4.62758129	3.37353952	Protein coding
PLEKHG5	pleckstrin homology domain containing, family G	1.858371049	2.03224899	Protein coding
SOX11	SRY (sex determining region Y)-box 11, transcription factor	4.234538566	4.107218641	Protein coding
CLEC12A	C-type lectin domain family 12, member A	-5.709574946	-4.675362953	Protein coding
IL20RB	interleukin 20 receptor beta	-5.121742683	-2.427950261	Protein coding
GRIA1	glutamate receptor	-3.561025711	-5.068887638	Protein coding
GSTM1	glutathion S transferase	-3.911425405	-3.500338869	Protein coding
TSPAN2	tetraspanin 2	-3.469786366	-3.8183497	Protein coding
UBL4B	ubiquitin-like protein 4b	-6.557094147	-6.640033107	Protein coding
CLEC2A	c-type lectin domain family 2A	-6.72183227	-3.21611715	Protein coding
OMD	osteomodulin	-2.66081377	-4.708887346	Protein coding
PILRB	paired immunoglobin-like type 2 receptors	-1.390971792	-1.894120381	Protein coding
TNFSF18	tumor necrosis factor (ligand) superfamily, member 18	-3.81028222	-4.723342904	Protein coding
L1TD1	LINE-1 type transposase domain containing 1	-3.617196089	-4.022066803	protein_coding
TBX5	t-box 5, transcription factor	-2.878300285	-5.488105064	Protein coding
KIF26A	kinesin family member 26A	-3.34455908	-4.127845901	Protein coding
AL162151.3		-2.21360557	-2.691774485	processed_pseudogene
HTATSF1P2	HIV-1 Tat specific factor 1 pseudogene 2	-2.556743643	-3.466975903	processed_pseudogene
RPL3P2	ribosomal protein L3 pseudogene	-2.096968531	-2.684915229	processed_pseudogene

RP5-857K21.11	unknown sequence, not overlapping with any gene	-5.501265385	-4.521465668	unprocessed_pseudogene
VTRNA1-2	vault RNA 1-2	-2.370807682	-2.280895671	misc_RNA
TARID	Homo sapiens TCF21 antisense RNA inducing promoter demethylation (TARID), long non-coding RNA	3.669128047	3.584094537	Antisense
HOTAIR	Hox transcript antisense RNA	5.264874941	7.642425264	Antisense
FLG-AS1		3.495582748	1.516653405	Antisense
TBX5-AS1		-3.423873961	-5.387431953	Antisense
LINC01397	long intergenic non-protein coding RNA 1397	-5.722161492	-6.540036225	Antisense
HOXC-AS2		3.48199326	4.271027646	processed_transcript
HOXC-AS3		4.513606333	4.446897002	processed_transcript
AC016757.3	unknown sequence	4.62825053	4.073858065	processed_transcript
AF131215.2	unknown sequence in intron of XKR6 gene, a bit overlapping with 5.9	2.797832461	2.7346828	sense_intronic
AF131215.9	unknown sequence in intron of XKR6 gene	2.887922063	2.363293297	sense_intronic
FLJ12825		3.009818227	3.660348996	lincRNA
RP1-15D23.2	unknown sequence, not overlapping with any gene	-3.955064919	-4.750905355	lincRNA
LINC00869		2.938100879	3.005697201	lincRNA

Table 7. List of common differentially expressed transcripts in RBM7 and EXOSC8 mutant fibroblasts compared to control.

Gene Symbol	RBM7 Log2 Fold Change	EXOSC8 Log2 Fold Change	ARE	Location
TBX5	-2.8783	-5.48811	CTATTTATTTATA	1201-1213
OMD	-2.66081	-4.70889	ATATATTTAGAAT	88-100
KLHL3	2.106159	1.809268	TAAAATTTATTAT	3741-3753
NTNG1	2.735819	3.235429	GATTATTTATAAT	2253-2265
SOX11	4.234539	4.107219	TTTTATTTAAAAA	4497-4509
PDE4B	1.41702	1.944872	ATTAATTTATATA	1008-1020
WNK3	2.694942	3.429504	TAATATTTACAAT	2498-2510
HOXC6	1.82723	2.372816	TTATATTTATGTT	638-650

Table 8. List of common differentially expressed ARE genes in *RBM7* and *EXOSC8* mutant fibroblasts compared to controls.

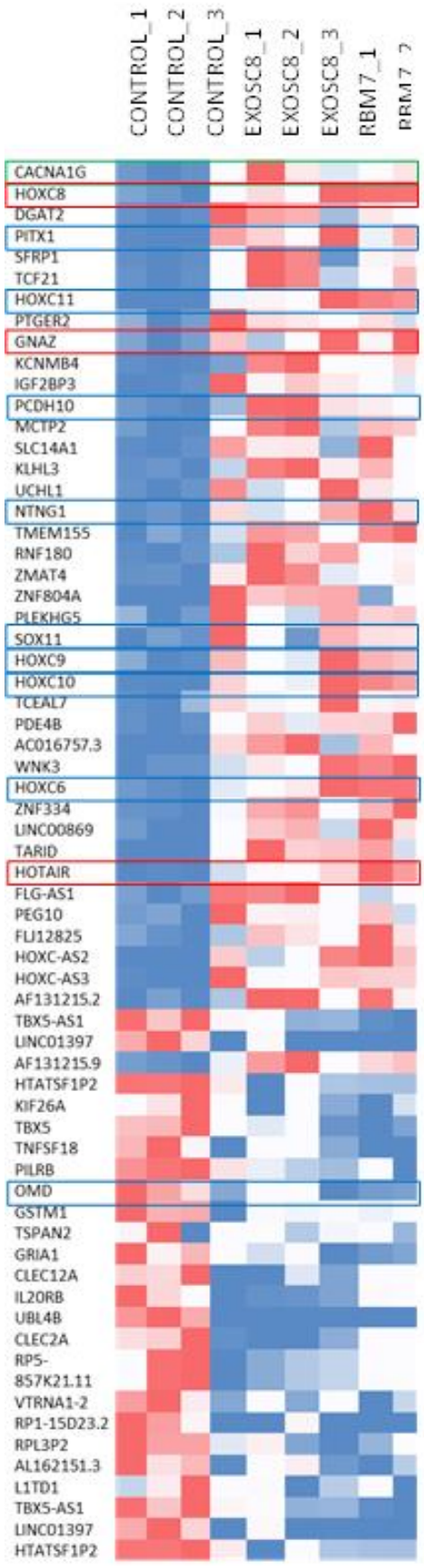

Figure 3.5 **Heatmap showing the pattern of expression of the 62 shared transcripts.** Red indicates higher counts, white average and blue low counts. Highlighted in Blue: genes listed on Pantherdb.org; in green listed on Reactome.org; red found function through PubMed.

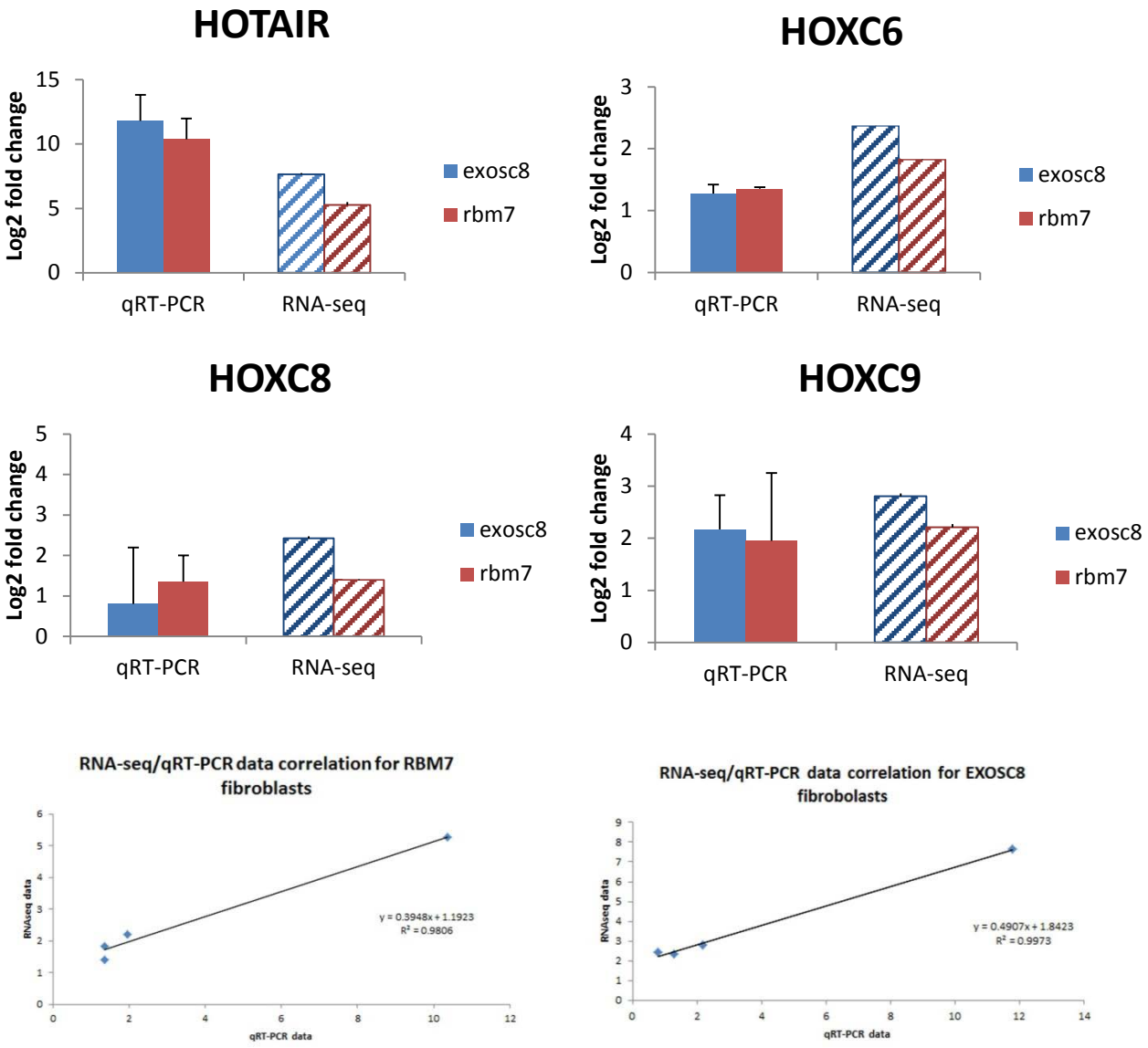

Figure 3.6 **RNA-seq data quality was confirmed by testing 4 transcripts via qRT-PCR (HOTAIR, HOXC6, HOXC8 and HOXC9).** The two datasets show a high correlation.

3.3.6 Alternative splicing analysis

Analysis of splicing isoforms in mutant cells was also performed. Pre-RNA splicing is known to be secondarily regulated by the exosome complex which, in turn, regulates the expression of splicing factors (Zhang et al., 2015).

Analysis was performed on the same RNA-seq data set (by Dr. Yaobo Xu) and shown as “sashimi plots” (Katz et al., 2015).

3.3.7 sashimi_plot

sashimi_plot is a graphic form for visualization of alternative splicing events in a given set of RNA-seq data, based on the MISO (mixture-of-isoforms) model (Katz et al., 2010).

The MISO model provides a series of parameters to identify alternative splicing events and their reliability in our transcriptome data such as the count of alternatively spliced isoforms, the type of event (Skipped Exons, Mutually exclusive exons, Retained Introns, Alternative 3’ splice sites, Alternative 5’ splice sites), significance of the differences (shown as “Bayes Factor” – BF), PSI (or Ψ - Percentage Spliced In).

The sashimi plot allows direct visualization of alternative events. Alignments in exons are represented as read densities, therefore exons result to be thicker and introns thinner. Splice junctions are drawn as arcs, connecting the two exons (Katz et al., 2015). Thickness of the arcs is proportional to the number of reads corresponding to a given splicing event (Fig. 3.8).

Several differential splicing events were identified. Some of them are also common between the two cell lines, meaning that they happen in the same locus and it is the same type of event (e.g. skipped exon), but in different proportions (Fig. 3.7).

RNA-seq analysis identified the same differential splicing event in *RBM7* and *EXOSC8* mutant cells in *TMEM119*, COL6A3, RPL17/C18ORF32 and finally an unknown transcript not mapped on ensemble (Fig. 3.8). The other events are summarized in Fig. 3.7

3.3.8 Biological function of the mis-spliced genes

TMEM119/*OBIF* (Transmembrane Protein 119/ Osteoblast Induction Factor) has 4 protein coding splicing variants (ENSG00000183160) of 28 aa, 44 aa, 140 aa, 283 aa.

OBIF is known to be expressed as a single transmembrane protein, strongly expressed in osteoblasts in mouse (Mizuhashi et al., 2012), knock-down of *OBIF* inhibits osteoblastic differentiation of pre-osteoblastic cells *in vitro*. *OBIF*$^{-/-}$ mice display reduced bone volume in the femur. Subsequently, the same group showed OBIF expression (the 283 aa isoform) is also important for bone mineralization and spermatogenesis suggesting that OBIF plays a role in differentiation of a number of tissues (Mizuhashi et al., 2015). TMEM119 was also shown to induce differentiation of myoblasts into osteoblasts and inhibit differentiation of myoblasts into myotubes (Tagliaferri et al., 2015). Furthermore, the same 283 aa isoform was found to be a stable marker of microglia in human and mouse (Satoh et al., 2016) (Bennett et al., 2016).

COL6A3 (Collagen Type VI Alpha 3) has 15 splicing variants, 10 of them being protein coding (ENSG00000163359). The longest isoform encodes for a 3,177 aa protein, the shortest for a 173 aa protein. Differentially spliced isoforms are present in pancreatic (Arafat et al., 2011) as well as colon, bladder and prostate cancer (Thorsen et al., 2008). *COL6A3* in human has 44 exons, mutations in this gene have been linked to dystonia. High level of expression in mouse was seen in brainstem and midbrain. Suppression of splicing of exon 41in zebrafish resulted in errors of motor neuron pathfinding, branching, and extension, suppression of other exons resulted in phenotypes more closely resembling other diseases related to COL6A3 such as Ullrich congenital muscular dystrophy or Bethlem myopathy(Balint and Bhatia, 2015). Interestingly, an overexpression of COL6A3 protein was observed in plasma, fibroblasts and iPS-derived motor neurons of SMA patients. In a review, Fuller and colleagues (Fuller et al., 2016) hypothesize that an overexpression of COL6A3 may be seen as an attempt of a protective response, as its overexpression protects neurons under cellular stress (Cheng et al., 2011). COL6A3 plays a role in neural crest development (Perris et al., 1993).
The role of RPL17/C18ORF32 is unknown.

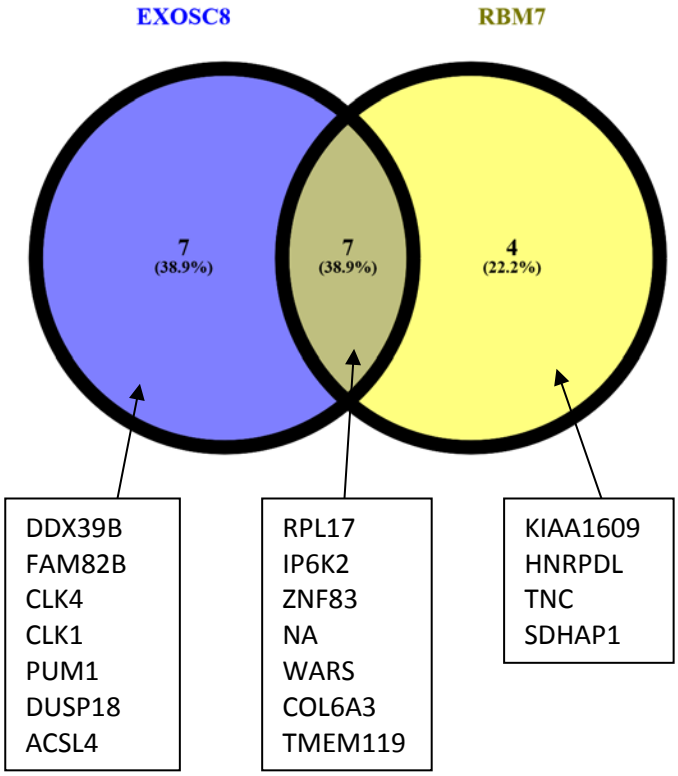

Figure 3.7 **Venn diagram illustrating the differential splicing events identified in *EXOSC8* and *RBM7* mutant cells.** RNAseq analysis identified 7 common genes in which some sort of differential splicing events occur in both cell lines. Only those which are exactly the same type of event and in exactly the same position are shown as *sashimi_plots* below.

TMEM119

Splice event ID chr12:108991746:108991894:-@chr12:108987940:108988321:-@chr12:108983622:108986173:-

EXOSC8

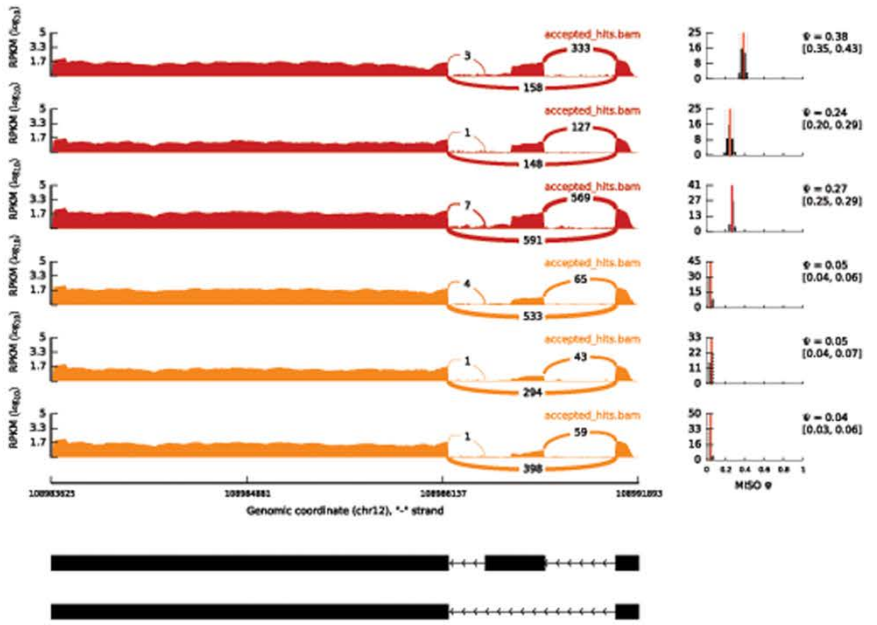

TYPE OF EVENT: SKIPPED EXON

Splice event ID chr12:108991746:108991894:-@chr12:108987940:108988321:-@chr12:108983622:108986173:-

RBM7

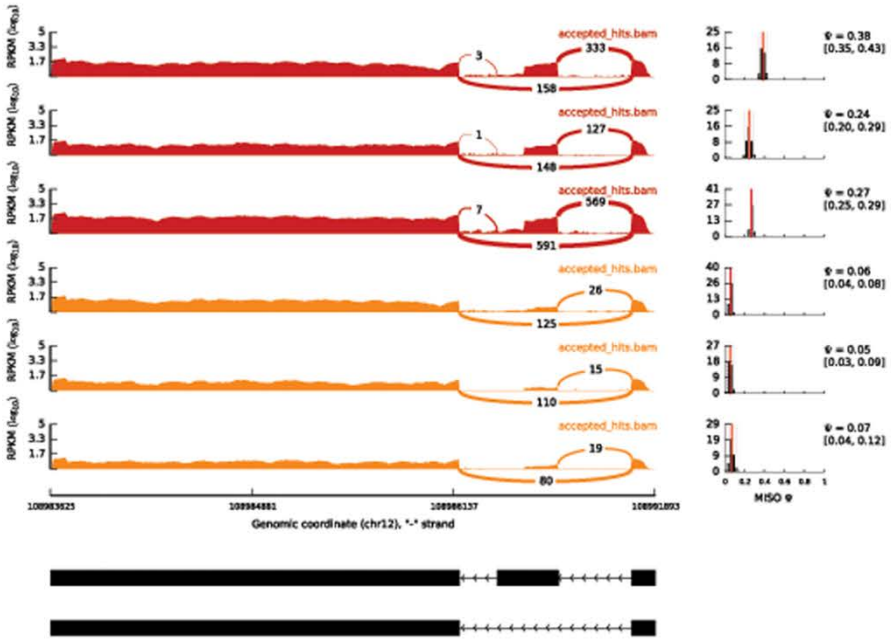

TYPE OF EVENT: SKIPPED EXON

TMEM119

Splice event ID chr12:108991746:108991894:-@chr12:108988113:108988321:-@chr12:108983622:108986173:-

EXOSC8

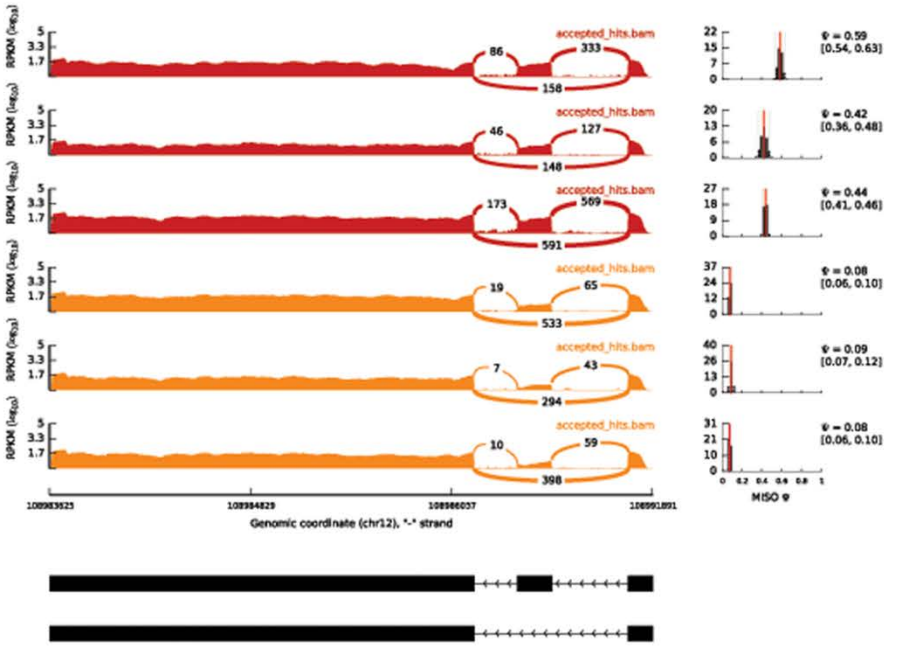

TYPE OF EVENT: SKIPPED EXON

Splice event ID chr12:108991746:108991894:-@chr12:108988113:108988321:-@chr12:108983622:108986173:-

RBM7

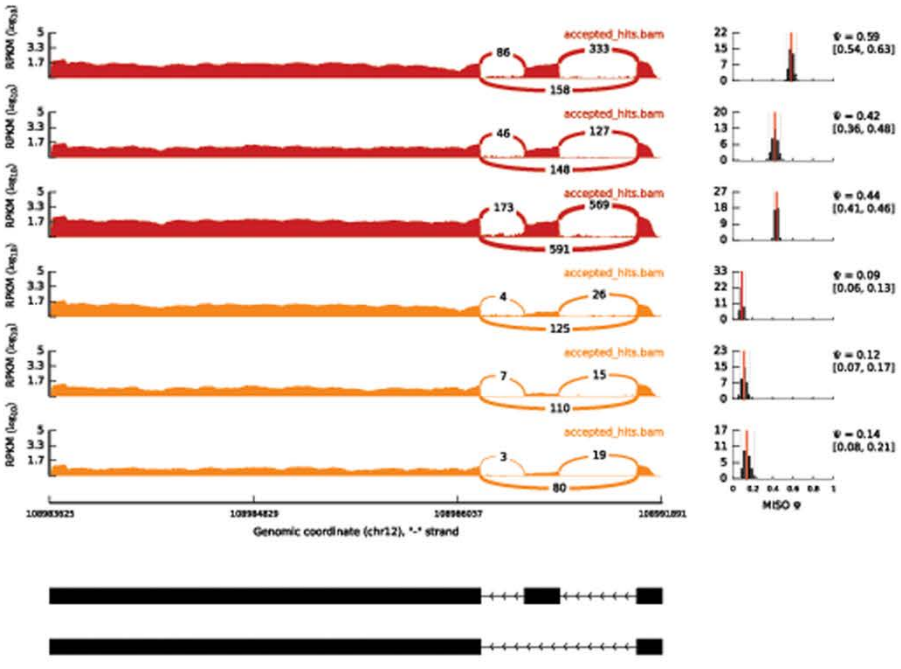

TYPE OF EVENT: SKIPPED EXON

COL6A3

Splice event ID chr2:238305370:238305490:-@chr2:238303230:238303847:-@chr2:238296225:238296827:-

EXOSC8

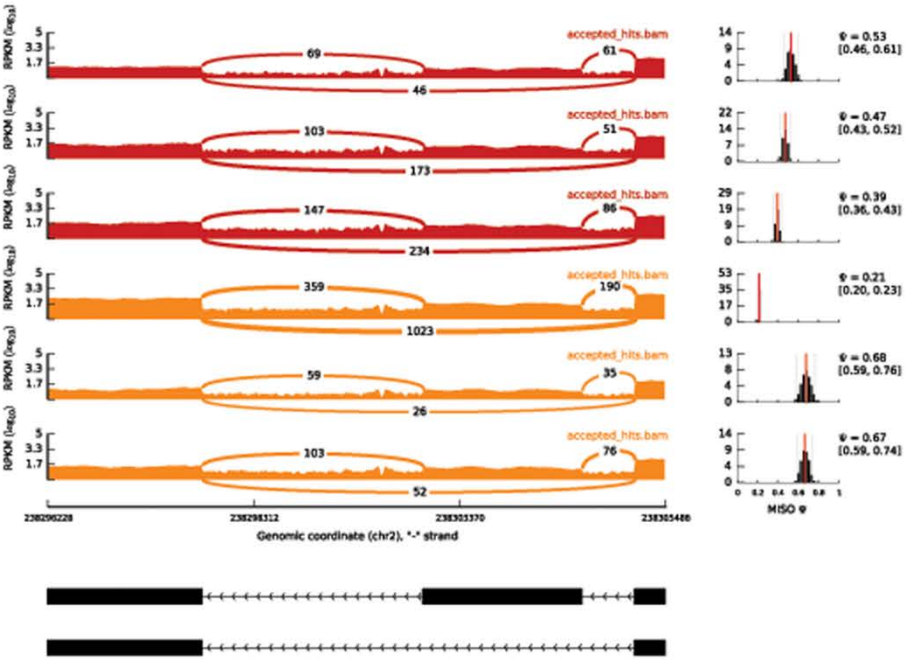

TYPE OF EVENT: SKIPPED EXON

Splice event ID chr2:238305370:238305490:-@chr2:238303230:238303847:-@chr2:238296225:238296827:-

RBM7

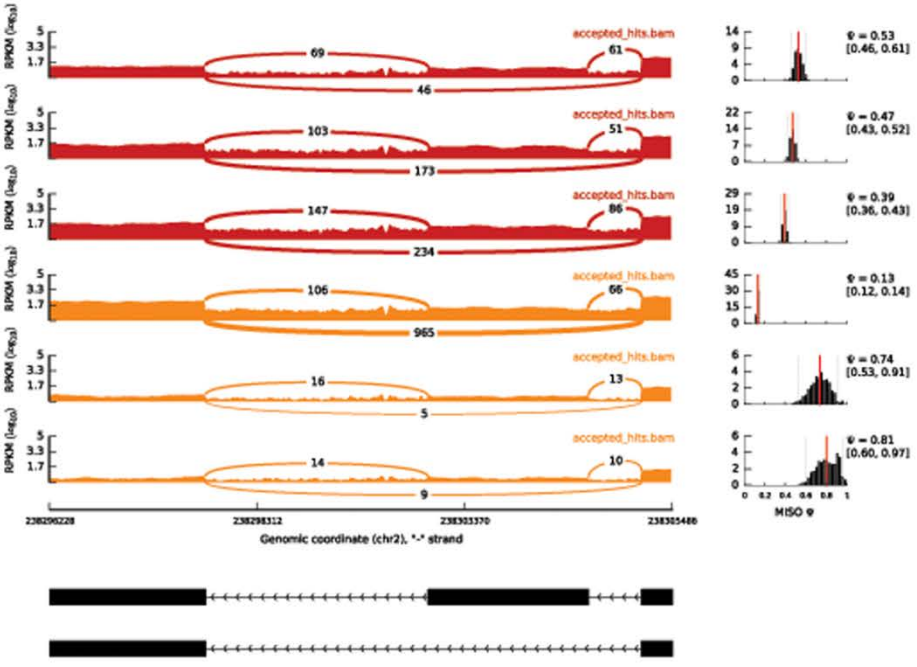

TYPE OF EVENT: SKIPPED EXON

Rpl17/C18ORF32

Splice event ID chr18:47018645:47018834:-@chr18:47017954|47018203:47017902:-

EXOSC8

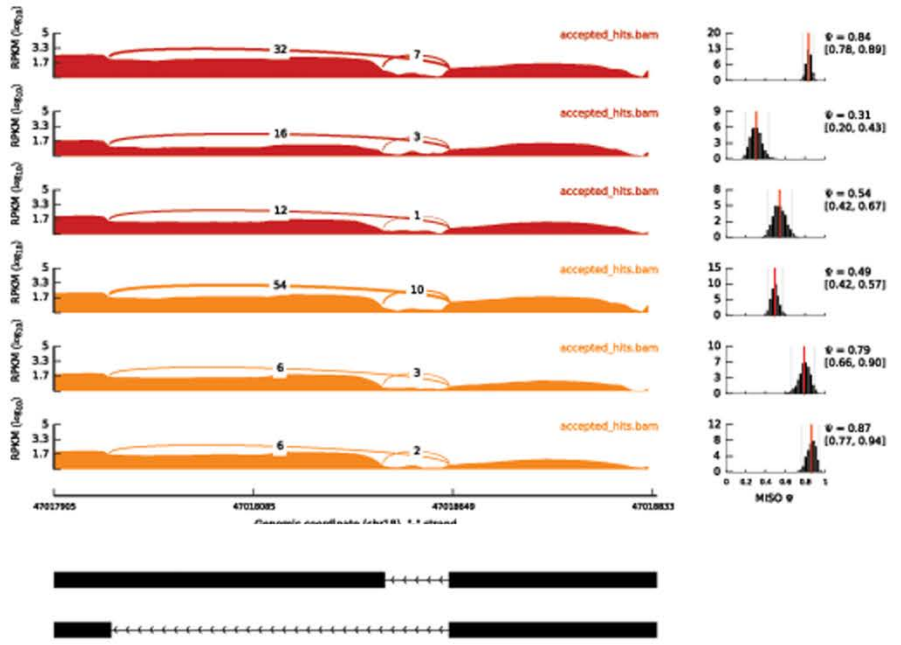

TYPE OF EVENT: ALTERNATIVE 3' SPLICE SITE

Splice event ID chr18:47018645:47018834:-@chr18:47017954|47018203:47017902:-

RBM7

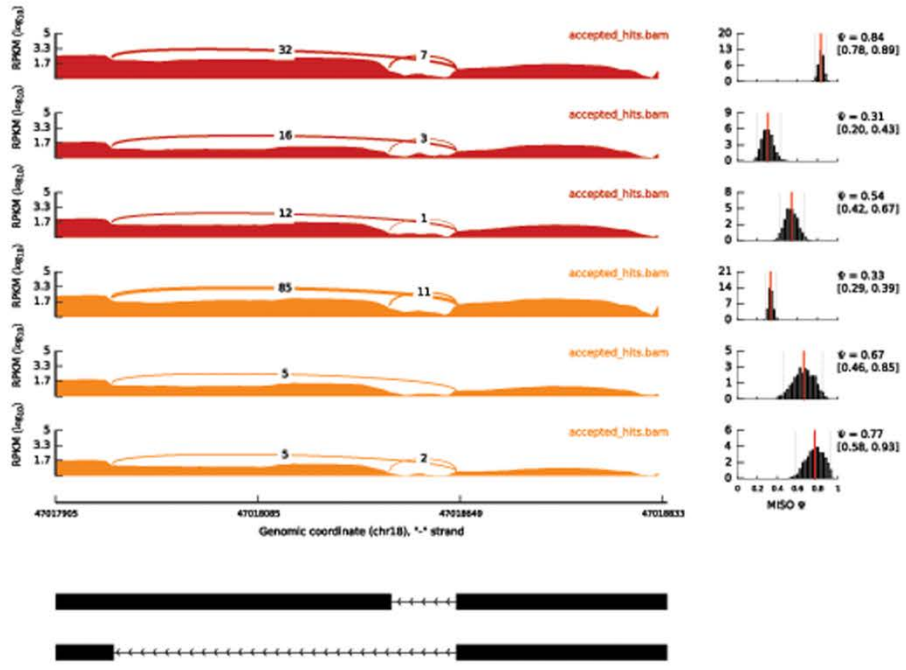

TYPE OF EVENT: ALTERNATIVE 3' SPLICE SITE

Unknown transcript

Splice event ID chr10:105156166:105156270:-@chr10:105155503:105155789:-@chr10:105153956:105154151:-

EXOSC8

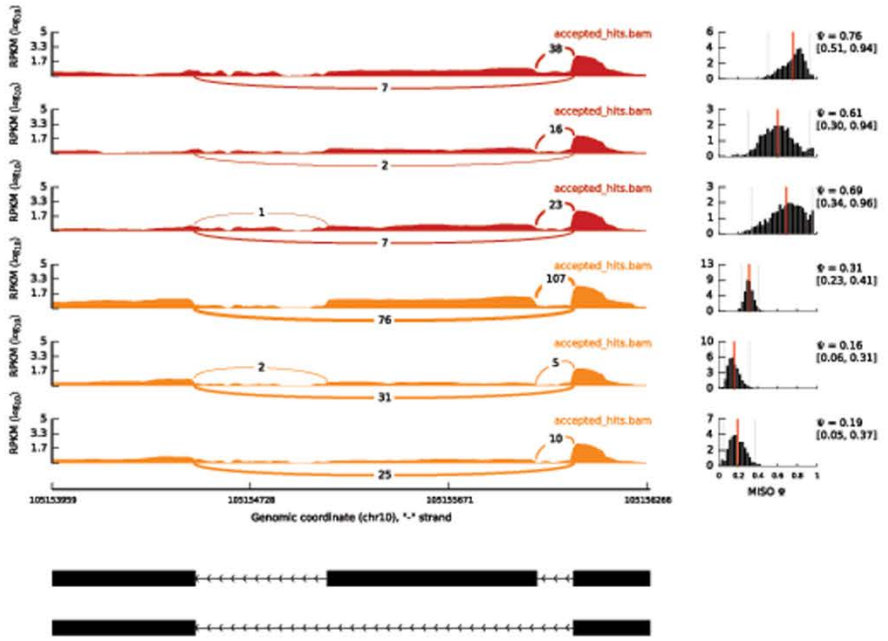

TYPE OF EVENT: SKIPPED EXON

Splice event ID chr10:105156166:105156270:-@chr10:105155503:105155789:-@chr10:105153956:105154151:-

RBM7

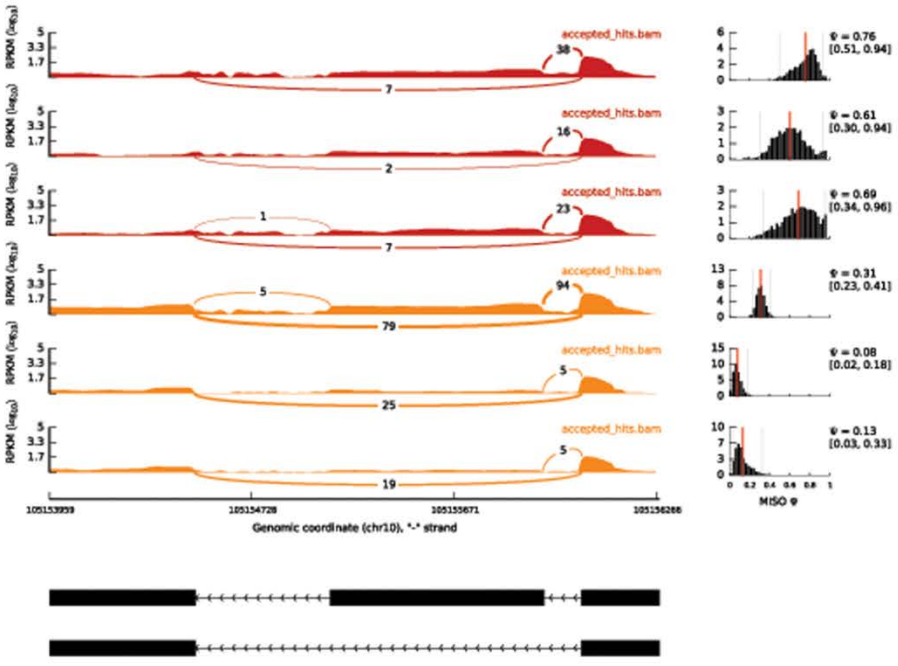

TYPE OF EVENT: SKIPPED EXON

Unknown transcript

Splice event ID 05156166:105156270:-@chr10:105155503:105155789:-@chr10:105153956:105154151:-@chr10:105152128:1051

EXOSC8

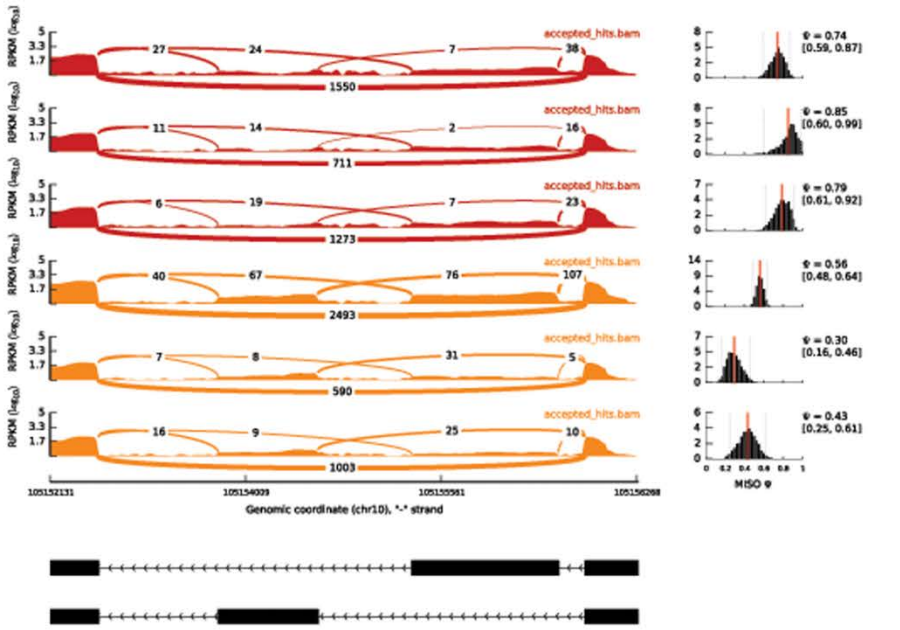

TYPE OF EVENT: MUTUALLY EXCLUSIVE EXONS

Splice event ID 05156166:105156270:-@chr10:105155503:105155789:-@chr10:105153956:105154151:-@chr10:105152128:1051

RBM7

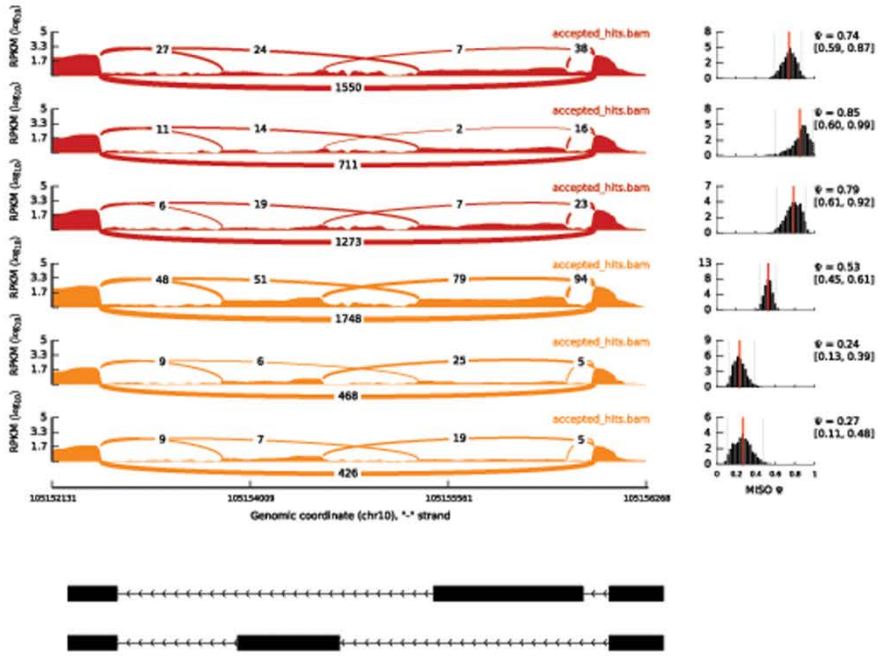

TYPE OF EVENT: MUTUALLY EXCLUSIVE EXONS

Figure 3.8 **Differential splicing events identified both in RBM7 and EXOSC8 mutant fibroblasts versus control.** Red: controls; yellow: mutants. Splice event ID refers to the genomic coordinates of the splicing event of the upstream (5') exon, the skipped exon, and the downstream (3') exon of this alternative splicing event, separated by @ symbols; Ψ denotes the fraction of mRNAs that represent the inclusion isoform. Overall splicing isoforms analysis indicates splicing defects in EXOSC8 and RBM7 cells. These data need to be confirmed by RT-PCR.

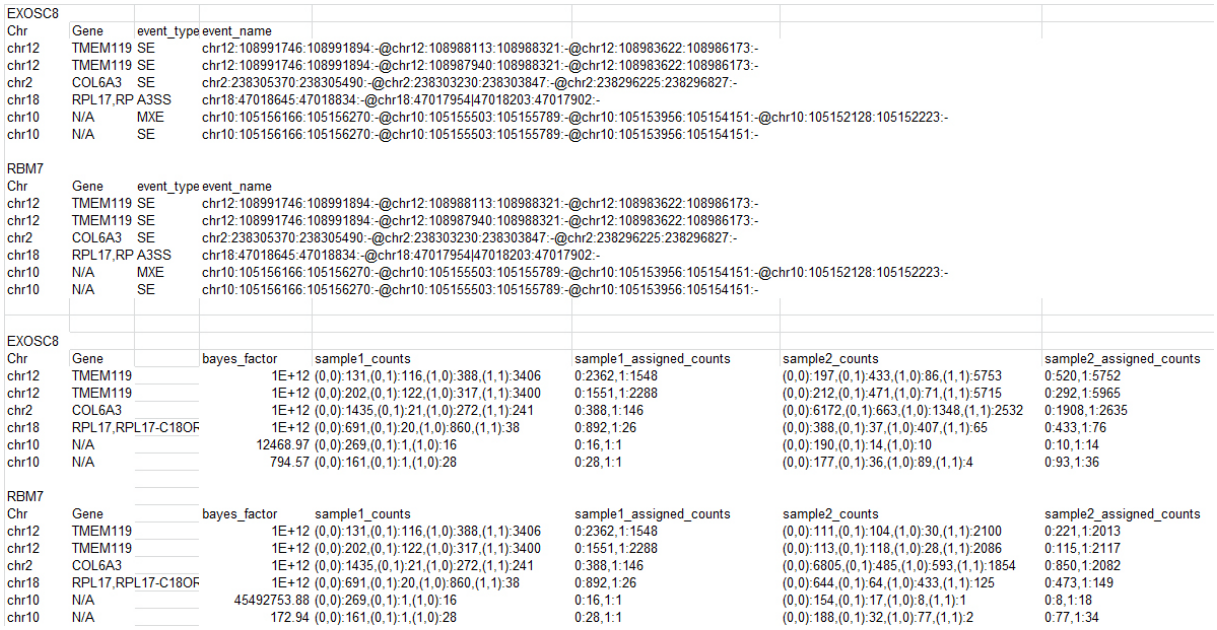

EXOSC8

Chr	Gene	event_type	event_name
chr12	TMEM119	SE	chr12:108991746:108991894:-@chr12:108988113:108988321:-@chr12:108983622:108986173:-
chr12	TMEM119	SE	chr12:108991746:108991894:-@chr12:108987940:108988321:-@chr12:108983622:108986173:-
chr2	COL6A3	SE	chr2:238305370:238305490:-@chr2:238303230:238303847:-@chr2:238296225:238296827:-
chr18	RPL17,RP	A3SS	chr18:47018645:47018834:-@chr18:47017954|47018203:47017902:-
chr10	N/A	MXE	chr10:105156166:105156270:-@chr10:105155503:105155789:-@chr10:105153956:105154151:-@chr10:105152128:105152223:-
chr10	N/A	SE	chr10:105156166:105156270:-@chr10:105155503:105155789:-@chr10:105153956:105154151:-

RBM7

Chr	Gene	event_type	event_name
chr12	TMEM119	SE	chr12:108991746:108991894:-@chr12:108988113:108988321:-@chr12:108983622:108986173:-
chr12	TMEM119	SE	chr12:108991746:108991894:-@chr12:108987940:108988321:-@chr12:108983622:108986173:-
chr2	COL6A3	SE	chr2:238305370:238305490:-@chr2:238303230:238303847:-@chr2:238296225:238296827:-
chr18	RPL17,RP	A3SS	chr18:47018645:47018834:-@chr18:47017954|47018203:47017902:-
chr10	N/A	MXE	chr10:105156166:105156270:-@chr10:105155503:105155789:-@chr10:105153956:105154151:-@chr10:105152128:105152223:-
chr10	N/A	SE	chr10:105156166:105156270:-@chr10:105155503:105155789:-@chr10:105153956:105154151:-

EXOSC8

Chr	Gene		bayes_factor	sample1_counts	sample1_assigned_counts	sample2_counts	sample2_assigned_counts
chr12	TMEM119		1E+12	(0,0):131,(0,1):116,(1,0):388,(1,1):3406	0:2362,1:1548	(0,0):197,(0,1):433,(1,0):86,(1,1):5753	0:520,1:5752
chr12	TMEM119		1E+12	(0,0):202,(0,1):122,(1,0):317,(1,1):3400	0:1551,1:2288	(0,0):212,(0,1):471,(1,0):71,(1,1):5715	0:292,1:5965
chr2	COL6A3		1E+12	(0,0):1435,(0,1):21,(1,0):272,(1,1):241	0:388,1:146	(0,0):6172,(0,1):663,(1,0):1348,(1,1):2532	0:1908,1:2635
chr18	RPL17,RPL17-C18OF		1E+12	(0,0):691,(0,1):20,(1,0):860,(1,1):38	0:892,1:26	(0,0):388,(0,1):37,(1,0):407,(1,1):65	0:433,1:76
chr10	N/A		12468.97	(0,0):269,(0,1):1,(1,0):16	0:16,1:1	(0,0):190,(0,1):14,(1,0):10	0:10,1:14
chr10	N/A		794.57	(0,0):161,(0,1):1,(1,0):28	0:28,1:1	(0,0):177,(0,1):36,(1,0):89,(1,1):4	0:93,1:36

RBM7

Chr	Gene		bayes_factor	sample1_counts	sample1_assigned_counts	sample2_counts	sample2_assigned_counts
chr12	TMEM119		1E+12	(0,0):131,(0,1):116,(1,0):388,(1,1):3406	0:2362,1:1548	(0,0):111,(0,1):104,(1,0):30,(1,1):2100	0:221,1:2013
chr12	TMEM119		1E+12	(0,0):202,(0,1):122,(1,0):317,(1,1):3400	0:1551,1:2288	(0,0):113,(0,1):118,(1,0):28,(1,1):2086	0:115,1:2117
chr2	COL6A3		1E+12	(0,0):1435,(0,1):21,(1,0):272,(1,1):241	0:388,1:146	(0,0):6805,(0,1):485,(1,0):593,(1,1):1854	0:850,1:2082
chr18	RPL17,RPL17-C18OF		1E+12	(0,0):691,(0,1):20,(1,0):860,(1,1):38	0:892,1:26	(0,0):644,(0,1):64,(1,0):433,(1,1):125	0:473,1:149
chr10	N/A		45492753.88	(0,0):269,(0,1):1,(1,0):16	0:16,1:1	(0,0):154,(0,1):17,(1,0):8,(1,1):1	0:8,1:18
chr10	N/A		172.94	(0,0):161,(0,1):1,(1,0):28	0:28,1:1	(0,0):188,(0,1):32,(1,0):77,(1,1):2	0:77,1:34

Figure 3.9 **Details of the splicing events listed in the sashimi plots above.** Sample1: control; sample2: mutant. Event type: SE skipped exon; MXE mutually exclusive exons; A3SS alternative 3' splice site. Event name same as event ID above. Sample count indicates the raw counts for each isoform. In parentheses, 1 and 0 indicate if the reads are consistent (1) or inconsistent (0) with the isoform. For example the first line entry is (0,0):131,(0,1):116,(1,0):388,(1,1):3406 where the numbers in brackets correspond to the first (inclusion of the exon) and second splicing event (exclusion of the exon). So 131 reads do not support both isoforms, 116 reads do not support the inclusion of the exon (first event, 0), but support the exclusion of it (second event, 1), 338 reads support the inclusion but not the exclusion, and 3406 reads support both isoforms. The read (0:0) are thrown out. Assigned counts: Inferred assignment of reads to isoforms; for example an entry like 0:2362, 1:1548 menas 2362 reads were assigned to the first isoform (0) and 1548 to the second isoform (1).

3.3.9 RT-PCR analysis of human fibroblasts WARS show differential splicing events in RBM7 and EXOSC8 cells compared to controls.

In order to confirm the data obtained through MISO and *sashimi_plot* I decided to perform RT-PCR to check if actual differential splicing events are taking place upon EXOSC8 and RBM7 impaired functions as the exosome complex is thought to secondarily affect splicing functions, being primarily involved in splicing factors' RNA processing (Zhang et al., 2015) and RBM7 has been very recently confirmed as directly involved in splicing (Guo et al., 2003) (Falk et al., 2016).

I decided to focus initially on WARS given the known roles of tRNA synthetase dysfunction in neurological disorders although WARS (Tryptophanyl-TRNA Synthetase) is not known to be linked to any disease.

WARS (ENSG00000140105) has 44 splice variants. Covering the whole length of the gene required designing of 8 pairs of primers. Results show that differential splicing events take place in either EXOSC8 and RBM7 fibroblasts compared to controls (Fig. X).

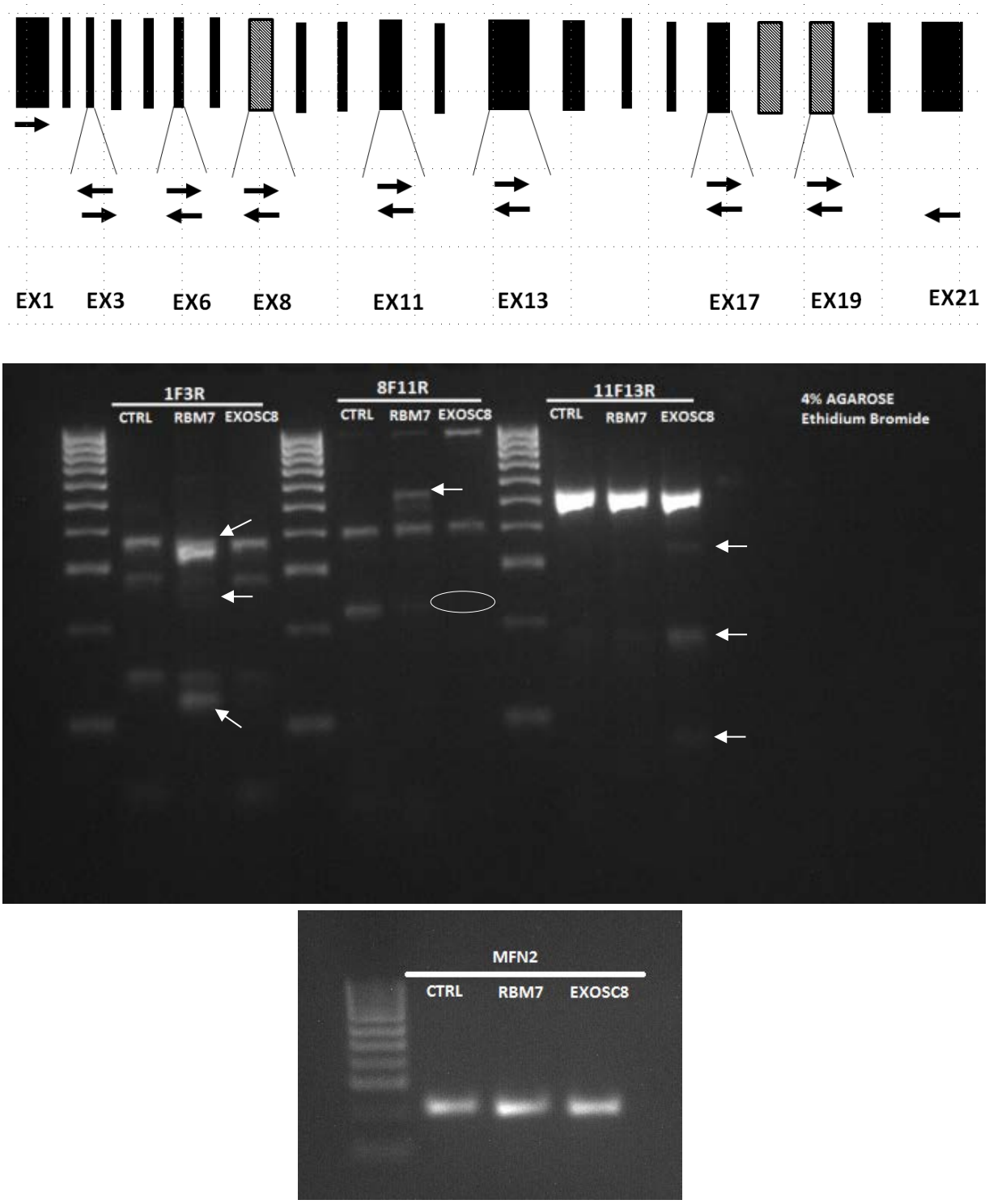

Figure 3.10. **Results of differential splicing analysis in *WARS* transcripts.** Top figure: schematic representation of the primers designed to cover the full length of *WARS*. Central image show differential splicing events identified using fprward primer on exon1 and reverse primer on exon3 (1F3R), forward primer on exon8 and reverse primer on exon 11 (8F11R) and forward primer on exon11 and reverse primer on exon 13 (11F13R). Arrows show [resence of a band which is missing in the control and ellipse show a missing band which is present in the control. Bottom image: MFN2 was used a sa control gene to show good quality of RNA and cDNA.

3.4 Discussion and future directions

Mutations in exosome related proteins constitute a novel sub-group of severe neurological disorders with childhood onset.

The mutations identified so far provide a very complex spectrum of symptoms (Fig. 3.10), some of them are unique for a specific gene, others are common features of different mutations.

Exosomal dysfunctions seem to cause a prevalent neurological spectrum of symptoms with little involvement of other systems, being the cerebellum and motor neurons the most affected tissues, therefore typical features of PCH1. Other features may be present too such as hypomyelination (PCH2, PCH4 and PCH5, PCH9 features), developmental delay (PCH7), or cortical involvement (PCH4, PCH10). One

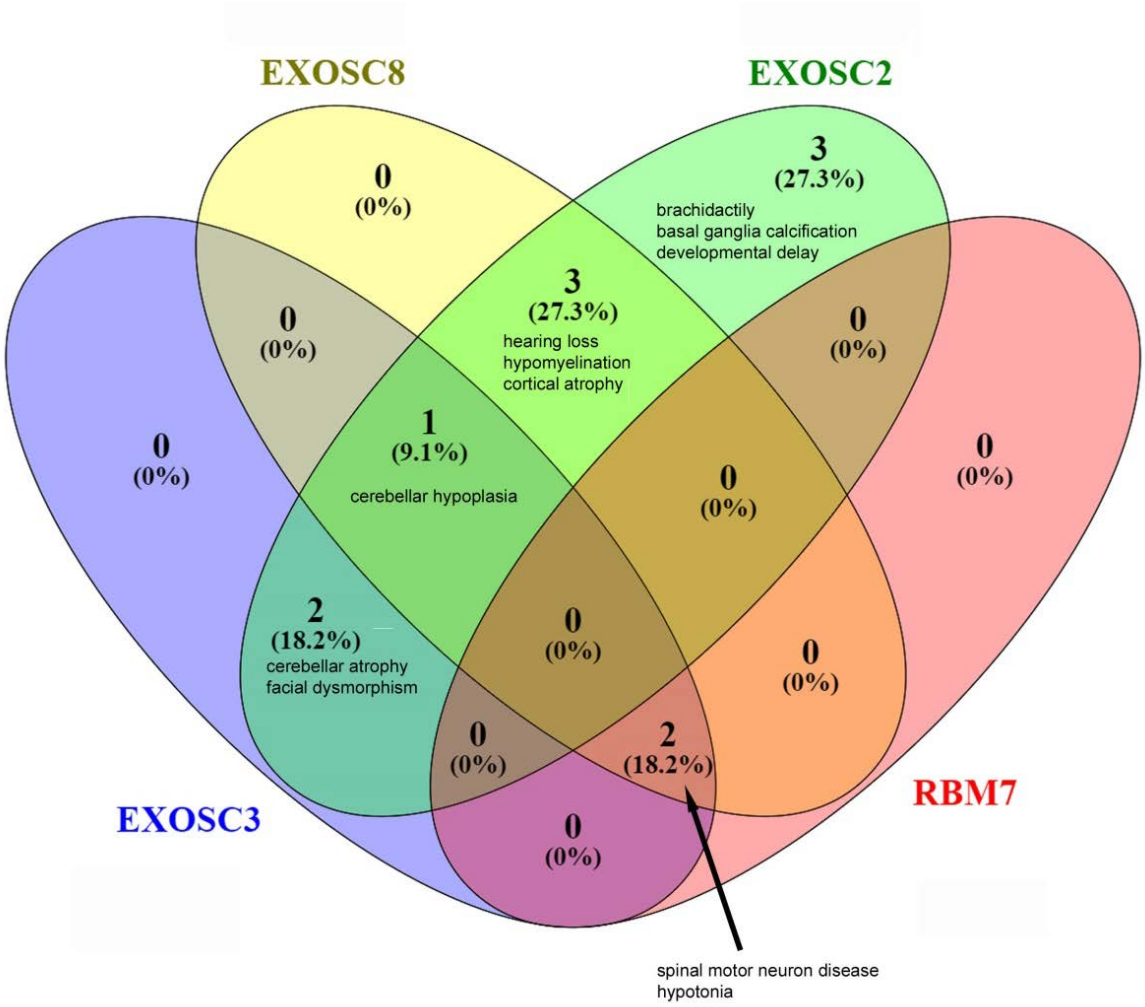

Figure 3.11 **Graphical representation of the complex pattern of overlapping symptoms caused by mutations in *EXOSC3*, *EXOSC8*, *EXOSC2* and *RBM7*.**

patient with *EXOSC8* mutation was reported to have cytochrome c negative muscle fibres and moderately decreased respiratory chain complexes I and IV activities. Mitochondrial disease is a feature of PCH6. The patient with *RBM7* mutation did not show any cerebellar impairment but clear motor neuron disease and hypotonia. For a more comprehensive list of PCH symptoms see Eggens, 2016.

Considering the fact that the exosome complex is present virtually in all cells of the body, the reasons underlying the neural specificity are unclear. In order to clarify this and other aspects of this novel subtype of neurological disorders, we extensively looked for new pathogenic mutations and identified a new variant in *RBM7*, a sub-unit of the NEXT complex which is a co-factor of the exosome complex. The identification of a new mutation in *RBM7* led us to develop new sets of experiments to study the functions of the exosome complex. Based on preliminary data on our *EXOSC8* deficient cells and zebrafish, we decided to further investigate the roles of these genes comparing zebrafish and primary fibroblasts data, which eventually led to publication of this work (Giunta et al., 2016).

We also identified new patients with variants in *EXOSC3* and *TSEN54* and another never reported gene, extending the knowledge of diseases caused by defective RNA metabolism.

RNA sequencing was performed to investigate which coding and non-coding RNAs are differentially expressed in *EXOSC8* and *RBM7* mutant primary fibroblast. Given the known role of the exosome complex in degrading/processing RNAs, it may be that an overexpression (or better, defective degradation) of some specific RNAs may be the underlying cause of the diseases. Indeed we identified 62 transcripts (14% of the total) commonly differentially expressed between the two cell lines. Of these 62, 13 transcripts (19%) are involved in neurodevelopment or neurological functions. It is also interesting to notice that all these 62 differentially expressed genes follow the same pattern of expression, showing a high level of correlation. A relatively high number of differentially expressed HOX genes was detected in fibroblasts, and given their known role in development of peripheral nervous system (Lacombe et al., 2013) (Wu et al., 2007) (Vermot, 2005) and in human neurological disorders (Quinonez and Innis, 2014), we hypothesize this may be one of the causes of the neurological defects observed in patients (Giunta et al., 2016). Expression of these genes in knock-down zebrafish models was then investigated, as explained in the next chapter.

Overexpression of *HOXC* genes well matches with overexpression of *HOTAIR* which is known to co-transcribe within the *HOXC* locus (Clark and Blackshaw, 2014) and silences expression of *HOXD* genes (Clark and Blackshaw, 2014). In support of this, *HOXD* genes were significantly downregulated in our *EXOSC8* mutant cells. The increase in HOTAIR was associated with a reduction of HOXD10, HOXD11 and HOXD13 of respectively -6.67, -5.37 and -4.10 Log2 fold change in expression.

Several other genes which resulted to be differentially expressed (CACNA1G, PITX1, GNAZ, PCDH10, NTNG1, SOX11, OMD) are important for the correct function of human neurons.

In vertebrates, PITX1 induces the expression of *HOXC11* (Park et al., 2014), which is itself expressed in the posterior neural tube and dorsal root ganglia in mouse during development (Hostikka and Capecchi, 1998). Both resulted to be upregulated in our data. Interestingly, SOX11 is expressed in the granule layer in the cerebellum (Rex et al., 1998), which is in turn essential for cerebellar layer differentiation (Kani et al., 2010), which may be important in the clinical presentation of these defects.

ARE genes analysis identified 8 AU-rich elements differentially expressed. Adenylate-Uridylate rich elements (ARE) are found within the 3' UTR of many transcripts and act as signals for rapid mRNA degradation (Barreau, 2005). The AU-rich RNAs identified here, however, are not the same as the ones we identified previously in myoblasts and oligodendroglia cells (Boczonadi et al., 2014), probably because of differences in tissue-specific gene expression. The exosome is known to degrade AU-rich elements (Mukherjee et al., 2002) but in our data we show that TBX5 and OMD are rather downregulated in exosome complex defective cells, while the other 6 ARE genes are upregulated as expected. This downregulation could be caused by inhibition of expression from some other over-represented transcripts, something similar to what *HOTAIR* transcript exerts on *HOXD* transcripts, inhibiting their expression as discussed above.

Non-coding RNAs represent an important fraction of the total of transcripts identified by our RNA-seq analysis (18 out of 62). Not much is known about the roles of non-coding RNAs. PubMed search could identify functional studies for only three of non-coding RNAs present in our data (a part from *HOTAIR* which is well studied): Tbx5-as1 (Eckalbar et al., 2016), *TARID* (Arab et al., 2014) and VTRNA1-3 (Helbo et al., 2015). Tbx5-as1 function is unknown, it maps close to *TBX5* gene. *TARID* is involved

in gene expression regulation, directing demethylation and VTRNA1-3 is associated with Myelodysplastic Syndrome, a hematopoietic disorder.

Non-coding RNAs are known to be related to gene expression regulation (Clark and Blackshaw, 2014), embryo development (Ulitsky et al., 2011), neuronal functions (Cao et al., 2006) (Qureshi and Mehler, 2013) as well as myelination (Lin et al., 2014).

HOTAIR functions are well established and it is indeed known to be involved in transcriptional regulation of gene expression (Rinn et al., 2007) and post-translational regulation (Yoon et al., 2013) of protein functions. *HOTAIR* is present in all mammals, although with poorly conserved sequence as it seems to have evolved very fast compared to its flanking genes *HOXC11* and *HOXC12* (He et al., 2011). It has a direct impact on nervous system development, being able to inhibit expression of *HOXD* genes as mentioned before (which are in turn involved in motor neuron development (de la Cruz et al., 1999) (Misra et al., 2009). HOTAIR also binds to ATXN1 protein (Yoon et al., 2013). Mutations in *ATXN1* cause Spinocerebellar ataxia 1 (OMIM 601556) as it is important for correct cerebellar development (Ebner et al., 2013).

Our analysis of alternative splicing confirms involvement of the exosome complex in splicing regulation, as previously shown by others (Zhang et al., 2015). RBM7 is also known to be involved in splicing (Guo et al., 2003) (Falk et al., 2016), therefore it is of particular interest to see some commonly mispliced transcripts in both *EXOSC8* and *RBM7* mutant cells. Some other genes are uniquely differentially spliced in one cell line or the other (not shown here) which, similarly to what observed for the differential expression analysis, may indicate a partially overlapping mechanism of disease.

On this matter it is worth to say that a complex pattern of differential splicing events was identified by RNA-seq analysis in WARS (tryptophanyl-tRNA synthetase) in both *RBM7* and *EXOSC8* mutant fibroblasts (not shown in this chapter because they are not exactly the same event), but it is of particular interest given the known role of aminoacyl-tRNA synthethases mutations in neurological disorders (described in the introduction chapter). A reduction in WARS expression (-1.61 Log2fold change) was also found only in *EXOSC8* mutant fibroblasts.

RT-PCR analysis seems to confirm differential splicing events in WARS in mutant cell lines. The experiments need to be repeated on more control lines and the bands will be sequenced to clearly understand which bits of the gene are mispliced.

WARS dysfunction may contribute to neurological symptoms triggering toxicity of tryptamine, a neurotoxic decarboxilated tryptophan analog which activates aryl-hydrocarbon receptors in the brain, causing axonal defects (Paley et al., 2013).

Tryptamine toxicity is triggered by tryptophanyl tRNA synthetase inhibition or downregulation which causes in turn synthesis of aberrant tryptophanyl-tRNA and synthesis of abnormal proteins (Paley et al., 2013).

In conclusion, through RNAseq analysis we could identify several potentially interesting patterns which may lead to neurodevelopmental defects: many genes which are listed on pathway analysis softwares (Reactome and Panther) as involved in neuronal functions (CACNA1G, HOXC8, PITX1, HOXC11, GNAZ, PCDH10, NTNG1, SOX11, HOXC9, HOXC10, HOXC6, HOTAIR, OMD) are differentially expressed; *HOTAIR* - a non-coding RNA - is known to be involved in neurodevelopmental regulation at transcriptional and post-transcriptional levels; splicing defects in several transcripts have also been identified, some of them in genes which may cause neurological impairments such as WARS.

It is difficult at present to speculate which ones of these defects may be relevant for the pathology or what are the causes of the neuronal specificity of the disease. Considering that we analysed transcriptome in fibroblasts and gene expression in this cell type is of course very different from neuronal gene expression, in order to clarify which of these transcript are relevant for the pathology,

Two hypothesis may be worth to mention about the tissue specificity of this conditions despite the systemic presence of the mutated proteins: Neurons are most affected because of their higher protein synthesis requirements compared to some other tissues and/or compensatory mechanism are present in other tissues but not in neurons. Anyway, these hypothesis would not explain why only a specific subset of neurons is affected (e.g. specifically the cerebellum but not the sensory neurons).

The following studies are in preparation to complete this project:

Our group have recently received from collaborators *EXOSC3* and *XXXX* primary fibroblasts mutant lines. Direct conversion of *EXOSC3*, *EXOSC8*, *XXXX* and *RBM7* mutant primary fibroblasts into neural cells will be performed (Meyer et al., 2014). Repeating RNA-seq on these cells will help to narrow down the number of non-specific transcripts and therefore reduce the candidates potentially related to the neural pathology. Comparing these human RNA-seq data to RNA-seq from mutant

zebrafish’ neurons (described in chapter 5), will help to identify conserved mechanisms underlying neurodevelopmental defects caused by the mutations.

4 Chapter 4: Results - Zebrafish models of exosomal protein deficiency through gene knock-down.

4.1 Gene knock-down in zebrafish

Zebrafish has been extensively used for investigating the pathomechanism of neurodevelopmental and neurodegenerative diseases (Xi et al., 2011) (Sumbre and de Polavieja, 2014). By using zebrafish as a model system to study deficiencies of RNA metabolism we aim to gain a better understanding of the molecular mechanisms underpinning neurodevelopmental defects in exosomal-related diseases.

To date and for the last 15 years, functional studies in zebrafish have been largely performed by gene-knock down in order to transiently down-regulate expression of a gene through morpholino technology (Blum et al., 2015; Nasevicius and Ekker, 2000). It is a relatively quick and easy way to specifically down-regulate gene expression in zebrafish.

Morpholinos phosphorodiamidate antisense oligonucleotides (MO) are synthetic DNA analogue molecules initially developed to overcome the expensive costs associated with DNA analogues back in 1989 (1989). MO are very stable within the cell as they are resistant to nucleases (Karkare and Bhatnagar, 2006; Hudziak et al., 1996). Morpholinos can be designed to bind on the AUG translation start site of the mRNA and then act through a translation-blocking mechanism (Kok et al., 2015) or can be designed to target a splicing site on the pre-mRNA which can be either an intron-exon or an exon-intron boundary, therefore causing a splicing defect (Morcos, 2007). These two different strategies lead to very different outcomes. For instance, targeting the AUG will also impair expression of maternal mRNA, while targeting a splice site will only affect zygotic mRNA (Bill et al., 2009). MOs have a narrow timeframe of availability and efficacy. It is usually injected in the yolk and this can only be done up to 8 cells stage (Bill et al., 2009). Later than that, uptake of morpholino from the yolk to the cells will stop or reduce. MOs are considered to work efficiently up to 5 dpf.

To overcome the fact that MOs need to be injected very early, therefore causing an early knock-down of gene isoforms that might not be related to the functions we are investigating (Eisen and Smith, 2008), some more advanced MOs have been developed. These types of photo-activated molecules can be turned on and off in a

spatially and timely restricted manner at need using a specific wavelength (Tallafuss et al., 2012).

4.1.1 Controversies about the use of morpholinos

MOs, as well as other gene knock-down technologies (Robu et al., 2007) (Jackson et al., 2003) (Fedorov, 2006) in zebrafish are known to cause off target effects such as activation of p53 - an apoptotic gene - and induce a non-specific p53 dependent cell death pathway (Robu et al., 2007). Therefore, co-injection of p53 morpholino together with a morpholino for our target sequence, should always be performed to reduce unspecific apoptotic effects (Robu et al., 2007). This is, however, a controversial topic itself, as some experts in the field do not agree

MOs have been used for more than 15 years to target genes in zebrafish and other animal models (Blum et al., 2015). Recently, the development of a new genome editing technique (CRISPR/Cas9) has allowed the easy targeting of genes and production of mutants, reviving the discussion about the off-target effects of knock-down technologies (Kok et al., 2015) (Law and Sargent, 2014) (Schulte-Merker and Stainier, 2014). Some authors argued that mutant fish phenotype for a specific gene do not recapitulate what observed in morphant fish for the same gene (Kok et al., 2015). Kok *et al.,* showed that in a screening of more than 20 genes, approximately 80% of the morphant phenotypes did not match the mutant phenotype indicating that off-target effects of morpholino might be much more prevalent than previously thought. One possible explanation for these discrepancies could be a genetic compensation effect induced by mutations but not by knock-down (Rossi et al., 2015). To investigate specificity of MO, Rossi and colleagues first created a mutant line for *egfl7*, which do not show any phenotype. They tested *egfl7*-MO specificity by injecting it in *egfl7*-null mutants, expecting that, if no off-target effects were caused by the morpholino, the morpholino itself should not have any effect on the mutant fish. They subsequently genotyped the fish showing a vascular defect and found that 53% of them were WT, 37 % were heterozygous and only 9% were homozygous mutant, showing that mutant fish were much less sensitive to morpholino implying a specificity of the morphant phenotype. They did notice a different phenotype between mutant and morphant fish though. To further investigate the reason of these differences they performed mass spectrometry and RNA profiling and identified some proteins which are upregulated in mutants but not in morphants (namely *emilin3a*, *emilin3b* and *emilin2a*) which were able to rescue morphants' phenotype.

Gene knock-down technologies can be very useful to study disease pathomechanisms and the function of genes, therefore morpholinos can be the first step before moving forward to mutagenesis. The results of MO studies have to be put in the right context, considering different aspects and not overestimating them. In this chapter we present interesting data we obtained by gene downregulation, where we showed for the first time the role played by the exosome complex and its co-factors in central and peripheral nervous system development in vertebrates. Nevertheless, further studies on mutant zebrafish will be conducted.

4.2 Results

4.2.1 Modelling exosomal protein deficiencies in zebrafish

We decided to investigate the role of the exosome complex-related genes in which mutations are known to cause severe neurological disorders such as *EXOSC8*, *EXOSC3* and *RBM7*. *EXOSC3* and *EXOSC8* protein deficiencies have already been modelled in zebrafish by our group (Boczonadi et al., 2014) and others (Wan et al., 2012) so we used the same translation blocking morpholinos to target *exosc8* (NM_001002865) and *exosc3* (NM_001029961) genes in zebrafish. Zebrafish exosc3 (NP_001025132) has 247 amino acids while human EXOSC3 has 275 AA (NP_057126) and share 55.4% identity and 70.7% similarity.

Zebrafish exosc8 (NP_001002865) has 277 amino acids while human EXOSC8 (NP_852480) has 276 AA and share 70% identity and 84 .5% similarity.

Although the overall homology between the human and zebrafish RBM7 protein is relatively low (43% identical and 59% similar protein sequences) and also the mutated amino acid is not conserved between the two species (it is substituted with a glutamine in zebrafish), if only the highly conserved region of the RRM (the first 94 amino acids in human, the first 93 in zebrafish) is considered, the degree of homology is much higher (14) (69.5% identity and 84% similarity. RBM7 deficiency (described in the previous chapter) have never been modelled in zebrafish before, so we designed 2 different new splicing morpholinos against *rbm7* - both causing skipping of exon 2 - and studied the phenotype of MO downregulated zebrafish (Fig. 4.1; 4.2). We identified only one *rbm7* gene in zebrafish which is on chr:18 (NM_199925), encoding a 252 amino acids protein. We obtained very similar phenotypes targeting 2 different parts of the transcript. MO1 was designed to target intron1-exon2 boundary and MO2 was designed to target exon2-intron2 boundary.

Efficiency of splicing morpholinos has been confirmed by RT-PCR (Fig. 4.3). Toxicity of *rbm7*-MOs was tested by performing injection of 3 different doses: 10 ng, 5 ng and 2.2 ng. Analysis of mortality rates between different morphant groups and controls indicated that 2.2. ng was the optimal dose for *rbm7*-MO1 injections, based on the evidence of the very high mortality rate of the other 2 doses. *rbm7*-MO1 is very toxic, indeed, already 2.2 ng give a high mortality rate (Fig. 4.4), but it provides a good spectrum of different phenotypes, which is essential in order to investigate the severity of the defects observed upon gene knock-down.

The same strategy for choosing the optimal dose was adopted for *rbm7*-MO2. In this case 1.1. ng was chosen as optimal dose. Upon injection of 2.2 ng of *rbm7*-MO1, 10 ng of *exosc8*-MO and 1.5 ng of *exosc3* we could observe defects in development and movements. *exosc8* and *exosc3* morphants were previously phenotyped (Wan et al., 2012; Boczonadi et al., 2014). *rbm7* morphants showed defective body morphology ranging from mild to severe phenotype (Fig. 4.4). Morphant fish were categorized in three phenotypical classes: mild, moderate and severe. Fish with a mild phenotype had slightly shorter body length and brain oedema. Mild phenotype fish were not able to normally swim away upon touch stimulation, indicating some sort of neuromuscular defect. Fish with a moderate phenotype had a curved body shape, smaller head with a more prominent brain oedema, and in addition heart oedema was observed. Fish with a severe phenotype had a disrupted body morphology with anatomical parts barely recognizable. Interestingly, in some severe fish, we could observe a partially external development of the spinal cord (Giunta *et al.*, 2016).

EXOSC3

```
#=======================================
#
# Aligned_sequences: 2
# 1: NP_057126
# 2: NP_001025132
# Matrix: EBLOSUM62
# Gap_penalty: 10.0
# Extend_penalty: 0.5
#
# Length: 280
# Identity:     155/280 (55.4%)
# Similarity:   198/280 (70.7%)
# Gaps:          38/280 (13.6%)
# Score: 799.5
#
#
#=======================================
```

EXOSC8

```
#=======================================
#
# Aligned_sequences: 2
# 1: NP_852480
# 2: NP_001002865
# Matrix: EBLOSUM62
# Gap_penalty: 10.0
# Extend_penalty: 0.5
#
# Length: 277
# Identity:     194/277 (70.0%)
# Similarity:   234/277 (84.5%)
# Gaps:           1/277 ( 0.4%)
# Score: 1051.0
#
#
#=======================================
```

RBM7

```
#=======================================
#
# Aligned_sequences: 2
# 1: NP_057174
# 2: NP_956219
# Matrix: EBLOSUM62
# Gap_penalty: 10.0
# Extend_penalty: 0.5
#
# Length: 286
# Identity:     124/286 (43.4%)
# Similarity:   168/286 (58.7%)
# Gaps:          54/286 (18.9%)
# Score: 486.5
#
#
#=======================================
```

```
#######################################
# Program: needle
# Rundate: Tue 17 Jan 2017 11:24:16
```

Figure 4.1. **Homology between human and zebrafish EXOSC3, EXOSC8 and RBM7 proteins.** EXOSC3 and EXOSC8 show an overall high degree of homology between the 2 species while RBM7 homology is relatively low if the whole protein is considered.

Alignment of NM_199925 and chr18:47305773-47311455

```
tatataaagc aacatcagag gtcattcatg cattttcttt ttccactagG  47308922
CTGGGCCATT GATCAAGGTT AAAATCCCTA AAgACAATGA AGGAAAGTCA  47308972
AAACTGTTTG CATTTGTaAA CTTCAAGCAT GAAGTGTCAG TGCCCTATGC  47309022
CTTGAACTTG CTGAATGGAA TCCGTCTGCA TGGACGACAG CTCAACATAA  47309072
AGTTCAAAAC CGgtaggact ttccttattg cgttgattta ttttgtgttt  47309122
```

Alignment of NM_001002865 and chr10:35058926-35067639

```
agcgggcgaa gaaagcgcag attccgccgt gaccaactga aatagcgcca  35058875
cacaccagag cggaggacgc gaagttctcc gcttttacgt cactgcagtt  35058925
ATTCACGTGG TGCTTCCAAA CATCATGGCG GCTGGTTTTA Agtgagctac  35058975
atgtgcaaat tgtttttata atactattaa tgatttatat aggtgtctaa  35059025
atagtgaggt gatgatttcg ctattttatt tcagctgaat catgttgtgt  35059075
```

Alignment of NM_001029961 and chr14:51760826-51764911

```
tttctgttgt ggacataaag ggttggagag gttttaatga gttaatttgt  51764962
ataggataag agtccccgtg ccggaagtgc tcagacacgt gtgtttgtgt  51764912
GTGTTTTCCG CTCCTCCATC ATGGACTCCT CAGTGCACAC TAGTCTGCTG  51764862
GAGAGGATAG GAGATGTGGT TCTTCCAGGC GAtCTGCTGT TCTCCTTCAG  51764812
TCCTCCTGAA GCCGGAGACG CGAACCCGAA AGCGGACAGG CTGATCTGCG  51764762
GCCCGGGGCT GCGGCGGAGC GGAGCGGAGA TCCGTGTGTG TAGAGCaGGA  51764712
GTCCTGAAAC ACAAACAACC CAACATGTAC TGGGTCAACT GTCAGCAGAG  51764662
ACGGgtcaga acacacacac acacaacatg tgccagcaca cactattgtt  51764612
```

Figure 4.2 **Localization of morpholinos against *rbm7* (NM_199925), *exosc8* (NM_001002865) and *exosc3* (NM_001029961).** Position of morpholinos is underlined. Two new morpholinos were designed to target *rbm7* exon 2 which caused skipping of the same. The other 2 morpholinos were designed against the ATG and previously described.

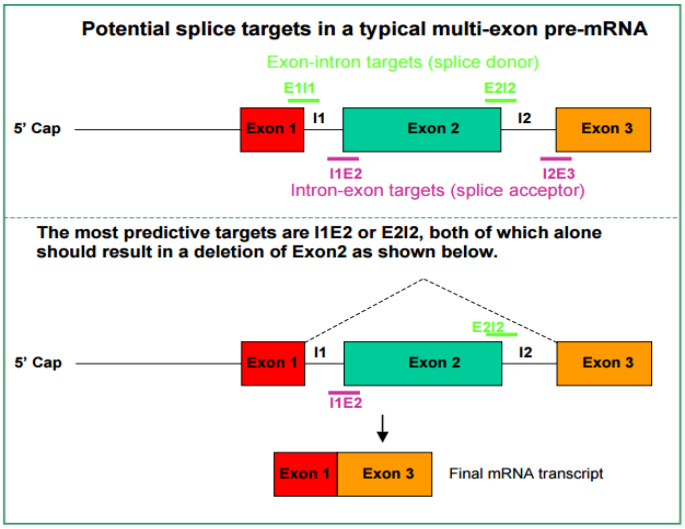

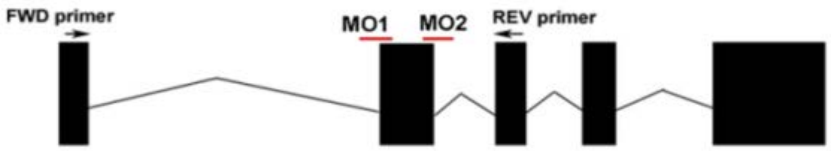

Figure 4.3 **Graphical representation of mode of action of splicing morpholinos and position of *rbm7*-MOs.** Morpholinos against intron-exon or exon-intron boundaries are predicted to cause exon skipping (top; image from Genetools website). Below, position of morpholinos against *rbm7* exon 2 and primers used to test efficiency (Giunta *et al*., 2016).

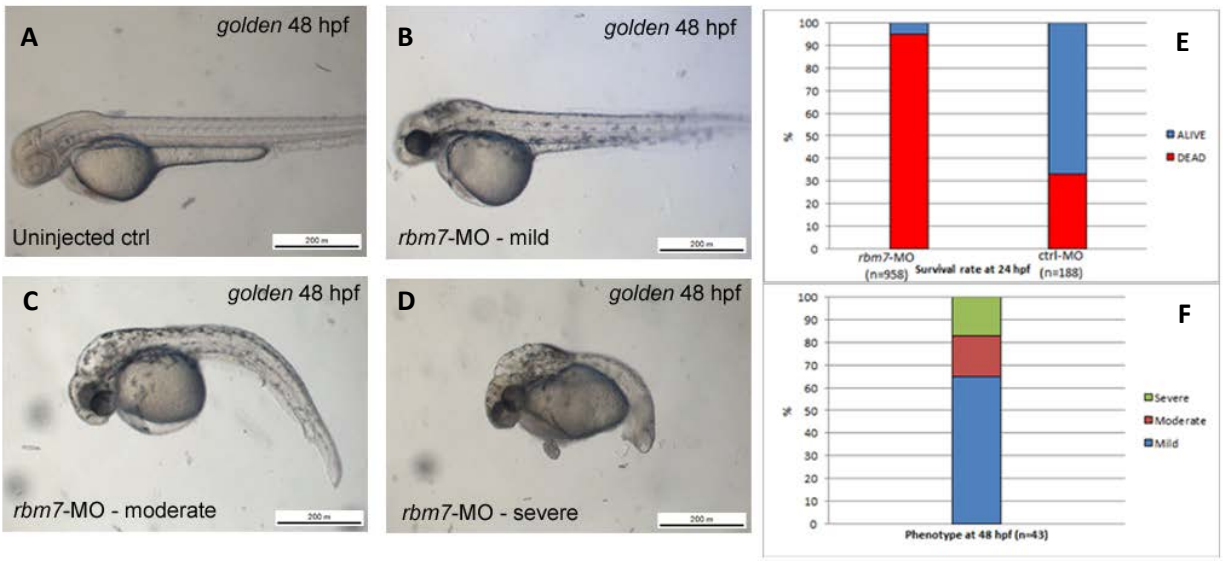

Figure 4.4 **Phenotypes (at 48 hpf) and mortality (at 24 hpf) caused by *rbm7* knock-down.** Mild phenotype fish (B) are slightly shorter than WT (A) and a brain oedema could be observed. Moderate fish (C) show smaller head and eyes and brain oedema becomes more pronounced. In severe fish (D) morphology is completely altered. Scalebar = 200 μm. Mortality is much higher compared to ctrl-MO injected fish, indicating that it is caused by *rbm7*-MO (E). Injection of 2.2 ng of *rbm7*-MO1 caused a range of different phenotypes which allowed an in-depth downstream analysis (F; images from Giunta et al., 2016).

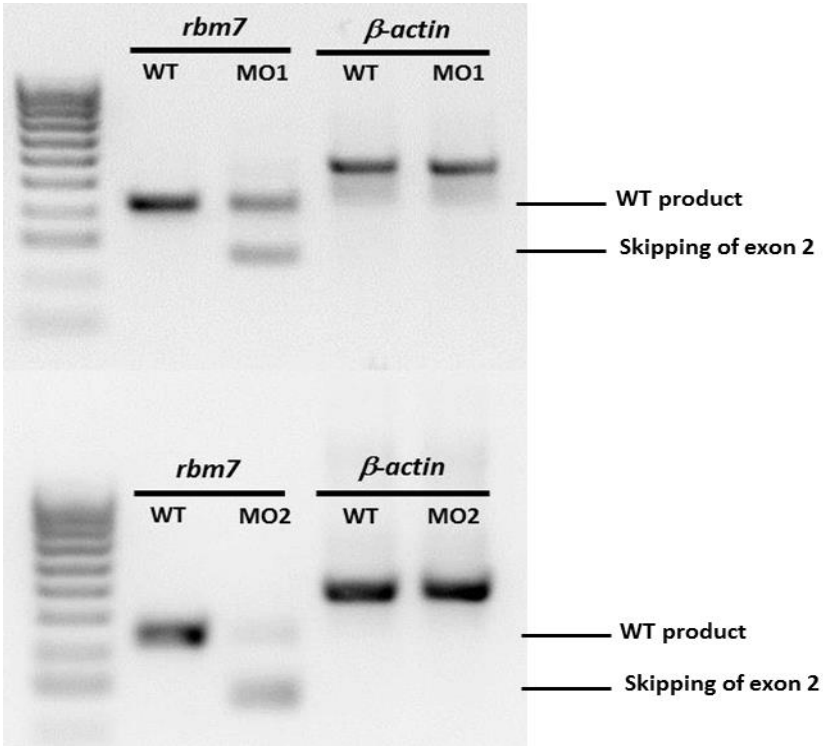

Figure 4.5 **Gel electrophoresis of *rbm7* RT-PCR of wild type and morphant fish.** Knock-down efficiency can be easily tested in splicing morpholinos. Both MO1 (top) and MO2 (bottom) cause exon 2 skipping (Giunta et al., 2016).

4.2.2 *Knock-down of rbm7, exosc8 and exosc3 cause defective hindbrain development in zebrafish*

Based on the observation of brainstem involvement in pontocerebellar hypoplasia type 1 (MedGen 335969) caused by *EXOSC3* and *EXOSC8* mutations in human, I decided to investigate development of brainstem nuclei in zebrafish upon knock-down of *rbm7*, *exosc8* and *exosc3*. We compared the phenotypes obtained, taking advantage of the *islet1*:GFP transgenic zebrafish line which expresses GFP in the brainstem cranial motorneurons (Lee et al., 2008). Zebrafish cranial motorneurons expressing *islet1* are divided into 5 nuclei, from rostral to caudal: III (oculomotor), IV (trochlear), V (trigeminal), VII (facial) and X (vagal; Higashijima et al., 2000) allowing visualization of defects in development of the hindbrain. Fish with a severe phenotype were not considered for this experiment, as important morphological defects are likely to affect brain structures. *rbm7*-MO had little effect on this anatomical area. At 48 hpf only the slightly shortened nuclei nX (vagal nerve) could be observed in mild *rbm7*-MO fish, compared to control (Fig. 4.5). Similar defects were also present in the moderately affected zebrafish. *exosc8*-MO fish showed similar defects of cranial neurons, as observed previously by us (Boczonadi et al., 2014) with a pattern of disruption which could be observed mostly in moderate fish

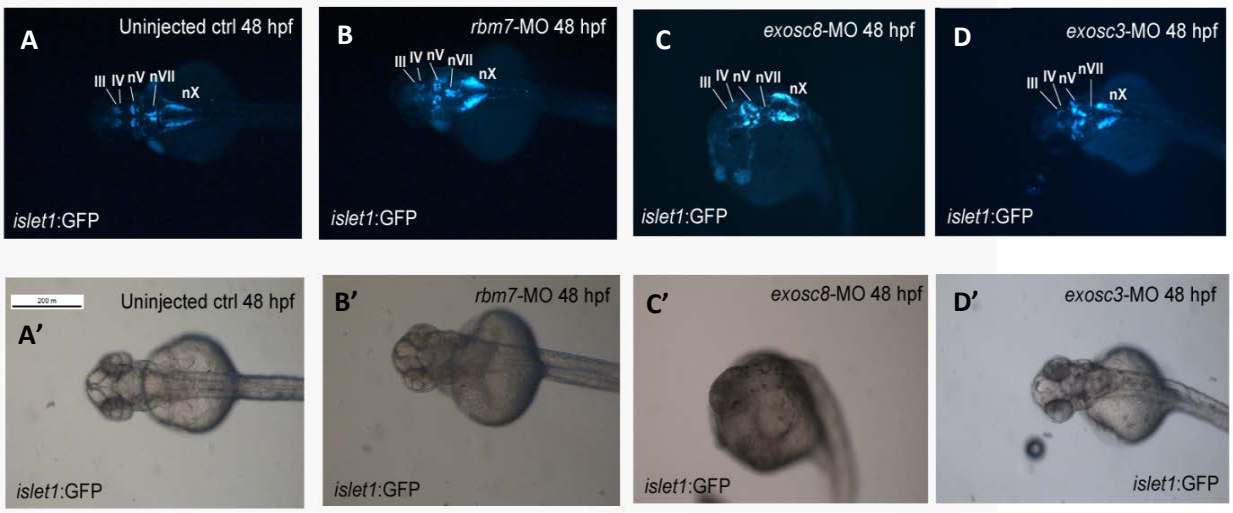

Figure 4.6. **Knock-down of *rbm7*, *exosc8* and *exosc3* affects cranial motor-neurons development.** In uninjected *islet1*:GFP fish (A, A'), five cranial motorneurons nuclei are clearly distinguishable. *rbm7*-MO seems to slightly affect nX(B, B'), which results to be shorter than in controls, even in mild fish. *exosc8*-MO fish have several defective structures (moderate phenotype; C, C'). *exosc3*-MO fish lack nVII, while the rest of the hindbrain seems to be relatively preserved (D, D'). Scale bar = 200 μm Image from Giunta *et al*., 2016.

(Fig. 4.5). *exosc3*-MO seem to affect mostly nuclei VII (facial nerve) even in the mildly affected embryos (Fig. 4.5). Interestingly, although the role of these three different genes in cranial nerve development was never studied before, similar disruption of cranial nerves has been observed in a zebrafish SMA model by others (Beattie et al., 2007). The authors could observe a defective development of facial motor neurons in SMN knock-down zebrafish.

4.2.3 Knock-Down of exosc8 in zebrafish causes defective myelination

Based on observation of defective myelination in the central nervous system in *EXOSC8* patients, I analysed myelination in zebrafish through electron microscopy upon knock down of *exosc8*. In order to confirm what observed we also analysed myelin in exosc8-MO zebrafish with a fluorescent dye which specifically stains myelin lipids (BrainStain, Thermofisher). Lipid staining was performed by Dr. Veronika Boczonadi, Newcastle University. We analysed in both cases myelination in the lateral line, as it is one of the first structures that start developing myelin sheaths.

Analysis of electron microscope images clearly show lack of myelin sheaths formation around axons, which appears to be rather well developed in zebrafish at 4 dpf. Lack of organelles such as mitochondria is also apparent (Fig 4.6. Boczonadi et al., 2014).

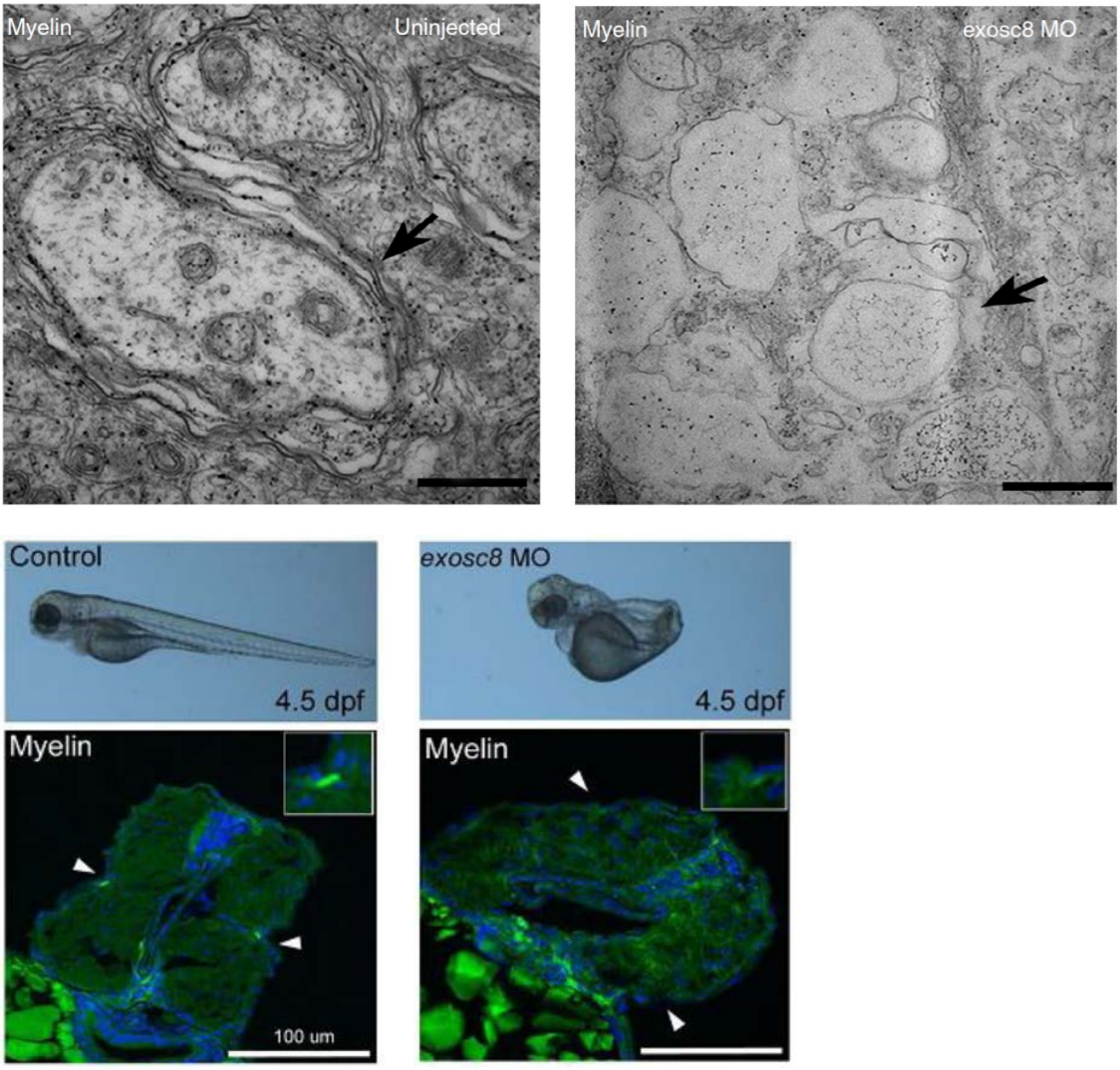

Figure 4.7 **Defective myelination caused by *exosc8* knock down in 4 dpf zebrafish.** Uninjected fish show normal development of myelin sheats around the axons at 4 dpf in the lateral line (arrow, top left) while *exosc8* downregulated fish of the same age do not show the beginning of the myelination process in the same anatomical area (arrow, top right). Below: in order to confirm myelination defects caused by *exosc8* knock-down in zebrafish we performed myelin staining on transversal section of 4.5 dpf zebrafish uninjected (bottom left) and *exosc8*-MO (bottom right) showing defective myelination. Images from Boczonadi et al., 2014. EM Scalebar = 500 nm.

4.2.4 Co-downregulation of mbp in exosc8 morphant zebrafish rescues hindbrain phenotype

Previous studies of transcript levels in *EXOSC8* mutant fibroblasts and myoblasts, showed higher levels of several ARE genes such as *SMN1*, *MOBP* and *MBP*. The exosome complex is known to be important for degradation of AU-rich elements, and dysfunctions of the same are likely to affect ARE genes levels. *MBP* level in particular was found to be much higher than the other two. In zebrafish, levels of *mbp* resulted to be 4 to 6 times higher upon downregulation of *exosc8* at 16 hpf (Boczonadi et al., 2014). *mbp* plays a key role in formation of myelin sheaths around the axons. Unbalance of its levels is likely to affect the myelination process, causing the phenotype observed in the patients.

To test if this was indeed causative of myelination issues in humans and *exosc8*-MO fish, we performed co-downregulation of *exosc8* and *mbp* in a transgenic zebrafish line expressing GFP in cranial motor neurons (*islet1*:GFP) resulting in a rescue of the hindbrain phenotype with better defined structures even in the severe fish (Fig. 4.7) and increased survival rate from from 59.3% of survival upon *exosc8* knock-down to 77.7% upon co-downregulation of *exosc8* and *mbp*. Myelin sheaths were not analysed after co-downregulation, but it is interesting to notice that *mbp* is also expressed in hindbrain oligodendrocytes at 48 hpf (Kazakova et al., 2006). Therefore an overexpression of *mbp* may affect hindbrain development as well, even before the onset of myelination process. RT-PCR analysis shows that both *mbpb* and *exosc8* are expressed since very early stages, even maternally in zebrafish (Fig. 4,9).

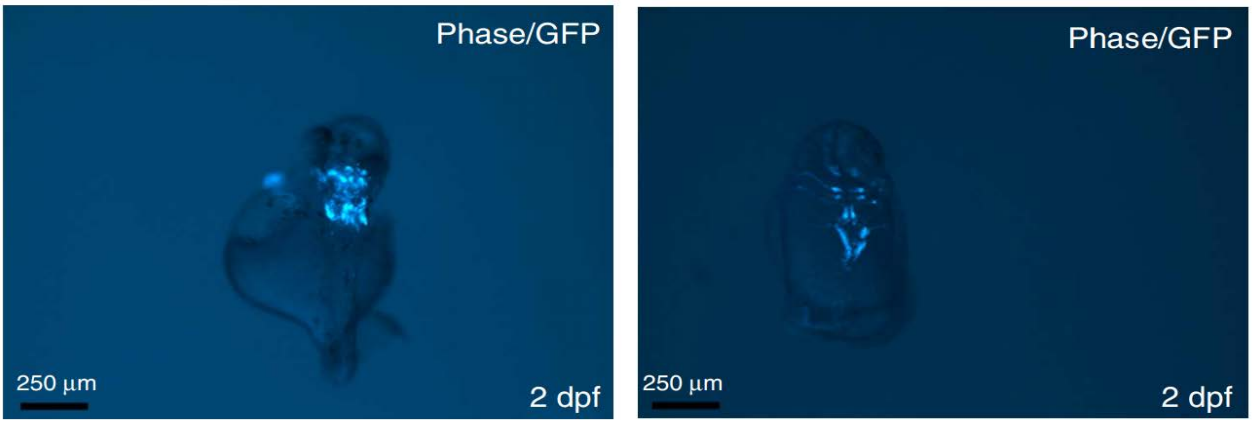

Figure 4.8. **Co-downregulation of *exosc8* and *mbp* rescued hindbrain phenotypes.** Downregulation of *exosc8* severely affects development of the hindbrain (left), especially in severe fish causing an overexpression of *mbp* (Boczonadi *et al.,* 2014). Co-downregulation of *exosc8* and *mbp* restores development of anatomical structures which are well defined even in severe phenotype (right). Images from Boczonadi et al., 2014.

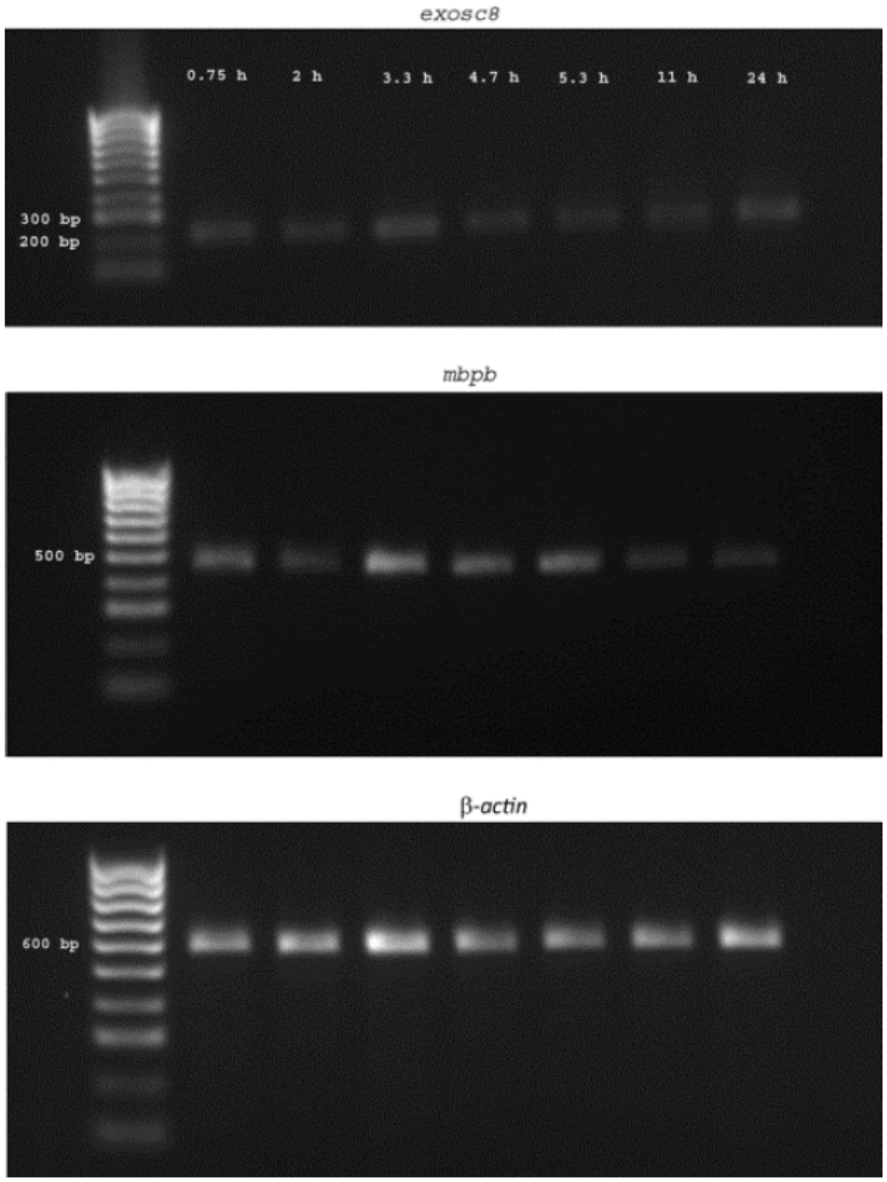

Figure 4.9. **RT-PCR of *exosc8* and *mbp* in zebrafish.** Both genes present maternal and zygotic expression. Interestingly *mbp* is expressed even before the onset of myelination.

4.2.5 Development of motor neurons in zebrafish

Neurogenesis of motor neurons in zebrafish has been well established. Two main classes of peripheral motor neurons that innervate axial muscles can be distinguished during development: primary and secondary motor neurons. Each class has some anatomical and cellular characteristics that make possible to discriminate between the two, although some of these characteristics may overlap in some cases (Myers, 1985) (Myers et al., 1986). Each primary motor neuron can be classified based on the antero-posterior position within each myotome in Rostral (RoP), Middle (MiP) and Caudal (CaP) (Fig. 4.8; Sanes et al., 2012). A fourth type of primary motor neuron is present in about half of the hemi-segments (whereas all the others are present in all segments, bilaterally). This neuron type is called Variable (VaP) as it is not always present (Eisen, 1992).

Primary motor neurons are larger in size (~ 11 μm somata diameter) and located in a dorsolateral position at 48 hpf (Myers et al., 1986). Secondary neurons are located more ventrally, they are smaller (~ 6 μm somata diameter) and their axons are thinner. Different primary motor neurons can be also recognized based on the direction of the axons (Myers et al., 1986) (Issa et al., 2012). At 48 hpf RoP axons direct caudally then descend toward the horizontal septum which separates the dorsal and ventral part of the somite, continuing elongating at this height in both directions. MiP axons extend caudally over the CaP somata and then start growing dorsally turning to the opposite hemisegment. Finally, CaP grows quite straight toward the ventral part, innervating those ventral muscles, suddenly dividing into two branches. Primary axon growth can be visualized staining axons with antibody against synaptic vesicle 2 (SV2) (Palaisa and Granato, 2007) (Sainath and Granato, 2013).

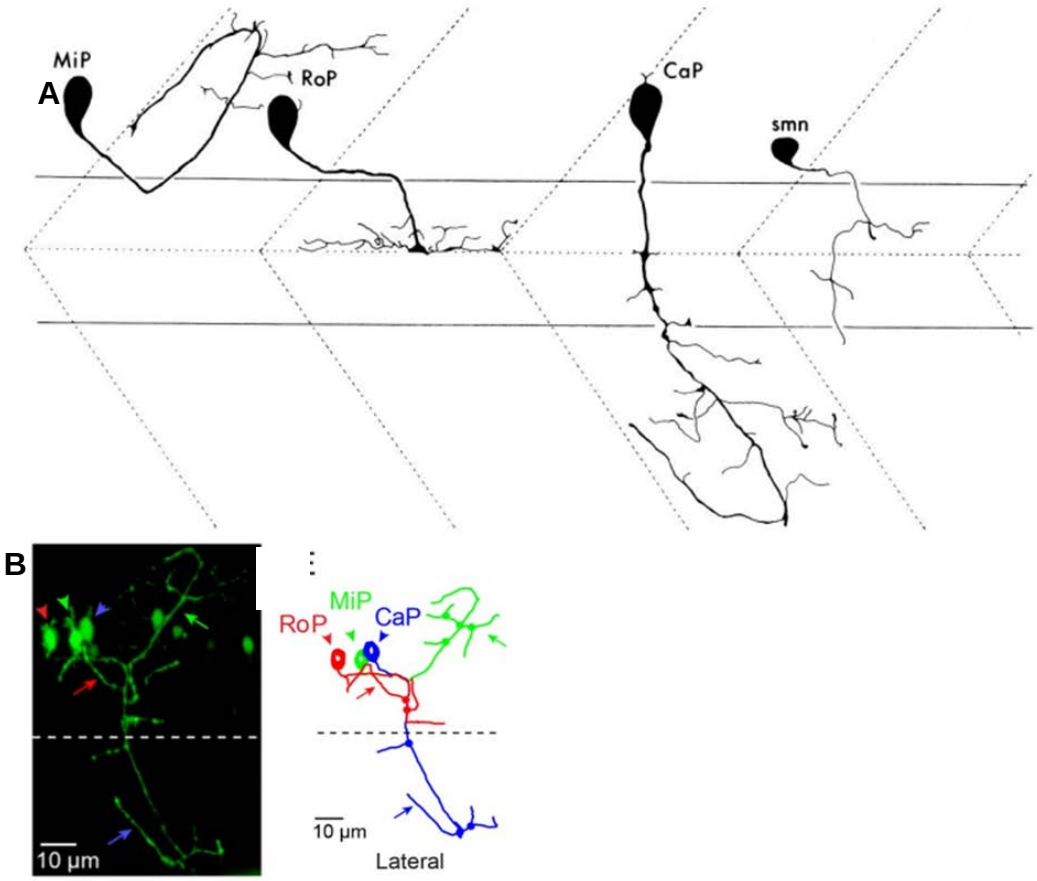

Figure 4.10 **Schematic representation of primary motor neuron development in zebrafish.** Primary motor neuron development in zebrafish follows a clear pattern. RoP (rostral) axons follow the notochord horizontal septum rostrally (solid horizontal line) before going ventrally and start branching along the horizontal septum (horizontal dotted line). MiP axons (middle) also go ventrally and rostrally until notochord and suddenly go up to the most dorsal part of the trunk. CaP (caudal) go straight down toward the ventral side and innervate that area where they branch. Secondary motor neurons are different in size of soma and axons (A). Confocal image of primary motor neurons and graphical representation of the same image (B). Images from Myers *et al.,* 1986 (top) and Issa *et al.,* 2012 (bottom).

4.2.6 Knock-down of rbm7, exosc8 and exosc3 causes defective growth of motor neuron axons in zebrafish

In order to understand the role of *rbm7*, *exosc8* and *exosc3* in neural development we analyzed the growth and pathfinding of motor neuron axons in all three morphants at 48 hpf. We stained synapses with SV2 antibody and α-bungarotoxin which bind respectively to pre-synaptic vesicles and AChRs.

In control fish SV2/αBGTX stainings show correct development of primary motor neurons. In all three morphants the axon growth was defective, specifically regarding CaP while growth of RoP and MiP seems to be overall correct. Sporadically, in *exosc8* and *exosc3* morphant fish, CaPs seem to branch earlier. In either case CaP fail to innervate the ventral trunk (Fig. 4.9). The phenotype resembles what observed in morphant zebrafish for *sema3a1*, a secreted class III of semaphorin (Sato-Maeda, 2006) and in a *smn* knock-down zebrafish model (McWhorter et al., 2003). The reduced length of the motor neurons resulted to be statistically sgnificant (Fig. 4.9).

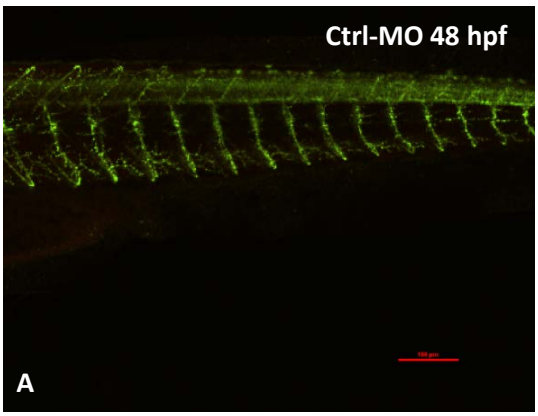
Ctrl-MO 48 hpf
A

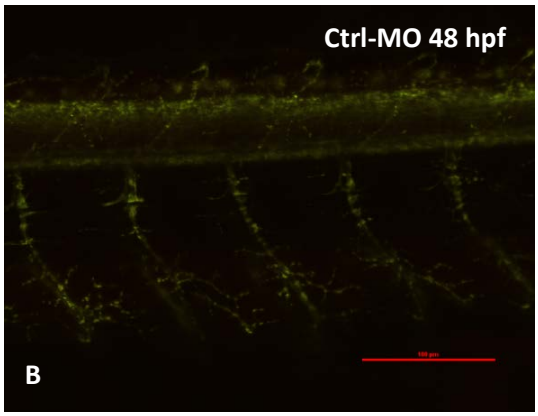
Ctrl-MO 48 hpf
B

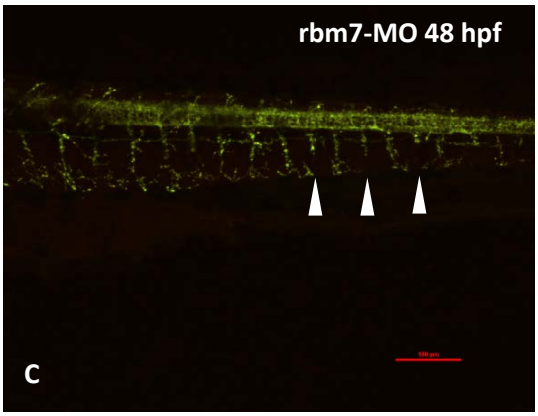
rbm7-MO 48 hpf
C

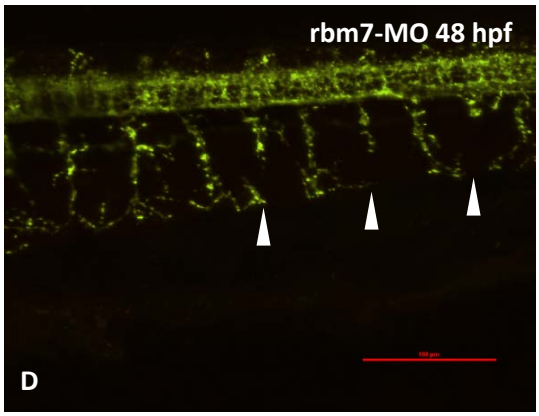
rbm7-MO 48 hpf
D

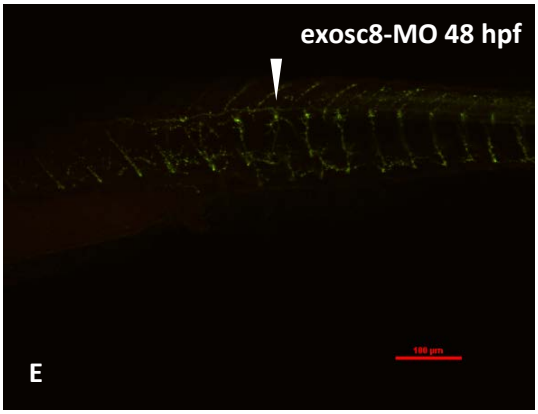
exosc8-MO 48 hpf
E

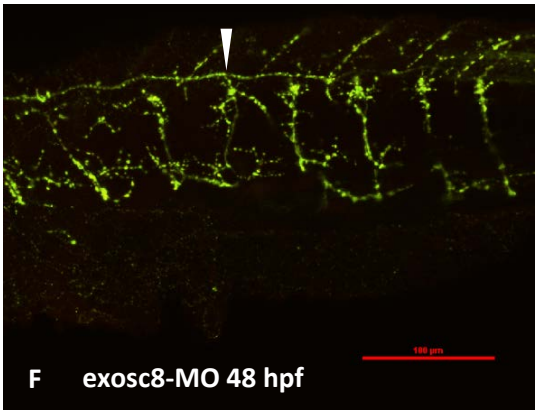
F exosc8-MO 48 hpf

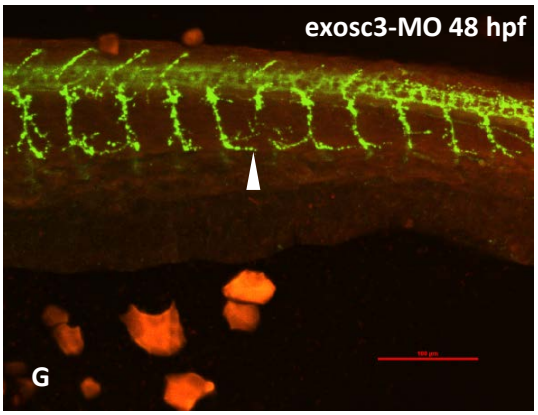
exosc3-MO 48 hpf
G

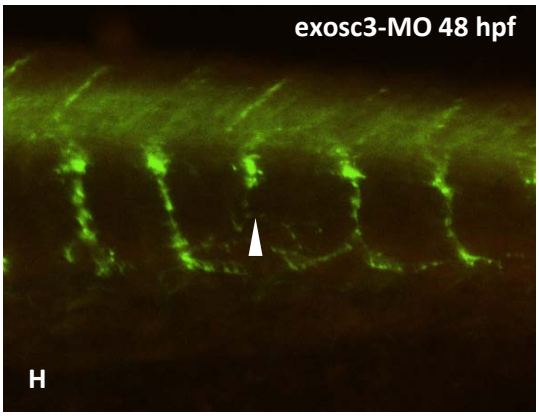
exosc3-MO 48 hpf
H

I

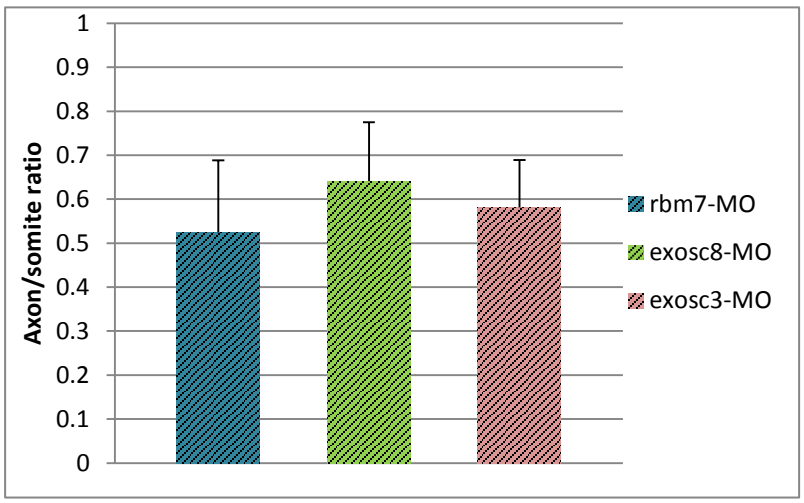

Figure 4.11 **Motor neuron axons defects in rbm7, *exosc8* and *exosc3* morphant fish and statistical analysis of axons length.** (A-H) Confocal images of motor neurons stained with SV2 (green) and αBGTX (red) in *rbm7*-MO, *exosc8*-MO and *exosc3*-MO. Structures of RoP, MiP and CaP can clearly be recognized in ctrl-MO fish. In all three morphants structure of CaP seem to be disrupted with premature stopping and defective branching. MiP seem to be relatively preserved. RoP seem to be missing in morphant fish. Scale bar = 100 μm. (I) axon/somite length ratio in morphant fish is significantly reduced compared to control injected fish (axon/somite length ratio = 1).

		Number of axons missing (*rbm7*-MO)							Total # of fish
		1	2	3	4	5	6	0	
# of fish/phenotype	Mild	1 (5.8%)	4 (23.5%)	3 (17.6%)	3 (17.6%)	-	-	6 (35%)	17
	Mod.	1 (16.6%)	-	1 (16.6%)	2 (33.2%)	1 (16.6%)	-	1 (16.6%)	6
	Ctrl	-	-	-	-	-	-	12	12

		Number of axons missing or defective branching (*exosc8*-MO)							Total # of fish
		1	2	3	4	5	6	0	
# of fish/phenotype	Mild	17 (48%)	3 (8.6%)	1 (2.8%)	-	-	-	14 (40%)	35
	Mod.	1 (4%)	8 (33.3%)	8 (33.3%)	6 (25%)	1 (4%)	-		24
	Ctrl	-	-	-	-	-	-	30	30

		Number of axons missing (*exosc3*-MO)							Total # of fish
		1	2	3	4	5	6	0	
# of fish/phenotype	Mild	10 (43.5%)	6 (26%)	-	1 (4%)	-	-	6 (26%)	23
	Mod.	4 (21%)	4 (21%)	4 (21%)	2 (10.5%)	2 (10.5%	2 (10.5%)	1 (5%)	19
	Ctrl	-	-	-	-	-	-	9	9

Table 9. **Axonal defects in different morphant and phenotypical classes.** Only mild and moderate phenotypes were considered for this analysis. Image from Giunta et al., 2016.

4.2.7 Imaging of Purkinje cells

In order to clarify the causes of defective cerebellar development in exosomal protein deficiencies, we analyzed differentiation of Purkinje cells (PCs) in zebrafish cerebellum. *rbm7*, *exosc8* and *exosc3* were downregulated and PCs were stained with an antibody against *pvalb7*, a well known marker of PCs (Bae et al., 2009). Knock-down of all three genes caused defective differentiation of PCs even in mild fish (Fig. 4.10). The layer of PCs in ctrl-MO fish has a peculiar wing-shaped structure, which fails to form in all three morphants. KD of all three genes results in a scattered structure which is never observed throughout the differentiating process. *pvalb*$^{+}$ cells are present since slightly before 3 dpf (Hamling et al., 2015) from progenitor cells expressing *ptf1a* (Kani et al., 2010) and since the beginning of cerebellar development the *pvalb*$^{+}$ layer has its characteristic shape.

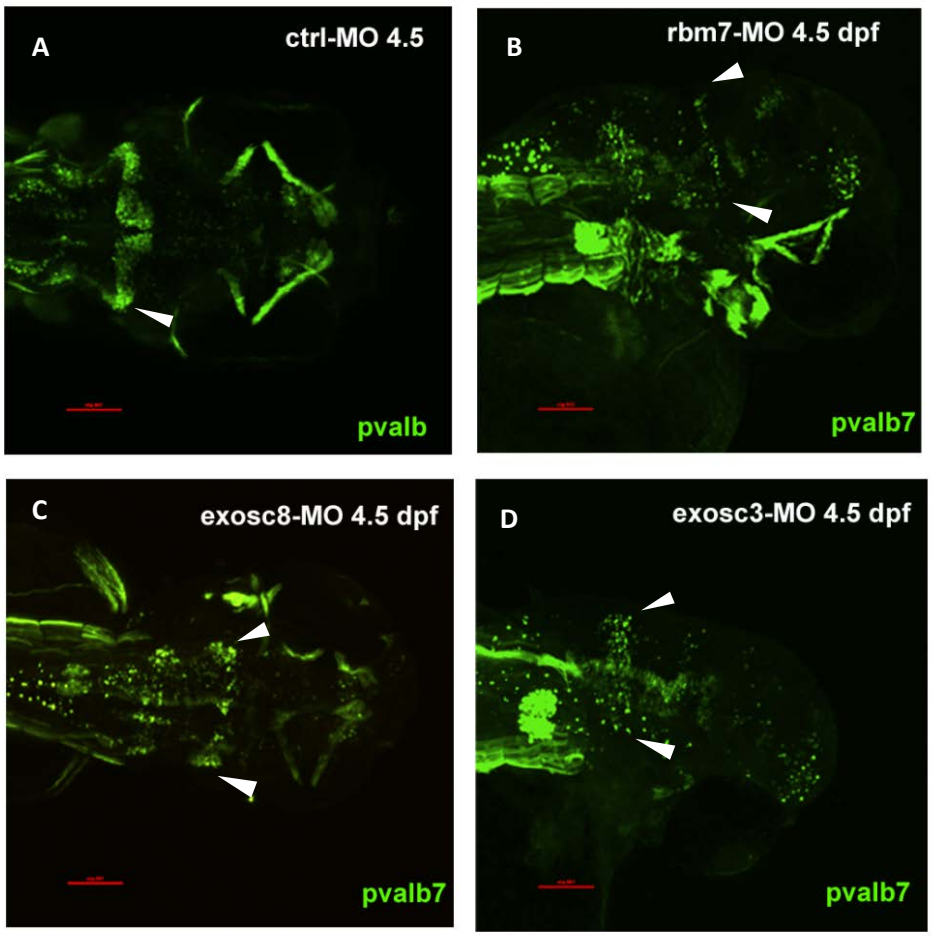

Figure 4.12 **Cerebellar structures in ctrl-MO, *rbm7*-MO, *exosc8*-MO and *exosc3*-MO injected fish.** Ctrl-MO injected fish show normal differentiation of PCs into the peculiar wing-shaped layer (arrowheads, A). Knock-down of all three genes cause defective differentiation of pvalb^{+} cells which result in a scattered layer of PCs (arrowheads, B-D). Only mild phenotype fish were considered for this analysis. 47% if *rbm7*-MO fish showed defects, 93% of *exosc3*-MO and 76% of *exosc8*-MO. Image from Giunta et al., 2016.

		Cerebellum (Purkinje cells)		Total # of fish
		Defective	Not defective	
rbm7-MO	Mild	9 (47%)	10 (53%)	19
	Mod.	5 (71%)	2 (29%)	7
exosc3-MO	Mild	14 (93%)	1 (7%)	15
	Mod.	13 (100%)	-	13
exosc8-MO	Mild	20 (76%)	6 (24%)	26
	Mod.	13 (100%)	-	13
	ctrl	-	20	20

Table 10. **Quantity and respective percentage of fish with cerebellar defects.** Only mild and moderate phenotypes were considered for this analysis. Image from Giunta et al., 2016.

4.2.8 Analysis of gene expression in morphant zebrafish

In order to understand the molecular pathomechanisms causing the neurodevelopmental defects observed in zebrafish after knock down of *rbm7*, *exosc8* and *exosc3,* transcript levels of several genes which were up or downregulated in mutant human fibroblasts have been analysed.

We tested the levels of *atxn1a*, *atxn1b*, *hoxc6a*, *hoxc6b*, *hoxc8*, *hoxc9*, hoxc10, *hoxc11a*, and *hoxc11b*. Gene expression was analysed for all three morphants (*rbm7*, *exosc8* and *exosc3*) in three different phenotypical classes (mild, moderate, severe) at four different developmental stages (12 hpf, 16 hpf, 24 hpf and 48 hpf). The analysis was repeated on three biological replicates. Because expression of reference genes (EF1-α and β-actin) was found to be very variable throughout development, expression levels of target genes was compared to expression levels of reference genes at the same developmental stage. Although small differences could be observed, analyses of *hox* genes did not show any statistically significant difference in transcript levels between morphants and uninjected controls. This may be due to tissue and/or species specificity of expression. Instead, *atxn1b* show a great increase in expression after knock down of all three genes (Fig 4.11).

ATXN1 is present in two paralogs in zebrafish: *atxn1a* and *atxn1b* (Carlson et al., 2009)*. atxn1a* (ENSDARG00000061687) is situated on Chr:19 while *atxn1b* (ENSDARG00000060862) is located on Chr:16. Interestingly, levels of *atxn1b* but not *atxn1a* were highly increased in morphants compared to controls at 12hpf, 16 hpf and 24 hpf. At 48 hpf *atxn1b* levels returned near to normal.

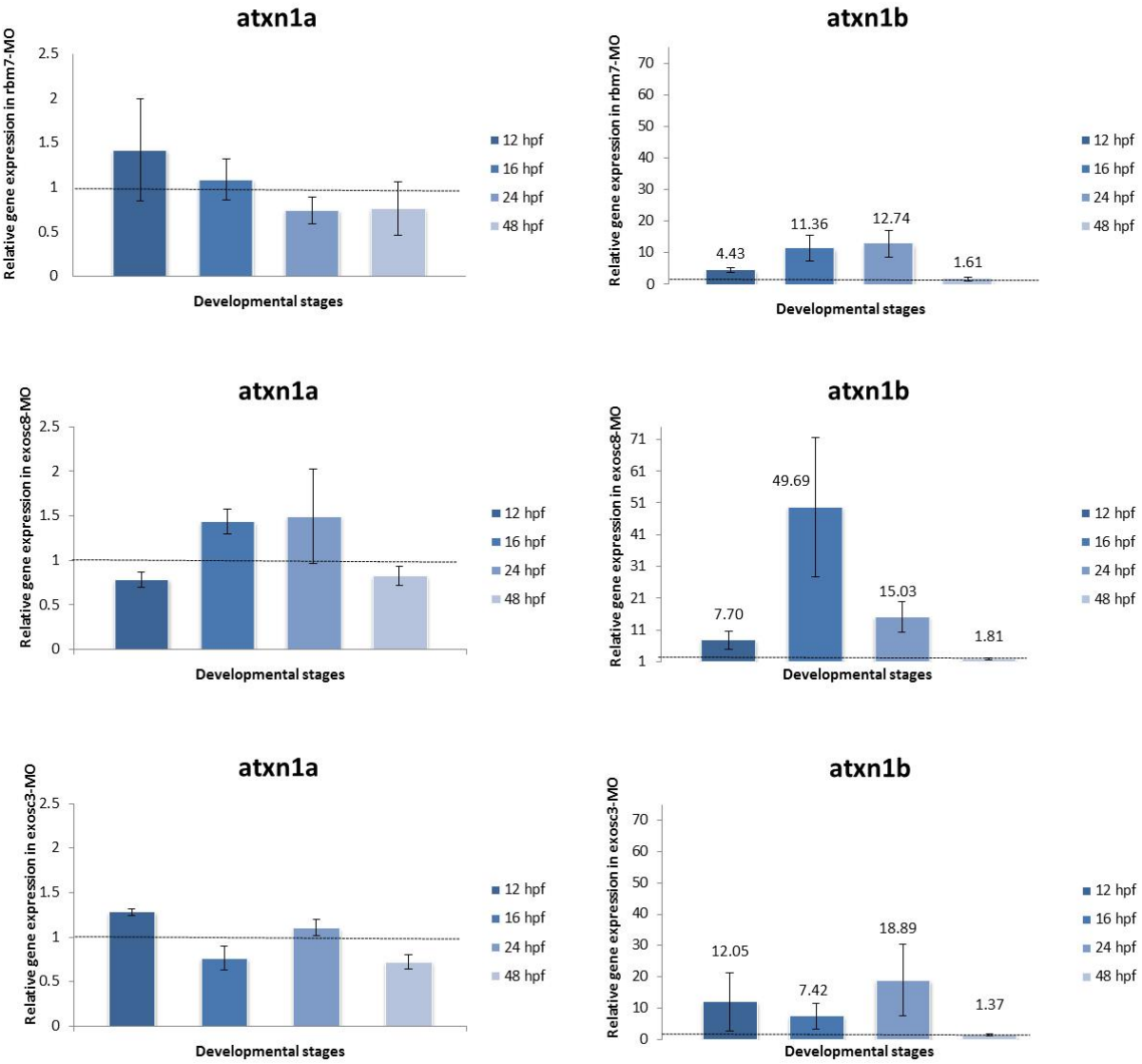

Figure 4.13 **Transcript levels of *atxn1a* and *atxn1b* after *rbm7*, *exosc8* and *exosc3* knock-down.** Gene expression was analysed at 4 different developmental stages in mild phenotype fish (from 24 hpf, when a phenotype could be seen). qRT-PCRs were repeated on 3 biological replicates. *atxn1a* did not show any significant change after gene knock-down (left column). *atxn1b* expression shows a dramatic increase after knock-down of all three genes (right column). Bars indicate S.D.

4.2.9 In silico analysis of AU content of ATXN1, atxn1a and atxn1b

Human *ATXN1* (ENSG00000124788) is located on Chr:6 and it has 2 protein coding isoforms of the same length (815 aa). Zebrafish *atxn1a* has 2 isoforms: which share exactly the same identity and similarity with the human gene (43% identity and 55% similarity). *atxn1b* has only one protein coding transcript which shares 36% identity and 48% similarity with the human homolog. Analysis of AU-rich element score through AREscore (Spasic et al., 2012) showed that human ATXN1 has a similar, high AREscore to *atxn1b* whereas *atxn1a* has a much lower score (table 6).

Name	Score	Pentamer count	Sequence length
H. sapiens ATXN1 ENST00000244769	21.65	17	12967
D. rerio *atxn1a* ENSDART00000167664	3.3	3	3139
D. rerio *atxn1b* ENSDART00000149411	19	16	8697

Table 11. In silico analysis of AU content in ATXN1, atxn1a and atxn1b. Analysis of AU content through AREscore (http://arescore.dkfz.de/arescore.pl) show *atxn1a* and *atxn1b* have a great difference in AU content. Human ATXN1 has a similar score to *atxn1b*.

4.3 Discussion and future directions

RNA processing and metabolism is known to be important for efficient development of neural system and functions. Mutations in *SMN* - a splicing factor - cause Spinal Muscular Atrophy (SMA) (Seng et al., 2015). Correct levels and structure of non-coding RNAs are involved in a variety of neurological diseases (Saitsu et al., 2011) (Lin et al., 2014) (Qureshi and Mehler, 2013). Incorrect tRNA transcription and processing also affects neural system (Breuss et al., 2016) (Simonati et al., 2011) (Li et al., 2015) (Antonellis et al., 2006)

Interestingly, among these neurological disorders, a specific subgroup is caused by mutations on sub-units or co-factor of the exosome complex, the main cellular RNA degradation machinery. Mutations in genes encoding exosomal subunits EXOSC3 (Wan et al., 2012), EXOSC8 (Boczonadi et al., 2014), EXOSC2 (Di Donato et al., 2016a) and exosome co-factor subunit RBM7 (Giunta et al., 2016) cause severe childhood-onset neurological symptoms including pontocerebellar hypoplasia, spinal

muscular atrophy and central nervous system demyelination, raising many questions about the pathomechanisms underlying these disorders. In this thesis I present a comparative analysis of functions of *rbm7*, *exosc8* and *exosc3* in zebrafish which further confirm the role of correct RNA processing in vertebrates neurodevelopment and highlights some new aspects of these pathologies.

These data show for the first time that the exosome complex has a role in axon development of motor neurons, specifically affecting the primary motor neurons. Knock down of *rbm7*, *exosc8* and *exosc3* cause defective axon growth and pathfinding of CaP in a very similar way to *smn* knock down zebrafish (McWhorter et al., 2003) suggesting that this early developmental defects may lead to subsequent neurodegeneration. The percentage of defective axons with defects at 48 hpf suggest that, analysing the level of motor neuron loss at later stages in the same morpholino-injected batch may be of interest, although it may be difficult to estimate, due to extended axons branching at later stages.

The molecular causes of these defects are not known. I compared the RNA-seq data from patient fibroblasts and identified many HOX genes differentially expressed. HOX genes are known to be involved in motor neuron development (Giunta et al., 2016) therefore that seemed a logical path to follow. I thorougly analyzed a set of HOX genes in zebrafish after gene knock down in order to find the downstream molecular events responsible for the defects but could not find any clear indication. Some of the HOX genes analyzed were slightly differentially expressed but always <2 fold change therefore not statistically significant. This may be due to the fact that analysing the whole embryo instead of the single cell introduces a lot of background signal during qRT-PCR analysis or, assuming that the human fibroblast data are reflecting the causes of neuronal defect, the downstream effects may be different from human to zebrafish.

Many other genes are involved in axonal growth. I tested in zebrafish the expression of another gene (*CACNA1G*), which is differentially expressed in both human fibroblasts carrying mutations in *EXOSC8* and *RBM7* which - according to Reactome (Fabregat et al., 2016) - is involved in axonal guidance through NCAM1 interactions (Reactome Reaction “NCAM1 interacts with T- and L-type VDCC”). Reactome is a pathways analysis software which is able to indicate which cellular pathways are affected by differential expression of genes. It can be very helpful for understanding

the meaning of large datasets obtained from analysis such RNA-seq, metabolomics and proteomics. However no differential expression could be found in zebrafish. We are confident that taking advantage of the *rbm7* (and *exosc8*) mutants we have created (which will be described in detail in the next chapter) we will be able to address these questions.

It will be interesting to analyse in detail the pathfinding of primary motor neuron axons using the *islet1*:GFP fish. This fish expresses GFP in the soma of neurons, and co-staining with SV2 will follow the growth of the axon. In future studies on mutant fish we will perform qRT-PCR of some genes which are known to be involved in axon pathfinding in zebrafish such as semaphorins (Sato-Maeda, 2006).

In the cerebellum the reduction of Purkinje cells is a clear hallmark of PCH1 (Eggens et al., 2014). It was already shown by others that *pvalb7* transcript levels were reduced in a zebrafish model of PCH1 (Wan et al., 2012). We wanted to test if protein expression was also reduced in all three knock-down models we have made: *rbm7*-MO, *exosc8*-MO and *exosc3*-MO. As expected we could observe defective *pvalb*$^{+}$ layer also in *exosc8* morphant fish, but rather unexpectedly we observed the same also in *rbm7*-MO, although less frequently.

The defects observed in downregulated fish at 4.5 dpf cannot be considered just as a developmental delay. Indeed, PCs start differentiating just before 3 dpf and throughout development not such a scattered structure can be observed (Kani et al., 2010) (Hamling et al., 2015).

A molecular explanation of the pathomechanism may be provided by the results of the qRT-PCR. Investigation of levels of *atxn1a* and *atxn1b* showed that *atxn1b* is present in much higher levels in knock down fish up to 48 hpf when they return close to normal levels. *In silico* analysis of the AU content of the gene shows it has a high score, similar to the human *ATXN1* gene. Here I note that the exosome complex is known to perform degradation of genes which expression is only transiently required, such as the AU rich element containing genes (Chen et al., 2001). *ATXN1* is important for correct cerebellar development, is linked to the pathogenesis of spinocerebellar ataxia type 1 (SCA1) (Matilla-Dueñas et al., 2008) causing neurodegeneration of PCs and other brainstem structures in human (Ju et al., 2014) and mice (Ebner et al., 2013) caused by either a toxic gain of function due to the polyQ extension or overexpression of the wild type gene. Overexpression of wild type

ATXN1 is toxic for PCs and lead to neural degeneration in mice and *D. melanogaster* (Tsuda et al., 2005) (Fernandez-Funez et al., 2000). A similar pathomechanism may occur in our model due to overexpression of *atxn1b* caused by impaired functionality of the exosome complex.

A similar pathomechanism driven by overexpression of an ARE gene (*mbp*) was found to cause defective myelination in a zebrafish *exosc8*-MO model. In that case also, defective functionality of the exosome complex caused reduced degradation of *mbp*, which supposedly impairs correct formation of myelin sheats around the axons (Boczonadi et al., 2014). It is interesting to notice the rescue of hindbrain structures caused by co-downregulation of *mbp* after knock-down of *exosc8*. Thisse et al., showed that *mbp* RNA is expressed much earlier than the onset of myelination in the oligodendrocites in the hindbrain (zfin.org). That may explain why defective *mbp* metabolism due to *exosc8* knock down has such a detrimental effect on hindbrain structures and also why downregulation of overexpressed *mbp* rescues the same structures.

A more detailed analysis of the defects observed in cranial motor neurons may provide further information. Through confocal microscopy, axon growth can be followed throughout de velopment. Live imaging of knocked down (or mutant) islet1:GFP fish may allow to understand which neurons are affected and which are not, and compare real-time development of cranial motorneurons in mutant and control fish.

5 Chapter 5: Results - Mutant zebrafish models of exosomal proteins deficiency through CRISPR/Cas9 technology

Very recently a new technology for site specific mutagenesis has been developed based on the CRISPR/Cas system (Cong et al., 2013) (Mali et al., 2013). Until then, previous mutagenesis technologies (zinc finger nucleases – ZFNS - and transcription activator-like effector nucleases - TALENS) had a much lower efficiency (Varshney et al., 2015).

The Clustered Regularly Interspaced Short Palindromic Repeats (CRISPR)/CRISPR Associated (Cas) is a natural defense system in prokaryotes (Haft et al., 2005), identified for the first time by Ishino and colleagues upstream of the *iap* gene in *E. coli* (Ishino et al., 1987).

Although at that time the biological role of these clustered repeats within the prokaryotic genome was unknown, few years later three independent *in silico* studies (Mojica et al., 2005) (Pourcel et al., 2005) (Bolotin et al., 2005) demonstrated homology between these repeats and extra-chromosomal elements such as viruses and plasmids, leading to the hypothesis that these repeated sequences were a defensive mechanism of archaea and bacteria against invading viruses and plasmids (Makarova et al., 2006) (Horvath and Barrangou, 2010) (van der Oost et al., 2009).

In order to build this defence system, microbes take up genetic material from invaders and build up these loci (CRISPR) which are able to target specific sequences of the intruders' genome. These CRISPR sequences (usually about 20 nt long) co-transcribe with Cas genes which encode for endonucleases. If Cas is co-transcribed with a specific sequence (CRISPR), able to target the exogenous genome, the CRISPR/Cas system will provide adaptive immunity against phages or plasmids. There are many types of Cas proteins. Bionformatic analysis has shown that there are about 65 different orthologous in different organisms, which can be classified in three different systems (Makarova et al., 2011). Cas9 - which contains at least 2 nuclease domains - belongs to type II CRISPR/Cas system (Makarova et al., 2011). CRISPR/Cas9 system needs a proto-spacer adjacent motif (PAM) sequence to work, which is an "NGG" (being "N" any nucleotide) sequence, downstream of the CRISPR target sequence (Fig. 5.1) (Wu et al., 2014). The predicted cut site on the target genome is 3 nucleotides upstream of the PAM sequence (Jiang et al., 2013)

(Jinek et al., 2012). Autoimmunity in microbes is prevented thanks to the lack of a PAM sequence within the CRISPR arrays.

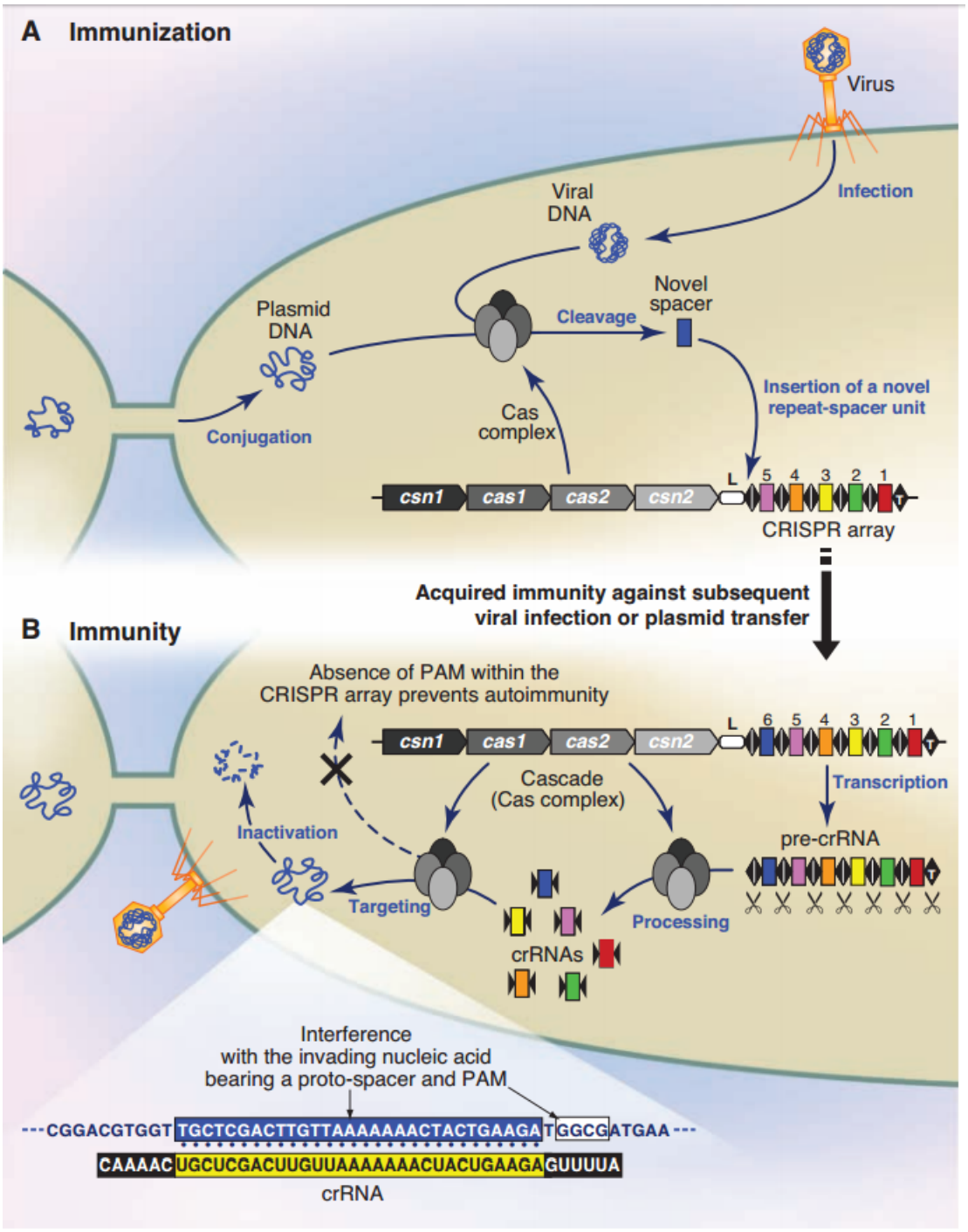

Figure 5.1 **CRISPR/Cas is an acquired immune system of bacteria and archaea.** During the first infective event, viral or plasmid DNA is cleaved and incorporated into the bacterial genome immunizing the cell from further infections (A). When a second infective event occurs, the previosuly incorporated exogenous DNA fragments act as guide RNAs, in fact "guiding" Cas protein to target regions of the invading genome, causing inactivation through cleavage (B). Autoimmunity is prevented due to lack of PAM sequences on the prokaryote genome (Image modified from Horvath and Barrangou, 2010).

The CRISPR/Cas9 system has been adapted to produce sequence specific double strand breaks (DSB) in eukaryote's genomes. For our purposes, the CRISPR sequence is substituted with a single-guide RNA (sgRNA) which is designed to target a specific sequence. The sgRNA is co-transcribed with Cas9 RNA, which will be subsequently translated, allowing the cleavage of the DNA introducing random deletions or insertions via the non-homologous end joining (NHEJ) system (Armstrong et al., 2016) (Irion et al., 2014).

5.1 Overview of the technique

5.1.1 Designing sgRNA and testing efficiency in the F0:

In order to perform mutagenesis in zebrafish two sgRNAs against 2 exons of *rbm7* were designed using CRISPRscan (Fig. 5.2; Moreno-Mateos et al., 2015; http://www.crisprscan.org/) targeting exon 2 and exon 4.

CRISPRscan categorizes all potential guide RNAs based on their efficiency. Score >70 is highly efficient sgRNA, >55 is efficient sgRNA. In the UCSC interface, bright green is for "high activity sgRNAs", grey-green is for "low CRISPRscan score", grey is for "sgRNA with potential off-target effects" (Fig. 5.2).

The selected sgRNAs have respectively a score of 56 (bright green) for exon 4 and score of 33 (grey-green) for exon 2 (Fig. 5.2).

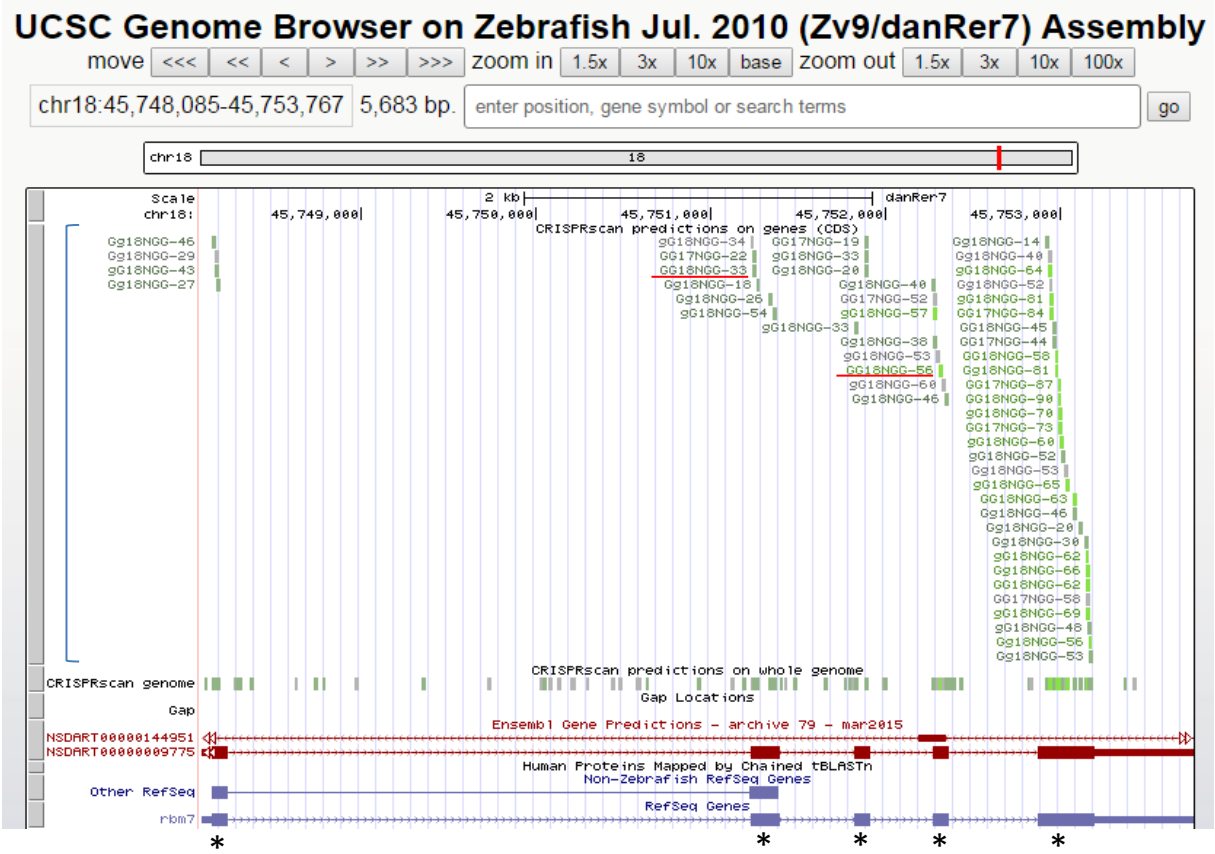

Figure 5.2 **Screenshot of the UCSC-based interface of CRISPRscan.** CRISPRscan works on a UCSCgenome based interface. Selecting the organism and typing the name of the gene we need automatically show this page with a graphical representation of the gene (RefSeq genes, blue) with exons (asterisks) and introns. All potential sgRNAs are listed above in different shades of green(blue bracket) corresponding to the exons. 2 sgRNAs were chosen for our experiment based on position on the gene and efficiency score (underlined in red).

Synthesis of sgRNA and purification was performed as described before (Varshney et al., 2015). Mutations in the F0 are known to be mosaic and we wanted to avoid mixing WT and mutant genomes when sequencing for testing the system, which would have resulted in a noisy electropherogram (or it would have caused impossibility to read the mutant sequences). Therefore, in order to test the efficiency of the sgRNAs and injection method, we injected sgRNA + Cas9 RNA in embryos at 1 cell stage of development, extracted genomic DNA from 10 injected embryos at 24 hpf, amplified the exon of interest by PCR and cloned it into a plasmid, which was subsequently transfected in *E.coli*. We then plated the bacteria and performed colony PCR in a 96 well plate and sequenced the PCR product. This system allowed having only one copy of the gene per colony and therefore a clear electropherogram.

5.2 Results:

5.2.1 Testing mutagenesis efficiency in F0

Considering that genomic DNA from 10 fish was extracted, we calculated efficiency % based on how many mutations were found in a 96 well-plate. An average efficiency of 6.5% for Exon 2 and 13% for Exon 4 was observed.

With sgRNA_56 against exon 4 we identified 3 different types of mutation in F0. Two of them were subsequently identified in F1 as well (Fig 5.3):

- c.440delCA (also found in F1)
- c.434delCCTCCACAG (also found in F1)
- c.442delGCACA (not found in F1)

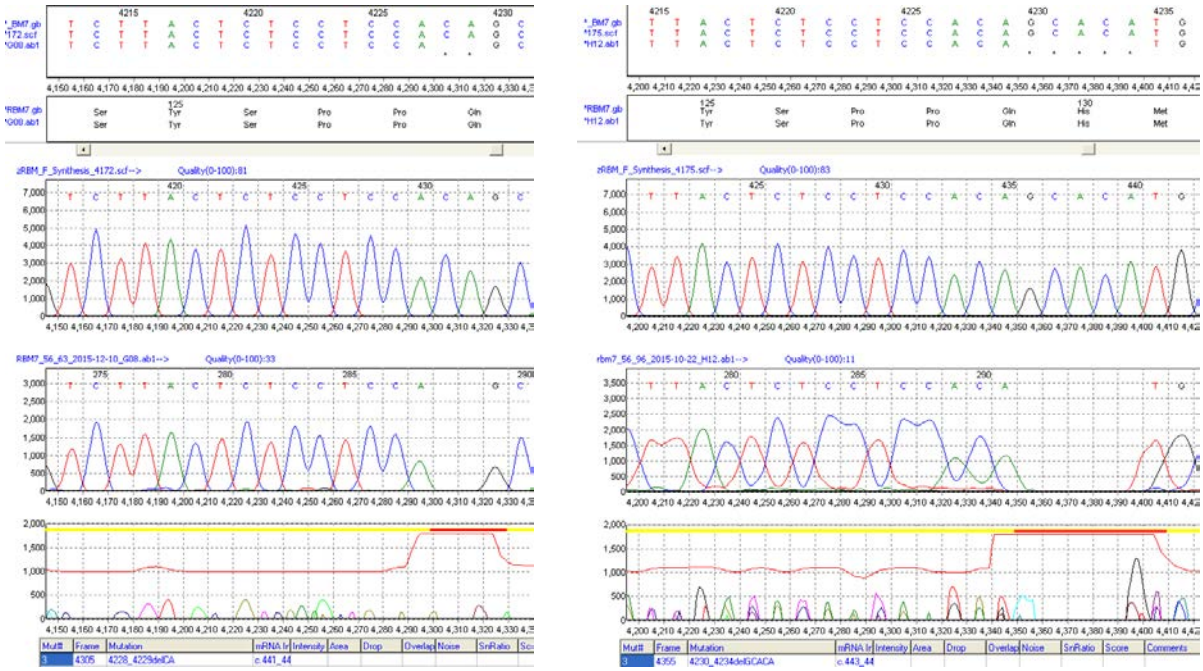

Figure 5.3 **Sequencing of *E. coli* colonies with insertion of Ex4.** Genomic DNA extraction and insertion into bacterial cells followed by Sanger sequencing allowed to clearly identify “homozygous” deletions within the exon. Red orizontal bars at the bottom show deletions.

Analysis of the predicted effect of the mutation on the protein structure with EMBOSS Transeq (http://www.ebi.ac.uk/Tools/st/emboss_transeq/) provided the following results:

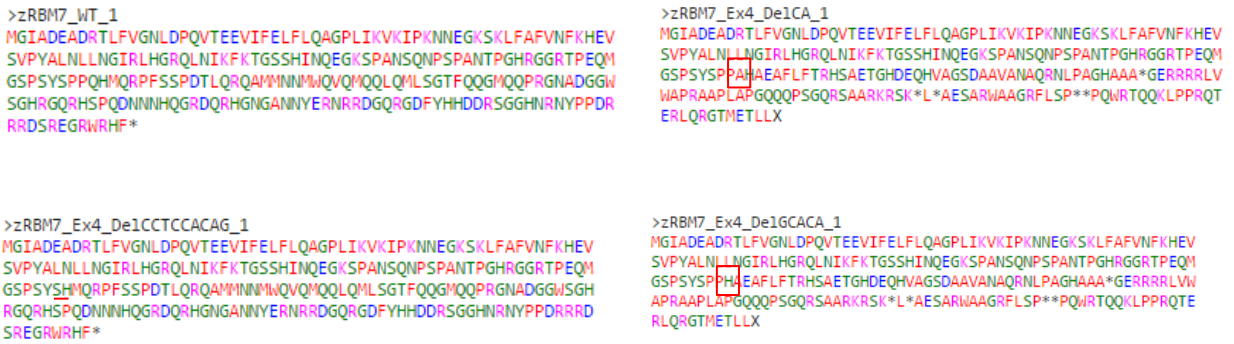

Figure 5.4 ***In silico* prediction of exon 4 mutations effects on amino acid sequence.** Top left: Wild type zebrafish *rbm7* sequence. Top right: the identified frameshift mutation 4228_4229delCA is just after the P highlighted by the red square. It is predicted to cause different downstream stop codons. In-frame deletion c.434delCCTCCACAG cause deletion of P-P-Q (underlined in red, bottom left). Frameshift deletion c.442delGCACA also creates several downstream stop codons, possibly causing a C-terminal truncated protein (bottom right).

Mutations c.440delCA and c.442delGCACA are frameshift deletions and predicted to create stop codons at different points within the amino acid sequence. c.434delCCTCCACAG is an in-frame deletion and predicted to remove three amino acids (P-P-Q) from the protein but does not cause a downstream stop codon (Fig. 5.4).

With sgRNA 33 for Exon2 we found 2 different types of mutation in the F0 (Fig. 5.5, Fig. 5.6):

- c.156delCA
- c.156delC

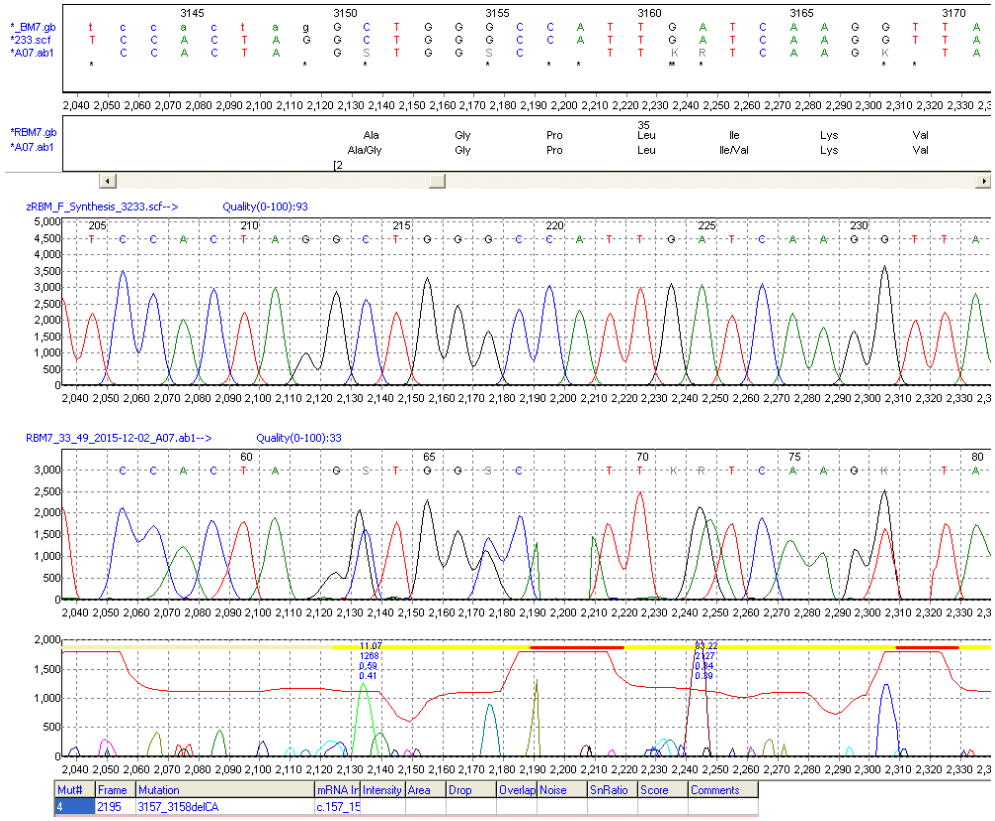

Figure 5.5 **Representative image of a deletion in exon 2.** Representative image of sequencing of *E. coli* colonies with insertion of *rbm7* exon2. Efficacy of the system could be easily checked thanks to the clarity of the electropherogram. Red orizontal bars show a deletion.

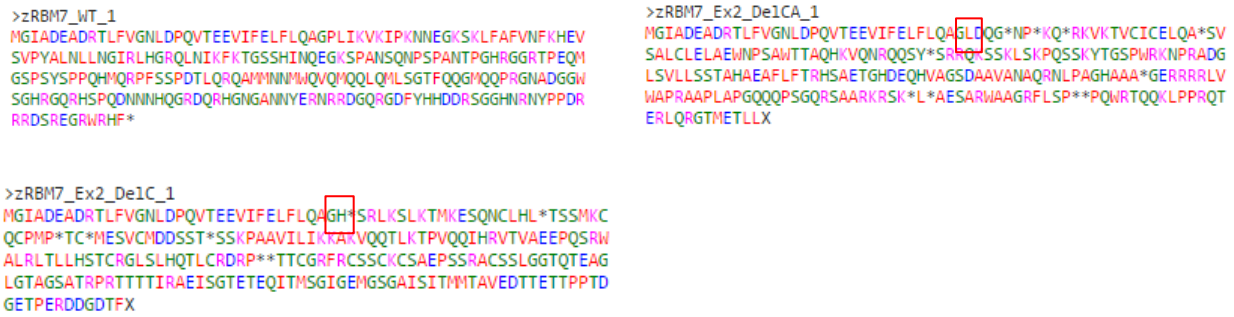

Figure 5.6 ***In silico* prediction of exon 2 mutations effects on amino acid sequence.** Either c.156delCA and c.156delC are frame-shift mutations (red square top right and bottom left) and predicted to create stop codons soon after the mutation itself, Because the stop codon is >50-55 nt before the next exon-exon boundary, these mutations are likely causing a *non-sense mediated* decay of RNA (Popp and Maquat, 2016).

5.3 Breeding strategy – overview.

F0 injected fish were left to grow up to 3 months of age, until sexual maturity was reached.

About fifteen F1 fish were screened for mutation transmission pairing two F0 injected fish. If at least one fish of the progeny was positive for the mutation, the two F0 fish were out-crossed with a WT *golden* fish to understand which one was the carrier of the mutation (male or female). Progenitors which resulted to have progeny negative for the mutation were discarded. From the outcrossing of positive F0 fish, some of the F1 were sequenced in order to discriminate the carrier of the mutation, and the rest was left to grow up to 3 months of age. Adult F1 fish were later screened by fin-clipping in order to separate them by mutation type (Fig. 5.7).

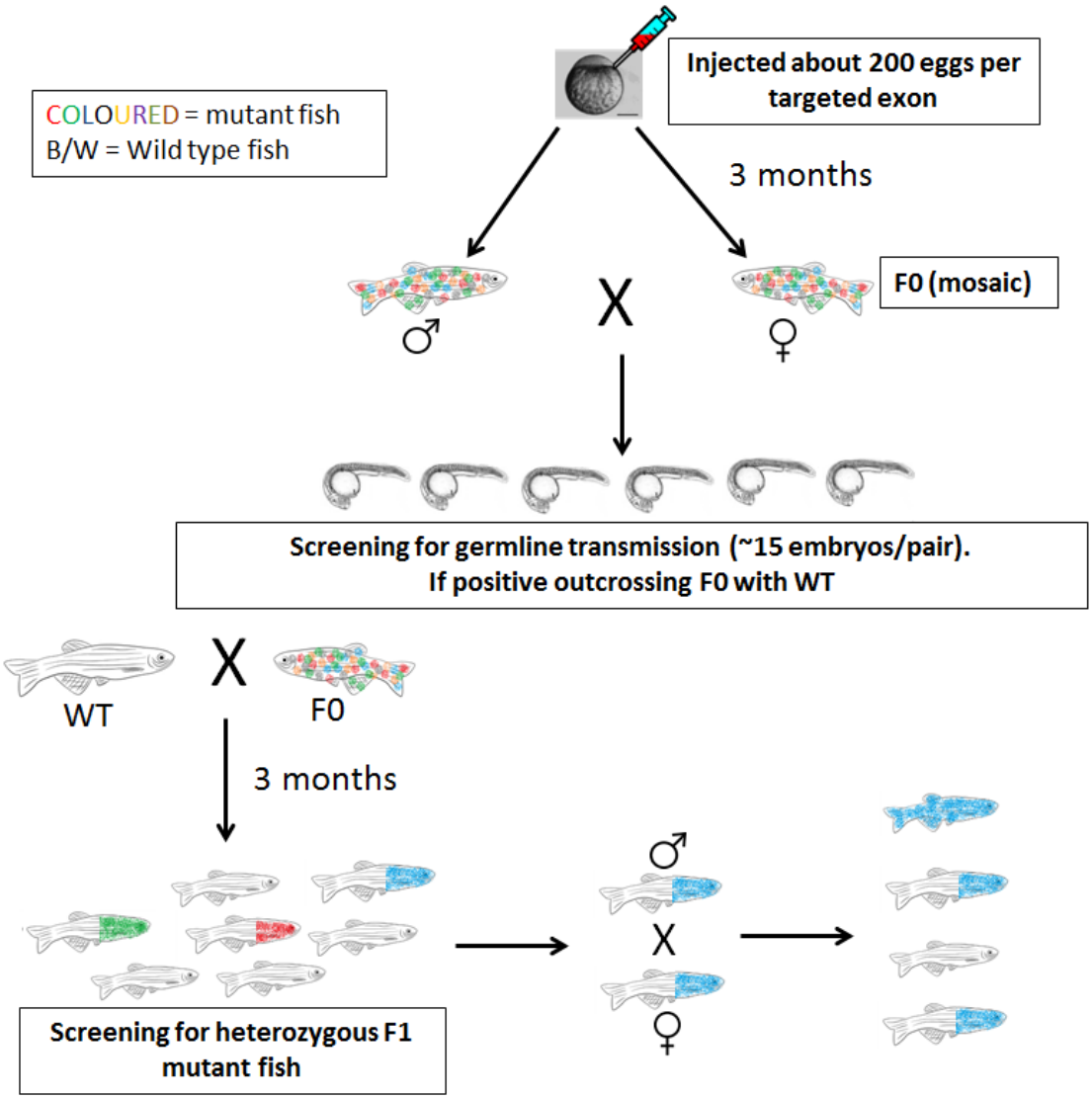

Figure 5.7 **Breeding strategy in order to obtain a stable mutant strain.** About 200 eggs from different batches were injected with sgRNA+Cas9 RNA in order to have enough F0 adults. F0 are known to be mosaic mutants so they may not carry the mutation into the germline and they may not be able to transmit it to their progeny. Therefore, a screening of the F1 embryos was carried out in order to identify those F0 adults able to transmit the mutation. Some batches resulted to be negative (0% transmission), some others resulted to be positive. From the positive batches, F0 fish were outcrossed with a wild type fish in order to understand which fish was the carrier (male or female). This heterozygous F1 has been left to grow and sequenced in order to separate the fish based on different types of mutations.

5.4 Genotyping of F1 zebrafish

Germline transmission resulted to be very variable. For some of the injected batches was 0%, for some others it was positive.

In the positive ones, a high germline transmission rate (Fig 5.8) could be observed. In order to better understand which one was the actual carrier of the mutation (male or female) F0 fish were outcrossed with a wild-type *golden* fish. In many cases both fish

were carrying mutation(s) in the germline. Furthermore, different types of mutations were identified in the germline from the same fish (Fig. 5.8).

For sgRNA_56_Ex4, 92 F1 embryos were screened from 8 outcrossed pairs, we found an overall germline transmission rate of 32.60% (n=30).

90% of the mutations were deletions and 10% insertions. 9 different types of deletions and 2 different types of insertions were found in all mutants. Up to 5 different types of mutations were found in the progeny of a single F0 fish (summarized in Fig. 5.8). F1 fish were let to grow and screened for mutations when adults by fin clipping. Different types of mutants will be grown and bred separately to study the role of different mutations on embryo development.

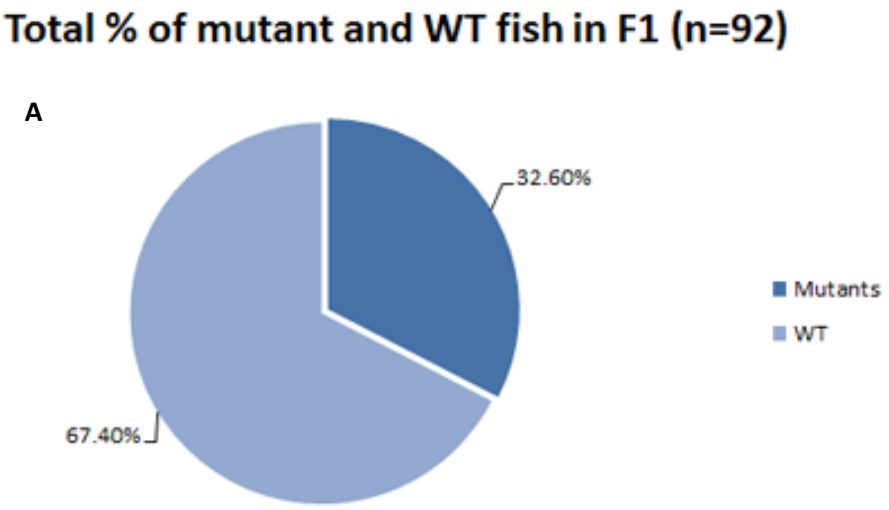
Total % of mutant and WT fish in F1 (n=92)
A
32.60%
67.40%
Mutants
WT

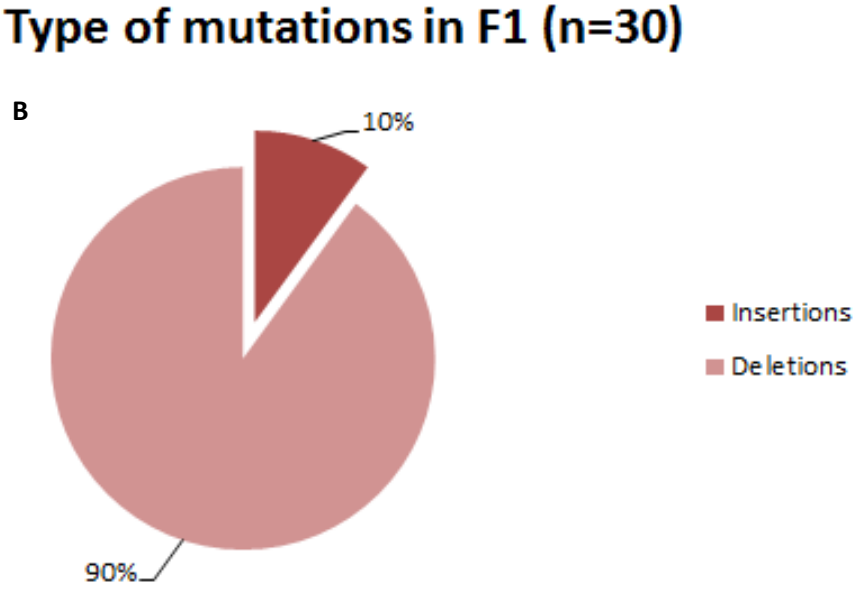
Type of mutations in F1 (n=30)
B
10%
90%
Insertions
Deletions

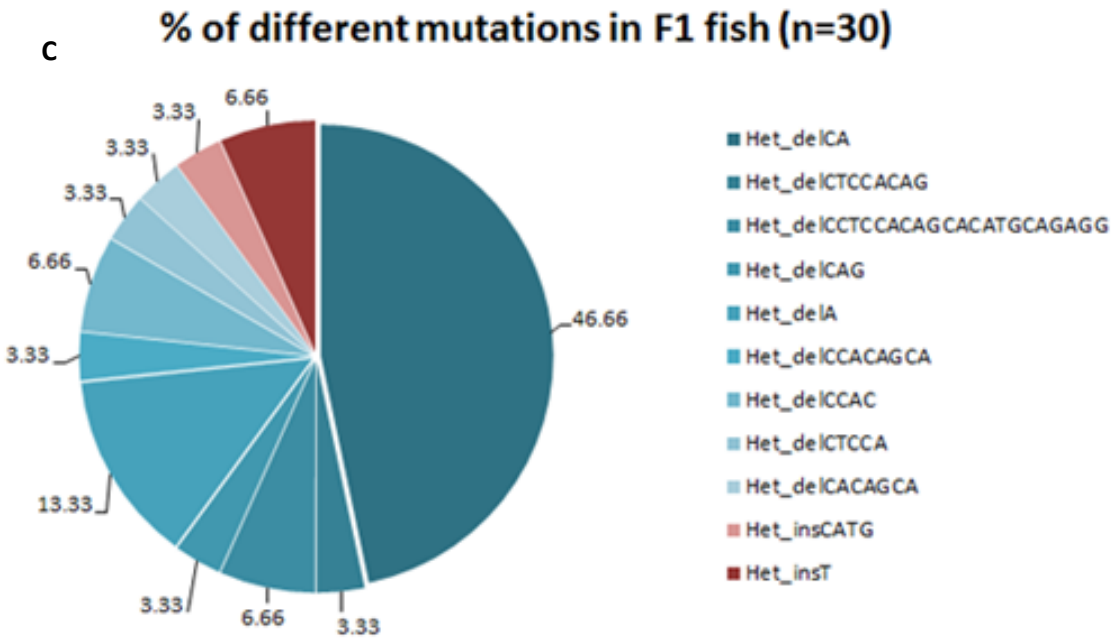
% of different mutations in F1 fish (n=30)
C
46.66
13.33
6.66
3.33
3.33
3.33
3.33
6.66
3.33
6.66
3.33
Het_delCA
Het_delCTCCACAG
Het_delCCTCCACAGCACATGCAGAGG
Het_delCAG
Het_delA
Het_delCCACAGCA
Het_delCCAC
Het_delCTCCA
Het_delCACAGCA
Het_insCATG
Het_insT

Germline transmission and mutation types relative to F0 fish #1 (♂) n=12

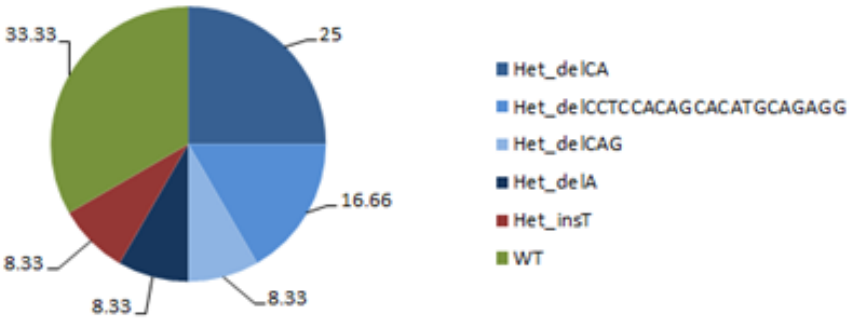

Germline transmission and mutation types relative to F0 fish #2 (♀) n=11

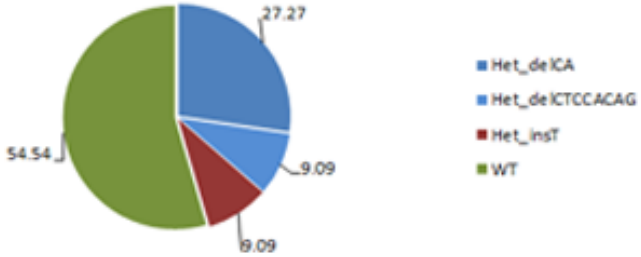

Germline transmission and mutation types relative to F0 fish #3 (♂) n=12

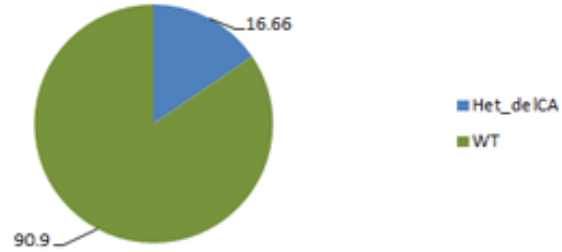

Germline transmission and mutation types relative to F0 fish #4 (♀) n=12

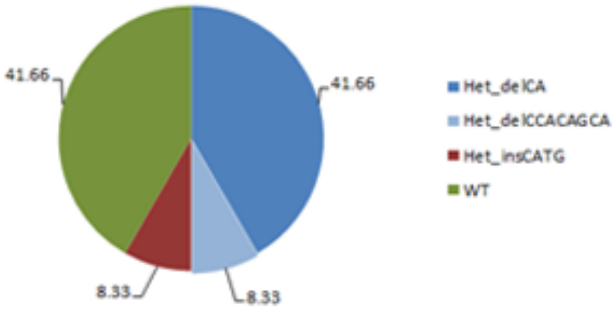

Germline transmission and mutation types relative to F0 fish #5 (♀) n=12

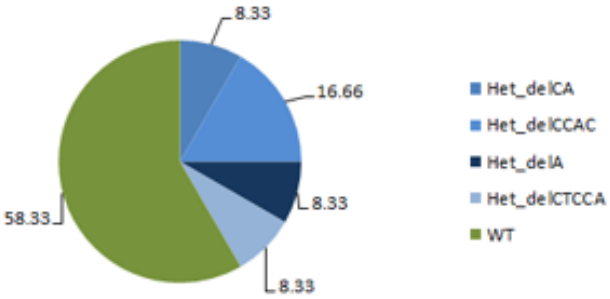

Germline transmission and mutatio n types relative to F0 fish #7 (♂) n=12

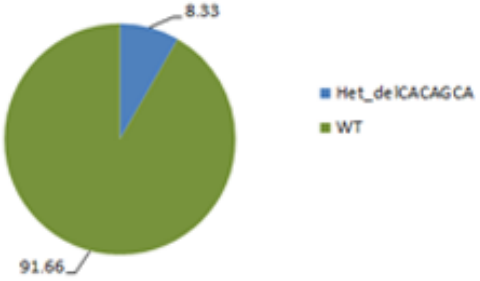

Germline transmission and mutation types relative to F0 fish #8 (♀) n=9

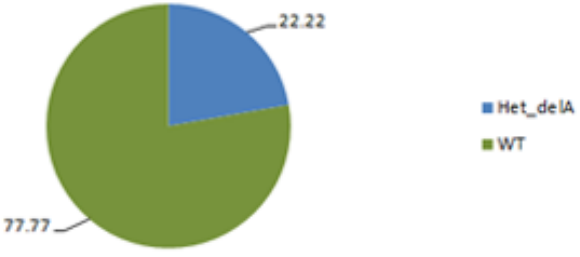

Figure 5.8 **Analysis of germline transmission for sgRNA_Ex4.** Total germline transmission in the F1 was similar to what previously reported by others (A); Several types of mutation were find for a single sgRNA, either insertions and/or deletions (B, C); Even within a single fish, the same sgRNA caused different types of mutations (E-L), fish #6 was not included in the analysis as it had 0% germline transmission. Overall the most frequent seems to be a frameshift deletion of CA.

Regarding *rbm7* exon 2 mutagenesis, the same number of eggs was injected with sgRNA for exon2 + Cas9 RNA. After three months, screening for germline transmission showed again that for some batches the injection and mutagenesis worked fine, for some others did not work. For those batches that contained mutations, germline transmission was about 20%. Types of mutations were different than for exon 4. Indeed in exon 2, other than insertions and deletions (accounting together for about 76% of total mutations), 23% were duplications (n=17). None of the mutations previously found in the F0 was identified in the F1.

8 different types of mutations were identified (4 deletions, 2 insertions and 2 duplications). Up to 3 different types of mutations were found in the progeny from a single F0 fish (Fig. 5.9).

For both sgRNAs, no clear differences in the types of mutation or % of germline transmission was seen between males and females.

Total % of mutant and WT fish in F1 (n=84)

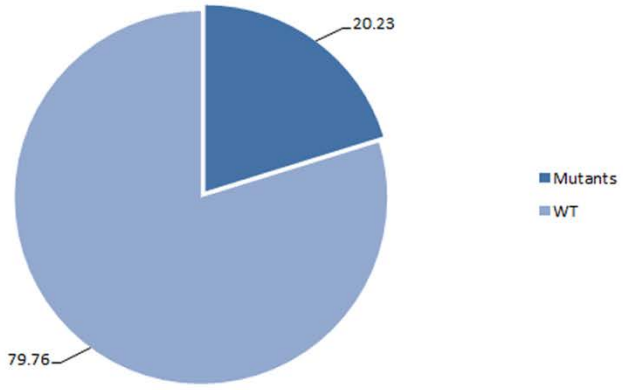

Type of mutations in F1 (n=17)

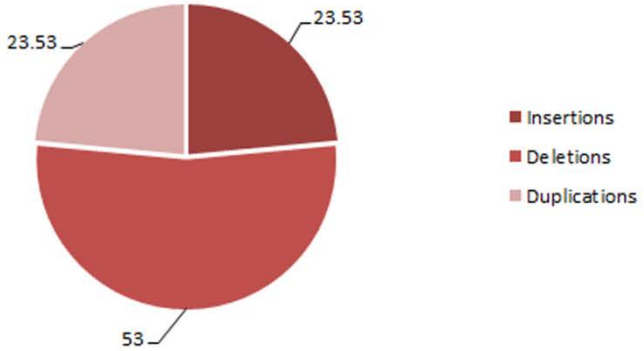

% of different mutations in F1 fish (n=17)

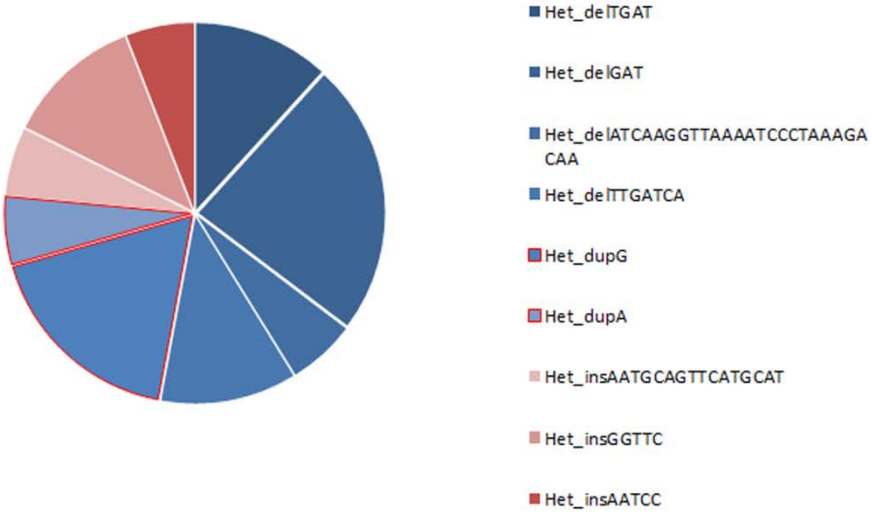

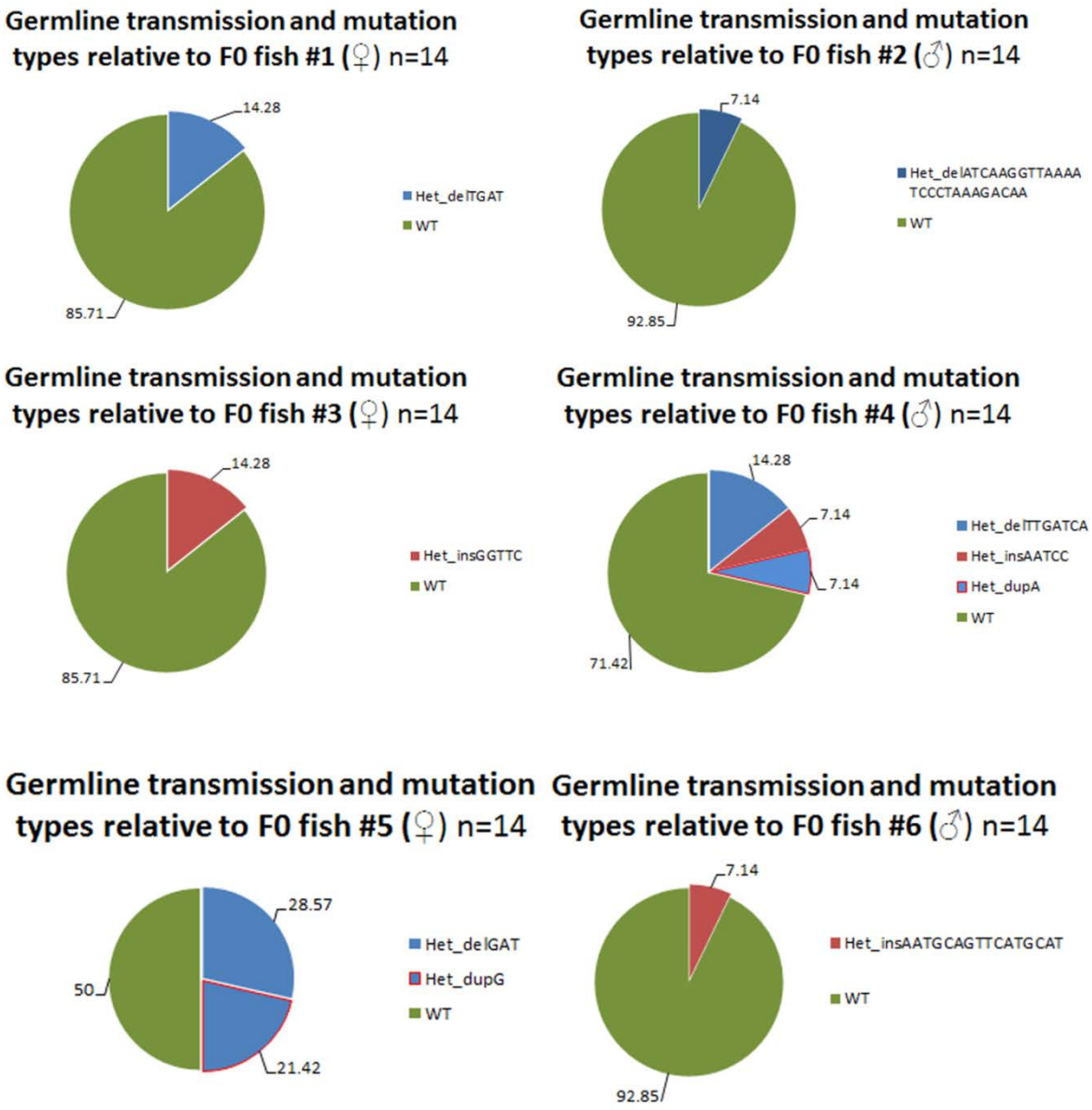

Figure 5.9 **Analysis of germline transmission for sgRNA_Ex2.** Overall transmission was lower than sgRNA_ex4. This may be due to lower predicted efficiency (A); ~23% of mutations were duplications, which were not present in mutants for exon 4 (B). The total number of different types of mutation was also lower than in exon 4 mutants (C), maybe again because of lower efficiency of sgRNA_Ex2 compared to sgRNA_Ex4. Also analysing mutation types per single fish, number of mutations is lower (E-I).

5.5 Selection of F1 adults mutation carriers and phenotype analysis in F2 embryos

Adult F1 fish were selected for genotyping through fin-clipping. 30 random fish from the pairs who carried the highest rate of mutation (#4 and #5) were selected for sequencing. The mutations identified and selected resulted to be a deletion of 3 nucleotides and a c.162DelATC_InsGTTA (Del3_Ins4) nucleotides. Sanger sequencing was performed with the help of summer student Alba Vilella.
The mutation c.164delCAA (Del3) is an inframe deletion resulting in a deletion of 2 amino acids (IK) and insertion of 1 (M) as follows:

```
>EMBOSS_WT
MGIADEADRTLFVGNLDPQVTEEVIFELFLQAGPLIKVKIPKNNEGKSKLFAFVNFKHEV
SVPYALNLLNGIRLHGRQLNIKFKTGSSHINQEGKSPANSQNPSPANTPGHRGGRTPEQM
GSPSYSPPQHMQRPFSSPDTLQRQAMMNNMWQVQMQQLQMLSGTFQQGMQQPRGNADGGW
SGHRGQRHSPQDNNNHQGRDQRHGNGANNYERNRRDGQRGDFYHHDDRSGGHNRNYPPDR
RRDSREGRWRHF*

>EMBOSS_Del3_Ex2
MGIADEADRTLFVGNLDPQVTEEVIFELFLQAGPLMVKIPKNNEGKSKLFAFVNFKHEVS
VPYALNLLNGIRLHGRQLNIKFKTGSSHINQEGKSPANSQNPSPANTPGHRGGRTPEQMG
SPSYSPPQHMQRPFSSPDTLQRQAMMNNMWQVQMQQLQMLSGTFQQGMQQPRGNADGGWS
GHRGQRHSPQDNNNHQGRDQRHGNGANNYERNRRDGQRGDFYHHDDRSGGHNRNYPPDRR
RDSREGRWRHF*
```

The second selected mutation c.162DelATC_InsGTTA results in a frameshift mutation which is predicted to introduce stop codons downstream of the InDel as shown below.

```
>EMBOSS_Del3_Ins4_Ex2
MGIADEADRTLFVGNLDPQVTEEVIFELFLQAGPLVKG*NP*KQ*RKVKTVCICELQA*S
VSALCLELAEWNPSAWTTAQHKVQNRQQSY*SRRQKSSKLSKPQSSKYTGSPWRKNPRAD
GLSVLLSSTAHAEAFLFTRHSAETGHDEQHVAGSDAAVANAQRNLPAGHAAA*GERRRRL
VWAPRAAPLAPGQQQPSGQRSAARKRSK*L*AESARWAAGRFLSP**PQWRTQQKLPPRQ
TERLQRGTMETLLX
```

Both mutations are located within the RNA Recognition Motif of RBM7, a highly conserved and catalytically active region of the protein (Hrossova et al., 2015).

5.6 Analysis of phenotype in F2 mutant embryos

In order to characterize a possible effect of the identified mutations on embryo development in zebrafish, a morphological analysis was carried out of both mutants throughout development up to 5 dpf. No clear morphological defect could be observed for the Del3 mutants, although it seemed that, starting from 2 dpf, swimming movements of some fish was not as effective as in wild type fish. Altough they were able to swim away upon touch stimulation, the number of movement events if not stimulated, efficacy of the movement and speed was decreased compared to control fish. The exact percentage of fish with behavioural defects is not known though, due to difficulties in identify a clear phenotype

Progenitor fish carrying the c.162DelATC_InsGTTA mutation on exon 2 were paired and a clear phenotype could be seen starting from 24 hpf. Embryos showed a variety of different phenotypes from milder to severe. Mild and moderate fish had shorter body length, heart oedema and smaller head. The most severe fish had completely altered body morphology with barely recognizable anatomical structures. ~50% of the fish showed a phenotype (Fig. 5.10). The experiment was repeated three times (with the same pair of F1 fish). Genotyping of fish these was not performed.

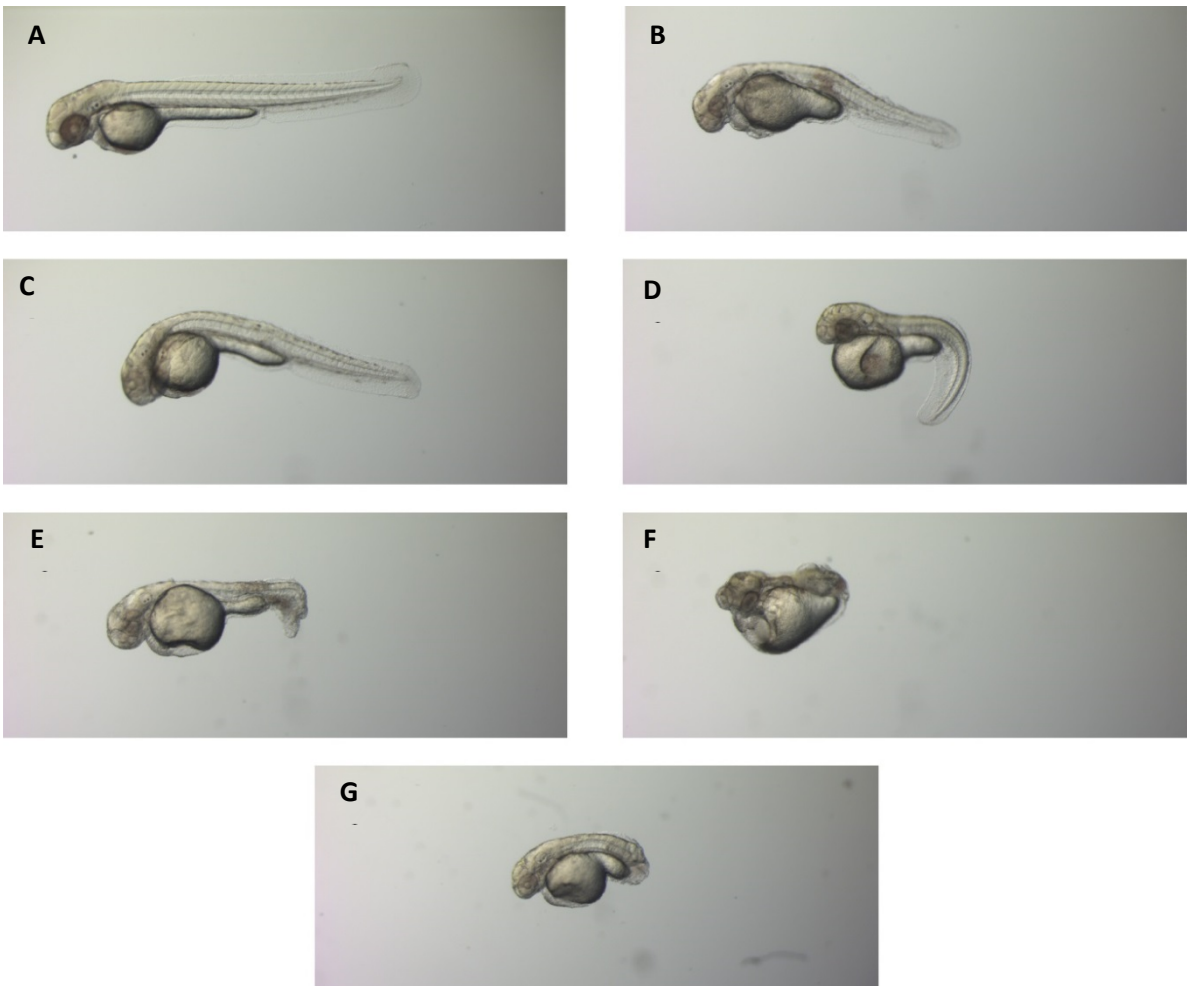

Figure 5.10 **F2 Zebrafish with the *rbm7* c.162DelATC_InsGTTA mutation display different phenotypes at 48 hpf.** Fish with a normal phenotype (A) were ~50% of the total. The other phenotypes look very different from each others (B-G). Head is generally smaller but overall the external morphology is preserved. Trunk and tail seem to be more affected by the mutation.

5.6.1 Immunostaining of F2 mutant embryos

Immunostaining on F2 embryos was performed in order to identify possible defects in motor neurons and/or cerebellum. Immunostaining of PCs was performed with an anti-parvalbumin7 antibody and immunostaining of neuromuscular junctions was performed with SV2 antibody which allows to visualize motor neurons, as previously described.

Analysis of PCs and motor neurons in the c.164delCAA mutants did not show any defect in cerebellar structures. pvalb7 is also expressed in muscle fibers, resembling expression of PARVALBUMIN in mammals muscle fibers (Hazama et al., 2002) (Racay et al., 2006). Incidentally, an analysis of muscular structure in mutant fish

could be performed on the same batch of samples showing a rather slightly disrupted structure of the fibers which display empty spaces between single fibers and do not look perfectly parallel and packed as they do in WT fish (Fig. 5.11).

The loose apperance of muscle fibers in mutant fish becomes more pronounced in larvae carrying a c.162DelATC_InsGTTA mutation (Fig. 5.11).
Analysis of c.162DelATC_InsGTTA mutants show also defective structure of the PCs layer at 5 dpf which seems to be thinner on the sides when observed from above in some cases and completely scattered in others. Analysis of motor neurons in c.162DelATC_InsGTTA fish showed defective growth and pathfinding of the axon of CaP neurons which seem to wrongly grow rostrally first and then suddenly move caudally. Also a branching defect of the neuron at midline level was observed, which may be due to defective branching of a RoP neuron (Fig. 5.11). These, however, are preliminary data and need further investigation in order to be confirmed.

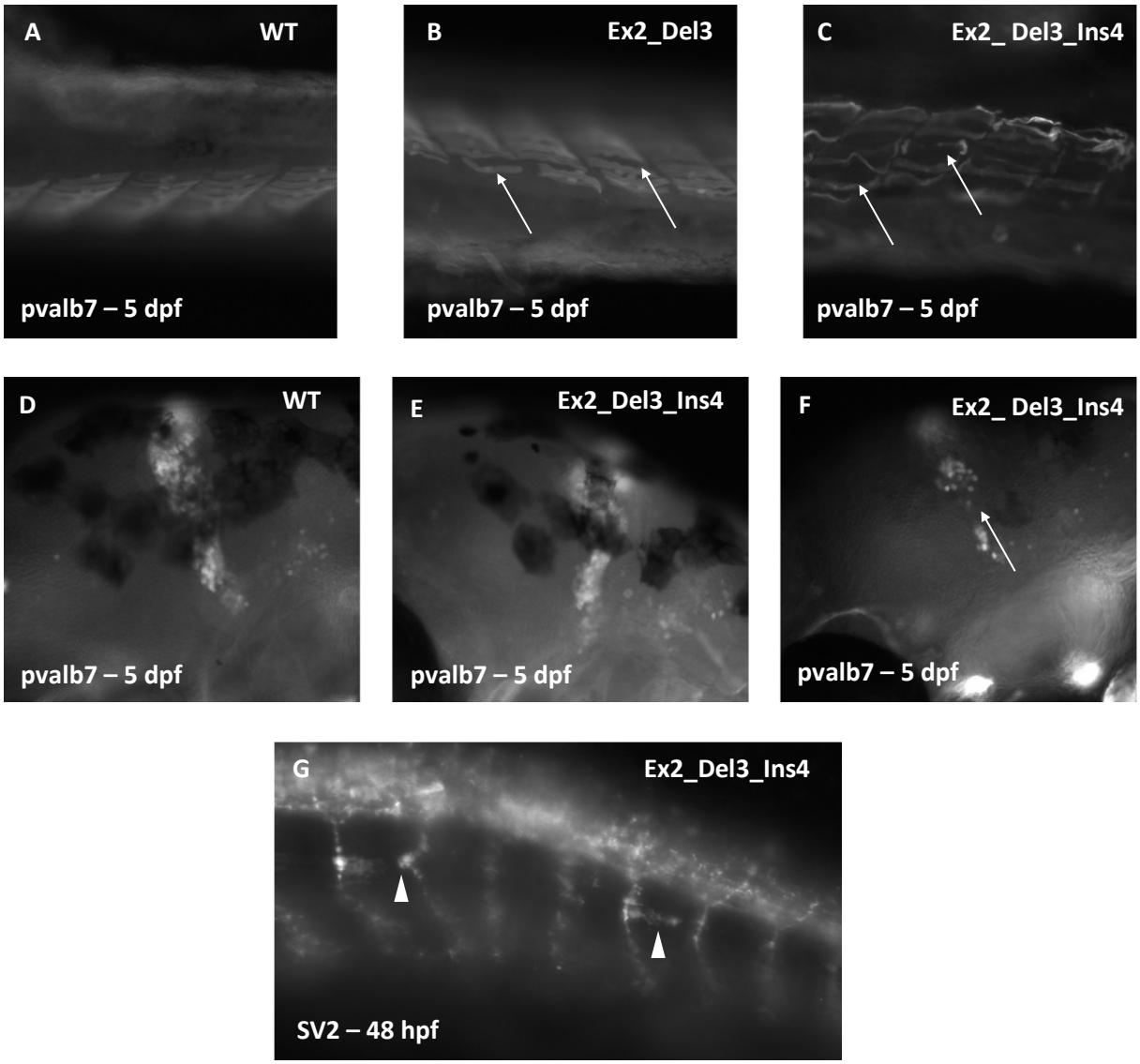

Figure 5.11. **Immunostaining of mutant zebrafish.** Muscle fibers show different degrees of disruption depending on the type of mutation (A-C). In WT fish, muscle fibers appear packed and parallel (A) while in fish with the inframe mutations are slightly looser (B, arrows). Muscle structure appears to be completely disrupted in mutants with the frameshift mutation (C. arrows). Purkinje Cells Layer has a defective structure in mutant fish (D-F). The external side of PCs layer appears thinner (E) compared to control (D). In other cases it is not well differentiated appearing scattered (F). No defects of PCs was observed in the in frame Del3 mutants. Motor neuron axons in frameshift mutants have growth and pathfinding defects (G, arrow-heads).

5.6.2 Update with most recent CRISPR-Cas9 data

Despite many efforts to identify a morphological or behavioural defect which could correlate with the mutation, genotyping of F2 fish carrying the c.162DelATC_InsGTTA which were displaying developmental disruption did not show any genotype-phenotype correlation. Upon identification of a restriction enzyme (BclI) which digests only the wild type sequence, it was possible to screen a larger number of adult fish in a much faster way (Fig. 5.12). Therefore I was able to identify other 2 fish with the same c.162DelATC_InsGTTA mutation.

Crossing of different pairs of fish with the same mutation did not show any severe phenotype anymore. Immunostaining for α-bungarotoxin/SV2 for neuromuscular junctions and phalloidin staining for slow and fast muscle fibers were comparable to controls.

In silico analysis of cryptic splice site within exon2 excluded the possibility that the mutation could have been somehow skipped.

Meanwhile some F2 fish I did breed from heterozygous fish had become adults and I was able to identify 2 adult fish homozygous for the c.162DelATC_InsGTTA.

This allowed me to have a progeny without any WT maternal contribution. Unfortunately, even pairing the 2 homozygous fish did not provide any clear phenotype.

RNA extraction from F3 *rbm7*$^{-/-}$ embryos allowed to sequence the transcript and check if the mutation is still present in the RNA. As expected I was able to see a clear electropherogram showing the mutation on an RNA level.

zRBM7_Ex2

GTATTATTAATCTACTTCATAATAAATGTAGTAGTAGTAGCTGTTGTTGTTGTTGTTGTT
ATTATTGCAGGCAATTTATAGTTCACAGAAACTAATAAATAAAGGACTTTTCTGTTTTGT
ATATAAAGCAACATCAGAGGTCATTCATGCATTTTCTTTTTCCACTAGGCTGGGCCATTG
ATCAAGGTTAAAATCCCTAAAGACAATGAAGGAAAGTCAAAACTGTTTGCATTTGTAAAC
TTCAAGCATGAAGTGTCAGTGCCCTATGCCTTGAACTTGCTGAATGGAATCCGTCTGCAT
GGACGACAGCTCAACATAAAGTTCAAAACCGGTAGGACTTTCCTTATTGCGTTGATTTAT
TTTGTGTTTTCTAAGGGTTGTCACTGTTCAACATTTCAGCATACCCTCATGCCGGCTGAT
TTGGTGACTGGGCTTTTTCACAATATTAAAGAATATGGTGTTAAAAATGTACTTCATGTT
TTTTGTTTGTTTGTTTTTTTCGTGATCATCTGAGTGATTCATGTGTAAATAATTTAGAAT

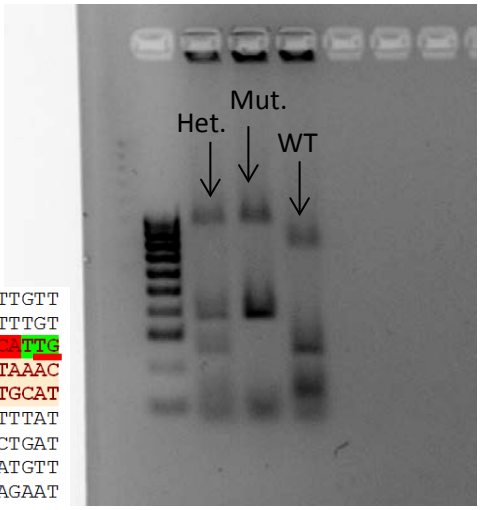

Figure 5.12. **BclI restriction enzyme digestion site and digested product on an agarose gel.** BclI works on a TGATCA sequence which - in this case - is right across the predicted CRISPR/Cas9 cut site, therefore it can be used for any kind of mutation identified so far. Highlighted in red the PAM sequence; underlined in red the enzyme digestion site; green: sgRNA complementary sequence; yellow: PCR primers (left). On the right: agarose gel of a digestion reaction of a heterozygous, homozygous mutant and homozygous WT fish.

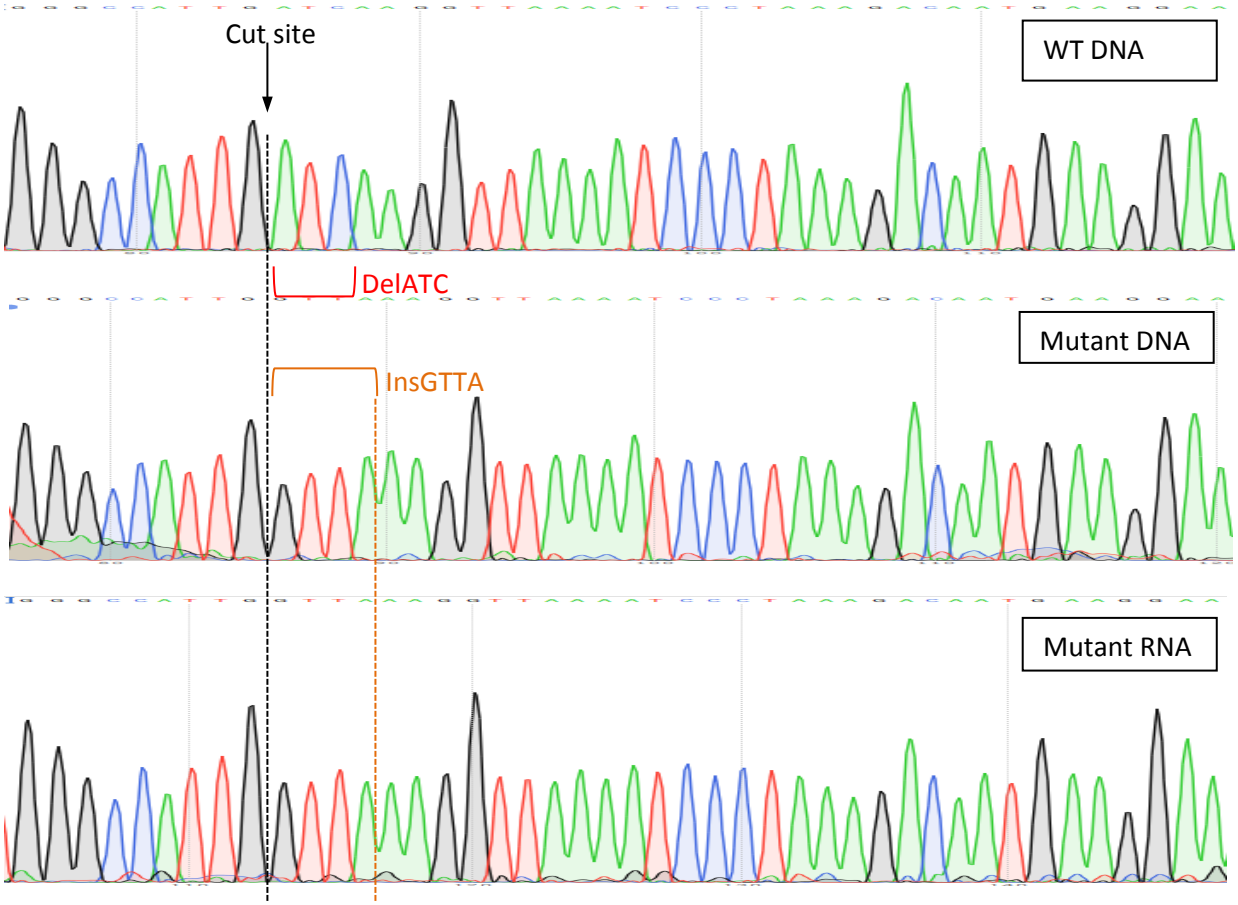

Figure 5.13. **Comparison of WT *rbm7*_Ex2 DNA sequence, mutant DNA and mutant RNA.** The delATC_Ins GTTA mutation is still present in the RNA

5.7 Discussion and future directions

With the advent of the CRISPR/Cas9 technology, mutagenesis has become easier to perform on-site than ever before. The critical step for an efficient CRISPR/Cas9 mutagenesis is to design a good quality guide RNA which needs to have specific characteristics such as a certain length (between 18 and 21 nucleotides, the shortest being more specific), it has to be near a PAM sequence on the target genome and to have a certain number of guanines, in specific positions within the sequence. This critical step has been overcome with the use of bioinformatic tools such as CRISPRscan (Moreno-Mateos et al., 2015).

Given the increasing number of controversies that are addressed over knock-down technologies (especially in zebrafish) and the opportunity of performing mutagenesis relatively easily, nowadays it is necessary to perform gene inactivation through mutagenesis if functions of a given gene are investigated.

Therefore, as we wanted to further delineate exosome complex functions in disease, we decided to create a mutant zebrafish strain. I decided to target exon 2 and exon 4 of RBM7 for two different reasons: the active domain of *rbm7* is predicted to be only within the first ~94 amino acids (Hrossova et al., 2015) so targeting exon 2 is most likely going to affect protein functions, even with an in-frame mutation. The guide RNA on exon 4 was predicted by CRISPRscan to be the most efficient (with a score of 56). Targeting the first exon is not advised, due to potentially alternative AUGs downstream to the canonical start codon.

Targeting exons downstream of the active domain of the protein should cause a loss-of-function effect anyways, if a stop codon is introduced (due to frame-shift mutations) >50-55 nt before an exon-exon junction, due to *non-sense mediated decay* (Popp and Maquat, 2016). In the case of mutations in exon 4, they are predicted to introduce a stop too close to the exon-exon junction. It may rather be that if a phenotype will be observed in exon 4 targeted fish this may be due to the synthesis of a C-terminal truncated protein (Barrangou et al., 2015).

Because this was the first time we tried such approach, we wanted to test the efficacy of our technique in creating a DSB in our target, therefore we decided to use the colony PCR approach followed by Sanger sequencing as previously described in

this chapter. This approach resulted probably in a lower estimation of the efficiency (between 6.5% and 13%) in the F0 but we confirmed the effectiveness of our system.

The reason for the lower efficiency is probably because of the mosaicism of the mutants. Amplification of genomic DNA extracted from 10 fish and insertion of single copies of the exons into *E. coli* may not give a proportional ratio of mutagenesis efficiency. It is anyway an efficient qualitative method to establish the presence or absence of the mutation, although it cannot be used as a quantitative assay.

The reason of mosaicism and presence of different types of mutations in the germline of a single fish is not completely clear. It could be that, although sgRNA+Cas9 RNA are all injected at one cell stage, the Cas9 RNA does not get translated and start working on the target genome straight away. Instead, it is moved between cells during cell division and gets translated at different time points in different cells, therefore causing different types of mutations (Tu et al., 2015). It is an issue that needs to be taken into account or chances are to have a mixed population of mutant and WT genomes therefore a lot of background when Sanger sequencing the F0.

Analysis of germline transmission in our experiments (~32% for exon4 and ~20% for exon2) is overall in accord with previous studies which reported an average transmission of 28% (Varshney et al., 2015).

A very high difference in mutagenesis efficiency was found between different batches of fish, which may be due to experimental set-up differences. For some batches efficiency was 0%, although on the batches where mutagenesis worked, efficiency was nearly 100%.

The initial observation of a phenotype in the *rbm7* mutant fish was proven to be wrong by further genotype-phenotype analysis. I may conclude the phenotype observed was probably due to some inbreeding issues. Indeed pairing those 2 fish carriers of the unknown mutation and raising the F2 generation (and of course getting rid of the most severe ones which could not survive until adult age) have washed away the defect-causing mutation and even pairing 2 homozygous mutants do not show any clear external phenotype. Neverthless, having managed to obtain 2 homozygous mutants is a useful step forward because it allows to get rid of the maternal WT contribution and allow to perform analysis without caring about selecting the actual 25% of homozygous mutants which raise from 2 heterozygous.

For example now I can extract RNA from 20 homozygous mutant embryos and perform qRT-PCR to check expression levels of those genes which were differentially expressed in the morphant fish (e.g. *atxn1*) or other genes which expression I may expect to be misregulated such as genes involved in muscle development or neuron development.

It is striking to observe such a strong difference between the effect of morpholino against *rbm7* – which appears to be very toxic - and a frameshift mutation on the same gene.

It is especially interesting because *rbm7* seems to be a key protein for RNA metabolism. It may be that some other proteins take over its functions in presence of a deleterious mutation in similar way to what observed by Rossi and colleagues (Rossi et al., 2015).

It could also be that the defects are there, just not as clear as with morpholino injections. Maybe the differences are more subtle, therefore the mutants need to be analysed more carefully – e.g. higher microscopy magnification.

Next step will be to perform qRT-PCR on the homozygous mutant embryos. It will be an relatively quick and easy way to screen differential expression of tens of genes involved in different pathways (muscle development, motor neuron development, etc.) and levels of *rbm7* itself. If some of these genes will result to be differentially expressed, then I will keep investigating in that direction via immunofluorescence imaging, *in situ* hybridization, histology analysis. In order to increase the chances to see a phenotype I may try to trigger a physiological reaction injecting a low dose of morpholino which would not cause any effect in WT embryos but may help to reduce the levels of mRNA.

Then I will analyse the phenotype in Ex4 mutant fish to understand the role of this part of the protein which is not known. Given that the first ~90 amino acid are all within the highly conserved RNA Recognition Motif and has a catalityc role, it may be that the rest of the protein could be involved in binding to MTR4 and ZCCHC8 forming the NEXT complex or perhaps binding to the other RBM7 molecules forming the ring-shaped pentameric structure presented in a recent publication (Sofos et al., 2016).

qRT-PCR analysis on the homozygous mutant fish will be a quick way to check the expression of a number of genes involved in different pathways (muscle development, motor neuron development, etc.) in order to identify a disruption in any of those and then investigate deeper the defects caused by a up or downregulation.

6 Chapter 6 - Summary, conclusions and future directions

Pontocerebellar hypoplasias (PCHs) are a rare and heterogeneous subtype of neurological disorders which share symptoms of hypoplasia of the cerebellum and pons and motor neuron disease. Common symptoms are severe psychomotor retardation and muscle weakness which often lead to premature death of the patients. Ten different subtypes of PCHs have been classified to date. Many different genes have been linked to the pathogenesis which seems to be related somehow to incorrect RNA metabolism and processing, suggesting that these mechanisms are specifically important in cerebellar Purkinje cells.

One of the issues investigators have to face when studying rare diseases is the lack of satisfactory number of samples, which makes the development of experimental models particularly important in this field. In this thesis I show the identification of a new human disease gene involved in RNA metabolism (*RBM7)* and investigated the pathomechanisms in both in vitro (primary fibroblasts) and in vivo (zebrafish) models. I showed that *RBM7* mutation results in a similar defect of RNA metabolism as mutations in *EXOSC8*, another exosomal defect. To further understand disease mechanisms I developed a zebrafish model of RBM7 deficiency and then compared phenotypical and molecular findings to previously published zebrafish PCH models. Furthermore here I present the creation of CRISPR/Cas9 induced zebrafish *rbm7* mutant lines , which may further help to understand this subset of disease. The results of this thesis show that a common pathomechanism exists in exosomal protein deficiency, indicated by common molecular and phenotypical findings between different disease models.

6.1 Identification and characterization of a novel pathogenic mutation in *RBM7*

RBM7 is known to be involved in RNA metabolism and splicing. Our collaborators in Jerusalem identified a patient from a consanguineous Palestinian family with symptoms of motor neuron disease. Exome sequencing identified a homozygous pathogenic mutation in *RBM7*, however even after intensive search, we could not confirm the clinical phenotype in a second patient. The pathogenic role of this RBM7 mutation was supported by lower protein level in fibroblasts, suggesting a loss-of-function effect of the mutation. The mutation in *RBM7* also caused a reduction of EXOSC8 protein, further supporting the hypothesis of *RBM7* mutation's role in the

disease. The c.236C>G; p.Pro79Arg mutation is located in a highly conserved RNA binding domain (RRM) and is predicted to alter protein stability (Giunta et al., 2016). RBM7 is known to be involved in RNA splicing and degradation of ncRNAs such as tRNA, rRNA, snRNA and PROMPTs, which are transcribed upstream of the promoters of many protein coding genes, competing with canonical downstream transcription for RNA polymerase II and other transcription factors. RNA-seq analysis showed defective metabolism of many coding and non-coding RNAs in both *RBM7* and *EXOSC8* mutant cells. We strongly believe that the identification of so many shared differentially expressed transcripts and alternative spliced RNAs between *EXOSC8* and *RBM7* mutant fibroblasts, also strengthens this hypothesis.
In the next months a deeper bionformatic analysis of differential splicing events will be performed on EXOSC3 and EXOSC9 fibroblasts and neuronal cells and data will be confirmed by standard RT-PCR. The identified bands will also be Sanger sequenced in order to clarifiy which part of the gene is mispliced and try to identify potential loss or gain of functions.

6.2 Zebrafish models of PCH

Zebrafish is an ideal model for studying disorders of the motor neurons and cerebellar Purkinje cells (Bae et al., 2009) (Babin et al., 2014). The development and comparison of three zebrafish models of exosomal protein deficiencies (rbm7-MO, exosc8-MO and exosc3-MO) seems to further confirm a common pathomechanism underlying the phenotype observed in all three models. The similar defects in motor neuron axons and in Purkinje cells, confirm an involvement of the exosome, specifically in these types of neuronal cells, which is a key aspect of the clinical presentation of exosomal protein defects. The defects observed in motor neurons of our morphant fish (defective growth and branching) are very similar to those observed in previous zebrafish models of SMA (McWhorter et al., 2003) as well as fish with deficiencies for proteins known to be involved in axon pathfinding (Sato-Maeda, 2006). It is interesting to notice that brainstem nuclei were severely affected upon gene knock down in zebrafish *exosc3*-MO and *exosc8*-MO models, but very mildly affected in *rbm7* knocked down fish. This resembles what observed in patients: *EXOSC3* and *EXOSC8* mutations cause PCH1 with severe involvement of the brainstem, while *RBM7* mutation caused motor neuron disease, with no apparent defects of the brainstem. Also, a smaller percentage of *rbm7*-MO fish show a cerebellar defect as indicated by our experiments.

It may be that the subset of genes differentially expressed only in *EXOSC8* mutant cells could be specific for the onset of PCH1 and hypomyelination while the shared genes differentially expressed both in *RBM7* and *EXOSC8* may underlie the cause of common symptoms of motor neuron disease. Performing RNA-seq on *EXOSC3* fibroblasts and coverted neurons will hopefully help to clarify this aspect.
The creation of the mutant line(s) is a step forward toward the understanding of such molecular mechanisms. It is well known that morphants may display a different phenotype than mutants due to off target effects or compensatory effects observed in mutants but not in morphants.

At present it is unclear why *rbm7* mutants do not show any phenotype at all or a much milder one. It may be because compensatory factors are induced by mutagenesis but not by gene knock down. It may be that the phenotype is milder therefore fish need to be analysed better.

A more detailed analysis of different structures at different developmental stages may show defects: investigation of motor neurons at 48 hpf, 3 dpf and 4 dpf with a higher magnification may indicate some smaller defects which may have been underestimated before.

A high throughput quantitative analysis of gene expression of genes involved in motor neuron development such as *olig2* (Park et al., 2002) will be performed in order to identify possible anatomical structures to look at.

I have already crossed mutant fish with *islet1*:GFP transgenic. This will allow to show possible defects during development of motor neurons under control of *islet1* promoter.

Analysis of mutants instead of morphants will abolish variability due to unavoidable quantitative differences during the morpholino injection. As we introduced different mutations into our new CRISPR/Cas9 zebrafish models, mutants will be sorted by mutation type, in order to investigate different roles of different mutations.

Trying to inject a very low dose of morpholino in the mutants or a stress test may also help to amplify defects which may be too small to be identified at the moment.

Having induced mutations on exon 2 and exon 4, likely able to cause stop codons and/or in-frame mutations, we may be able to understand different roles of the protein through the synthesis of proteins truncated at different levels.

High throughput behavioural studies of zebrafish larvae can be performed in a standardized manner using software which are able to track movements of a single larvae over a given amount of time and directly compare speed, number of events and length of the event between mutant and WT fish (Ingebretson and Masino, 2013)

Using technologies such as single cell laser micro dissection and/or magnetic activate cell sorting (MACS) or flow cytometry it will be possible to extract high quality RNA for whole transcriptomic analysis from specific cell types, without contamination from neighbouring cells (Bandyopadhyay et al., 2014) (Welzel et al., 2015).

One issue with laser microdissection may be the degradation of RNA due to processing time and high temperature. The creation of mutant zebrafish strain will further help to investigate the *in vivo* molecular mechanism underlying the disease.

On the other hand, if no phenotype or defects is actually identified, RNAseq analysis of *rbm7* mutant fish may help to understand which are – if any – the compensatory mechanism that allow the fish to do not develop a motor neuron phenotype.

Moreover, direct conversion of patients' fibroblasts into neuronal cells (Meyer et al., 2014) and subsequent RNA-seq (and possibly proteomic) analysis will also narrow down the number of candidates transcripts and enable validating our previous data in better cellular models.

Comparing the two sets of data is likely going to give some insights on the RNA species which are commonly differentially expressed and regulated in human patient's neurons and mutant fish.

Furthermore, the development of a stable, closely resembling model of RNA processing related disease (and specifically, exosome complex related disease) like our *rbm7* mutant zebrafish models is fundamental in order to perform drug discovery, whenever a therapeutic approach will be possible to be tested on animal models or to do large high-throughput screening of chemical compounds (Gibert et al., 2013) (MacRae and Peterson, 2015). If a specific gene will result to be upregulated in exosome complex deficiency, it would be a suitable target for downregulation or pharmacological inhibition of related pathways. As we showed in chapter 3, co-downregulation of *exosc8* and *mbp* – which was overexpressed upon knock down of *exosc8* – resulted in better preserved brain structure and increased survival. ATXN1 levels are regulated by the RAS–MAPK–MSK1 pathway, which can itself be regulated pharmacologically (Park et al., 2013). On a pure speculative basis this

could be a possible approach to test RAS-MAPK-MSK1 as a potential target to rescue cerebellar phenotype in PCH in our zebrafish model.The opposite could be performed in those cases where there is an over-degradation of certain RNAs. Reducing physiological functions of the exosome complex may have a positive effect on the symptoms. This obviously has to be finely regulated in order to do not interfere with other functions of the exosome complex.

Zebrafish mutants could be used for testing a new possible therapeutic approach which was recently published by Fasken and colleagues: they modelled different mutations in Rrp40/EXOSC3 in yeast and show that, upon impossibility of the mutated sub-unit to join the exosome complex, the mutated protein it is degraded by the proteasome. This well matches with our previous finding of reduced protein levels in EXOSC8 and RBM7 mutants cells. Even more importantly though, they show that if the WT protein is provided together with the mutant protein, this is even more unstable and gets targeted by the exosome complex even more. Therefore the WT protein is successfully able to replace the mutant one and get assembled within the exsome complex either in yeast and mouse cells (Fasken et al., 2017).

Overall, this thesis expands the knowledge about mechanisms underlying neurological disorders caused by defective RNA metabolism. Furthermore it forms the basis for further studies using new experimental models such as *rbm7* mutant fish and - ideally – neuronal cells directly converted from patients fibroblasts. Understanding the roles of different exosome specific factors may potentially be useful to take advantage of the exosome complex as a therapeutic strategy in RNA processing deficiency diseases.

7 References

1000 Genomes Project Consortium, Abecasis, G.R., Altshuler, D., Auton, A., Brooks, L.D., Durbin, R.M., Gibbs, R.A., Hurles, M.E., and McVean, G.A. (2010). A map of human genome variation from population-scale sequencing. Nature *467*, 1061–1073.

Adzhubei, I., Jordan, D.M., and Sunyaev, S.R. (2013). Predicting Functional Effect of Human Missense Mutations Using PolyPhen-2. In Current Protocols in Human Genetics, J.L. Haines, B.R. Korf, C.C. Morton, C.E. Seidman, J.G. Seidman, and D.R. Smith, eds. (Hoboken, NJ, USA: John Wiley & Sons, Inc.), p. 7.20.1-7.20.41.

Ahmed, M.Y., Chioza, B.A., Rajab, A., Schmitz-Abe, K., Al-Khayat, A., Al-Turki, S., Baple, E.L., Patton, M.A., Al-Memar, A.Y., Hurles, M.E., et al. (2015). Loss of PCLO function underlies pontocerebellar hypoplasia type III. Neurology *84*, 1745–1750.

Akizu, N., Cantagrel, V., Schroth, J., Cai, N., Vaux, K., McCloskey, D., Naviaux, R.K., Van Vleet, J., Fenstermaker, A.G., Silhavy, J.L., et al. (2013). AMPD2 Regulates GTP Synthesis and Is Mutated in a Potentially Treatable Neurodegenerative Brainstem Disorder. Cell *154*, 505–517.

Andersen, P.R., Domanski, M., Kristiansen, M.S., Storvall, H., Ntini, E., Verheggen, C., Schein, A., Bunkenborg, J., Poser, I., Hallais, M., et al. (2013). The human cap-binding complex is functionally connected to the nuclear RNA exosome. Nat. Struct. Mol. Biol. *20*, 1367–1376.

Antonellis, A., Lee-Lin, S.-Q., Wasterlain, A., Leo, P., Quezado, M., Goldfarb, L.G., Myung, K., Burgess, S., Fischbeck, K.H., and Green, E.D. (2006). Functional analyses of glycyl-tRNA synthetase mutations suggest a key role for tRNA-charging enzymes in peripheral axons. J. Neurosci. Off. J. Soc. Neurosci. *26*, 10397–10406.

Arab, K., Park, Y.J., Lindroth, A.M., Schäfer, A., Oakes, C., Weichenhan, D., Lukanova, A., Lundin, E., Risch, A., Meister, M., et al. (2014). Long noncoding RNA TARID directs demethylation and activation of the tumor suppressor TCF21 via GADD45A. Mol. Cell *55*, 604–614.

Arafat, H., Lazar, M., Salem, K., Chipitsyna, G., Gong, Q., Pan, T.-C., Zhang, R.-Z., Yeo, C.J., and Chu, M.-L. (2011). Tumor-specific expression and alternative splicing of the COL6A3 gene in pancreatic cancer. Surgery *150*, 306–315.

Argenton, F., Giudici, S., Deflorian, G., Cimbro, S., Cotelli, F., and Beltrame, M. (2004). Ectopic expression and knockdown of a zebrafish sox21 reveal its role as a transcriptional repressor in early development. Mech. Dev. *121*, 131–142.

Armstrong, G.A.B., Liao, M., You, Z., Lissouba, A., Chen, B.E., and Drapeau, P. (2016). Homology Directed Knockin of Point Mutations in the Zebrafish tardbp and fus Genes in ALS Using the CRISPR/Cas9 System. PLOS ONE *11*, e0150188.

Babin, P.J., Goizet, C., and Raldúa, D. (2014). Zebrafish models of human motor neuron diseases: advantages and limitations. Prog. Neurobiol. *118*, 36–58.

Bae, Y.-K., Kani, S., Shimizu, T., Tanabe, K., Nojima, H., Kimura, Y., Higashijima, S., and Hibi, M. (2009a). Anatomy of zebrafish cerebellum and screen for mutations affecting its development. Dev. Biol. *330*, 406–426.

Bae, Y.-K., Kani, S., Shimizu, T., Tanabe, K., Nojima, H., Kimura, Y., Higashijima, S., and Hibi, M. (2009b). Anatomy of zebrafish cerebellum and screen for mutations affecting its development. Dev. Biol. *330*, 406–426.

Baertling, F., Alhaddad, B., Seibt, A., Budaeus, S., Meitinger, T., Strom, T.M., Mayatepek, E., Schaper, J., Prokisch, H., Haack, T.B., et al. (2016). Neonatal encephalocardiomyopathy caused by mutations in VARS2. Metab. Brain Dis.

Balint, B., and Bhatia, K.P. (2015). Hot topic: Recessive mutations in the a3(VI) collagen gene COL6A3 cause early-onset isolated dystonia: Hot Topics. Mov. Disord. *30*, 1622–1622.

Bamshad, M.J., Ng, S.B., Bigham, A.W., Tabor, H.K., Emond, M.J., Nickerson, D.A., and Shendure, J. (2011). Exome sequencing as a tool for Mendelian disease gene discovery. Nat. Rev. Genet. *12*, 745–755.

Bandyopadhyay, U., Fenton, W.A., Horwich, A.L., and Nagy, M. (2014). Production of RNA for Transcriptomic Analysis from Mouse Spinal Cord Motor Neuron Cell Bodies by Laser Capture Microdissection. J. Vis. Exp.

Barrangou, R., Birmingham, A., Wiemann, S., Beijersbergen, R.L., Hornung, V., and Smith, A. v. B. (2015). Advances in CRISPR-Cas9 genome engineering: lessons learned from RNA interference. Nucleic Acids Res. *43*, 3407–3419.

Barreau, C. (2005). AU-rich elements and associated factors: are there unifying principles? Nucleic Acids Res. *33*, 7138–7150.

Beattie, C.E., Carrel, T.L., and McWhorter, M.L. (2007). Fishing for a mechanism: using zebrafish to understand spinal muscular atrophy. J. Child Neurol. *22*, 995–1003.

Becker, J., Semler, O., Gilissen, C., Li, Y., Bolz, H.J., Giunta, C., Bergmann, C., Rohrbach, M., Koerber, F., Zimmermann, K., et al. (2011). Exome Sequencing Identifies Truncating Mutations in Human SERPINF1 in Autosomal-Recessive Osteogenesis Imperfecta. Am. J. Hum. Genet. *88*, 362–371.

Bennett, M.L., Bennett, F.C., Liddelow, S.A., Ajami, B., Zamanian, J.L., Fernhoff, N.B., Mulinyawe, S.B., Bohlen, C.J., Adil, A., Tucker, A., et al. (2016). New tools for studying microglia in the mouse and human CNS. Proc. Natl. Acad. Sci. *113*, E1738–E1746.

Benson, E.A., Eadon, M.T., Desta, Z., Liu, Y., Lin, H., Burgess, K.S., Segar, M.W., Gaedigk, A., and Skaar, T.C. (2016). Rifampin Regulation of Drug Transporters Gene Expression and the Association of MicroRNAs in Human Hepatocytes. Front. Pharmacol. *7*.

Bierhals, T., Korenke, G.C., Uyanik, G., and Kutsche, K. (2013). Pontocerebellar hypoplasia type 2 and TSEN2: review of the literature and two novel mutations. Eur. J. Med. Genet. *56*, 325–330.

Bill, B.R., Petzold, A.M., Clark, K.J., Schimmenti, L.A., and Ekker, S.C. (2009). A Primer for Morpholino Use in Zebrafish. Zebrafish *6*, 69–77.

Blum, M., De Robertis, E.M., Wallingford, J.B., and Niehrs, C. (2015). Morpholinos: Antisense and Sensibility. Dev. Cell *35*, 145–149.

Boczonadi, V., Müller, J.S., Pyle, A., Munkley, J., Dor, T., Quartararo, J., Ferrero, I., Karcagi, V., Giunta, M., Polvikoski, T., et al. (2014). EXOSC8 mutations alter mRNA metabolism and cause hypomyelination with spinal muscular atrophy and cerebellar hypoplasia. Nat. Commun. *5*.

Boggs, J.M. (2006). Myelin basic protein: a multifunctional protein. Cell. Mol. Life Sci. CMLS *63*, 1945–1961.

Bolotin, A., Quinquis, B., Sorokin, A., and Ehrlich, S.D. (2005). Clustered regularly interspaced short palindrome repeats (CRISPRs) have spacers of extrachromosomal origin. Microbiol. Read. Engl. *151*, 2551–2561.

Bonanomi, D., and Pfaff, S.L. (2010). Motor Axon Pathfinding. Cold Spring Harb. Perspect. Biol. *2*, a001735–a001735.

Bova, G.S., Kallio, H.M.L., Annala, M., Kivinummi, K., Högnäs, G., Häyrynen, S., Rantapero, T., Kivinen, V., Isaacs, W.B., Tolonen, T., et al. (2016). Integrated clinical, whole-genome, and transcriptome analysis of multisampled lethal metastatic prostate cancer. Mol. Case Stud. *2*, a000752.

Br�samle, C., and Halpern, M.E. (2002). Characterization of myelination in the developing zebrafish. Glia *39*, 47–57.

Breuss, M.W., Sultan, T., James, K.N., Rosti, R.O., Scott, E., Musaev, D., Furia, B., Reis, A., Sticht, H., Al-Owain, M., et al. (2016). Autosomal-Recessive Mutations in the tRNA Splicing Endonuclease Subunit TSEN15 Cause Pontocerebellar Hypoplasia and Progressive Microcephaly. Am. J. Hum. Genet. *99*, 228–235.

Buckley, C.E., Goldsmith, P., and Franklin, R.J.M. (2008). Zebrafish myelination: a transparent model for remyelination? Dis. Model. Mech. *1*, 221–228.

Buckley, C.E., Marguerie, A., Alderton, W.K., and Franklin, R.J.M. (2010). Temporal dynamics of myelination in the zebrafish spinal cord. Glia *58*, 802–812.

Buckner, R.L. (2013). The Cerebellum and Cognitive Function: 25 Years of Insight from Anatomy and Neuroimaging. Neuron *80*, 807–815.

Campagnoni, A.T., and Skoff, R.P. (2001). The pathobiology of myelin mutants reveal novel biological functions of the MBP and PLP genes. Brain Pathol. Zurich Switz. *11*, 74–91.

Cao, X., Yeo, G., Muotri, A.R., Kuwabara, T., and Gage, F.H. (2006). Noncoding RNAs in the mammalian central nervous system. Annu. Rev. Neurosci. *29*, 77–103.

Carlson, K.M., Melcher, L., Lai, S., Zoghbi, H.Y., Clark, H.B., and Orr, H.T. (2009). Characterization of the zebrafish atxn1/axh gene family. J. Neurogenet. *23*, 313–323.

Cassandrini, D., Biancheri, R., Tessa, A., Di Rocco, M., Di Capua, M., Bruno, C., Denora, P.S., Sartori, S., Rossi, A., Nozza, P., et al. (2010). Pontocerebellar hypoplasia: clinical, pathologic, and genetic studies. Neurology *75*, 1459–1464.

Chen, C.Y., and Shyu, A.B. (1994). Selective degradation of early-response-gene mRNAs: functional analyses of sequence features of the AU-rich elements. Mol. Cell. Biol. *14*, 8471–8482.

Chen, C.Y., Gherzi, R., Ong, S.E., Chan, E.L., Raijmakers, R., Pruijn, G.J., Stoecklin, G., Moroni, C., Mann, M., and Karin, M. (2001). AU binding proteins recruit the exosome to degrade ARE-containing mRNAs. Cell *107*, 451–464.

Cheng, I.H., Lin, Y.-C., Hwang, E., Huang, H.-T., Chang, W.-H., Liu, Y.-L., and Chao, C.-Y. (2011). Collagen VI protects against neuronal apoptosis elicited by ultraviolet irradiation via an Akt/Phosphatidylinositol 3-kinase signaling pathway. Neuroscience *183*, 178–188.

Chi, K.R. (2016). Finding function in mystery transcripts. Nature *529*, 423–425.

Chlebowski, A., Lubas, M., Jensen, T.H., and Dziembowski, A. (2013). RNA decay machines: the exosome. Biochim. Biophys. Acta *1829*, 552–560.

Clark, B.S., and Blackshaw, S. (2014). Long non-coding RNA-dependent transcriptional regulation in neuronal development and disease. Front. Genet. *5*.

Cong, L., Ran, F.A., Cox, D., Lin, S., Barretto, R., Habib, N., Hsu, P.D., Wu, X., Jiang, W., Marraffini, L.A., et al. (2013). Multiplex genome engineering using CRISPR/Cas systems. Science *339*, 819–823.

Cooper, T.A., Wan, L., and Dreyfuss, G. (2009). RNA and Disease. Cell *136*, 777–793.

de la Cruz, C.C., Der-Avakian, A., Spyropoulos, D.D., Tieu, D.D., and Carpenter, E.M. (1999). Targeted disruption of Hoxd9 and Hoxd10 alters locomotor behavior, vertebral identity, and peripheral nervous system development. Dev. Biol. *216*, 595–610.

Cunningham, T.J., and Duester, G. (2015). Mechanisms of retinoic acid signalling and its roles in organ and limb development. Nat. Rev. Mol. Cell Biol. *16*, 110–123.

Dangel, A.W., Shen, L., Mendoza, A.R., Wu, L.C., and Yu, C.Y. (1995). Human helicase gene SKI2W in the HLA class III region exhibits striking structural similarities to the yeast antiviral gene SKI2 and to the human gene KIAA0052: emergence of a new gene family. Nucleic Acids Res. *23*, 2120–2126.

D'Arrigo, S., Riva, D., and Valente, E.M. (2014). Paediatric neurological disorders with cerebellar involvment diagnosis and management (Montrouge: J. Libbey Eurotext).

Davis-Dusenbery, B.N., Williams, L.A., Klim, J.R., and Eggan, K. (2014). How to make spinal motor neurons. Development *141*, 491–501.

Del Bo, R., Locatelli, F., Corti, S., Scarlato, M., Ghezzi, S., Prelle, A., Fagiolari, G., Moggio, M., Carpo, M., Bresolin, N., et al. (2006). Coexistence of CMT-2D and distal SMA-V phenotypes in an Italian family with a GARS gene mutation. Neurology *66*, 752–754.

Detrich, H.W., Westerfield, M., and Zon, L.I. (1999). Overview of the Zebrafish system. Methods Cell Biol. *59*, 3–10.

Di Donato, N., Neuhann, T., Kahlert, A.-K., Klink, B., Hackmann, K., Neuhann, I., Novotna, B., Schallner, J., Krause, C., Glass, I.A., et al. (2016a). Mutations in EXOSC2 are associated with a novel syndrome characterised by retinitis pigmentosa, progressive hearing loss, premature ageing, short stature, mild intellectual disability and distinctive gestalt. J. Med. Genet.

Di Donato, N., Neuhann, T., Kahlert, A.-K., Klink, B., Hackmann, K., Neuhann, I., Novotna, B., Schallner, J., Krause, C., Glass, I.A., et al. (2016b). Mutations in *EXOSC2* are associated with a novel syndrome characterised by retinitis pigmentosa, progressive hearing loss, premature ageing, short stature, mild intellectual disability and distinctive gestalt. J. Med. Genet. *53*, 419–425.

Di Mauro, S., Tanji, K., and Hirano, M. (2007). LAMP-2 deficiency (Danon disease). Acta Myol. Myopathies Cardiomyopathies Off. J. Mediterr. Soc. Myol. Ed. Gaetano Conte Acad. Study Striated Muscle Dis. *26*, 79–82.

Do, R., Kathiresan, S., and Abecasis, G.R. (2012). Exome sequencing and complex disease: practical aspects of rare variant association studies. Hum. Mol. Genet. *21*, R1-9.

Doma, M.K., and Parker, R. (2006). Endonucleolytic cleavage of eukaryotic mRNAs with stalls in translation elongation. Nature *440*, 561–564.

Dori-Bachash, M., Shema, E., and Tirosh, I. (2011). Coupled Evolution of Transcription and mRNA Degradation. PLoS Biol. *9*, e1001106.

Ebner, B.A., Ingram, M.A., Barnes, J.A., Duvick, L.A., Frisch, J.L., Clark, H.B., Zoghbi, H.Y., Ebner, T.J., and Orr, H.T. (2013). Purkinje Cell Ataxin-1 Modulates Climbing Fiber Synaptic Input in Developing and Adult Mouse Cerebellum. J. Neurosci. *33*, 5806–5820.

Eckalbar, W.L., Schlebusch, S.A., Mason, M.K., Gill, Z., Parker, A.V., Booker, B.M., Nishizaki, S., Muswamba-Nday, C., Terhune, E., Nevonen, K.A., et al. (2016). Transcriptomic and epigenomic characterization of the developing bat wing. Nat. Genet. *48*, 528–536.

Edvardson, S., Shaag, A., Kolesnikova, O., Gomori, J.M., Tarassov, I., Einbinder, T., Saada, A., and Elpeleg, O. (2007). Deleterious Mutation in the Mitochondrial Arginyl–Transfer RNA Synthetase Gene Is Associated with Pontocerebellar Hypoplasia. Am. J. Hum. Genet. *81*, 857–862.

Eggens, V.R. (2016). On the origin of pontocerebellar hypoplasia: Finding genes for a rare disease. PhD thesis. University of Amsterdam - Faculty of Medicine (AMC-UvA).

Eggens, V.R., Barth, P.G., Niermeijer, J.-M.F., Berg, J.N., Darin, N., Dixit, A., Fluss, J., Foulds, N., Fowler, D., Hortobágyi, T., et al. (2014). EXOSC3 mutations in pontocerebellar hypoplasia type 1: novel mutations and genotype-phenotype correlations. Orphanet J. Rare Dis. *9*, 23.

Eisen, J.S. (1992). The role of interactions in determining cell fate of two identified motoneurons in the embryonic zebrafish. Neuron *8*, 231–240.

Eisen, J.S., and Smith, J.C. (2008). Controlling morpholino experiments: don't stop making antisense. Development *135*, 1735–1743.

Ekert, K., Groeschel, S., Sánchez-Albisua, I., Frölich, S., Dieckmann, A., Engel, C., and Krägeloh-Mann, I. (2016). Brain morphometry in Pontocerebellar Hypoplasia type 2. Orphanet J. Rare Dis. *11*.

Fabre, A., and Badens, C. (2014). Human Mendelian diseases related to abnormalities of the RNA exosome or its cofactors. Intractable Rare Dis. Res. *3*, 8–11.

Fabregat, A., Sidiropoulos, K., Garapati, P., Gillespie, M., Hausmann, K., Haw, R., Jassal, B., Jupe, S., Korninger, F., McKay, S., et al. (2016). The Reactome pathway Knowledgebase. Nucleic Acids Res. *44*, D481–D487.

Falk, S., Weir, J.R., Hentschel, J., Reichelt, P., Bonneau, F., and Conti, E. (2014). The Molecular Architecture of the TRAMP Complex Reveals the Organization and Interplay of Its Two Catalytic Activities. Mol. Cell *55*, 856–867.

Falk, S., Finogenova, K., Melko, M., Benda, C., Lykke-Andersen, S., Jensen, T.H., and Conti, E. (2016). Structure of the RBM7-ZCCHC8 core of the NEXT complex reveals connections to splicing factors. Nat. Commun. *7*, 13573.

Fasken, M.B., Losh, J.S., Leung, S.W., Brutus, S., Avin, B., Vaught, J.C., Potter-Birriel, J., Craig, T., Conn, G.L., Mills-Lujan, K., et al. (2017). Insight into the RNA Exosome Complex Through Modeling Pontocerebellar Hypoplasia Type 1b Disease Mutations in Yeast. Genetics *205*, 221–237.

Fedorov, Y. (2006). Off-target effects by siRNA can induce toxic phenotype. RNA *12*, 1188–1196.

Feng, J.-M. (2007). Minireview: expression and function of golli protein in immune system. Neurochem. Res. *32*, 273–278.

Feng, T., Niu, M., Ji, C., Gao, Y., Wen, J., Bu, G., Xu, H., and Zhang, Y.-W. (2015). SNX15 Regulates Cell Surface Recycling of APP and Aβ Generation. Mol. Neurobiol.

Fernandez-Funez, P., Nino-Rosales, M.L., de Gouyon, B., She, W.C., Luchak, J.M., Martinez, P., Turiegano, E., Benito, J., Capovilla, M., Skinner, P.J., et al. (2000). Identification of genes that modify ataxin-1-induced neurodegeneration. Nature *408*, 101–106.

Foo, J.-N., Liu, J.-J., and Tan, E.-K. (2012). Whole-genome and whole-exome sequencing in neurological diseases. Nat. Rev. Neurol. *8*, 508–517.

Forconi, M., and Herschlag, D. (2009). Metal Ion-Based RNA Cleavage as a Structural Probe. In Methods in Enzymology, (Elsevier), pp. 91–106.

Friedrichs, S., Malzahn, D., Pugh, E.W., Almeida, M., Liu, X.Q., and Bailey, J.N. (2016). Filtering genetic variants and placing informative priors based on putative biological function. BMC Genet. *17*.

Frischmeyer, P.A., van Hoof, A., O'Donnell, K., Guerrerio, A.L., Parker, R., and Dietz, H.C. (2002). An mRNA surveillance mechanism that eliminates transcripts lacking termination codons. Science *295*, 2258–2261.

Fuller, H.R., Gillingwater, T.H., and Wishart, T.M. (2016). Commonality amid diversity: Multi-study proteomic identification of conserved disease mechanisms in spinal muscular atrophy. Neuromuscul. Disord. *26*, 560–569.

Fulton, D., Paez, P.M., and Campagnoni, A.T. (2010). The multiple roles of myelin protein genes during the development of the oligodendrocyte. ASN Neuro *2*, e00027.

Gibert, Y., Trengove, M.C., and Ward, A.C. (2013). Zebrafish as a genetic model in pre-clinical drug testing and screening. Curr. Med. Chem. *20*, 2458–2466.

Gilbert, S.F. (2000). Developmental biology, Early development in fish. (Sunderland, Mass: Sinauer Associates).

Giunta, M., Edvardson, S., Xu, Y., Schuelke, M., Gomez-Duran, A., Boczonadi, V., Elpeleg, O., Müller, J.S., and Horvath, R. (2016). Altered RNA metabolism due to a homozygous *RBM7* mutation in a patient with spinal motor neuropathy. Hum. Mol. Genet. ddw149.

Goodarzi, H., Nguyen, H.C.B., Zhang, S., Dill, B.D., Molina, H., and Tavazoie, S.F. (2016). Modulated Expression of Specific tRNAs Drives Gene Expression and Cancer Progression. Cell *165*, 1416–1427.

Griffith, M., Walker, J.R., Spies, N.C., Ainscough, B.J., and Griffith, O.L. (2015). Informatics for RNA Sequencing: A Web Resource for Analysis on the Cloud. PLOS Comput. Biol. *11*, e1004393.

Güngör, O., Özkaya, A.K., Şahin, Y., Güngör, G., Dilber, C., and Aydın, K. (2016). A compound heterozygous EARS2 mutation associated with mild leukoencephalopathy with thalamus and brainstem involvement and high lactate (LTBL). Brain Dev.

Guo, T.B., Boros, L.G., Chan, K.C., Hikim, A.P.S., Hudson, A.P., Swerdloff, R.S., Mitchell, A.P., and Salameh, W.A. (2003). Spermatogenetic expression of RNA-binding motif protein 7, a protein that interacts with splicing factors. J. Androl. *24*, 204–214.

Guyon, J.R., Steffen, L.S., Howell, M.H., Pusack, T.J., Lawrence, C., and Kunkel, L.M. (2007). Modeling human muscle disease in zebrafish. Biochim. Biophys. Acta BBA - Mol. Basis Dis. *1772*, 205–215.

Haft, D.H., Selengut, J., Mongodin, E.F., and Nelson, K.E. (2005). A Guild of 45 CRISPR-Associated (Cas) Protein Families and Multiple CRISPR/Cas Subtypes Exist in Prokaryotic Genomes. PLoS Comput. Biol. *1*, e60.

Halbach, F., Reichelt, P., Rode, M., and Conti, E. (2013). The yeast ski complex: crystal structure and RNA channeling to the exosome complex. Cell *154*, 814–826.

Hamaguchi, Y., Fujimoto, M., Matsushita, T., Kaji, K., Komura, K., Hasegawa, M., Kodera, M., Muroi, E., Fujikawa, K., Seishima, M., et al. (2013). Common and Distinct Clinical Features in Adult Patients with Anti-Aminoacyl-tRNA Synthetase Antibodies: Heterogeneity within the Syndrome. PLoS ONE *8*, e60442.

Hamling, K.R., Tobias, Z.J.C., and Weissman, T.A. (2015). Mapping the development of cerebellar Purkinje cells in zebrafish. Dev. Neurobiol.

Hazama, M., Watanabe, D., Suzuki, M., Mizoguchi, A., Pastan, I., and Nakanishi, S. (2002). Different regulatory sequences are required for parvalbumin gene expression in skeletal muscles and neuronal cells of transgenic mice. Mol. Brain Res. *100*, 53–66.

He, S., Liu, S., and Zhu, H. (2011). The sequence, structure and evolutionary features of HOTAIR in mammals. BMC Evol. Biol. *11*, 102.

Heap, L.A., Goh, C.C., Kassahn, K.S., and Scott, E.K. (2013). Cerebellar output in zebrafish: an analysis of spatial patterns and topography in eurydendroid cell projections. Front. Neural Circuits *7*, 53.

Helbo, A.S., Treppendahl, M., Aslan, D., Dimopoulos, K., Nandrup-Bus, C., Holm, M.S., Andersen, M.K., Liang, G., Kristensen, L.S., and Grønbæk, K. (2015). Hypermethylation of the VTRNA1-3 Promoter is Associated with Poor Outcome in Lower Risk Myelodysplastic Syndrome Patients. Genes *6*, 977–990.

Higashijima, S. -i. (2004). Engrailed-1 Expression Marks a Primitive Class of Inhibitory Spinal Interneuron. J. Neurosci. *24*, 5827–5839.

Higashijima, S., Hotta, Y., and Okamoto, H. (2000). Visualization of cranial motor neurons in live transgenic zebrafish expressing green fluorescent protein under the control of the islet-1 promoter/enhancer. J. Neurosci. Off. J. Soc. Neurosci. *20*, 206–218.

Hill, C.M.D., Libich, D.S., and Harauz, G. (2005). Assembly of tubulin by classic myelin basic protein isoforms and regulation by post-translational modification. Biochemistry (Mosc.) *44*, 16672–16683.

Hiraishi, N., Ishida, Y., and Nagahama, M. (2015). AAA-ATPase NVL2 acts on MTR4-exosome complex to dissociate the nucleolar protein WDR74. Biochem. Biophys. Res. Commun. *467*, 534–540.

Horvath, P., and Barrangou, R. (2010). CRISPR/Cas, the immune system of bacteria and archaea. Science *327*, 167–170.

Hostikka, S.L., and Capecchi, M.R. (1998). The mouse Hoxc11 gene: genomic structure and expression pattern. Mech. Dev. *70*, 133–145.

Houseley, J., LaCava, J., and Tollervey, D. (2006). RNA-quality control by the exosome. Nat. Rev. Mol. Cell Biol. *7*, 529–539.

Howe, K., Clark, M.D., Torroja, C.F., Torrance, J., Berthelot, C., Muffato, M., Collins, J.E., Humphray, S., McLaren, K., Matthews, L., et al. (2013). The zebrafish reference genome sequence and its relationship to the human genome. Nature *496*, 498–503.

Hrdlickova, R., Toloue, M., and Tian, B. (2016). RNA-Seq methods for transcriptome analysis: RNA-Seq. Wiley Interdiscip. Rev. RNA.

Hrossova, D., Sikorsky, T., Potesil, D., Bartosovic, M., Pasulka, J., Zdrahal, Z., Stefl, R., and Vanacova, S. (2015). RBM7 subunit of the NEXT complex binds U-rich sequences and targets 3'-end extended forms of snRNAs. Nucleic Acids Res.

Hudziak, R.M., Barofsky, E., Barofsky, D.F., Weller, D.L., Huang, S.B., and Weller, D.D. (1996). Resistance of morpholino phosphorodiamidate oligomers to enzymatic degradation. Antisense Nucleic Acid Drug Dev. *6*, 267–272.

Hutchinson, S.A., Cheesman, S.E., Hale, L.A., Boone, J.Q., and Eisen, J.S. (2007). Nkx6 proteins specify one zebrafish primary motoneuron subtype by regulating late islet1 expression. Development *134*, 1671–1677.

Ingebretson, J.J., and Masino, M.A. (2013). Quantification of locomotor activity in larval zebrafish: considerations for the design of high-throughput behavioral studies. Front. Neural Circuits *7*, 109.

Irion, U., Krauss, J., and Nusslein-Volhard, C. (2014). Precise and efficient genome editing in zebrafish using the CRISPR/Cas9 system. Development *141*, 4827–4830.

Ishino, Y., Shinagawa, H., Makino, K., Amemura, M., and Nakata, A. (1987). Nucleotide sequence of the iap gene, responsible for alkaline phosphatase isozyme conversion in Escherichia coli, and identification of the gene product. J. Bacteriol. *169*, 5429–5433.

Issa, F.A., Mock, A.F., Sagasti, A., and Papazian, D.M. (2012). Spinocerebellar ataxia type 13 mutation that is associated with disease onset in infancy disrupts axonal pathfinding during neuronal development. Dis. Model. Mech. *5*, 921–929.

Jackson, A.L., Bartz, S.R., Schelter, J., Kobayashi, S.V., Burchard, J., Mao, M., Li, B., Cavet, G., and Linsley, P.S. (2003). Expression profiling reveals off-target gene regulation by RNAi. Nat. Biotechnol. *21*, 635–637.

Januszyk, K., and Lima, C.D. (2010). Structural components and architectures of RNA exosomes. Adv. Exp. Med. Biol. *702*, 9–28.

Januszyk, K., and Lima, C.D. (2014). The eukaryotic RNA exosome. Curr. Opin. Struct. Biol. *24C*, 132–140.

Jessen, K.R., and Mirsky, R. (2005). The origin and development of glial cells in peripheral nerves. Nat. Rev. Neurosci. *6*, 671–682.

Jiang, W., Zhou, H., Bi, H., Fromm, M., Yang, B., and Weeks, D.P. (2013). Demonstration of CRISPR/Cas9/sgRNA-mediated targeted gene modification in Arabidopsis, tobacco, sorghum and rice. Nucleic Acids Res. *41*, e188–e188.

Jinek, M., Chylinski, K., Fonfara, I., Hauer, M., Doudna, J.A., and Charpentier, E. (2012). A programmable dual-RNA-guided DNA endonuclease in adaptive bacterial immunity. Science *337*, 816–821.

Johnston, J.J., and Biesecker, L.G. (2013). Databases of genomic variation and phenotypes: existing resources and future needs. Hum. Mol. Genet. *22*, R27-31.

Ju, H., Kokubu, H., and Lim, J. (2014). Beyond the glutamine expansion: influence of posttranslational modifications of ataxin-1 in the pathogenesis of spinocerebellar ataxia type 1. Mol. Neurobiol. *50*, 866–874.

Kanehisa, M., and Goto, S. (2000). KEGG: kyoto encyclopedia of genes and genomes. Nucleic Acids Res. *28*, 27–30.

Kani, S., Bae, Y.-K., Shimizu, T., Tanabe, K., Satou, C., Parsons, M.J., Scott, E., Higashijima, S., and Hibi, M. (2010). Proneural gene-linked neurogenesis in zebrafish cerebellum. Dev. Biol. *343*, 1–17.

Karkare, S., and Bhatnagar, D. (2006). Promising nucleic acid analogs and mimics: characteristic features and applications of PNA, LNA, and morpholino. Appl. Microbiol. Biotechnol. *71*, 575–586.

Kasher, P.R., Namavar, Y., van Tijn, P., Fluiter, K., Sizarov, A., Kamermans, M., Grierson, A.J., Zivkovic, D., and Baas, F. (2011). Impairment of the tRNA-splicing endonuclease subunit 54 (tsen54) gene causes neurological abnormalities and larval death in zebrafish models of pontocerebellar hypoplasia. Hum. Mol. Genet. *20*, 1574–1584.

Katz, Y., Wang, E.T., Airoldi, E.M., and Burge, C.B. (2010). Analysis and design of RNA sequencing experiments for identifying isoform regulation. Nat. Methods *7*, 1009–1015.

Katz, Y., Wang, E.T., Silterra, J., Schwartz, S., Wong, B., Thorvaldsdóttir, H., Robinson, J.T., Mesirov, J.P., Airoldi, E.M., and Burge, C.B. (2015). Quantitative visualization of alternative exon expression from RNA-seq data. Bioinformatics *31*, 2400–2402.

Kazakova, N., Li, H., Mora, A., Jessen, K.R., Mirsky, R., Richardson, W.D., and Smith, H.K. (2006). A screen for mutations in zebrafish that affect myelin gene expression in Schwann cells and oligodendrocytes. Dev. Biol. *297*, 1–13.

Kelley, L.A., Mezulis, S., Yates, C.M., Wass, M.N., and Sternberg, M.J.E. (2015). The Phyre2 web portal for protein modeling, prediction and analysis. Nat. Protoc. *10*, 845–858.

Kiebler, M.A., Scheiffele, P., and Ule, J. (2013). What, where, and when: the importance of post-transcriptional regulation in the brain. Front. Neurosci. *7*.

Kilchert, C., Wittmann, S., and Vasiljeva, L. (2016). The regulation and functions of the nuclear RNA exosome complex. Nat. Rev. Mol. Cell Biol. *17*, 227–239.

Kimmel, C.B., Warga, R.M., and Schilling, T.F. (1990). Origin and organization of the zebrafish fate map. Dev. Camb. Engl. *108*, 581–594.

Kimmel, C.B., Ballard, W.W., Kimmel, S.R., Ullmann, B., and Schilling, T.F. (1995). Stages of embryonic development of the zebrafish. Dev. Dyn. Off. Publ. Am. Assoc. Anat. *203*, 253–310.

Knogler, L.D., and Drapeau, P. (2014). Sensory gating of an embryonic zebrafish interneuron during spontaneous motor behaviors. Front. Neural Circuits *8*.

Kok, F.O., Shin, M., Ni, C.-W., Gupta, A., Grosse, A.S., van Impel, A., Kirchmaier, B.C., Peterson-Maduro, J., Kourkoulis, G., Male, I., et al. (2015). Reverse genetic screening reveals poor correlation between morpholino-induced and mutant phenotypes in zebrafish. Dev. Cell *32*, 97–108.

Kopajtich, R., Murayama, K., Janecke, A.R., Haack, T.B., Breuer, M., Knisely, A.S., Harting, I., Ohashi, T., Okazaki, Y., Watanabe, D., et al. (2016). Biallelic IARS Mutations Cause Growth Retardation with Prenatal Onset, Intellectual Disability, Muscular Hypotonia, and Infantile Hepatopathy. Am. J. Hum. Genet. *99*, 414–422.

Krämer-Albers, E.-M., and White, R. (2011). From axon-glial signalling to myelination: the integrating role of oligodendroglial Fyn kinase. Cell. Mol. Life Sci. CMLS *68*, 2003–2012.

Ku, C.-S., Naidoo, N., and Pawitan, Y. (2011). Revisiting Mendelian disorders through exome sequencing. Hum. Genet. *129*, 351–370.

Kumar, P., Henikoff, S., and Ng, P.C. (2009). Predicting the effects of coding non-synonymous variants on protein function using the SIFT algorithm. Nat. Protoc. *4*, 1073–1081.

Kutmon, M., Riutta, A., Nunes, N., Hanspers, K., Willighagen, E.L., Bohler, A., Mélius, J., Waagmeester, A., Sinha, S.R., Miller, R., et al. (2016). WikiPathways: capturing the full diversity of pathway knowledge. Nucleic Acids Res. *44*, D488-494.

Lacombe, J., Hanley, O., Jung, H., Philippidou, P., Surmeli, G., Grinstein, J., and Dasen, J.S. (2013). Genetic and Functional Modularity of Hox Activities in the Specification of Limb-Innervating Motor Neurons. PLoS Genet. *9*, e1003184.

Lai, H.C., Seal, R.P., and Johnson, J.E. (2016). Making sense out of spinal cord somatosensory development. Development *143*, 3434–3448.

Law, S.H.W., and Sargent, T.D. (2014). The serine-threonine protein kinase PAK4 is dispensable in zebrafish: identification of a morpholino-generated pseudophenotype. PloS One *9*, e100268.

Lee, S.-K. (2005). Olig2 and Ngn2 function in opposition to modulate gene expression in motor neuron progenitor cells. Genes Dev. *19*, 282–294.

Lee, T.I., and Young, R.A. (2013). Transcriptional Regulation and Its Misregulation in Disease. Cell *152*, 1237–1251.

Lee, J.-A., Anholt, R.R.H., and Cole, G.J. (2008). Olfactomedin-2 mediates development of the anterior central nervous system and head structures in zebrafish. Mech. Dev. *125*, 167–181.

Lejeune, F., Li, X., and Maquat, L.E. (2003). Nonsense-mediated mRNA decay in mammalian cells involves decapping, deadenylating, and exonucleolytic activities. Mol. Cell *12*, 675–687.

Lewis, K.E., and Eisen, J.S. (2003). From cells to circuits: development of the zebrafish spinal cord. Prog. Neurobiol. *69*, 419–449.

Li, Z., Schonberg, R., Guidugli, L., Johnson, A.K., Arnovitz, S., Yang, S., Scafidi, J., Summar, M.L., Vezina, G., Das, S., et al. (2015). A novel mutation in the promoter of RARS2 causes pontocerebellar hypoplasia in two siblings. J. Hum. Genet. *60*, 363–369.

Lin, S.-T., Heng, M.Y., Ptáček, L.J., and Fu, Y.-H. (2014). Regulation of Myelination in the Central Nervous System by Nuclear Lamin B1 and Non-coding RNAs. Transl. Neurodegener. *3*, 4.

Lloret-Llinares, M., Mapendano, C.K., Martlev, L.H., Lykke-Andersen, S., and Jensen, T.H. (2016). Relationships between PROMPT and gene expression. RNA Biol. *13*, 6–14.

Lubas, M., Christensen, M.S., Kristiansen, M.S., Domanski, M., Falkenby, L.G., Lykke-Andersen, S., Andersen, J.S., Dziembowski, A., and Jensen, T.H. (2011). Interaction profiling identifies the human nuclear exosome targeting complex. Mol. Cell *43*, 624–637.

Lubas, M., Andersen, P.R., Schein, A., Dziembowski, A., Kudla, G., and Jensen, T.H. (2015). The human nuclear exosome targeting complex is loaded onto newly synthesized RNA to direct early ribonucleolysis. Cell Rep. *10*, 178–192.

Luz, J.S., Tavares, J.R., Gonzales, F.A., Santos, M.C.T., and Oliveira, C.C. (2007). Analysis of the Saccharomyces cerevisiae exosome architecture and of the RNA binding activity of Rrp40p. Biochimie *89*, 686–691.

Lyons, D.A., and Talbot, W.S. (2015). Glial cell development and function in zebrafish. Cold Spring Harb. Perspect. Biol. *7*, a020586.

MacRae, C.A., and Peterson, R.T. (2015). Zebrafish as tools for drug discovery. Nat. Rev. Drug Discov. *14*, 721–731.

Makarova, K.S., Grishin, N.V., Shabalina, S.A., Wolf, Y.I., and Koonin, E.V. (2006). A putative RNA-interference-based immune system in prokaryotes: computational analysis of the predicted enzymatic machinery, functional analogies with eukaryotic RNAi, and hypothetical mechanisms of action. Biol. Direct *1*, 7.

Makarova, K.S., Haft, D.H., Barrangou, R., Brouns, S.J.J., Charpentier, E., Horvath, P., Moineau, S., Mojica, F.J.M., Wolf, Y.I., Yakunin, A.F., et al. (2011). Evolution and classification of the CRISPR–Cas systems. Nat. Rev. Microbiol. *9*, 467–477.

Makino, D.L., Baumgärtner, M., and Conti, E. (2013). Crystal structure of an RNA-bound 11-subunit eukaryotic exosome complex. Nature *495*, 70–75.

Mali, P., Yang, L., Esvelt, K.M., Aach, J., Guell, M., DiCarlo, J.E., Norville, J.E., and Church, G.M. (2013). RNA-guided human genome engineering via Cas9. Science *339*, 823–826.

Martín-Jiménez, R., Campanella, M., and Russell, C. (2015). New zebrafish models of neurodegeneration. Curr. Neurol. Neurosci. Rep. *15*, 33.

Marty, M.C., Alliot, F., Rutin, J., Fritz, R., Trisler, D., and Pessac, B. (2002). The myelin basic protein gene is expressed in differentiated blood cell lineages and in hemopoietic progenitors. Proc. Natl. Acad. Sci. U. S. A. *99*, 8856–8861.

Matilla-Dueñas, A., Goold, R., and Giunti, P. (2008). Clinical, genetic, molecular, and pathophysiological insights into spinocerebellar ataxia type 1. Cerebellum Lond. Engl. *7*, 106–114.

McLaughlin, H.M., Sakaguchi, R., Liu, C., Igarashi, T., Pehlivan, D., Chu, K., Iyer, R., Cruz, P., Cherukuri, P.F., Hansen, N.F., et al. (2010). Compound heterozygosity for loss-of-function lysyl-tRNA synthetase mutations in a patient with peripheral neuropathy. Am. J. Hum. Genet. *87*, 560–566.

McWhorter, M.L., Monani, U.R., Burghes, A.H.M., and Beattie, C.E. (2003). Knockdown of the survival motor neuron (Smn) protein in zebrafish causes defects in motor axon outgrowth and pathfinding. J. Cell Biol. *162*, 919–931.

Meyer, A., and Schartl, M. (1999). Gene and genome duplications in vertebrates: the one-to-four (-to-eight in fish) rule and the evolution of novel gene functions. Curr. Opin. Cell Biol. *11*, 699–704.

Meyer, K., Ferraiuolo, L., Miranda, C.J., Likhite, S., McElroy, S., Renusch, S., Ditsworth, D., Lagier-Tourenne, C., Smith, R.A., Ravits, J., et al. (2014). Direct conversion of patient fibroblasts demonstrates non-cell autonomous toxicity of astrocytes to motor neurons in familial and sporadic ALS. Proc. Natl. Acad. Sci. *111*, 829–832.

Min, Y., Kristiansen, K., Boggs, J.M., Husted, C., Zasadzinski, J.A., and Israelachvili, J. (2009). Interaction forces and adhesion of supported myelin lipid bilayers modulated by myelin basic protein. Proc. Natl. Acad. Sci. *106*, 3154–3159.

Mirrakhimov, A.E. (2015). Antisynthetase syndrome: a review of etiopathogenesis, diagnosis and management. Curr. Med. Chem. *22*, 1963–1975.

Misra, M., Shah, V., Carpenter, E., McCaffery, P., and Lance-Jones, C. (2009). Restricted patterns of Hoxd10 and Hoxd11 set segmental differences in motoneuron subtype complement in the lumbosacral spinal cord. Dev. Biol. *330*, 54–72.

Mizuhashi, K., Kanamoto, T., Ito, M., Moriishi, T., Muranishi, Y., Omori, Y., Terada, K., Komori, T., and Furukawa, T. (2012). OBIF, an osteoblast induction factor, plays an essential role in bone formation in association with osteoblastogenesis. Dev. Growth Differ. *54*, 474–480.

Mizuhashi, K., Chaya, T., Kanamoto, T., Omori, Y., and Furukawa, T. (2015). Obif, a Transmembrane Protein, Is Required for Bone Mineralization and Spermatogenesis in Mice. PLOS ONE *10*, e0133704.

Mochida, G.H., Ganesh, V.S., de Michelena, M.I., Dias, H., Atabay, K.D., Kathrein, K.L., Huang, H.-T., Hill, R.S., Felie, J.M., Rakiec, D., et al. (2012). CHMP1A encodes an essential regulator of BMI1-INK4A in cerebellar development. Nat. Genet. *44*, 1260–1264.

Mojica, F.J.M., Díez-Villaseñor, C., García-Martínez, J., and Soria, E. (2005). Intervening sequences of regularly spaced prokaryotic repeats derive from foreign genetic elements. J. Mol. Evol. *60*, 174–182.

Monies, D.M., Rahbeeni, Z., Abouelhoda, M., Naim, E.A., Al-Younes, B., Meyer, B.F., and Al-Mehaidib, A. (2015). Expanding phenotypic and allelic heterogeneity of tricho-hepato-enteric syndrome. J. Pediatr. Gastroenterol. Nutr. *60*, 352–356.

Moraes, K.C.M. (2010). RNA surveillance: molecular approaches in transcript quality control and their implications in clinical diseases. Mol. Med. Camb. Mass *16*, 53–68.

Morcos, P.A. (2007). Achieving targeted and quantifiable alteration of mRNA splicing with Morpholino oligos. Biochem. Biophys. Res. Commun. *358*, 521–527.

Moreno-Mateos, M.A., Vejnar, C.E., Beaudoin, J.-D., Fernandez, J.P., Mis, E.K., Khokha, M.K., and Giraldez, A.J. (2015). CRISPRscan: designing highly efficient sgRNAs for CRISPR-Cas9 targeting in vivo. Nat. Methods *12*, 982–988.

Mukherjee, D., Gao, M., O'Connor, J.P., Raijmakers, R., Pruijn, G., Lutz, C.S., and Wilusz, J. (2002). The mammalian exosome mediates the efficient degradation of mRNAs that contain AU-rich elements. EMBO J. *21*, 165–174.

Müller, C., Bauer, N.M., Schäfer, I., and White, R. (2013). Making myelin basic protein -from mRNA transport to localized translation. Front. Cell. Neurosci. *7*, 169.

Myers, P.Z. (1985). Spinal motoneurons of the larval zebrafish. J. Comp. Neurol. *236*, 555–561.

Myers, P.Z., Eisen, J.S., and Westerfield, M. (1986). Development and axonal outgrowth of identified motoneurons in the zebrafish. J. Neurosci. Off. J. Soc. Neurosci. *6*, 2278–2289.

Nahorski, M.S., Asai, M., Wakeling, E., Parker, A., Asai, N., Canham, N., Holder, S.E., Chen, Y.-C., Dyer, J., Brady, A.F., et al. (2016). CCDC88A mutations cause PEHO-like syndrome in humans and mouse. Brain J. Neurol. *139*, 1036–1044.

Namavar, Y., Barth, P.G., Poll-The, B., and Baas, F. (2011a). Classification, diagnosis and potential mechanisms in Pontocerebellar Hypoplasia. Orphanet J. Rare Dis. *6*, 50.

Namavar, Y., Barth, P.G., Kasher, P.R., van Ruissen, F., Brockmann, K., Bernert, G., Writzl, K., Ventura, K., Cheng, E.Y., Ferriero, D.M., et al. (2011b). Clinical, neuroradiological and genetic findings in pontocerebellar hypoplasia. Brain J. Neurol. *134*, 143–156.

Namavar, Y., Chitayat, D., Barth, P.G., van Ruissen, F., de Wissel, M.B., Poll-The, B.T., Silver, R., and Baas, F. (2011c). TSEN54 mutations cause pontocerebellar hypoplasia type 5. Eur. J. Hum. Genet. *19*, 724–726.

Nasevicius, A., and Ekker, S.C. (2000). Effective targeted gene “knockdown” in zebrafish. Nat. Genet. *26*, 216–220.

Nawaz, S., Schweitzer, J., Jahn, O., and Werner, H.B. (2013). Molecular evolution of myelin basic protein, an abundant structural myelin component. Glia *61*, 1364–1377.

Norbury, C.J. (2011). Regional specialization: the NEXT big thing in nuclear RNA turnover. Mol. Cell *43*, 502–504.

Oddone, A., Lorentzen, E., Basquin, J., Gasch, A., Rybin, V., Conti, E., and Sattler, M. (2007). Structural and biochemical characterization of the yeast exosome component Rrp40. EMBO Rep. *8*, 63–69.

van der Oost, J., Jore, M.M., Westra, E.R., Lundgren, M., and Brouns, S.J.J. (2009). CRISPR-based adaptive and heritable immunity in prokaryotes. Trends Biochem. Sci. *34*, 401–407.

Palaisa, K.A., and Granato, M. (2007). Analysis of zebrafish sidetracked mutants reveals a novel role for Plexin A3 in intraspinal motor axon guidance. Development *134*, 3251–3257.

Paley, E.L., Perry, G., and Sokolova, O. (2013). Tryptamine induces axonopathy and mitochondriopathy mimicking neurodegenerative diseases via tryptophanyl-tRNA deficiency. Curr. Alzheimer Res. *10*, 987–1004.

Park, H.-C., Mehta, A., Richardson, J.S., and Appel, B. (2002). olig2 Is Required for Zebrafish Primary Motor Neuron and Oligodendrocyte Development. Dev. Biol. *248*, 356–368.

Park, J., Al-Ramahi, I., Tan, Q., Mollema, N., Diaz-Garcia, J.R., Gallego-Flores, T., Lu, H.-C., Lagalwar, S., Duvick, L., Kang, H., et al. (2013). RAS–MAPK–MSK1 pathway modulates ataxin 1 protein levels and toxicity in SCA1. Nature *498*, 325–331.

Park, S., Infante, C.R., Rivera-Davila, L.C., and Menke, D.B. (2014). Conserved regulation of *hoxc11* by pitx1 in *Anolis* lizards: CONSERVED REGULATION OF *hoxc11* BY pitx1. J. Exp. Zoolog. B Mol. Dev. Evol. *322*, 156–165.

Paschaki, M., Lin, S.-C., Wong, R.L.Y., Finnell, R.H., Dollé, P., and Niederreither, K. (2012). Retinoic Acid-Dependent Signaling Pathways and Lineage Events in the Developing Mouse Spinal Cord. PLoS ONE *7*, e32447.

Perris, R., Kuo, H.-J., Glanville, R.W., and Bronner-Fraser, M. (1993). Collagen type VI in neural crest development: Distribution in situ and interaction with cells in vitro. Dev. Dyn. *198*, 135–149.

Phillips, S.A., Barr, V.A., Haft, D.H., Taylor, S.I., and Haft, C.R. (2001). Identification and characterization of SNX15, a novel sorting nexin involved in protein trafficking. J. Biol. Chem. *276*, 5074–5084.

Pogoda, H.-M., Sternheim, N., Lyons, D.A., Diamond, B., Hawkins, T.A., Woods, I.G., Bhatt, D.H., Franzini-Armstrong, C., Dominguez, C., Arana, N., et al. (2006). A genetic screen identifies genes essential for development of myelinated axons in zebrafish. Dev. Biol. *298*, 118–131.

Popp, M.W., and Maquat, L.E. (2016). Leveraging Rules of Nonsense-Mediated mRNA Decay for Genome Engineering and Personalized Medicine. Cell *165*, 1319–1322.

Poulos, M.G., Batra, R., Charizanis, K., and Swanson, M.S. (2011). Developments in RNA Splicing and Disease. Cold Spring Harb. Perspect. Biol. *3*, a000778–a000778.

Pourcel, C., Salvignol, G., and Vergnaud, G. (2005). CRISPR elements in Yersinia pestis acquire new repeats by preferential uptake of bacteriophage DNA, and provide additional tools for evolutionary studies. Microbiol. Read. Engl. *151*, 653–663.

Preker, P., Nielsen, J., Kammler, S., Lykke-Andersen, S., Christensen, M.S., Mapendano, C.K., Schierup, M.H., and Jensen, T.H. (2008). RNA Exosome Depletion Reveals Transcription Upstream of Active Human Promoters. Science *322*, 1851–1854.

Preker, P., Almvig, K., Christensen, M.S., Valen, E., Mapendano, C.K., Sandelin, A., and Jensen, T.H. (2011). PROMoter uPstream Transcripts share characteristics with mRNAs and are produced upstream of all three major types of mammalian promoters. Nucleic Acids Res. *39*, 7179–7193.

Pyle, A., Nightingale, H.J., Griffin, H., Abicht, A., Kirschner, J., Baric, I., Cuk, M., Douroudis, K., Feder, L., Kratz, M., et al. (2015). Respiratory chain deficiency in nonmitochondrial disease. Neurol. Genet. *1*, e6.

Quinonez, S.C., and Innis, J.W. (2014). Human HOX gene disorders. Mol. Genet. Metab. *111*, 4–15.

Qureshi, I.A., and Mehler, M.F. (2013). Long Non-coding RNAs: Novel Targets for Nervous System Disease Diagnosis and Therapy. Neurotherapeutics *10*, 632–646.

Racay, P., Gregory, P., and Schwaller, B. (2006). Parvalbumin deficiency in fast-twitch muscles leads to increased “slow-twitch type” mitochondria, but does not affect the expression of fiber specific proteins. FEBS J. *273*, 96–108.

Raphael, A.R., and Talbot, W.S. (2011). New insights into signaling during myelination in zebrafish. Curr. Top. Dev. Biol. *97*, 1–19.

Reon, B.J., and Dutta, A. (2016). Biological Processes Discovered by High-Throughput Sequencing. Am. J. Pathol. *186*, 722–732.

Rex, M., Church, R., Tointon, K., Ichihashi, R.M.., Mokhtar, S., Uwanogho, D., Sharpe, P.T., and Scotting, P.J. (1998). Granule cell development in the cerebellum is punctuated by changes in Sox gene expression. Mol. Brain Res. *55*, 28–34.

Richardson, W.D., Kessaris, N., and Pringle, N. (2006). Oligodendrocyte wars. Nat. Rev. Neurosci. *7*, 11–18.

Rick Brouwer, Wilma TM Vree Egberts, Gerald JD Hengstman, Reinout Raijmakers, Baziel GM van Engelen, Hans Peter Seelig, Manfred Renz, Rudolf Mierau, Ekkehard Genth, Ger JM Pruijn, et al.

(2002). Autoantibodies directed to novel components of the PM/Scl complex, the human exosome. Arthritis Res *4(2)*, 134–138.

Rinn, J.L., Kertesz, M., Wang, J.K., Squazzo, S.L., Xu, X., Brugmann, S.A., Goodnough, L.H., Helms, J.A., Farnham, P.J., Segal, E., et al. (2007). Functional Demarcation of Active and Silent Chromatin Domains in Human HOX Loci by Noncoding RNAs. Cell *129*, 1311–1323.

Robu, M.E., Larson, J.D., Nasevicius, A., Beiraghi, S., Brenner, C., Farber, S.A., and Ekker, S.C. (2007). p53 Activation by Knockdown Technologies. PLoS Genet. *3*, e78.

Rogowska, A.T. (2005). Balance between Transcription and RNA Degradation Is Vital for Saccharomyces cerevisiae Mitochondria: Reduced Transcription Rescues the Phenotype of Deficient RNA Degradation. Mol. Biol. Cell *17*, 1184–1193.

Rolfe, A.J., Bosco, D.B., Wang, J., Nowakowski, R.S., Fan, J., and Ren, Y. (2016). Bioinformatic analysis reveals the expression of unique transcriptomic signatures in Zika virus infected human neural stem cells. Cell Biosci. *6*.

Rossi, A., Kontarakis, Z., Gerri, C., Nolte, H., Hölper, S., Krüger, M., and Stainier, D.Y.R. (2015). Genetic compensation induced by deleterious mutations but not gene knockdowns. Nature *524*, 230–233.

Safka Brozkova, D., Deconinck, T., Griffin, L.B., Ferbert, A., Haberlova, J., Mazanec, R., Lassuthova, P., Roth, C., Pilunthanakul, T., Rautenstrauss, B., et al. (2015). Loss of function mutations in HARS cause a spectrum of inherited peripheral neuropathies. Brain J. Neurol. *138*, 2161–2172.

Sager, J.J., Bai, Q., and Burton, E.A. (2010). Transgenic zebrafish models of neurodegenerative diseases. Brain Struct. Funct. *214*, 285–302.

Sainath, R., and Granato, M. (2013). Plexin A3 and Turnout Regulate Motor Axonal Branch Morphogenesis in Zebrafish. PLoS ONE *8*, e54071.

Saitsu, H., Osaka, H., Sasaki, M., Takanashi, J., Hamada, K., Yamashita, A., Shibayama, H., Shiina, M., Kondo, Y., Nishiyama, K., et al. (2011). Mutations in POLR3A and POLR3B Encoding RNA Polymerase III Subunits Cause an Autosomal-Recessive Hypomyelinating Leukoencephalopathy. Am. J. Hum. Genet. *89*, 644–651.

Sander, M. (2000). Ventral neural patterning by Nkx homeobox genes: Nkx6.1 controls somatic motor neuron and ventral interneuron fates. Genes Dev. *14*, 2134–2139.

Sanes, D.H., Reh, T.A., and Harris, W.A. (2012). Development of the nervous system (Amsterdam ; Boston : Burlington, MA: Elsevier ; Academic Press).

Satoh, J., Kino, Y., Asahina, N., Takitani, M., Miyoshi, J., Ishida, T., and Saito, Y. (2016). TMEM119 marks a subset of microglia in the human brain: Human microglial marker TMEM119. Neuropathology *36*, 39–49.

Sato-Maeda, M. (2006). Sema3a1 guides spinal motor axons in a cell- and stage-specific manner in zebrafish. Development *133*, 937–947.

Scalise, K., Shimizu, T., Hibi, M., and Sawtell, N.B. (2016). Responses of cerebellar Purkinje cells during fictive optomotor behavior in larval zebrafish. J. Neurophysiol. jn.00042.2016.

Schaffer, A.E., Eggens, V.R.C., Caglayan, A.O., Reuter, M.S., Scott, E., Coufal, N.G., Silhavy, J.L., Xue, Y., Kayserili, H., Yasuno, K., et al. (2014). CLP1 Founder Mutation Links tRNA Splicing and Maturation to Cerebellar Development and Neurodegeneration. Cell *157*, 651–663.

Schier, A.F., and Talbot, W.S. (1998). The zebrafish organizer. Curr. Opin. Genet. Dev. *8*, 464–471.

Schmidt, K., and Butler, J.S. (2013). Nuclear RNA surveillance: role of TRAMP in controlling exosome specificity. Wiley Interdiscip. Rev. RNA *4*, 217–231.

Schmidt, R., Strähle, U., and Scholpp, S. (2013). Neurogenesis in zebrafish – from embryo to adult. Neural Develop. *8*, 3.

Schmitz, S.U., Grote, P., and Herrmann, B.G. (2016). Mechanisms of long noncoding RNA function in development and disease. Cell. Mol. Life Sci. *73*, 2491–2509.

Schroeder, A., Mueller, O., Stocker, S., Salowsky, R., Leiber, M., Gassmann, M., Lightfoot, S., Menzel, W., Granzow, M., and Ragg, T. (2006). The RIN: an RNA integrity number for assigning integrity values to RNA measurements. BMC Mol. Biol. *7*, 3.

Schulte-Merker, S., and Stainier, D.Y.R. (2014). Out with the old, in with the new: reassessing morpholino knockdowns in light of genome editing technology. Dev. Camb. Engl. *141*, 3103–3104.

Seng, C.O., Magee, C., Young, P.J., Lorson, C.L., and Allen, J.P. (2015). The SMN structure reveals its crucial role in snRNP assembly. Hum. Mol. Genet. *24*, 2138–2146.

Sidova, M., Tomankova, S., Abaffy, P., Kubista, M., and Sindelka, R. (2015). Effects of post-mortem and physical degradation on RNA integrity and quality. Biomol. Detect. Quantif. *5*, 3–9.

Simonati, A., Cassandrini, D., Bazan, D., and Santorelli, F.M. (2011). TSEN54 mutation in a child with pontocerebellar hypoplasia type 1. Acta Neuropathol. (Berl.) *121*, 671–673.

Smith, G.S.T., Paez, P.M., Spreuer, V., Campagnoni, C.W., Boggs, J.M., Campagnoni, A.T., and Harauz, G. (2011). Classical 18.5-and 21.5-kDa isoforms of myelin basic protein inhibit calcium influx into oligodendroglial cells, in contrast to golli isoforms. J. Neurosci. Res. *89*, 467–480.

Smith, G.S.T., De Avila, M., Paez, P.M., Spreuer, V., Wills, M.K.B., Jones, N., Boggs, J.M., and Harauz, G. (2012). Proline substitutions and threonine pseudophosphorylation of the SH3 ligand of 18.5-kDa myelin basic protein decrease its affinity for the Fyn-SH3 domain and alter process development and protein localization in oligodendrocytes. J. Neurosci. Res. *90*, 28–47.

Smith, G.S.T., Samborska, B., Hawley, S.P., Klaiman, J.M., Gillis, T.E., Jones, N., Boggs, J.M., and Harauz, G. (2013). Nucleus-localized 21.5-kDa myelin basic protein promotes oligodendrocyte proliferation and enhances neurite outgrowth in coculture, unlike the plasma membrane-associated 18.5-kDa isoform. J. Neurosci. Res. *91*, 349–362.

Sofos, N., Winkler, M.B.L., and Brodersen, D.E. (2016). RRM domain of human RBM7: purification, crystallization and structure determination. Acta Crystallogr. Sect. F Struct. Biol. Commun. *72*, 397–402.

Spasic, M., Friedel, C.C., Schott, J., Kreth, J., Leppek, K., Hofmann, S., Ozgur, S., and Stoecklin, G. (2012). Genome-Wide Assessment of AU-Rich Elements by the AREScore Algorithm. PLoS Genet. *8*, e1002433.

Staals, R.H.J., and Pruijn, G.J.M. (2011). The human exosome and disease. Adv. Exp. Med. Biol. *702*, 132–142.

Staugaitis, S.M., Colman, D.R., and Pedraza, L. (1996). Membrane adhesion and other functions for the myelin basic proteins. BioEssays News Rev. Mol. Cell. Dev. Biol. *18*, 13–18.

Stewart, A.M., Braubach, O., Spitsbergen, J., Gerlai, R., and Kalueff, A.V. (2014). Zebrafish models for translational neuroscience research: from tank to bedside. Trends Neurosci. *37*, 264–278.

Stickney, H.L., Barresi, M.J., and Devoto, S.H. (2000). Somite development in zebrafish. Dev. Dyn. Off. Publ. Am. Assoc. Anat. *219*, 287–303.

Strehlow, D., Heinrich, G., and Gilbert, W. (1994). The fates of the blastomeres of the 16-cell zebrafish embryo. Dev. Camb. Engl. *120*, 1791–1798.

Sudo, H., Nozaki, A., Uno, H., Ishida, Y.-I., and Nagahama, M. (2016). Interaction properties of human TRAMP-like proteins and their role in pre-rRNA 5'ETS turnover. FEBS Lett.

Sumbre, G., and de Polavieja, G.G. (2014). The world according to zebrafish: how neural circuits generate behavior. Front. Neural Circuits *8*.

Svensson, A., Libelius, R., and Tågerud, S. (2008). Semaphorin 6C expression in innervated and denervated skeletal muscle. J. Mol. Histol. *39*, 5–13.

Synowsky, S.A., and Heck, A.J.R. (2007). The yeast Ski complex is a hetero-tetramer. Protein Sci. *17*, 119–125.

Sztal, T.E., Zhao, M., Williams, C., Oorschot, V., Parslow, A.C., Giousoh, A., Yuen, M., Hall, T.E., Costin, A., Ramm, G., et al. (2015). Zebrafish models for nemaline myopathy reveal a spectrum of nemaline bodies contributing to reduced muscle function. Acta Neuropathol. (Berl.) *130*, 389–406.

Taft, R.J., Vanderver, A., Leventer, R.J., Damiani, S.A., Simons, C., Grimmond, S.M., Miller, D., Schmidt, J., Lockhart, P.J., Pope, K., et al. (2013). Mutations in DARS cause hypomyelination with brain stem and spinal cord involvement and leg spasticity. Am. J. Hum. Genet. *92*, 774–780.

Tagliaferri, C., Wittrant, Y., Davicco, M.-J., Walrand, S., and Coxam, V. (2015). Muscle and bone, two interconnected tissues. Ageing Res. Rev. *21*, 55–70.

Tallafuss, A., Gibson, D., Morcos, P., Li, Y., Seredick, S., Eisen, J., and Washbourne, P. (2012). Turning gene function ON and OFF using sense and antisense photo-morpholinos in zebrafish. Dev. Camb. Engl. *139*, 1691–1699.

Thomas, F.P., Guergueltcheva, V., Gondim, F.A.A., Tournev, I., Rao, C.V., Ishpekova, B., Kinsella, L.J., Pan, Y., Geller, T.J., Litvinenko, I., et al. (2016). Clinical, neurophysiological and morphological study of dominant intermediate Charcot-Marie-Tooth type C neuropathy. J. Neurol. *263*, 467–476.

Thorsen, K., Sorensen, K.D., Brems-Eskildsen, A.S., Modin, C., Gaustadnes, M., Hein, A.-M.K., Kruhoffer, M., Laurberg, S., Borre, M., Wang, K., et al. (2008). Alternative Splicing in Colon, Bladder, and Prostate Cancer Identified by Exon Array Analysis. Mol. Cell. Proteomics *7*, 1214–1224.

Torres-Torronteras, J., Rodriguez-Palmero, A., Pinós, T., Accarino, A., Andreu, A.L., Pintos-Morell, G., and Martíí, R. (2011). A novel nonstop mutation in TYMP does not induce nonstop mRNA decay in a MNGIE patient with severe neuropathy. Hum. Mutat. *32*, E2061-2068.

Tsuda, H., Jafar-Nejad, H., Patel, A.J., Sun, Y., Chen, H.-K., Rose, M.F., Venken, K.J.T., Botas, J., Orr, H.T., Bellen, H.J., et al. (2005). The AXH domain of Ataxin-1 mediates neurodegeneration through its interaction with Gfi-1/Senseless proteins. Cell *122*, 633–644.

Ulitsky, I., Shkumatava, A., Jan, C.H., Sive, H., and Bartel, D.P. (2011). Conserved Function of lincRNAs in Vertebrate Embryonic Development despite Rapid Sequence Evolution. Cell *147*, 1537–1550.

Varshney, G.K., Pei, W., LaFave, M.C., Idol, J., Xu, L., Gallardo, V., Carrington, B., Bishop, K., Jones, M., Li, M., et al. (2015a). High-throughput gene targeting and phenotyping in zebrafish using CRISPR/Cas9. Genome Res. *25*, 1030–1042.

Varshney, G.K., Pei, W., LaFave, M.C., Idol, J., Xu, L., Gallardo, V., Carrington, B., Bishop, K., Jones, M., Li, M., et al. (2015b). High-throughput gene targeting and phenotyping in zebrafish using CRISPR/Cas9. Genome Res. *25*, 1030–1042.

Vermot, J. (2005). Retinaldehyde dehydrogenase 2 and Hoxc8 are required in the murine brachial spinal cord for the specification of Lim1+ motoneurons and the correct distribution of Islet1+ motoneurons. Development *132*, 1611–1621.

Vinograd-Byk, H., Sapir, T., Cantarero, L., Lazo, P.A., Zeligson, S., Lev, D., Lerman-Sagie, T., Renbaum, P., Reiner, O., and Levy-Lahad, E. (2015). The spinal muscular atrophy with pontocerebellar hypoplasia gene VRK1 regulates neuronal migration through an amyloid-β precursor protein-dependent mechanism. J. Neurosci. Off. J. Soc. Neurosci. *35*, 936–942.

Wan, J., Yourshaw, M., Mamsa, H., Rudnik-Schöneborn, S., Menezes, M.P., Hong, J.E., Leong, D.W., Senderek, J., Salman, M.S., Chitayat, D., et al. (2012). Mutations in the RNA exosome component gene EXOSC3 cause pontocerebellar hypoplasia and spinal motor neuron degeneration. Nat. Genet. *44*, 704–708.

Wang, K., Li, M., and Hakonarson, H. (2010). ANNOVAR: functional annotation of genetic variants from high-throughput sequencing data. Nucleic Acids Res. *38*, e164–e164.

Weis, J.S. (1968). Analysis of the development of the nervous system of the zebrafish, Brachydanio rerio. II. The effect of nerve growth factor and its antiserum on the nervous system of the zebrafish. J. Embryol. Exp. Morphol. *19*, 121–135.

Weitzer, S., Hanada, T., Penninger, J.M., and Martinez, J. (2015). CLP1 as a novel player in linking tRNA splicing to neurodegenerative disorders: CLP1 in linking tRNA splicing to neurodegenerative disorders. Wiley Interdiscip. Rev. RNA *6*, 47–63.

Welzel, G., Seitz, D., and Schuster, S. (2015). Magnetic-activated cell sorting (MACS) can be used as a large-scale method for establishing zebrafish neuronal cell cultures. Sci. Rep. *5*, 7959.

Wilkinson, R.N., Elworthy, S., Ingham, P.W., and van Eeden, F.J.M. (2013). A method for high-throughput PCR-based genotyping of larval zebrafish tail biopsies. BioTechniques *55*.

Wilson, L., and Maden, M. (2005). The mechanisms of dorsoventral patterning in the vertebrate neural tube. Dev. Biol. *282*, 1–13.

Wolf, N.I., Salomons, G.S., Rodenburg, R.J., Pouwels, P.J.W., Schieving, J.H., Derks, T.G.J., Fock, J.M., Rump, P., van Beek, D.M., van der Knaap, M.S., et al. (2014). Mutations in RARS cause hypomyelination. Ann. Neurol. *76*, 134–139.

Wolfe, J.F., Adelstein, E., and Sharp, G.C. (1977). Antinuclear antibody with distinct specificity for polymyositis. J. Clin. Invest. *59*, 176–178.

Wu, X., Kriz, A.J., and Sharp, P.A. (2014). Target specificity of the CRISPR-Cas9 system. Quant. Biol. *2*, 59–70.

Wu, Y., Wang, G., Scott, S.A., and Capecchi, M.R. (2007). Hoxc10 and Hoxd10 regulate mouse columnar, divisional and motor pool identity of lumbar motoneurons. Development *135*, 171–182.

Xi, Y., Noble, S., and Ekker, M. (2011). Modeling Neurodegeneration in Zebrafish. Curr. Neurol. Neurosci. Rep. *11*, 274–282.

Yoon, J.-H., Abdelmohsen, K., Kim, J., Yang, X., Martindale, J.L., Tominaga-Yamanaka, K., White, E.J., Orjalo, A.V., Rinn, J.L., Kreft, S.G., et al. (2013). Scaffold function of long non-coding RNA HOTAIR in protein ubiquitination. Nat. Commun. *4*.

Zhang, L., Wan, Y., Huang, G., Wang, D., Yu, X., Huang, G., and Guo, J. (2015). The exosome controls alternative splicing by mediating the gene expression and assembly of the spliceosome complex. Sci. Rep. *5*, 13403.

Zhang, X., Ling, J., Barcia, G., Jing, L., Wu, J., Barry, B.J., Mochida, G.H., Hill, R.S., Weimer, J.M., Stein, Q., et al. (2014). Mutations in QARS, encoding glutaminyl-tRNA synthetase, cause progressive microcephaly, cerebral-cerebellar atrophy, and intractable seizures. Am. J. Hum. Genet. *94*, 547–558.

Zhu, B., Mandal, S.S., Pham, A.-D., Zheng, Y., Erdjument-Bromage, H., Batra, S.K., Tempst, P., and Reinberg, D. (2005). The human PAF complex coordinates transcription with events downstream of RNA synthesis. Genes Dev. *19*, 1668–1673.

Zhu, X., Petrovski, S., Xie, P., Ruzzo, E.K., Lu, Y.-F., McSweeney, K.M., Ben-Zeev, B., Nissenkorn, A., Anikster, Y., Oz-Levi, D., et al. (2015). Whole-exome sequencing in undiagnosed genetic diseases: interpreting 119 trios. Genet. Med. *17*, 774–781.

Zon, L.I. (1999). Zebrafish: a new model for human disease. Genome Res. *9*, 99–100.

(1989). Discoveries in antisense nucleic acids (The Woodlands, Tex. : Houston: Portfolio Pub. Co. ; Gulf Pub. Co).

(1997). Embryology: constructing the organism (Sunderland, MA: Sinauer Associates).

8 Chapter 8 - Publications arising from this work

- Giunta M, Edvardson S, Xu Y, Schuelke M, Gomez-Duran A, Boczonadi V, Elpeleg O, Müller JS, Horvath R. **Altered RNA metabolism due to a homozygous RBM7 mutation in a patient with spinal motor neuropathy.** *Hum Mol Genet.* 2016 May 18. pii: ddw149. [Epub ahead of print].
- Müller JS, Giunta M, Horvath R. **Exosomal Protein Deficiencies: How Abnormal RNA Metabolism Results in Childhood-Onset Neurological Diseases.** *J Neuromuscul Dis.* 2015;2(Suppl 2):S31-S37.
- Boczonadi V, Müller JS, Pyle A, Munkley J, Dor T, Quartararo J, Ferrero I, Karcagi V, Giunta M, Polvikoski T, Birchall D, Princzinger A, Cinnamon Y, Lützkendorf S, Piko H, Reza M, Florez L, Santibanez-Koref M, Griffin H, Schuelke M, Elpeleg O, Kalaydjieva L, Lochmüller H, Elliott DJ, Chinnery PF, Edvardson S, Horvath R. **EXOSC8 mutations alter mRNA metabolism and cause hypomyelination with spinal muscular atrophy and cerebellar hypoplasia.** *Nat Commun.* 2014 Jul 3;5:4287.